The Thesis Committee for Nicolás Bruno Tiburzi
Certifies that this is the approved version of the following thesis:

Evaluation of Volume Changes and Cracking Potential of Low Water-to-Cementitious Material Ratio Concrete Mixtures

APPROVED BY
SUPERVISING COMMITTEE:

Supervisor:

Kevin J. Folliard

Thanos Drimalas

Evaluation of Volume Changes and Cracking Potential of Low Water-to-Cementitious Material Ratio Concrete Mixtures

by

Nicolás Bruno Tiburzi, B.E.

Thesis

Presented to the Faculty of the Graduate School of

The University of Texas at Austin

in Partial Fulfillment

of the Requirements

for the Degree of

Master of Science in Engineering

The University of Texas at Austin

August 2015

Acknowledgements

I would like to thank my supervisor and co-supervisor, Dr. Kevin Folliard and Dr. Thanos Drimalas, for their guidance, advice, and support over these two years. Dr. Folliard, working under your supervision has been a truly fulfilling experience. I am very grateful for all the support and the opportunity you gave me to work in this project and continuously learn from you. Dr. Drimalas, I could never have finished without your help. Thank you for your constant advice and help with all the experimental work, and for being a great mentor and friend.

I would really like to thank the assistance and friendship of all of my colleagues at the lab. Thank you for all the fun discussions and for creating such a great work environment. Thank you Fred, Stephen, Anthony, Mitch, Racheal, Trevor, Simon, Saamiya, J.C., Beth Anne, Zia, and Aasiyah. Fred, Mitch, Anthony, J.C., Stephen and Racheal, thank you for all the help with the big mixes and for always being ready to help regardless of what you were doing.

I would like to thank Michael Rung and Sherian Williams for their help and support. Mike, thank you for your assistance with all the equipment, technology, and testing procedures. Sherian, thank you for managing and taking care of our finances and any of the orders.

I would really like to thank everyone back in Argentina that has contributed to my education and helped make this thesis possible. Thank you Marcelo, Carlos, Claudio, Jorge, Roberto, María Angélica y Raúl.

Last but far from least, I would like to thank my family. Mom, Dad, and Mauro, thank you for your continuous encouragement and endless love. Being away from home

has shown me how much I value your love and support. Thank you for everything. I would finally like to thank my wife Adela for her patience and support. I can never express to her how grateful for all the love she has given me I am. Thank you for so many nights of sleeping with the light on to allow me to write.

Abstract

Evaluation of Volume Changes and Cracking Potential of Low Water-to-Cementitious Material Ratio Concrete Mixtures

Nicolás Bruno Tiburzi, M.S.E

The University of Texas at Austin, 2015

Supervisor: Kevin J. Folliard

This thesis presents the results of a comprehensive evaluation of volume changes and cracking potential of low water-to-cementitious materials ratio concrete mixtures. This work was initiated due to observed cracking of prestressed concrete beams in Texas that typically becomes visible after one to two years of service. This study evaluated various forms of volume change, including chemical shrinkage, autogenous shrinkage, and drying shrinkage. A subset of the mixtures from this study was evaluated using a restrained shrinkage frame, where the stress development was monitored along with the development of mechanical properties. A range of materials and mixture proportions were evaluated, including various portland cements, supplementary cementitious materials, aggregate types, and high-range water reducer types. Overall, it was determined that the most important parameter determining cracking potential was the volume change caused by autogenous deformations at early ages. The results of the laboratory investigations were complemented by large scale exposure blocks that were stored outdoors in Austin, TX. Only a small number of blocks cracked during the course

of this study, but the long term behavior of these blocks will continue to be monitored to better correlate laboratory results to field performance.

Table of Contents

List of Tables

List of Figures

Chapter 1: Introduction

1.1 Description of the Problem

Despite having been cast under stringent alkali-silica reaction (ASR) and delayed ettringite formation (DEF) specifications, cracking looking similar to distress from ASR and/or DEF, has been observed in several precast bridge girders at most of the largest precast yards in Texas since the mid- to late-2000's. The type of cracking is typically observed about 18 to 24 months after casting. The pathology has affected girders at most precast producers in Texas. As a result of the observed cracking, a large number of beams have been rejected for use or have been destroyed. This has resulted in substantial costs as a means of inspection reports and all the costs associated with the production, destruction and disposal of the rejected beams. More important, however, the impact of all the girders that did not remain at the precast yard and are now in service will be.

Having been determined that ASR and/or DEF are not the causes of the distress, a study started at the University of Texas at Austin to investigate potential sources of volume changes of concrete mixtures specifically used for bridge girder production in that 18 to 24 month window where cracking has been observed, since they represent the main driving forces behind cracking.

1.2 Background and Scope

Volume changes represent the main driving forces behind cracking due to internal and external restraints to the deformation tensile stresses that develop in the concrete, which may induce cracking. The net volume changes in concrete are often a combination of different mechanisms. At very early ages, the main mechanisms responsible for volume changes are autogenous and thermal deformations. At later times, when the

concrete is exposed to the environment, drying shrinkage and, to a lesser extent carbonation shrinkage represent the principal mechanisms driving the volume change.

Knowledge of the free deformation resultant from the mechanisms mentioned before does not provide the whole picture to explain, model and predict concrete cracking. The phenomenon is more complex, and an approach that considers all the mechanisms of volume change involved, the development of the mechanical properties, creep (relaxation), size and restraint conditions of the concrete system is needed.

In the last years the use of high-performance concrete (HPC) has been fueled by the benefits that can be achieved regarding workability, early strength gain, permeability, and durability. This is especially important in precast production, where excellent workability and high early strength development are critical parameters, together with long-term durability. Concrete mixtures typically used in precast bridge girders production are characterized by very low w/cm (typical in the range of 0.28 to 0.33), a high cement content, incorporation of SCMs and superplasticizers (currently polycarboxylate-based). But in addition to the mentioned improvements, this type of concrete may be more prone to early – age cracking, since it can experience significant autogenous shrinkage. This can considerably impact aesthetics, strength and its durability.

Research is needed to understand the primary causes of the distress observed. This knowledge will allow The Texas Department of Transportation (TxDOT) to evaluate the modification of specifications in order to protect against this form of distress. In this regard, a set of laboratory experiments was performed in order to examine the influence of different mixture parameters on sources of volume changes of precast concrete mixtures. In addition, a smaller set of tests was performed to assess the cracking

potential of the same concrete mixtures used for bridge girders production. The work program was divided in two major parts: cement paste testing, and concrete testing.

1.3 CONTENT

The following content outlines the chapters that will be provided in this Thesis

Chapter 2 presents a description of the problematic that is object of this research. In addition, a review of the literature concerning the factors contributing to the observed phenomenon is presented.

Chapter 3 describes the materials used in this project which are common to what is currently used in pre-cast yards in Texas.

Chapter 4 describes the set of experiments performed in the laboratory in order to examine sources of volume changes and cracking potential of precast concrete mixtures, focusing on the influence of different mixture parameters. The work program was divided in two major parts: cement paste testing, and concrete testing. Tests performed on cement paste include the determination of chemical shrinkage, autogenous deformation and isothermal calorimetry. Test in concrete include drying shrinkage, autogenous deformation, stress development under restrained deformation and the evaluation of mechanical development properties.

Chapter 5 presents the field work performed in this project as a complement to the laboratory testing focus of the previous sections. A wide set of mixtures were selected to cast exposure blocks. The objective of these exposure blocks was to have a reference for each concrete mixture subjected to outdoor conditions to analyze the time at which cracks become visible and their severity. Analogously, two visits to the TxDOT exposure site were made in order to perform a visual examination of similar concrete blocks cast between August 2010 and October 2012.

Chapter 6 summarizes the key findings and provides recommendations for future testing.

Chapter 2: Literature Review

2.1 INTRODUCTION

The following sections will provide a description of the problematic that is object of this research. In addition, a review of the literature concerning the factors contributing to the observed phenomenon is presented.

2.2 OBSERVED CRACKING

Despite having been cast under stringent ASR and DEF specifications, cracking with similar visual observations to distress from ASR and/or DEF, has been observed in several precast bridge girders at most of the largest precast yards in Texas beginning in the mid-2000's

This type of cracking is typically observed about 18 to 24 months after casting. It typically starts off as a "starburst pattern," like random map cracking. With time the cracking tends to become more extensive and in some cases a preferred alignment becomes visible, which is often associated with distress due to ASR and/or DEF. Figures 1 and 2 show pictures of the typical distress observed on the bridge girders and in an exposure block.

Fig. 1 Typical cracking observed on precast beams

Fig. 2 Typical cracking observed on an exposure block

Researchers at the University of Texas at Austin (UT) have worked closely with TxDOT engineers since 2010 to determine if the cracking was, in fact, caused by ASR and/or DEF. In this regard, researchers funded under the Federal Highway Administration (FHWA) ASR Development and Deployment Program (led by Dr. Kevin Folliard, Dr. Michael Thomas, and Dr. Benoit Fournier) started to monitor (for expansion, cracking, and internal relative humidity) four girders that had been rejected for use by TxDOT and exhibited the characteristic cracking.

These beams are stored in New Braunfels, TX and the mixtures had w/cm ratios between 0.33 and 0.35. Three of them were straight cement mixtures, and one mixture contained 20 % Class F fly ash. Cores were taken from the girders and evaluated petrographically by Dr. Benoit Fournier at the University of Laval. The evaluation mainly consisted of the Damage Rating Index (DRI), a method that provides a semi-quantitative assessment of the degree of damage in concrete based on a count of petrographic features of deterioration generally associated with alkali-silica reaction (ASR). Very low Damage Rating Indices ranging from 36 to 66 were obtained for the New Braunfels cores. In fact, the cores showed no significant signs of ASR or noticeable deterioration.

As a subsequent step, laboratory testing was conducted to evaluate the reactivity of both the coarse and fine aggregates used in the distressed girders. This included ASTM C1260 (accelerated mortar bar test) and ASTM C 1293 (concrete prism test) testing for each of the aggregate sources. Outdoor exposure blocks for both the coarse and fine aggregate were also cast using the same mixture in ASTM C 1293. In addition, "replicate" concrete mixtures using the same materials and proportions as two of the distressed girders (one without fly ash, one with 20 percent Class F fly ash) were tested under ASTM C 1293 conditions (the actual mixture was used in the tests) and used to

cast exposure blocks. The aggregates used in the girders were found to be reactive in ASTM C1260, but very little expansion was measured in ASTM C 1293 for the concrete prisms or the outdoor exposure blocks. Both replicate mixtures, with and without fly ash, showed no expansion under ASTM C 1293 conditions. Although no measurable expansion was observed, both replicate exposure blocks exhibited very similar distress as the New Braunfels girders. The cracking was first noticed between about 18 and 24 months after casting. It should be mentioned that cracking was not observed in mixtures using similar materials but with a w/cm ratio in the range of 0.42 and 0.45. Fig. 3 and Fig. 4 show pictures of replicate exposure blocks.

Fig. 3 Replicate exposure block to precast girders. Block with 20 % Class F fly ash

Fig. 4 Replicate exposure block to precast girders. Block with straight cement mixture

Based on the expansion results mentioned, coupled with the petrographic results, there is little likelihood of ASR being the cause of distress in the girders.

Continuing with the investigation, in mid-2013, Dr. Folliard and Dr. Drimalas visited five of the highest volume producers of precast girders in Texas, including visiting plants in San Antonio, San Marcos, Waco, Eagle Lake, and Victoria. The visits included visual examinations of a range of girders at each plant, with focus on girders that had been in the yards for a significant length of time. Similar types of distress that were observed in the New Braunfels girders were also evident at each of the five plants, with varying degrees of severity. Fig. 5 shows photographs from four of the plants, showing the telltale starburst cracking pattern, which ranges from discrete blemishes to more continuous, aligned, cracks.

Fig. 5 Typical crack patterns observed on some precast girders cast at different precast plants in Texas

In addition to the observations already presented, it must be mentioned that most of the girders that are showing this distress were cast using polycarboxylate-based superplasticizers. However, there was at least one girder examined visually that was reported to contain naphthalene as the superplasticizer. Currently, polycarboxylates are used in all precast concrete mixtures, and the majority of precast producers have migrated to self-consolidating concrete (SCC). Typical w/cm ratios are in the range of 0.28 to 0.33. In addition to polycarboxylates, most producers use a viscosity-modifying admixture (VMA) to minimize segregation. A few plants also use calcium nitrite as an accelerator for mixtures containing polycarboxylate superplasticizers.

Based on this previous work and observations, the research presented in this thesis will focus on volume changes of concrete mixtures specifically used in precast girders production, as they are the main driving forces behind cracking. The influence of

polycarboxylate-based superplasticizers and other mixture parameters will be studied through a comprehensive work plan.

2.3 VOLUME CHANGES

Concrete volume changes are the main driving forces behind cracking. Due to internal and external restraints to the deformation tensile stresses develop in the concrete, which may induce cracking. The net volume changes in concrete are often a combination of different mechanisms. In this section some of the main mechanisms responsible for volume changes at early ages and in the long-term will be reviewed: autogenous deformation, plastic shrinkage, drying shrinkage and thermal deformation.

2.3.1 Chemical and Autogenous shrinkage

2.3.1.1 Definitions and mechanisms

In the past few years the use of high-performance concrete (HPC) has been fueled by the benefits that can be achieved regarding workability, high early strength, permeability, and durability. HPC mixtures are characterized by a low (<0.4) w/cm, a high cement content, incorporation of SCMs and superplasticizers (Bentz and Jensen 2004). In addition to the mentioned improvements, this type of concrete can experience significant autogenous shrinkage that can induce micro- or macro-cracking, therefore impacting aesthetics, strength and its durability (Lura et al. 2003). Autogenous shrinkage is extremely dependent on w/cm ratio, and is more pronounced as the w/cm is lowered below 0.35. For the same w/cm and degree of hydration, autogenous shrinkage is greater the finer the cement used (Bentz 2008).

Autogenous deformation is defined as “the bulk (apparent) deformation of a closed, isothermal, cementitious material system not subjected to external forces” (Jensen

and Hansen 2001). The terms isothermal and closed mean that temperature is constant and there is no matter exchange with the environment. Autogenous shrinkage is the external volume reduction as a result of the chemical shrinkage associated with the hydration reactions.

Three mechanisms have been proposed to explain the observed phenomena. Variations in capillary pressure, surface tension and disjoining pressure are the factors that have been suggested; however, only the first of them has been relatively easily and successfully applied to hardening cement paste systems and provided quantitative information (Lura et al. 2003) (Barcelo et al. 2005).

From the moment that water and cement are put in contact, the absolute volume of the hydrating cement paste decreases because the volume of the hydration products is smaller than the volume of the initial reactants (Barcelo et al. 2005) (Jensen and Hansen 2001) (Lura et al. 2003). This internal volume reduction is known as chemical shrinkage (Jensen and Hansen 2001). Before setting, while the cement paste is fluid, the chemical shrinkage is entirely converted into an external volume change. Some authors (Barcelo et al. 2005) have referred to this phenomenon as “autogenous plastic shrinkage”. Therefore, measurements of autogenous and chemical shrinkage overlap during this period. At and beyond setting, as the connection between solid particles increases due to the progress of cement hydration, the deformation of the paste is restrained. The chemical shrinkage is not completely transformed into an external volume change and autogenous shrinkage becomes a small portion of chemical shrinkage. If the system is kept sealed empty pores are created and curved liquid-vapor interfaces (menisci) are formed (Bentz 2008) (Barcelo et al. 2005) (Radlinska et al. 2008). The menisci produce tensile stresses (negative pressure, known as capillary tension Pcap) in the pore solution causing the

volume change. This process is called self-desiccation and is principally responsible for the observed autogenous shrinkage.

Linear shrinkage due to capillary stresses can be approximated as shown in Equation 1 (Bentz and Jensen 2004) (Radlinska et al. 2008):

$$\varepsilon = \frac{S}{3} \mathrm{Pcap} \left[\frac{1}{K} - \frac{1}{Ks}\right] \qquad \text{Equation 1}$$

where Pcap is the capillary tension in the fluid, S is the degree of saturation of the cement paste, K is the bulk modulus of the paste, and Ks is the modulus of solid framework inside the cement paste. The relationship between the capillary pressure generated and the radius of curvature of the formed menisci is given by the Laplace equation:

$$\mathrm{Pcap} = - \frac{2\,\gamma \cos(\theta)}{r} \qquad \text{Equation 2}$$

where Pcap is the capillary tension, γ is the surface tension of the pore solution, θ is the contact angle between the pore solution and the capillary pore walls, and r is the meniscus radius of curvature. It is shown that the capillary tension in the pore solution is inversely proportional to the radius of curvature of the liquid–gas menisci. Formation of menisci corresponds with a reduction in internal RH. This proportionality can be observed if we combine Equation 2 with the Kelvin equation, which relates capillary pressure to RH:

$$\mathrm{Pcap} = \frac{R\,T\,\ln(RH)}{Vm} \qquad \text{Equation 3}$$

where R is the universal gas constant (8.314 J/mol*K), T is temperature (K), RH is the internal RH and Vm is the molar volume of the pore solution, obtaining the Kelvin–Laplace equation:

$$RH = \exp\left[\frac{-2\gamma\cos(\theta)}{r} * \frac{Vm}{RT}\right] \qquad \text{Equation 4}$$

As stated above and according to this mechanism, the monitoring of the capillary stresses can be performed by measuring the evolution of the internal RH (Barcelo et al. 2005) (Lura et al. 2003) (Bentz 2008) (Radlinska et al. 2008).

2.3.1.2 Test methods

2.3.1.2.1 Chemical shrinkage

Chemical shrinkage is commonly used to track the progression of hydration reactions (Bentz 2013). There are different test methods to measure chemical shrinkage. They are based on the measurement of the amount of water that is sorbed by the hydrating cement paste, which is kept in saturated conditions. Three main tests are found in the literature: volumetric method (dilatometry), density method (pycnometry) and buoyancy method (gravimetry). These are depicted in Fig 6, as shown by Bouasker et al. (Bouasker et al. 2008).

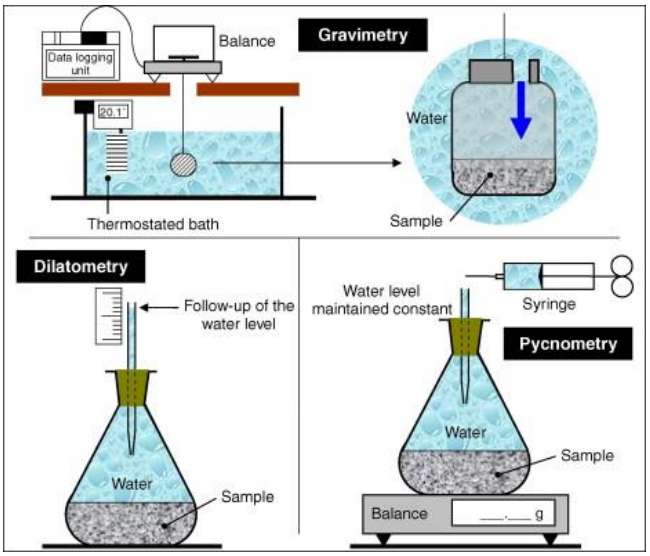

Fig. 6 Chemical shrinkage test methods (Bouasker et al. 2008)

The first two mentioned correspond to the standard test method ASTM C1608. In this section the dilatometry and buoyancy methods will be reviewed since they are the most widely used.

In the dilatometry method a small cement paste sample (between 3 mm and 10 mm thick) is placed in a glass vial. The sample is consolidated and de-aired water is added up to filling the glass vial to the top. A rubber stopper with a graduated capillary tube is inserted into the top of the vial. The level of water inside the pipette will rise. Then a drop of oil is placed on top to prevent evaporation. The sample is placed in a water bath at 23 °C to keep isothermal conditions. The initial level is recorded. The amount of water that is absorbed by the sample is measured by monitoring the change in height (decrease) of water inside the tube with time. An automated version of the dilatometry method was used in the research presented in this thesis. Further details of the specific test setup used are provided in Chapter 4. Chemical shrinkage at time t,

CS(t), (mL/g cement) is calculated as the mL of sorbed water per gram of cement in the paste specimen:

$$CS(t)=\frac{h(t)-h(60min)}{Mcement}$$

where h(t) is the water level(ml) in capillary tube at time t.

The buoyancy method monitors the change in buoyancy of a cement paste sample kept in saturated conditions (covered with a layer of water or pore solution) that is suspended in paraffin oil (Sant et al. 2006). A picture of the test setup is shown in Fig. 7.

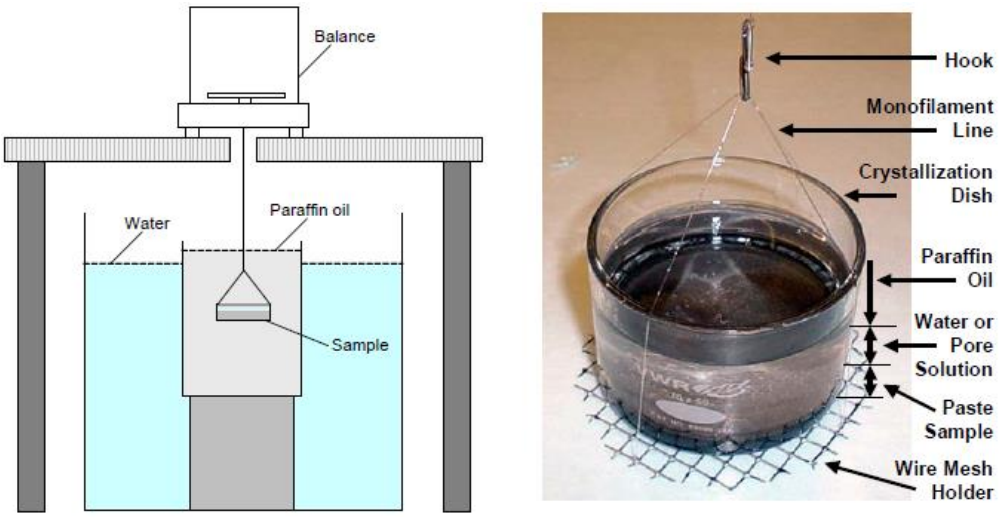

Fig. 7 Test set up of the buoyancy method (Sant et al. 2006).

As water is sorbed into the sample, the consequent change in buoyancy is automatically recorded. Chemical shrinkage is calculated as follows:

$$VCS=\frac{\Delta Vpaste(t)}{gcem}=\frac{Wsub(t)-Wsub(30)}{\rho par*gcem}$$

where ΔVpaste(t) is the volume change of the paste at time t (ml), gcem is the cement content by mass of the cement paste (g), Wsub(t) is the submerged weight of the paste at time t (g), Wsub(30) is the initial submerged weight of the paste 30 minutes after water addition (g), and ρpar is the density of the paraffin oil in the buoyancy bath at 23ºC (g/ml).

2.3.1.2.2 Autogenous deformation

Several different techniques have been developed to measure autogenous deformation of paste, mortar and concrete. There is a significant amount of literature that analyzes and compares the different test methods regarding their accuracy, repeatability, applicability to different systems and ease of implementation (Jensen and Hansen 2001) (Sant et al. 2006) (Lura and Jensen 2007). Tests can be grouped in two categories: measurement of linear strain and measurement of volumetric strain.

Linear measurements are performed by placing the fresh sample in a mold that provides little or no restraint to deformation and recording the change in length at the end of the specimen. Two main methods are discussed in this section: the corrugated tube (dilatometer) method and the free deformation frame method.

In the corrugated tube method the sample is cast in a corrugated polyethylene mold and sealed. The specimen is then placed in a dilatometer and kept in isothermal conditions. Measurements to record the change in length are performed automatically by using a data-logging device and displacement transducers (Sant et al. 2006) (Lura and Jensen 2007) (Jensen and Hansen 1995). A picture of the test set up is shown in Fig. 8.

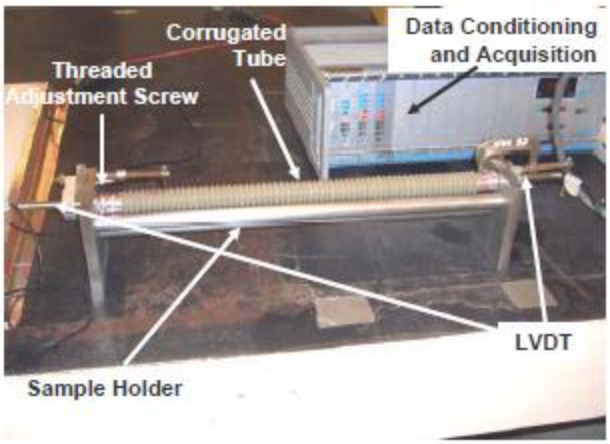

Fig. 8 Corrugated tube method set up – (Sant et al. 2006)

This method has been standardized in ASTM C 1698. In the standard it is specified that measurements start at the time of final setting. Although this method is currently the standard specified to measure autogenous strain of paste and mortars, the volumetric method was chosen in this research project due to the good agreement between both techniques (Sant et al. 2006) (Lura and Jensen 2007), the possibility of capturing very early-age behavior and previous experience in the laboratory at The University of Texas at Austin (Bentivegna 2012).

The free deformation frame method allows the tracking of autogenous deformation of concrete specimens (Riding et al. 2008) (Slatnick et al. 2011). In this technique fresh concrete specimens are cast in a temperature-controlled rigid formwork, shown in Fig. 9.

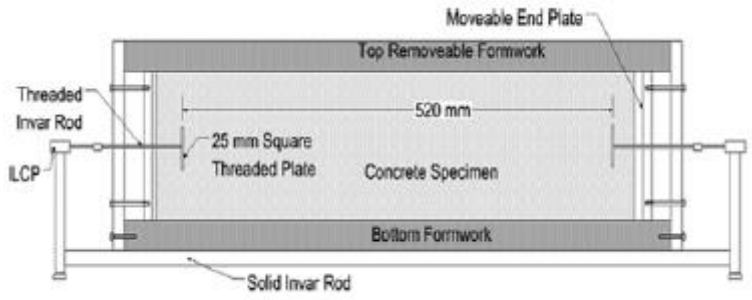

Fig. 9 Schematic Free deformation frame (Riding et al. 2008)

The concrete specimen is isolated from the form by using two layers of plastic between them, which are also lubricated with oil, in order to minimize the restraint. To prevent drying and ensure autogenous conditions a plastic layer is placed on the top surface of the sample. Two invar bars are embedded into the concrete at each end of the specimen and connected to respective linear variable displacement transducers (LDVT) to capture the length change. An automatic data-logging system is used to record the data with a 5 minutes frequency. The frame is surrounded by a system of copper pipes connected to a programmable water bath. This allows the active control of the temperature of the specimen (isothermal) by the circulation of a fluid (mixture of water and coolant). Two thermocouples are inserted into the concrete and connected to the data acquisition system, which continuously records and controls the temperature of the water bath. The concrete is held in place with the end steel plates from the moment of casting until the time of initial setting, as determined by ASTM C 403 - time of setting by penetration resistance of mortar cured to match the temperature of the concrete sample in the frame. At the time of initial setting the specimen is released by backing away both steel end plates so that the concrete is free to contract or expand. The strain is zeroed at this point.

The volumetric or buoyancy method involves casting fresh cement paste sample in a membrane that is submerged in paraffin oil (Lura and Jensen 2007). The temperature is maintained constant by placing the paraffin oil container in a water bath. A scheme of the tests set up is presented in Fig. 10.

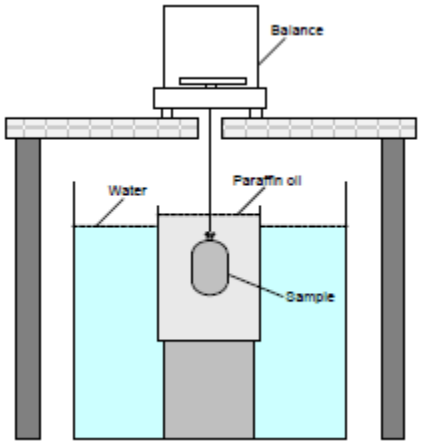

Fig. 10 Volumetric method for measuring of autogenous deformation (Sant et al. 2006)

The change in volume is determined by measuring the change in the amount of liquid displaced by the suspended specimen, what is accomplished by recording the change in its weight. The membranes consist in polyurethane condoms which are wiped to remove any lubricant. A small sample of cement paste is mixed according to ASTM C 305 and placed inside the condom using a funnel. Then the specimen is vibrated to remove any air bubbles. The condom is closed using a zip-tie with a fishing line pre-tied to it. At this point care must be taken to ensure that no air bubbles are left inside. The tail-ends of the zip-tie and the condom with some paste are cut and weighed. The cut part of the condom is washed to remove any paste and weighed. With this information the actual weight of the cement paste sample can be determined. The specimen is hung from the scale using a hook at the other end of the fishing line. Measurements start instantaneously

and are recorded automatically every 60 s by a data-logging system connected to the scale. At the end of the test, the specimen is removed from the setup and weighed to determine if there has been transport of paraffin oil through the membrane. The volumetric strain, εvol, is calculated as follows:

$$\varepsilon vol = \frac{\Delta Vpaste(t)}{Vpaste(initial)} = \frac{Wsub(t)-Wsub(initial)}{\rho par * Vpaste(initial)}$$

where ΔVpaste(t) is the volume change of the paste at time t (ml), Vpaste(t) is the volume of the paste at time t (ml), Wsub(t) is the submerged weight of the paste at time t (g), and ρpar is the density of the paraffin oil in the buoyancy bath at 23ºC (g/ml). Linear strain is obtained assuming isotropic deformations and dividing the volumetric strain by a factor of 3.

The volumetric method has been object of considerable research that tried to identify the factors influencing the divergence in the results with respect to the linear method (Jensen and Hansen 2001) (Lura and Jensen 2005) (Sant et al. 2006) (Lura and Jensen 2007). Several studies indicated that sources of error that should receive special consideration are: entrapment of air bubbles, tightness of the membrane, bleeding and water uptake through the membrane (type of membrane and type of buoyancy liquid influences on measurements were investigated and recommendations on these points provided).

Another important fact related to autogenous deformation testing is the determination of the point at which strain measurements should start or be zeroed. This point corresponds to the time at which autogenous and chemical shrinkage measurements start to diverge and is generally agreed to coincide with the final set according to the Vicat test. Sant et al. (Sant et al. 2006) discuss various analysis procedures used to

identify the time-zero in a hydrating cementitious system. Chemical shrinkage and autogenous strain measurements, the Vicat test, electrical conductivity and acoustic emission were used to determine time-zero.

2.3.2 Plastic shrinkage

2.3.2.1 Definition and mechanisms

The mechanism responsible for plastic shrinkage involves a combination of internal and external factors. It is related to the loss of water to the environment while the concrete is still in the plastic state and the development of capillary pressure as water evaporates from the surface of the concrete faster than it is replaced by bleeding. If shrinkage is not uniform or it is restrained, tensile stresses develop and can lead to cracking due to the almost negligible tensile strength of the concrete at this very early age (Banthia 2006). Plastic shrinkage cracking may have negative aesthetic and durability consequences to the concrete structure, since cracks represent weak planes for further distress or pathways for the ingress of aggressive agents (Qi et al. 2003) (Slowik et al. 2009) (Dao et al. 2010) (Lura et al. 2007) (Leemann et al. 2014). Plastic shrinkage is particularly a problem in elements that have a large surface to volume ratio (Leemann et al. 2014) (Mora-Ruacho et al. 2009). Higher strength concrete, with lower water-cementitious material ratio, lower bleed capacity, and higher contents of cement or finer cement, and fine materials such as silica fume, has an increased susceptibility to plastic shrinkage cracking (Dao et al. 2010) (Mora-Ruacho et al 2009) (Lura et al. 2007).

Lura et al. (Lura et al. 2007) described four main driving forces that contribute to plastic shrinkage cracking: the rapid evaporation of water, differential settlement, differential thermal dilation in which a temperature gradient develops inside fresh concrete due to evaporation of water from the surface, and autogenous shrinkage in the

plastic phase. An explanation of the mechanism of plastic shrinkage cracking as provided by the authors follows (Lura et al. 2007).

Immediately after placement of the concrete, the drying environment causes evaporation from a layer of bleed water. In this case, the rate of evaporation is similar to that of bulk water at the same temperature. Settlement of the solid body occurs mainly due to gravity and this causes the mixture to densify and the bleed water to be transported to the surface.

If evaporation occurs faster than the rate of bleeding the layer of water on the surface is evaporated and air-liquid menisci are formed in the liquid between the solid particles on the surface. These menisci create a capillary tension in the pore fluid. This capillary tension compresses the porous media, particularly near the top surface. In this case, in addition to the densification occurring at the bottom of the specimen during settlement/bleeding, significant local densification may also occur near the top surface of the specimen (Bentz 2008). As a consequence, the pore fluid is drawn to the surface of the concrete. The higher the capillary pressure, the more fluid is forced out of the porous network and this water is available for evaporation. In this period the bulk deformation of the system is equal to the volume of water that is lost by evaporation. As evaporation proceeds, the radius of the liquid-air menisci decreases, which causes a higher capillary stress that further consolidates the solid.

When the plasticity of the concrete is lost, due to consolidation of the concrete under the capillary pressure and the loss of water, the settlement almost stop and the deformation becomes isotropic (Leemann et al. 2014).At this point, a peak negative capillary pressure develops as the menisci reach a minimum possible radius and form in lower layers of the specimen, inducing maximum internal tensile stresses. Cracking is

most likely to happen at this critical point (Lura et al. 2007). Further evaporation leads to the opening of the crack until the concrete hardens (Mora-Ruacho et al 2009).

2.3.2.2 Testing

The ASTM C1579 - Standard Test Method for Evaluating Plastic Shrinkage Cracking of Restrained Fiber Reinforced Concrete (Using a Steel Form Insert) is commonly used to study plastic shrinkage cracking. The test exposes concrete specimens to restrain and drying conditions severe enough to cause cracking before final setting. A scheme of the test set up is presented in Fig. 11.

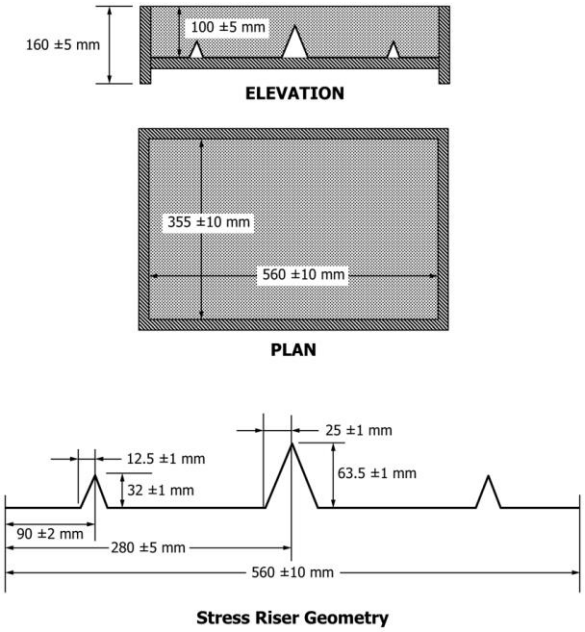

Fig. 11 Specimen and Stress Riser Geometry (ASTM C 1579 - 13)

Concrete samples are casted in the molds shown in Fig. 11 and placed in a climate chamber with specific temperature, relative humidity, and wind velocity (ASTM C1579-13). The set up allows deformation to localize, leading to cracking in a specific cross-

section. The test is terminated at the time of final setting of the concrete. At 24 h from initial mixing, the average crack width is determined. Several variations of this test method are found in literature with respect to the environmental conditions, additional parameters that are monitored (settlement, capillary pressure, mass loss, internal temperature, bleeding), and the data acquisition and analysis (Qi et al. 2003) (Lura et al. 2007) (Leemann et al. 2014).

2.3.3 Drying shrinkage

2.3.3.1 Definition and mechanisms

Drying can be classified depending on the conditions a specimen is exposed to. In sealed systems drying occurs due to consumption of water by the hydration reactions of cement and is referred to as self-desiccation. Shrinkage caused by this internal drying is known as autogenous shrinkage. In unsealed specimens, in addition to self-desiccation, loss of water to the adjacent environment, which is drier than the pore space of the drying material, occurs. Shrinkage caused by this external drying is known as drying shrinkage (Radlinska et al. 2008) (Wittmann 2009).

Drying shrinkage has been a matter of concern for many years because of the effects shrinkage can have on the durability of concrete. Drying shrinkage originates in the cement paste phase; therefore it is strongly influenced by the paste content and properties. As a general trend, for given cement content, higher w/cm will result in higher paste content, higher porosity and lower modulus of elasticity, thus increasing drying shrinkage. The aggregate phase, considered volumetrically stable, will restraint the deformation. Therefore higher aggregate content and aggregate modulus will reduce drying shrinkage. When a specimen is exposed to drying conditions (i.e. external RH lower than the internal) water will evaporate at the surface and moisture will migrate

towards the outside zone to equilibrate the external conditions. Water is first lost from the largest pores, and, as drying continues, smaller pores are emptied, being the pores smaller than 50 nm most responsible for drying shrinkage (Mindess 2003). The difference between the RH at the core of the specimen (function of self-desiccation) and the surface (function of boundary conditions), together with the transport properties of the system (function of mixture composition and curing) will determine the magnitude of the moisture gradient between the core and the surface of the structure, the concrete thickness involved, the time to reach equilibrium, and accordingly, the moisture distribution (Baroghel-Bouny 2002).

Extensive research has been conducted for decades trying to elucidate the mechanism responsible for drying shrinkage. No general agreement has been achieved regarding this point due to the complicated nature of the process and the number of chemical and physical factors involved. It is generally believed that several mechanisms acting simultaneously or consecutively may explain the observed volume change depending on the relative humidity (Ferraris and Wittmann 1987) (Hansen 1987) (Bisschop 2002) (Mindess 2003) (Wittmann 2009) (Maruyama 2010) (Lura et al. 2003) The four main proposed mechanisms are: surface free energy, capillary tension, movement of interlayer water, and disjoining pressure. The capillary tension approach, applicable at RH greater than 45%, was already described in Section 2.3.1.1. The reader is referred to the literature for explanation of the other mechanisms.

2.3.3.2 Testing

The ASTM C157 test is the most commonly used to determine the change in length of hardened concrete specimens due to drying shrinkage. In this test, concrete specimens are casted in rigid molds. After casting the specimens are cured in a moist

cabinet or room in accordance with ASTM C511 until the age of 23 ½ +/- ½ hours, then they are demolded. Upon removal from the molds, the specimens are placed in lime-saturated water at 23 °C for a minimum of 15 or 30 min depending on the cross section of the specimen. This is done to minimize variations in length due to variation in temperature. At an age of 24 +/- 1⁄2 h after the addition of water to the cement, specimens are removed from the water storage and immediately the initial comparator reading is taken. After this initial reading, the specimens are stored in lime-saturated water at 23°C until they have reached an age of 28 days. At the end of the curing period, a second comparator reading is taken and specimens are stored at RH of 50% and 23°C. Successive readings are taken at the ages of 4, 7, 14, and 28 days, and after 8, 16, 32, and 64 weeks. In addition to length change determinations, mass change is recorded at each specific age. Length change ΔLx (%) is calculated as follows:

$$\Delta Lx = \frac{CRD - CRDinitial}{G} x\ 100$$

where CRD is the difference between the comparator reading of the specimen and the reference bar at any age and G is the gage length (250 mm).

2.3.4 Thermal Deformation

2.3.4.1 Definition and mechanisms

Due to the exothermic nature of the hydration reactions, the temperature of the concrete will increase after placement. As the rate of heat evolution due to hydration decreases, the concrete temperature will decrease in order to reach equilibrium with ambient temperature. Then the heat exchange with the environment will govern the temperature of the concrete. Thermal deformation of concrete caused by changes in

temperature is a big concern when is restrained. In addition to the external restraint provided by adjacent elements, internal restraints can contribute to the buildup of significant stresses. Self-restraint is caused by non-uniform thermal deformations within the concrete structure, which result from temperature gradients in the member. This is particularly applicable to mass concrete where the heat released during cement hydration cannot dissipate uniformly, producing a large thermal gradient between the core and surface areas. Furthermore, internal restrains are also the result of differential deformation of the different concrete components (aggregates, cement paste, reinforcement) (Wyrzykowski and Lura 2013). If the stresses generated exceed concrete's tensile strength cracking occurs.

It is generally agreed that thermal deformation of hardened cement paste can be described by three coexisting mechanisms (Bazant 1970). The first is pure thermal dilation of the paste components (solid phases and water) resulting from their coefficients of thermal expansion. According to this mechanism, with a fast increase in temperature paste shows an immediate deformation (ID) and a delayed or time-dependent deformation (DD). DD occurs as water flows out of the smallest pores, releasing the pressure caused by the differential expansion of the phases (water has a higher CTE than the solid phases). Therefore DD happens in the opposite direction to the ID, representing a recovery of thermal dilation (Bazant 1970). This DD may be observed as ID depending on the speed of the pressure release, which is given by the permeability of the system and the distance to partially empty pores or the exterior (Sellevold and Bjøntegaard 2006).

The second mechanism is delayed thermal shrinkage or swelling. This deformation is related to the differences in entropies between the gel water (referring to the water present in very small pores, with lower entropy) and the capillary water (referring to water present in larger pores, with higher entropy) (Bazant 1970) (Sellevold

and Bjøntegaard 2006). With a fast temperature increase, a higher decrease in free energy occurs in the capillary water than in gel water. As a result water flows from gel pores to capillary pores in order to reestablish equilibrium and shrinkage is observed. On the other hand, delayed expansion is observed on cooling.

The third mechanism is hygrothermic dilation and involves the change in RH due to a change in temperature. Thermal dilation is caused by a change in capillary pressure (or disjoining pressure for RH< 45%) in the pore fluid at constant water content. With an increase in temperature, water expands, resulting in an increase of the radius of curvature of meniscus, which leads to an increase in RH according to Kelvin equation, thus resulting in deformation in the same direction as the pure thermal component. Another explanation relates the increase in RH to the decrease in surface tension of water as the temperature is increased (Bazant 1970) (Sellevold and Bjøntegaard 2006) (Grasley and Lange 2007).

When assessing the response of concrete to temperature changes a key parameter is its coefficient of thermal expansion (CTE). It is important to calculate early-age thermal stresses. The CTE is defined as the unit change in length due to a unit change in temperature (Mehta and Monteiro 2006).

When analyzing thermal deformation at early ages, it is critical to know the development of the CTE of the hardening concrete. It is known that the CTE varies considerably during the initial hydration period. The CTE starts at high values before setting, and drops during the setting process (Sellevold and Bjøntegaard 2006) (Kada et al. 2002). The high CTE before setting is attributed to the fact that in the fresh state no solid structure is formed and the water phase, which has a much higher CTE, is the dominant. After setting, the CTE has been reported to increase as self-desiccation occurs -showing the strong dependence of CTE on RH- (Sellevold and Bjøntegaard 2006), or to

remain relatively constant (Kada et al. 2002). There is a significant amount of publications analyzing the factors that influence the concrete's CTE. As aggregates represent the major volume of concrete, the CTE of concrete is mainly influenced by the CTE of the aggregates. In this regard, the type and volume % of aggregate are key (Won 2005) (Alungbe et al. 1992) (Tran et al. 2008). The internal RH of concrete has a strong influence on the CTE. It has been shown that a maximum CTE is obtained for partially saturated systems at RH around 50-75 %. Fully saturated and dried systems show lower CTE (Grasley and Lange 2007) (Sellevold and Bjøntegaard 2006) (Bazant 1970). The dependence of CTE on moisture content can be explained by the hygrothermic dilation mechanism presented before (Sellevold and Bjøntegaard 2006) (Bazant 1970). A more detailed review of the influence of other parameters on the CTE can be found in (Jahangirnejad 2009).

2.3.4.2 CTE testing

To determine the CTE of concrete TxDOT specifies the Tex-428-A method, which is a modification of the AASHTO TP60 test method (Won 2005). The CTE test setup consists of a water bath, a frame that provides support to the specimen, a LVDT to monitor the change in length of the specimen, and a data acquisition system for continuous data collection. First, specimens are conditioned in saturated limewater for at least 48 hours at 23 °C. The length of specimen is recorded at room temperature as L. Then the specimens are placed in the water bath and are stabilized at temperature of 10°C for 1 hour. Then the water bath temperature is increased to 50°C in a period of 130 min and maintained at this temperature for 1 hour. The temperature is then lowered to 10°C in 130 min and also maintained for 1 hour. Readings of the temperature, LVDT (displacement), and time are taken at 1-minute intervals for the entire duration of the test.

This cycle is repeated two more times, for a total of three cycles. Temperature vs. displacement is plotted using only increasing or decreasing temperature points. A straight line is fitted to the data and the slope M is calculated. CTE is calculated as:

$$CTE = \frac{M}{L} + Cf$$

where M is the slope of line (mm/°C), L is the length of the specimen (mm), and Cf is the correction factor that accounts for the deformation of the support frame.

As it was already described for autogenous deformation, free shrinkage frames can be used to measure unrestrained thermal deformation of concrete specimens at early age under real time-temperature histories (Riding 2007).

2.3.5 Cracking induced by volume changes

2.3.5.1 Background

Concrete volume changes are the main driving forces behind cracking. But knowledge of the free deformation resultant from the mechanisms presented before does not provide the whole picture to explain, model and predict concrete cracking. The phenomenon is more complex, and an approach that considers all the mechanisms of volume change involved, mechanical properties development, creep, size and restraint conditions of the concrete system is needed (Bentur 2002).

When shrinkage of concrete is restrained, internally or externally, tensile stresses develop in the system. Cracking occurs when these tensile stresses are greater than the tensile strength of the concrete. When considering the stresses generated, one must take into account creep effects, since these will produce a relaxation of the stresses predicted by Hooke's law from the restrained portion of the free shrinkage and elastic modulus

(Weiss 1999). As a result of this stress relaxation the age of cracking is increased. This phenomenon is presented in Fig 12.

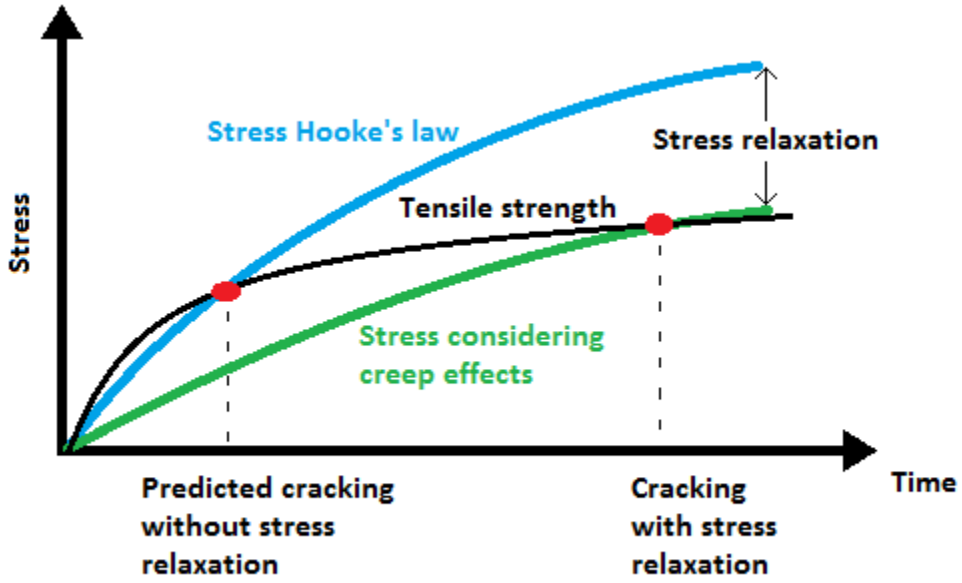

Fig. 12 Shrinkage, creep and strength development influences on cracking. Adapted from (Weiss 1999)

The consequences of the restrained volume changes are the development of stresses and possibly cracking. In addition of the magnitude of the volume change, stresses and cracking are dependent on the restraining conditions, the development of the mechanical properties (E and tensile strength) and the relaxation effects. Therefore, in order to assess the cracking potential of concrete mixtures the development of stresses and the time at which cracking occurs must be analyzed. This is accomplished by the use of restrained shrinkage tests, which evaluate the behavior of a concrete specimen in a setup that restraints its deformation.

2.3.5.2 Testing

Among restrained shrinkage tests, the most widely employed are ring tests and longitudinal tests.

The ring test has been standardized as ASTM C1581. In the test, concrete is cast around a steel ring. As the specimen tries to shrink the steel ring restraints the deformation, inducing tensile stresses in the concrete specimen. The strain in the steel ring is measured with strain gauges and is used to quantify the stress development in the concrete specimen. The stress rate development in the concrete and the time to cracking are used to classify the cracking potential of the system (See et al. 2004). In addition, there are procedures to evaluate the effects of creep (relaxation) in the concrete specimen. A more detailed overview of the characteristics and developments on the ring test can be found in (ACI 231R-10).

Longitudinal tests can be classified into several groups depending on the mode of restraint. A review of the different variants can be found in (Bentur and Kovler 2003). The following sections will focus on the testing approach selected for this research project, which consists in the use of rigid cracking frames to measure stresses due to restrained deformation, together with free shrinkage frames to measure free deformation and the evaluation of mechanical property development.

2.3.5.2.1 Rigid cracking frame

The rigid cracking frame is composed of an insulated formwork and a restraining frame. The restraining frame consists of two crossheads that are connected by two Invar bars. A schematic image and an actual picture of the setup are presented in Fig. 13 and Fig. 14 respectively.

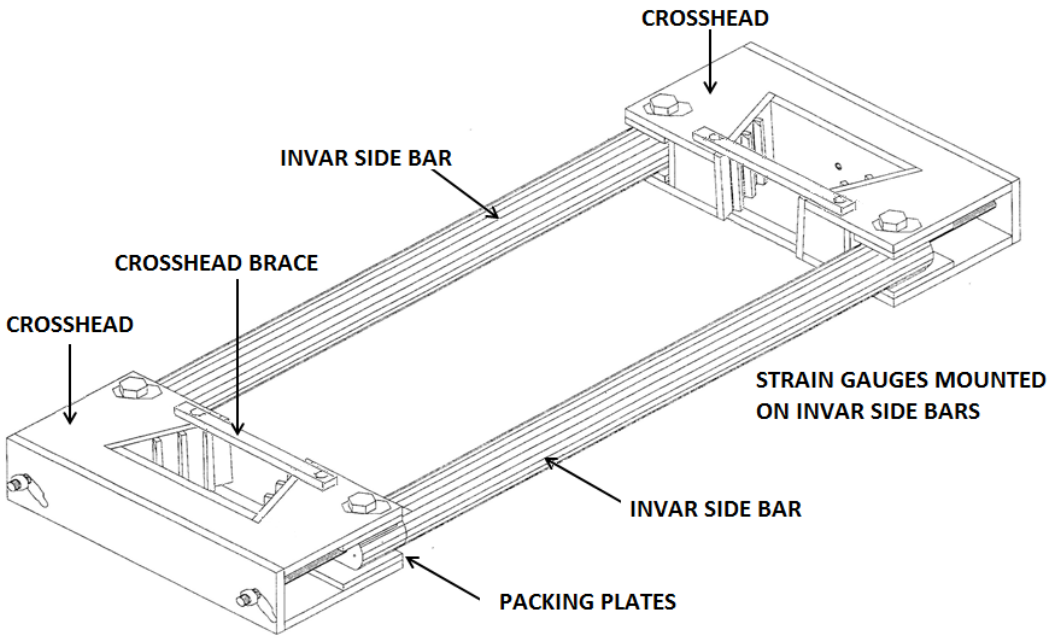

Fig. 13 Scheme of the restraining frame (Adapted from Whigham 2005)

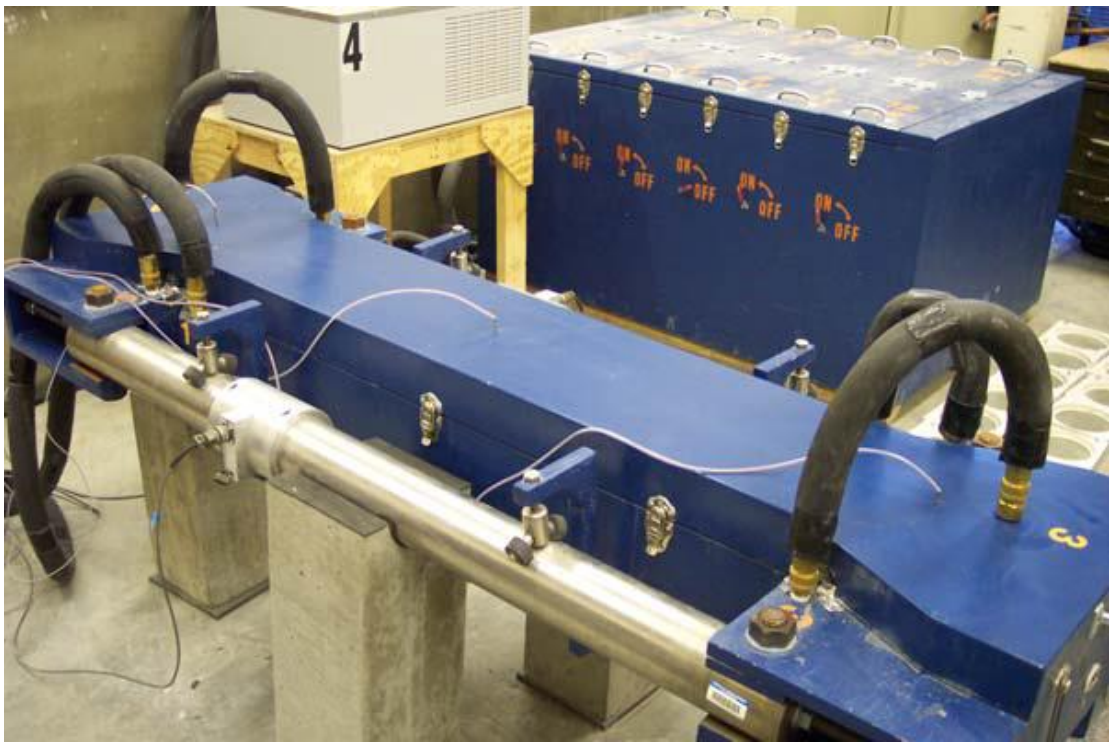

Fig. 14 Cracking frame with formwork (Whigham 2005)

The two crossheads have projections to grip the concrete. The two side bars are made of Invar, an alloy with a very low coefficient of thermal expansion, in order to minimize the deformation of the bars due to changes in temperature. A strain gauge is mounted on each restraining bar to measure the strain imposed by the deformation of the concrete specimen.

The formwork and crossheads have a system of copper pipes connected to a water bath that allows the control of the temperature of the concrete. Tests can be performed in isothermal regime in order to establish autogenous conditions or the temperature can be adjusted continuously to simulate any time-temperature history of a desired structural member. In this last case, isothermal and semi-adiabatic calorimetry tests are previously performed to determine the mixture hydration parameters. With these data, a simulation is run to obtain the temperature distribution throughout the specific structural member considering particular environmental and boundary conditions (Riding 2007) (Poole2007). Thermocouples are inserted into the fresh concrete in the middle section and in the crossheads and are connected to a software to control the temperature of the water bath.

The fresh concrete is placed in the frame and is sealed to prevent any moisture loss. The portion of the concrete autogenous (and thermal, if no isothermal conditions are imposed) deformation that is restrained induces a strain in the restraining bars that is constantly recorded by the strain gauges. This strain is used to calculate the stress development in the concrete specimen by knowing the Invar bar modulus of elasticity. The degree of restraint δ (%) provided by the cracking frame changes as a function of the modulus of elasticity of the concrete and can be calculated as follows (Mangold 1998):

$$\delta = \frac{100}{1 + \frac{EcAc}{EsAs}}$$

where Ec is the concrete elastic modulus (MPa); Ac is the concrete cross-sectional area (m2); Es is the restraining bar modulus (MPa); and As is the restraining bars cross-sectional area (m2). Since the length of the restraining bars changes due to temperature changes the strain measured is not the actual induced only by the restrained concrete deformation. The temperature of the restraining bars is measured to calculate their change in length. This thermal deformation, εTadj, must be subtracted from the strain measured by the gauges in order to determine the concrete stress (Riding 2007):

$$\varepsilon Tadj = \Delta Tib \times \alpha ib \times \delta$$

where ΔTib is the temperature change of the bar at the strain gauge (°C), and αib is the coefficient of thermal expansion of the Invar bar (m/m/°C).

A free shrinkage frame is used to measure the free autogenous (and thermal) deformation, as it was presented in Section 2.3.1.2.2. The free shrinkage frame's temperature is controlled to match the temperature in the rigid cracking frame.

In order to measure the mechanical property development, concrete cylinders are cast and cured following the same time-temperature history as the rigid cracking frame and free shrinkage frame. The cylinders are tested at 16 hours, 1, 3, 7, and 28 days for compressive strength, splitting tensile strength and modulus of elasticity (Riding 2007).

2.3.5.2.2 Early-age concrete creep behavior

The results of the rigid cracking frame, free shrinkage frame and mechanical property development can be used to model the early-age creep response of a concrete mixture. The principle of superposition is used to calculate the stress development (Riding 2007) (Byard and Schindler 2015). The strains of both the free shrinkage frame and the rigid cracking frame are discretized into changes in strain over small time steps. The total (restrained) change in strain (difference between the two measured strains) over each time step is divided by the compliance function to obtain the stress development for each time (and strain) step (Byard and Schindler 2015). By means of the principle of superposition, the stress response is obtained by adding all individual responses. The stress development calculated considering creep effects is then compared to the actual stress measured in the rigid cracking frame and the creep parameters are changed to obtain a good fit of the measured data (Riding 2007). This approach allows for the modeling of early-age stresses. In order to predict the stresses in the long term, models of long term creep must be considered. In a recent study (Byard and Schindler 2015) the B3 Model, designed for long term creep prediction, was modified to characterize the early-age concrete creep behavior and estimate the development of stresses at early ages. The modified version provided a better fit and prediction of the relaxation response at early ages than the original model and little to no change in the later-age prediction. This work represents a clear example of a model that may provide a good transition from early to long term creep response.

Since plastic and drying shrinkage are not evaluated using the presented approach, models or other methods have to be used to consider their contribution to cracking potential.

Chapter 3: Materials

3.1 Introduction

The following sections describe the materials used throughout this project.

3.2 Portland Cement

Two Type III and one Type I portland cements (ASTM C 150) were used in this study. The materials chosen are commercial available cements from two different Texas sources. Type III cement is employed in precast applications due to the higher early strength that can be obtained as a result of its increased rate of hydration. Table 1 shows the oxide analysis for the different cements.

Cement	SiO_2	Al_2O_3	Fe_2O_3	CaO	MgO	SO_3	Na_2O	K_2O
	mass %	mass %	mass %	mass %	mass %	mass %	mass %	mass %
PC-III-A	19.8	4.3	3.1	64.2	0.6	4.1	0.1	0.7
PC-III-B	19.8	5.1	1.9	63.5	1.1	5.0	0.1	0.6
PC-I-A	18.6	5.4	2.6	64.9	1.1	3.3	0.1	1.0

Table 1 Oxide analysis for the different cements

3.3 Fly Ash

One Class F fly ash (ASTM C618) from Texas was used in this study. Table 2 provides the chemical composition of the fly ash.

Fly ash	SiO2	Al2O3	Fe2O3	CaO	MgO	SO3	NA2O	K20
	mass %	mass %	mass %	mass %	mass %	mass %	mass %	mass %
Class F	52.07	23.07	3.95	11.65	2.06	0.48	0.403	0.74

Table 2 Oxide analysis for Class F Fly ash

3.4 AGGREGATES

3.4.1 Coarse Aggregates

Two sources of coarse aggregates from Texas were used for this research. The grading size was 57. A siliceous river (CA-R) and a limestone (CA-L) aggregates were used. Table 3 presents the physical properties of the coarse aggregates.

Material	Type	Specific Gravity	Absorption Capacity
CA-R	Siliceous	2.54	1.31
CA-L	Limestone	2.47	3.25

Table 3 Physical properties of the coarse aggregates

3.4.2 Fine Aggregates

Three fine aggregates from Texas were used for this study. A siliceous river sand (FA-R), a limestone sand (FA-L) and a light-weight fine aggregate (FA-LW) were used. Table 4 presents the physical properties of the fine aggregates.

Material	Type	Specific Gravity	Absorption Capacity
FA-R	Siliceous	2.62	0.42
FA-L	Limestone	2.54	2.68
FA-LW	Manufactured	1.86	22.50

Table 4 Physical properties of the fine aggregates

3.5 ADMIXTURES

A wide range of admixtures were used in this project. Four polycarboxylate-based high-range water reducers (HR-P1, HR-P2, HR-P3, HR-P4), a melamine-based high-range water reducer (HR-M), a naphthalene-based high-range water reducer (HR-N), a normal range water reducing and retarding (Type D ASTM C494) admixture (NR), and a shrinkage reducing admixture (SRA). All admixtures used are commercially available. Table 5 shows the characteristics of the admixtures used.

Admixture	Base – ASTM C494 type	Specific gravity	Typical dosage (fl. oz./100 lb cm)
HR-P1	Polycarboxylate - F	1.1	3-12
HR-P2	Polycarboxylate - F	1.1	5-12
HR-P3	Polycarboxylate - F	1.1	3-12
HR-P4	Polycarboxylate - F	1.1	3-12
HR-M	Melamine - F		
HR-N	Naphthalene- F	1.2	10-25
NR	Normal range water reducing and retarding – B and D	1.2	2-4
SRA	Shrinkage reducing admixture	0.91	1% to 2.5% by weight of cement

Table 5 Admixtures used in the project

3.6 FIBERS

Two types of polypropylene fibers were used as mitigation strategies in this project, a micro fiber, and a macro fiber. The properties of each one are presented in Table 6. Fig. 15 and Fig. 16 show a picture of the micro and macro fiber, respectively.

Fiber type	Material	Length (mm)	Aspect ratio	Specific Gravity	Modulus of Elasticity (ksi)	Tensile Strength (ksi)	Typical Dosage (lb/yd^3)
Micro fiber	Polypropylene	19	-	0.91	500	-	0.5 to 3
Macro fiber	Polypropylene	40	90	0.92	1378	90	3 to 12

Table 6 Fibers used in the project

Fig. 15 Micro fiber used

Fig. 16 Macro fiber used

Chapter 4: Laboratory Testing Results

The following sections will describe the set of experiments performed in the laboratory in order to examine sources of volume changes and cracking potential of precast concrete mixtures, focusing on the influence of different mixture parameters. The work program was divided in two major parts: cement paste testing, and concrete testing. Cement paste testing includes the determination of chemical shrinkage, autogenous deformation and isothermal calorimetry. Concrete testing includes drying shrinkage, autogenous deformation, stress development under restrained deformation and the evaluation of mechanical property development.

4.1 CHEMICAL SHRINKAGE

4.1.1 Procedure and experimental setup

To measure chemical shrinkage of cement paste specimens, the procedure specified in ASTM C1608 was used. The paste samples were mixed in a Hobart mixer according to ASTM C305. The water used in the mixture was previously de-aerated by boiling it and then stored at room temperature. The mixed paste was placed in small plastic vials. A sample height of approximately 3 mm or less was used in this project as recommended by ASTM C1608 for mixtures of very low w/cm ratio. The sample was then consolidated in a vibrating table for a few seconds. The sample was weighed to determine the amount of paste placed in the vial. The vial was filled with de-aerated water up to the top. A rubber stopper with a 2 ml capillary tube inserted in it was tightly positioned into the vial. As a result, the level of water inside the pipette rises. Following this step, red transmission oil was placed on top of the water in the pipette in order to prevent water evaporation. The sample is weighed and is then placed in a water bath at 23

°C to keep isothermal conditions. The amount of water that is absorbed by the sample is measured by monitoring the change in height (decrease) of water inside the tube with time.

In this project, an automated system was used to monitor the height of water in the capillary tube. The data are captured by a web camera, which takes a picture of the samples every 5 minutes and is connected to a computer to store the images. All the pictures are then processed by image analysis software developed by Bishnoi at École Polytechnique Fédérale de Lausanne, Switzerland (2009), which uses the red oil as the reference point to determine the height of water in the capillary tube. Fig. 17 shows the test setup at the University of Texas at Austin.

Fig. 17 Automated system at UT Austin for continuous measurement of chemical shrinkage

As shown in Fig. 17, the sample holder placed on top of a water bath faces two webcams. As a result, this setup is capable of testing 4 mixtures (3 samples per mixture) at the same time. Foam insulation is used over the water bath to moderate evaporation and temperature changes.

4.1.2 Mixture proportions and testing matrix

A total of 32 different mixtures were tested as a part of this project with varying combinations of w/cm ratios, cement sources, chemical admixtures types and dosages. The polycarboxylate mixtures are the reference mixtures for the most part of the study since they are the type of HRWR currently used in precast production. Tests were carried out at 23 °C for 7 days. Table 7 shows the mixture proportions of the samples tested and the measured chemical shrinkage at the age of 1, 5, and 7 days since 30 min after initial contact of water + cement. Each individual value in Table 7 is the average of three samples measured by the automated setup previously described.

w/c	Cement type	Admixtures					Chemical shrinkage (mL of H2O/g of cm)		
		Type	(floz/ 100 lb cm)	Type	(floz/ 100 lb cm)	SRA % cm	1d	5d	7d
0.28	PC-III-A	HR-P1	5	-	-	-	0.050	0.091	0.101
				NR	3	-	0.047	0.077	0.088
			12	-	-	-	0.041	0.067	0.076
		HR-P2	5	NR	3	-	0.056	0.084	0.089
			12	-	-	-	0.038	0.069	0.075
				NR	3	-	0.053	0.073	0.078
0.31	PC-III-A	HR-P2	12	-	-	-	0.035	0.062	0.074
	PC-III-B	HR-P2	12	-	-	-	0.041	0.071	0.082

Table 7 Mixture proportions and chemical shrinkage at 1, 5 and 7 days values

w/c	Cement type	Admixtures					Chemical shrinkage (mL of H2O/g of cm)		
		Type	(floz/ 100 lb cm)	Type	(floz/ 100 lb cm)	SRA % cm	1d	5d	7d
0.33	PC-III-A	-	-	-	-	-	0.053	0.074	0.074
		HR-P1	3	-	-	-	0.051	0.076	0.078
			5	-	-	-	0.041	0.075	0.085
				NR	3	-	0.047	0.088	0.099
			6	-	-	-	0.052	0.080	0.081
			9	-	-	-	0.048	0.076	0.078
			12	-	-	-	0.047	0.072	0.077
				NR	3	-	0.039	0.072	0.085
		HR-P2	5	-	-	-	0.047	0.077	0.086
				NR	3	-	0.043	0.063	0.079
				-	-	1.5	0.050	0.086	0.095
			12	-	-	-	0.038	0.071	0.079
				NR	3	-	0.051	0.081	0.089
		HR-M	25	-	-	-	0.045	0.085	0.091
		HR-N	29	-	-	-	0.039	0.074	0.081
	PC-III-B	HR-P1	5	-	-	-	0.045	0.071	0.079
				-	-	1.5	0.042	0.074	0.083
		HR-P2	5	NR	3	-	0.051	0.063	0.087
			12	-	-	-	0.039	0.074	0.079
0.35	PC-III-A	HR-P1	12	-	-	-	0.051	0.088	0.096
		HR-P2	12	-	-	-	0.043	0.077	0.082
0.4	PC-III-A	HR-P1	12	-	-	-	0.046	0.084	0.092
		HR-P2	5	-	-	-	0.059	0.084	0.091
			12	-	-	-	0.050	0.084	0.090

(cont.) Table 7 Mixture proportions and chemical shrinkage at 1, 5 and 7 days values

4.1.3 Results

In the following sections, the effect of several factors on chemical shrinkage of cement paste samples will be analyzed. The chemical shrinkage curves for all mixtures can be found in Appendix I.

4.1.3.1 Influence of w/c ratio

Fig. 18 shows the chemical shrinkage curves for the mixtures with PC-III-A, same amount of polycarboxylate -based HRWR and varying w/c ratio from 0.28 to 0.4.

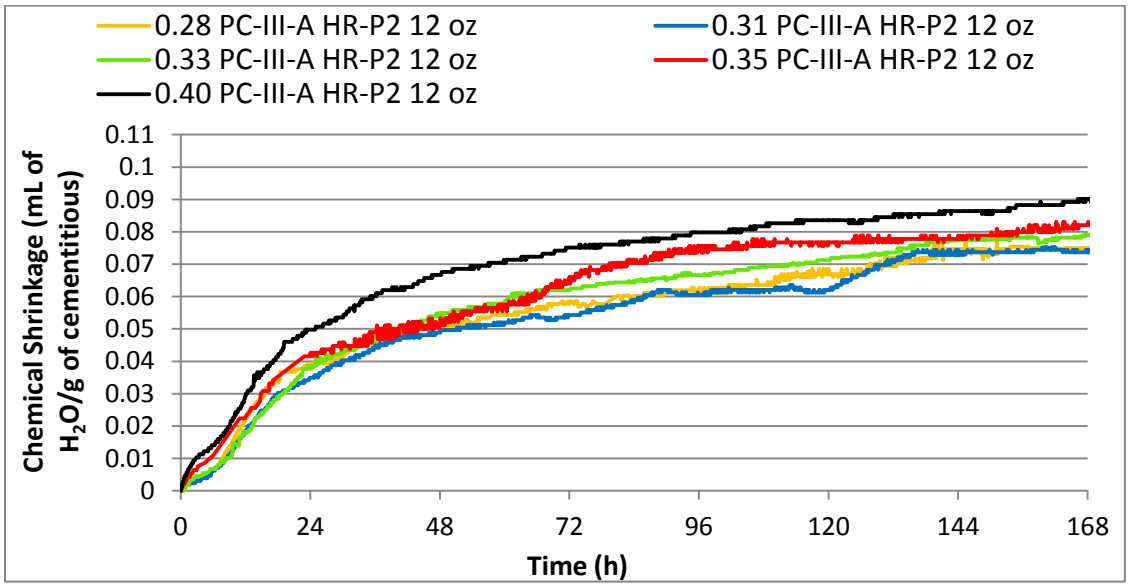

Fig. 18 Effect of w/c ratio on chemical shrinkage of cement paste specimens

As it is observed in Fig 18, there was a small increase in the chemical shrinkage value at 7 days with the increase in w/c ratio. This increase can be explained by the fact that lower w/c mixtures form a less open, more densely packed structure, thus reducing

the accessibility of external water. However, the increase in the values measured was not very significant and was much less noticeable in the lowest w/c range from 0.28 to 0.35. This is in agreement with results presented by other researchers (Baroghel-Bouny et al. 2006) (Holt 2005) (Justnes et al. 1996), who found minor and unsystematic variations in chemical shrinkage with w/cm.

4.1.3.2 Effect of cement source

Fig. 19 shows chemical shrinkage curves for equivalent mixtures with PC-III-A and PC-III-B cements.

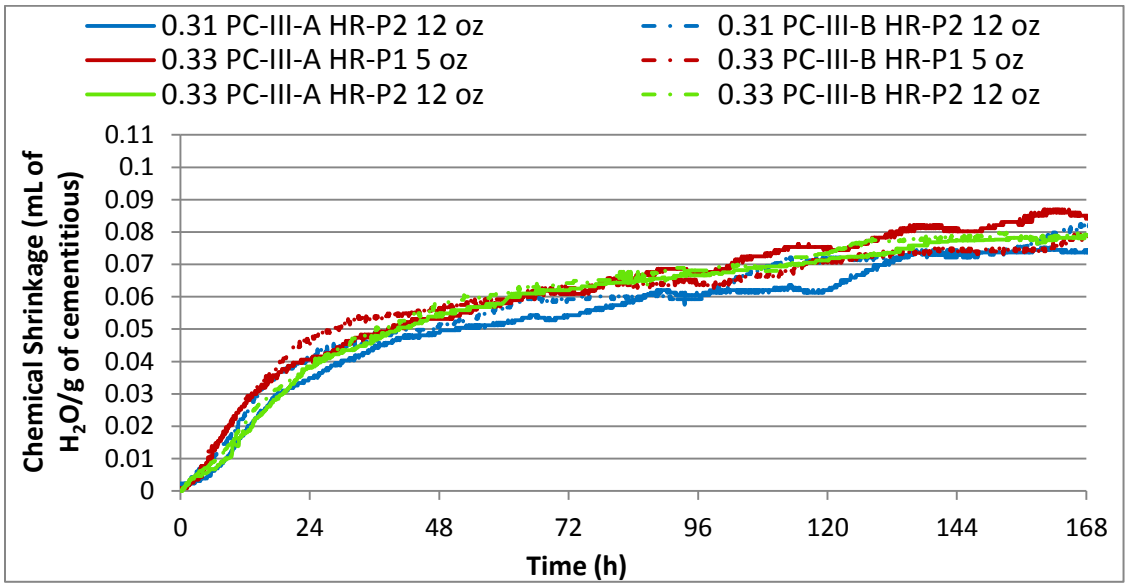

Fig. 19 Chemical shrinkage curves for different cement source

As it can be seen, no significant difference was observed between both equivalent mixtures within each pair (same line color means same mixture parameters but cement

source). This fact was independent of w/cm ratio, as it was shown before, and also independent of the type of polycarboxylate used.

4.1.3.3 Influence of HRWR type and Polycarboxylate-based HRWR dosage

Fig. 20 shows the chemical shrinkage curves for mixtures with PC-III-A with the same w/c ratio (0.33) and varying HRWR type. Fig. 21 shows chemical shrinkage curves for PC-III-A with the same w/c ratio (0.33) and varying polycarboxylate dosage.

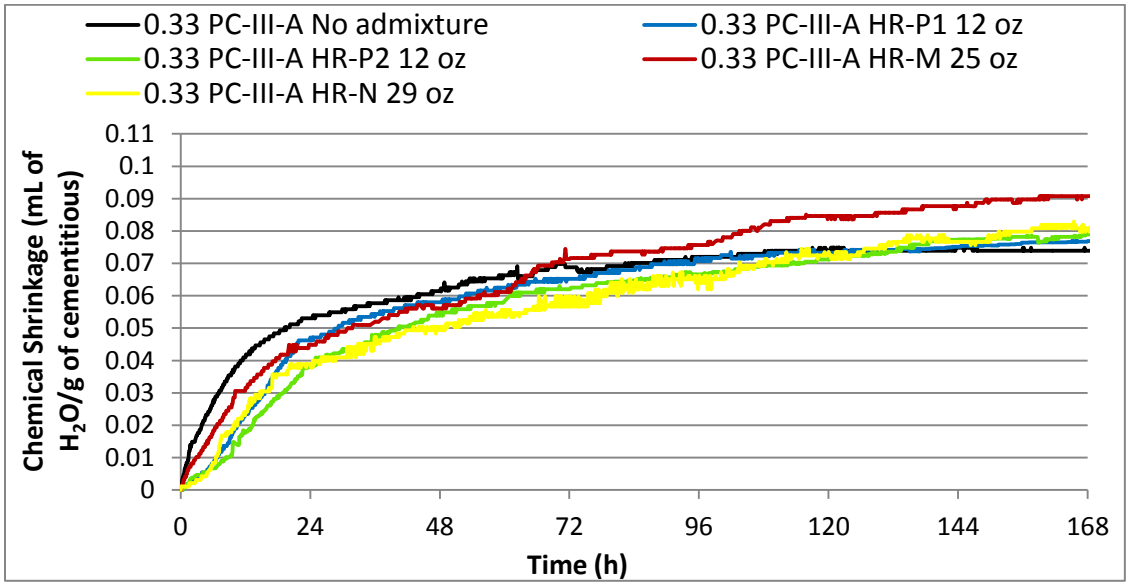

Fig. 20 Chemical shrinkage curves for different HRWR types

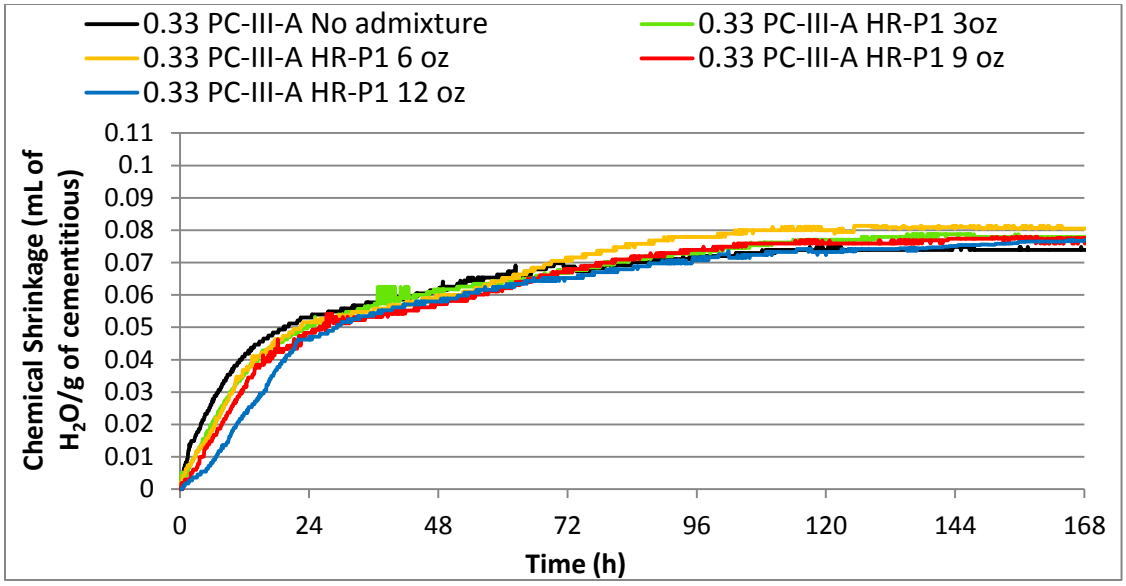

Fig. 21 Chemical shrinkage curves showing effect of polycarboxylate (HR-P1) dosage

It can be observed in Fig. 20 and Fig. 21 that the control mixture with no admixture showed a higher initial rate of chemical shrinkage. This rate then decreased, resulting in the lowest measured shrinkage at 7 days. The initial slower rate of chemical shrinkage in the mixtures with chemical admixtures can be a result of the retardation of the hydration reactions caused by the HRWR incorporation. This phenomenon is further observed in Fig. 21, where the progressive increase in HRWR dosage caused the initial slopes of the curves to slightly decrease and shift to the right. The mixtures that incorporated a HRWR showed slightly higher chemical shrinkage than the control mixture without admixtures at the end of the test period. This result may be attributable to a better dispersion and disaggregation of the cement particles, therefore improving their access to water.

Among all HRWR mixtures, the HR-M mixture showed the highest chemical shrinkage and this value was slightly different from all other HRWR mixtures, which

presented similar shrinkage values. In the case of the polycarboxylate-based HRWR showed in Fig. 21, the small increase in chemical shrinkage at the end of the test as a result of the HRWR incorporation compared to the control mixture was not proportional to the increase in admixture dosage. The greatest chemical shrinkage value was obtained for the intermediate dosage of 6 fl oz/ 100 lb cement, as shown more clearly in Fig. 22. This agrees with the results obtained with isothermal calorimetry testing presented later in this thesis.

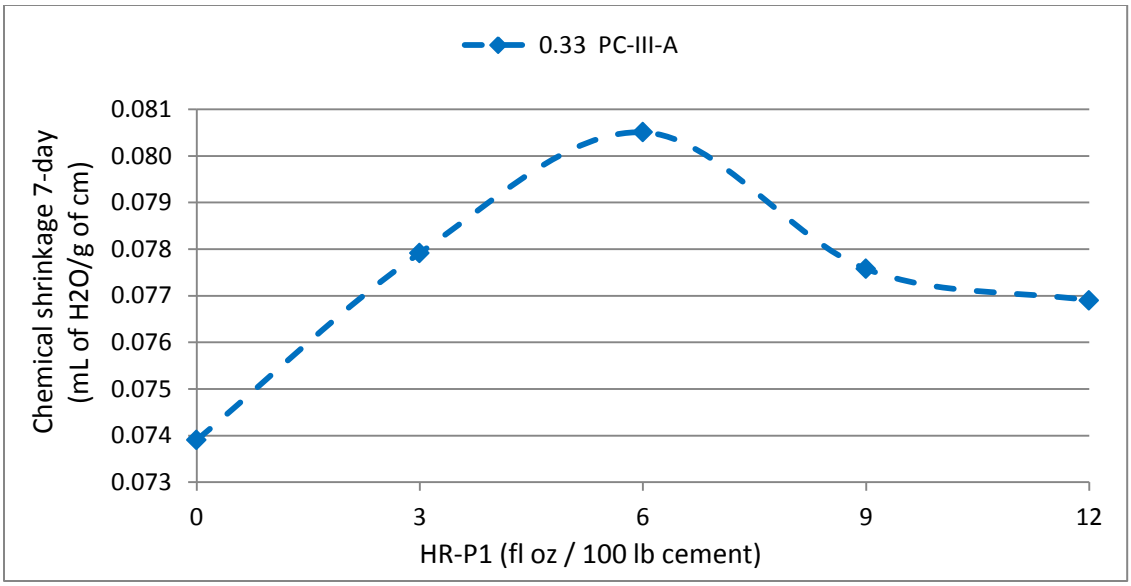

Fig. 22 Chemical shrinkage at 7 days - Effect of admixture (HR-P1) dosage

The mixtures that incorporated a normal range water reducer (NR) in combination with the polycarboxylate-based HRWR showed unsystematic results, but in the same range as the mixtures presented in this section. No clear trend was found. The chemical shrinkage for those mixtures can be found in Appendix I.

The effects of changing type of HRWR and dosage of polycarboxylate on chemical shrinkage were very small in magnitude. When a normal range water reducer (NR) was used in combination with the polycarboxylate-based HRWR, unsystematic but similar values were obtained compared to analogous mixtures without NR. The final chemical shrinkage values for pastes with different types of HRWR lie in the same small range. The same occurs with increasing polycarboxylate dosage. Therefore, according to the results obtained in this section, the type of HRWR and dosage of polycarboxylate do not seem to have a strong influence on the chemical shrinkage experienced by the cement paste. These results agree with the conclusions of Justnes et al. (Justnes et al. 2000), who found that the addition of a plasticizer (sodium lignosulphonate) and two different types of super-plasticizer (sodium salts of sulphonated melamine - formaldehyde condensate and naphthalene sulphonate - formaldehyde condensate) did not impact directly the chemical shrinkage of cement paste samples in a significant way.

4.1.3.4 Influence of SRA

Fig. 23 shows the influence of SRA incorporation on the chemical shrinkage of two sets of mixtures, with PC-III-A and PC-III-B with the same w/c ratio (0.33) and different HRWR types.

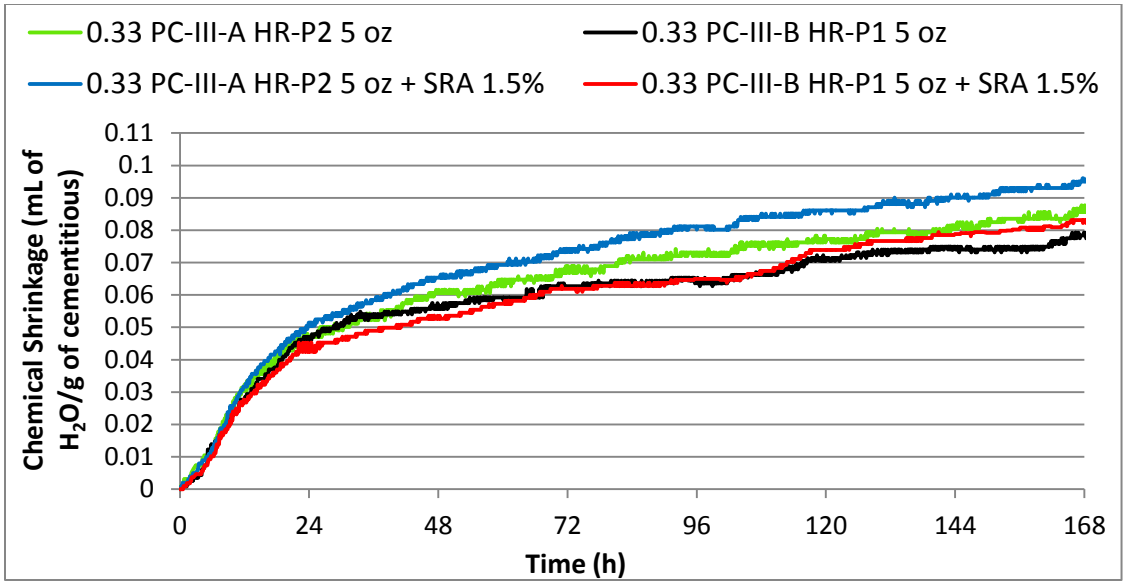

Fig. 23 Chemical shrinkage curves showing effect of SRA incorporation

As can be seen in Fig. 23, the incorporation of SRA produces an increase in the chemical shrinkage value at 7 days. This is in agreement with the results obtained by Fu (Fu 2011). However the behavior at earlier times (before 48 hours) shows two different trends. In the set with PC-III-A, the mixture with SRA presents higher values of chemical shrinkage than the non-SRA mixture at the same age. This is different from what we expected since retardation is often observed as a result of the SRA addition (Sant 2007) (Rajabipour et al. 2008), as can be seen in the results of isothermal calorimetry testing that will be presented later. On the other hand, the mixture with PC-III-B and SRA shows lower chemical shrinkage values than the corresponding non-SRA mixture at the same age. It must be mentioned that the relative differences between the curves are very small, and, similarly to the graphs presented before, the trends could be slightly different depending on the variability and accuracy of the test method.

4.1.4 Summary and Conclusions

Based on the results of this section the following conclusions can be made:

- The increase in w/cm ratio produced a small increase in the chemical shrinkage at 7 days. However, the increase in the values measured was not very significant and was much less noticeable in the lowest w/c range.
- No significant difference in chemical shrinkage was observed between different Type III cement sources.
- The incorporation of all HRWRs reduced the initial rate of chemical shrinkage. This may be a result of the retardation of the hydration reactions caused by the HRWR incorporation. This phenomenon was further observed for the case of polycarboxylates with the progressive increase in dosage.
- The incorporation of all HRWRs slightly increased the chemical shrinkage at 7 days. This result may be attributable to a better dispersion and disaggregation of the cement particles.
- Among all HRWR mixtures, the HR-M mixture showed the highest chemical shrinkage and this value was slightly different from all other HRWR mixtures, which presented similar shrinkage values.
- In the case of the polycarboxylate-based HRWR the small increase in chemical shrinkage at 7 days compared to the control was not proportional to the increase in admixture dosage. The greatest chemical shrinkage value was obtained for an intermediate dosage.
- The incorporation of a normal range water reducer (NR) in combination with the polycarboxylate-based HRWR showed unsystematic results, but in the same range as the analogous mixtures without NR.

- According to the results obtained in this section, the type of HRWR and dosage of polycarboxylate do not seem to have a strong influence on the chemical shrinkage experienced by the cement paste.
- The incorporation of SRA produced a small increase in the chemical shrinkage value at 7 days. No retardation was observed in the SRA mixtures as opposed to expected.
- It must be mentioned that the relative differences between chemical shrinkage curves were very small, and the trends found could be slightly different depending on the variability and accuracy of the test method.

4.2 AUTOGENOUS DEFORMATION

4.2.1 Procedure and experimental setup

In order to measure autogenous deformation in cement paste samples, the volumetric method described in Chapter 2 was used. A picture of the test setup is shown in Fig. 24.

Fig. 24 Test setup to measure autogenous deformation of cement paste

The setup at UT Austin allows the measurement of two samples at the same time. Two scales are placed on top of a concrete countertop, which has two holes to allow the specimens to hang from the bottom of the scales, and are covered to isolate them from air circulation and obtain more stable readings. The scales are connected directly to two computers to record the readings. Below, there are two glass containers filled with paraffin oil immersed in a water bath that keeps the temperature at 23 ºC.

The membranes used consisted in polyurethane condoms (Trojan Supra) which were wiped to remove any lubricant. The paste samples (between 100 g and 150 g) were mixed in a Hobart mixer according to ASTM C305. The water used in the mixture was previously de-aerated by boiling it and then stored at room temperature until the moment of the test. The cement paste was placed inside the condom using a funnel. Then the specimen was vibrated to remove any air bubbles. The condom was closed using a zip-tie with a fishing line pre-tied to it. Care was taken to ensure that no air bubbles were left inside.

The tail-ends of the zip-tie and the condom with some paste were cut and weighed. The cut part of the condom was washed to remove any paste and weighed. With this information the actual weight of the cement paste sample was determined. The specimen was hung from the scale using a hook at the other end of the fishing line. Measurements started instantaneously and were recorded automatically every 60 s. At the end of the test, the specimen was removed from the setup and weighed to determine if there was transport of paraffin oil through the membrane.

As it was mentioned in Chapter 2, an important factor related to autogenous shrinkage testing is the determination of the point at which strain measurements should start or be zeroed. This point corresponds to the time at which autogenous and chemical shrinkage measurements start to diverge and is generally agreed to coincide with the final set according to the Vicat test (Sant et al. 2006). The time at which autogenous and chemical shrinkage started to diverge was selected in this study as the zero point for autogenous shrinkage values. An example is presented in Fig. 25, where the zero point is indicated.

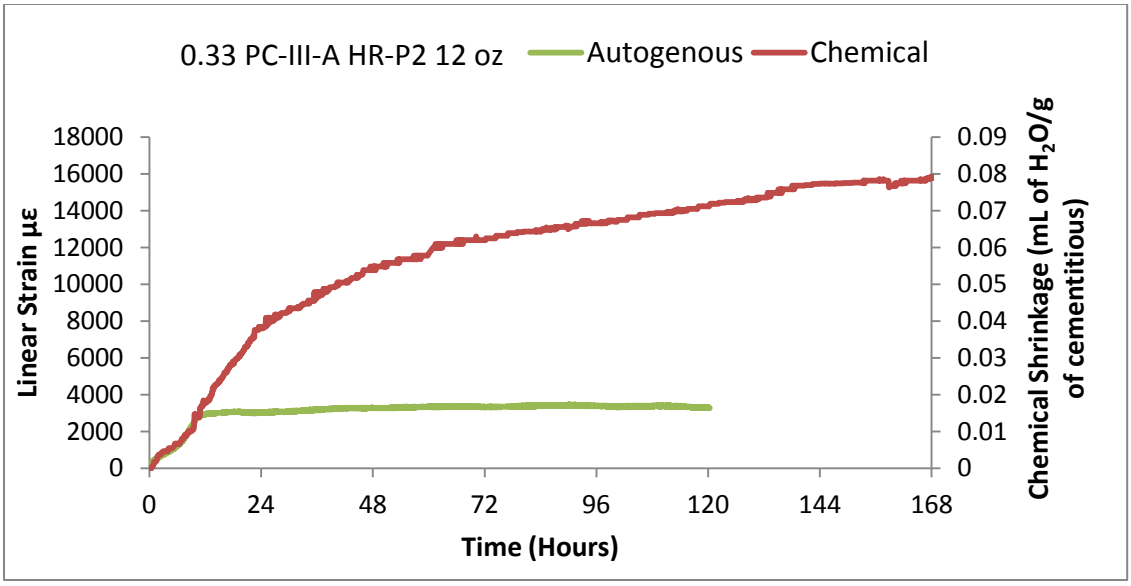

Fig. 25 Example of the determination of the zero point for autogenous shrinkage

4.2.2 Mixture proportions and testing matrix

Different mixtures were tested as a part of this project with varying combinations of w/cm ratios, chemical admixtures types and dosages. The polycarboxylate mixtures are the reference mixtures for the most part of the study since they are the type of HRWR currently used in precast production. Tests were carried out at 23 °C for 5 days. Table 8 shows the mixture proportions of the samples tested, the estimated time of final setting, and the autogenous shrinkage (linear strain, με) measured from time zero until 120 hours after initial contact of water + cement. Each individual value in Table 8 is the average of two samples.

w/c	Cement type	Admixtures		Other mixture parameters	Estimated set time (hr)	Linear strain (με)
		Type	(floz/ 100 lb cm)			
0.28	PC-III-A	HR-P1	12	-	10.9	1394.2
		HR-P2	12	-	9.9	667.3
0.33	PC-III-A	-	-	-	3.2	1256.6
		HR-P1	5	-	7.0	934.8
				SRA 1.5 %	8.4	-75.0
			12	-	11.9	758.4
		HR-P2	12	-	10.1	559.7
			5	SRA 1.5 %	8.7	-205.9
		HR-M	25	-	9.0	1596.7
		HR-N	29	-	23.5	898.7
0.4	PC-III-A	HR-P1	12	-	12.5	700.5
		HR-P2	12	-	10.8	265.7

Table 8: Mixture proportions and autogenous shrinkage at 5 days

4.2.3 Results

In the following sections, the effect of several factors on autogenous shrinkage of cement paste samples will be analyzed. The autogenous shrinkage curves for all mixtures can be found in Appendix II.

4.2.3.1 Influence of w/c ratio

Fig. 26 shows the autogenous shrinkage curves for two sets of mixtures, each prepared with a different HRWR at the same dosage, varying w/c ratio from 0.28 to 0.4. Fig. 27 shows the linear strain values at 120 h (from time zero) for each w/c and HRWR type considered.

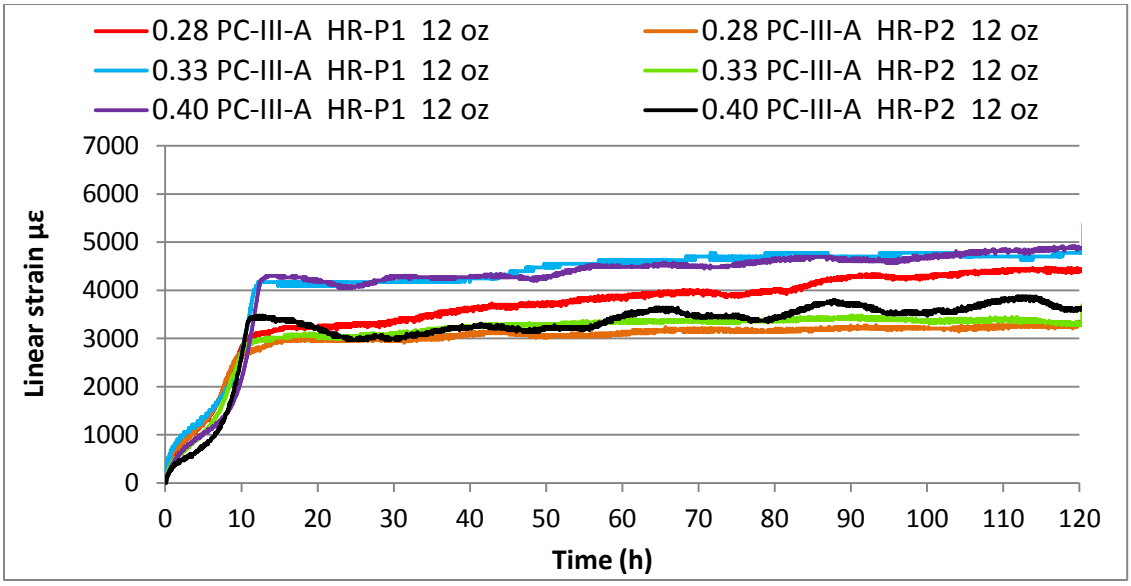

Fig. 26 Autogenous shrinkage curves for different w/c and polycarboxylate type

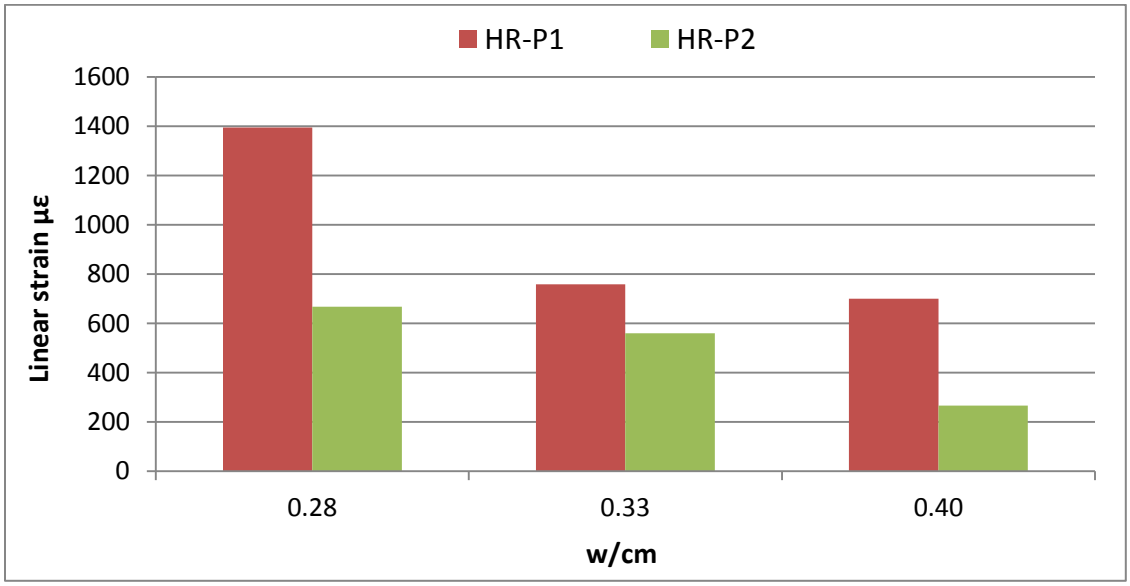

Fig. 27 Autogenous shrinkage values from time zero to 120 h for different w/c and polycarboxylate type

As expected, it is observed in Fig. 26 and Fig. 27 that the reduction in w/cm ratio produced an increase in the autogenous shrinkage measured from time zero until the end of the test (120 h). This fact was observed for the use of both types of polycarboxylate-based HRWR.

The mixtures with HR-P1 showed higher autogenous shrinkage at 120 h at every w/cm than the mixtures with HR-P2. Even at w/cm 0.40 the linear strain value for the mixture with HR-P1 (700.5 με) was higher than the value for w/cm 0.28 for the mixture with HR-P2 (667.3 με).

Another observation derived from Fig 26 is the fact that the mixtures with w/cm 0.40 for both types of HRWR showed an initial swelling period after setting followed by continued shrinkage. These periods lasted 10.1 hours for the mixture with HR-P1and 14.1 hours for the mixture with HR-P2. This phenomenon is consistent with the results obtained by other researchers (Barcelo et al. 2005) (Baroghel-Bouny et al. 2006) where autogenous swelling was also observed for cement pastes at medium and high w/cm ratios. This autogenous swelling may be related to crystallization pressure due to the growth of hydration products such as Aft and calcium hydroxide (Baroghel-Bouny and Kheirbek 2000). The swelling intensity has been observed to be dependent on the sulfate-to-alkali ratio of the clinker and the amount of free lime (Barcelo et al. 2005) and it is not detected in lower w/cm pastes due to the higher relative importance of self-desiccation, which occurs at the same time as autogenous swelling (Barcelo et al. 2005) (Baroghel-Bouny and Kheirbek 2000).

4.2.3.2 Influence of HRWR type

Fig. 28 shows the autogenous shrinkage curves for cement pastes with 0.33 w/cm ratio and different HRWR types. Fig. 29 shows the linear strain values at 120 h (from time zero) for each HRWR type considered.

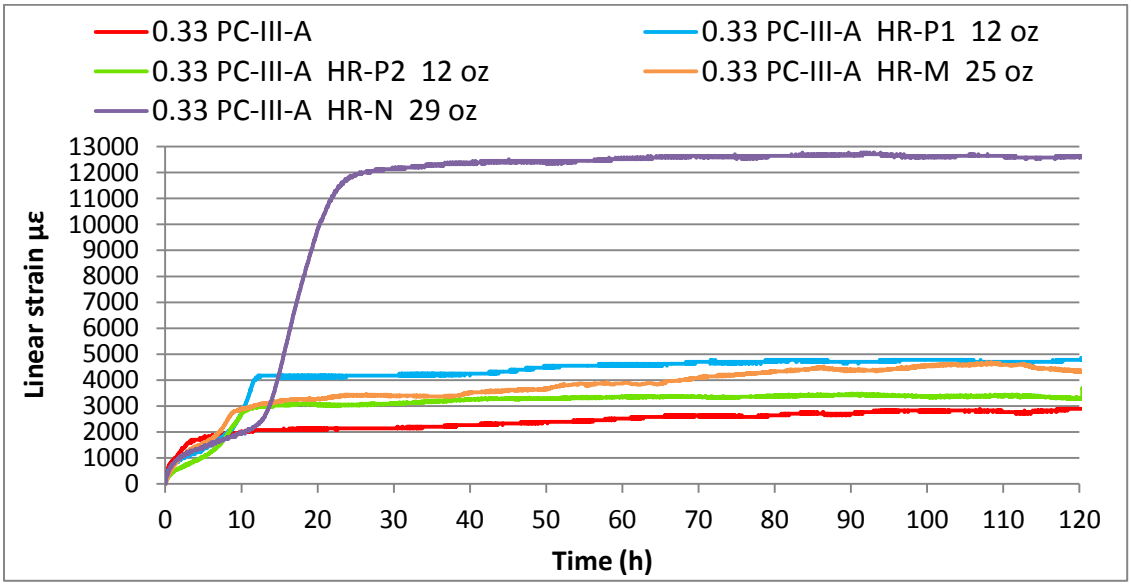

Fig. 28 Autogenous shrinkage curves for different HRWR types

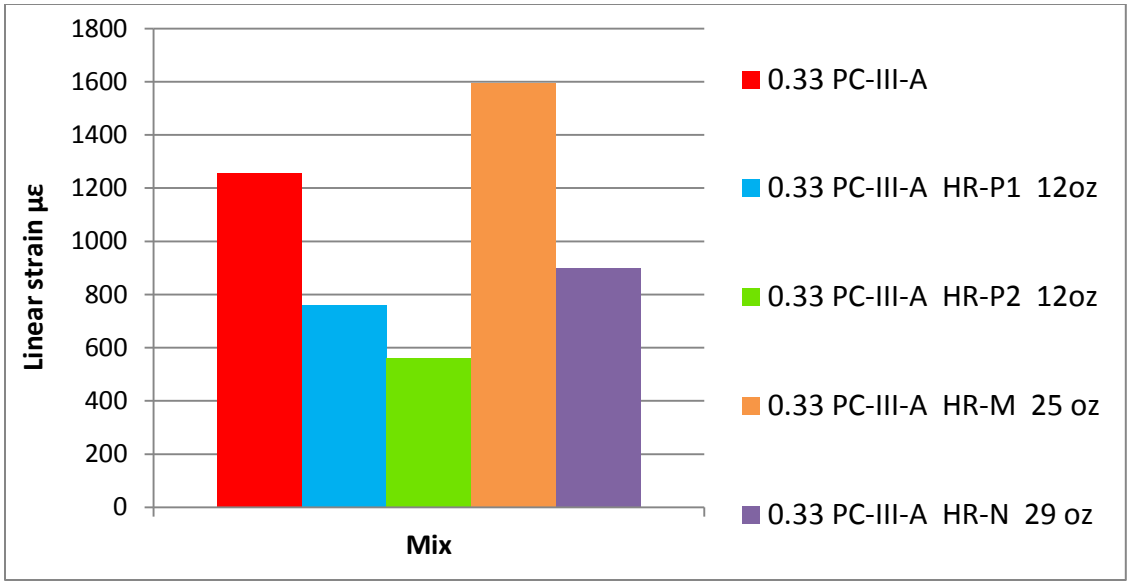

Fig. 29 Autogenous shrinkage values from time zero to 120 h for different HRWR types

The dosage of each type of admixture was selected based on trial mixtures in concrete in order to obtain the adequate consistency for precast application. It is observed that all HRWRs with the exception of the melamine-based superplasticizer (27 % increase in shrinkage) reduced the autogenous shrinkage measured from time zero until 120 hours compared to the control mixture. The lowest autogenous shrinkage was obtained for the mixtures with polycarboxylate-based superplasticizers, the mixture with HR-P2 (decreased 55 %) showing lower shrinkage than the HR-P1 mixture (decreased 40 %). The mixture with naphthalene-based superplasticizer exhibited greater autogenous shrinkage than the polycarboxylate mixtures (decreased 28 %). Another interesting fact is the substantial retardation obtained with the use of HR-N.

4.2.3.3 Influence of Polycarboxylate-based HRWR dosage

Fig. 30 shows the effect of polycarboxylate-based superplasticizer dosage on autogenous shrinkage for mixtures with PC-III-A and w/cm 0.33. Fig. 31 shows the linear strain values at 120 h (from time zero) for each HRWR dosage considered.

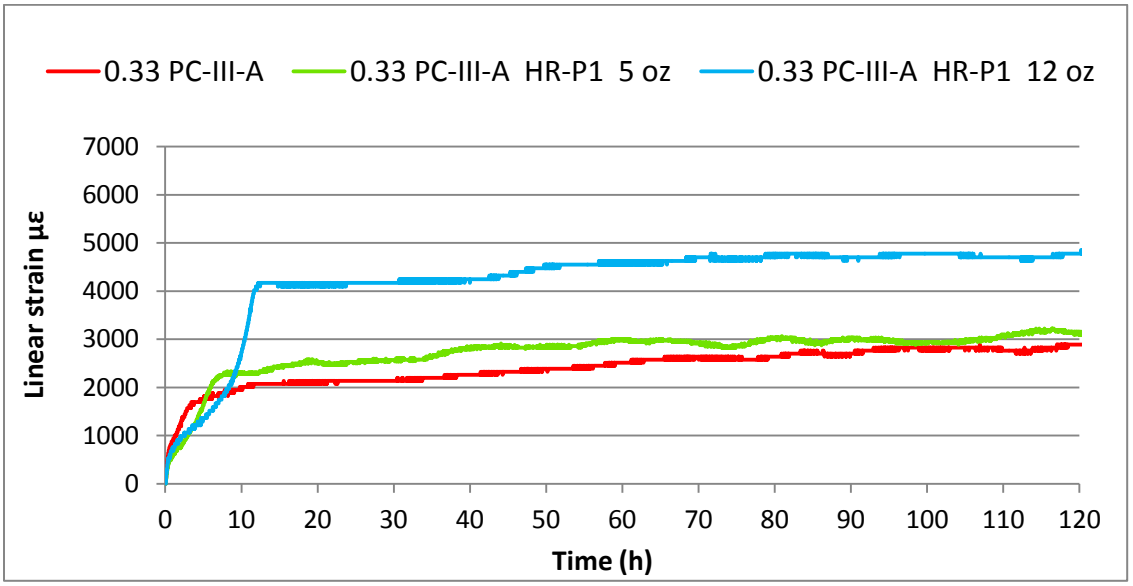

Fig. 30 Autogenous shrinkage curves for different polycarboxylate dosage

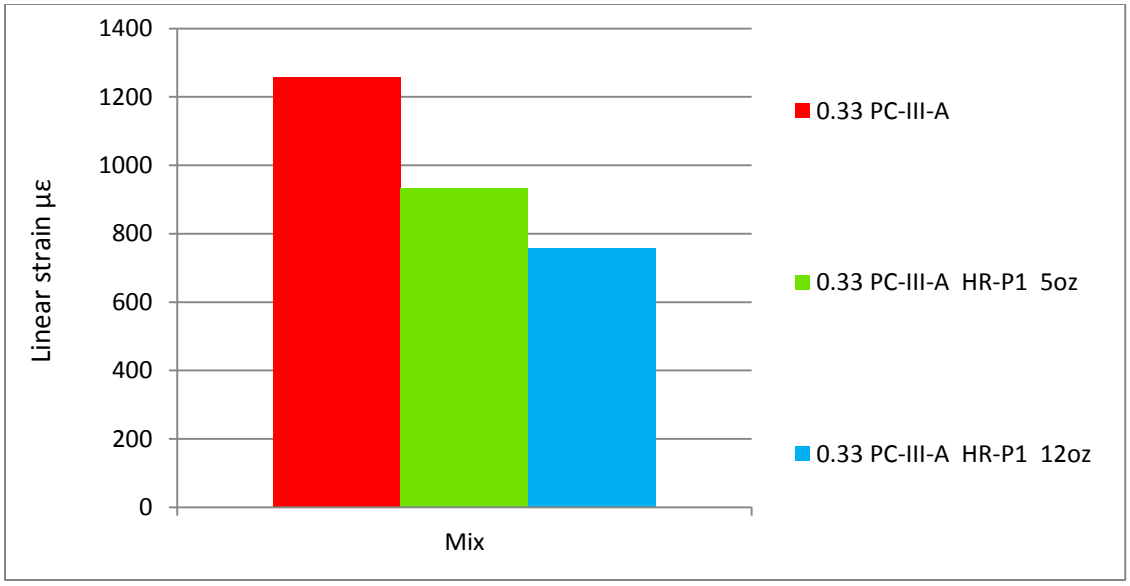

Fig. 31 Autogenous shrinkage values from time zero until 120 hours for different polycarboxylate dosage

As it is shown in Fig. 30, the increase in polycarboxylate dosage produced a retardation evidenced by the shift of the time zero point to the right, which coincides with the time of final setting (Sant et al. 2006). Fig. 31 shows that autogenous shrinkage at 120 hours was reduced by the increase in admixture dosage. The reduction in shrinkage from time zero until the end of the test was more significant between the control mixture with no admixture and the intermediate dosage (control – 5 oz), being the reduction obtained with a similar further increase in dosage (5 oz – 12 oz) lower.

4.2.3.4 Influence of SRA incorporation

Fig. 32 shows the effect of the use of SRA on autogenous shrinkage of cement paste.

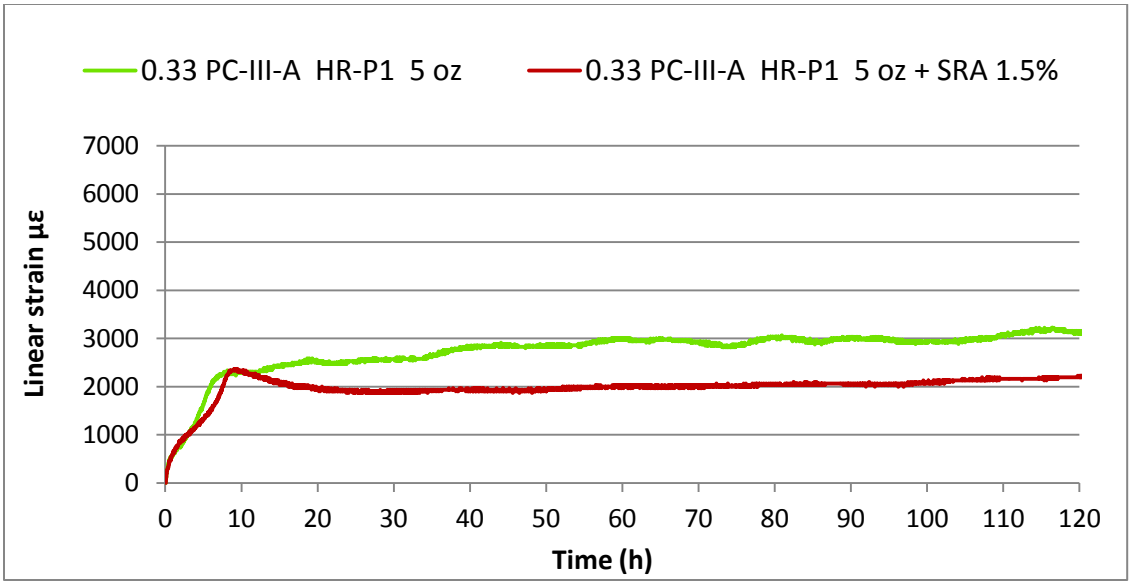

Fig. 32 Autogenous shrinkage curves showing the effect of SRA incorporation

The incorporation of SRA considerably changed the behavior of the hydrating cement paste. Table 8 and Fig. 32 show that the use of SRA significantly reduced the autogenous shrinkage measured at 120 hours. In this project, in fact, a final net expansion was measured from time zero until 120 hours in the mixtures with SRA. As it can be seen in Fig. 32, the mixture without SRA showed an initial period of constant volume after setting, which was followed by continued shrinkage until the end of the test. The plateau observed is, as it was explained in section 4.2.3.1 (w/cm effect), the result of simultaneous swelling and shrinkage processes (Barcelo et al. 2005) (Baroghel-Bouny and Kheirbek 2000) (Sant et al. 2011). On the other hand, the SRA mixture showed an initial expansion after setting, followed by sustained shrinkage. The initial expansion is a major responsible for the reduction of the autogenous shrinkage measured at later ages (Sant et al. 2011).

4.2.4 Summary and Conclusions

Based on the results of this section the following conclusions can be made:

- The reduction in w/cm ratio produced an increase in autogenous shrinkage
- Mixtures with the highest w/cm showed an initial swelling period after setting followed by continued shrinkage. This initial swelling was not as evident or observed at all in the lower w/cm pastes. The higher relative importance of self-desiccation, which occurs at the same time as autogenous swelling may explain this observation.
- All HRWRs, with the exception of the melamine-based superplasticizer, reduced the autogenous shrinkage measured. The lowest autogenous shrinkage was obtained for the mixtures with polycarboxylate-based superplasticizers. HR-P1 showed higher autogenous shrinkage than HR-P2 mixtures. The mixture with naphthalene-based superplasticizer exhibited greater autogenous shrinkage than both polycarboxylate-based mixtures.
- Autogenous shrinkage was reduced by the increase in polycarboxylate dosage. The increase in dosage produced a retardation evidenced by the shift of the time zero point to the right.
- The incorporation of SRA considerably changed the behavior of the hydrating cement paste. The SRA significantly reduced the autogenous shrinkage measured. A final net expansion was measured in the mixtures with SRA. The extent of the initial expansion observed in the SRA systems after setting is a major responsible for the reduction of the autogenous shrinkage measured at later ages.

4.3 ISOTHERMAL CALORIMETRY

4.3.1 Procedure and experimental setup

Isothermal calorimetry was used to measure the heat of hydration of different cement paste samples. Tests were performed at 23°C using a TAM AIR conduction calorimeter.

The instrument is equipped with eight channels. Each channel has one side for the sample and one side for an inert reference. For the tests performed in this research, water was used as reference material. Fig. 33 shows a picture of the setup.

Fig. 33 Isothermal calorimetry setup

Paste samples were mixed in a Hobart mixer following the procedure in ASTM C305. The materials used in the mixture were stored at room temperature until the moment of the test. After mixing, the paste sample was placed in a glass vial and the

sample mass was recorded. After capping the vial, the sample was inserted in the calorimeter. Heat flow data was recorded by the calorimeter every 20s for 60 h.

In order to analyze in detail the hydration kinetics a series of parameters were obtained from the heat flow curves (Zhang et al 2015). A typical heat flow curve of cement hydration is shown in Fig. 34.

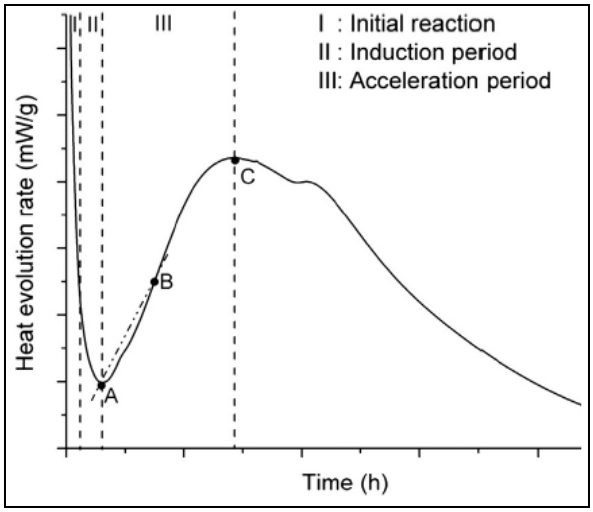

Fig. 34 Typical exothermic heat flow curve of cement hydration (Zhang et al 2015)

As depicted in the figure, tA represents the time corresponding to the minimum heat evolution rate; tB the point that corresponds to the maximum acceleration rate (maximum slope) on the heat flow curve and tC indicates the time point of the maximum heat generation rate due to alite hydration. The parameters (dQ/dt)A and (dQ/dt)C represent the heat evolution rates at the respective times. The secant slopes between A and B, KA-B, and B and C, KB–C, represent the acceleration rate of the heat flow.

4.3.2 Mixture proportions and testing matrix

Table 9 shows the mixture proportions for the cement paste mixtures considered in this study. The polycarboxylate mixtures are the reference mixtures for the most part of the study since they are the type of HRWR currently used in precast production.

w/c	Cement type	Admixtures				Other mixture parameters	Mixture ID number
		Type	(floz/ 100 lb cm)	Type	(floz/ 100 lb cm)		
0.28	PC-III-A	HR-P1	5	-	-	-	1
			12	-	-	-	2
		HR-P2	12	-	-	-	3
			12	-	-	Fly ash 25 % repl.	4
		HR-N	29	-	-	-	5
			29	-	-	Fly ash 25 % repl.	6
		HR-M	25	-	-	-	7
			25	-	-	Fly ash 25 % repl.	8

Table 9 Mixture proportions and testing matrix

w/c	Cement type	Admixtures				Other mixture parameters	Mixture ID number
		Type	(floz/ 100 lb cm)	Type	(floz/ 100 lb cm)		
0.33	PC-I-A	HR-P1	12	-	-	-	9
		HR-P2	12	-	-	-	10
	PC-III-A	-	-	-	-	-	11
		HR-P1	3	-	-	-	12
			5	-	-	-	13
			5	NR	3	-	14
			5	-	-	SRA 1.5 %	15
			6	-	-	-	16
			9	-	-	-	17
			12	-	-	-	18
			12	NR	3	-	19
			12	-	-	Fly ash 25 % repl.	20
		NR	3	-	-	-	21
		HR-N	29	-	-	-	22
			29	-	-	Fly ash 25 % repl.	23
		HR-M	25	-	-	-	24
		HR-P4	5	-	-	-	25
			12	-	-	-	26
	PC-III-B	-	-	-	-	-	27
		HR-P1	3	-	-	-	28
			6	-	-	-	29
			12	-	-	-	30
		HR-N	29	-	-	-	31
		HR-M	25	-	-	-	32
0.40	PC-III-A	HR-P1	5	-	-	-	33
			12	-	-	-	34

(cont.) Table 9 Mixture proportions and testing matrix

4.3.3 Results

Table 10 shows the calculated parameters described above for each mixture considered in this study.

Mixture ID number	Parameters - Heat flow curve							Cumulative heat (mJ/g cementitious)
	tA (h)	tB (h)	tC (h)	(dQ/dt)A (mW/g)	(dQ/dt)C (mW/g)	KA–B (mW/(g·h))	KB–C (mW/(g·h))	
1	1.9	6.4	9.1	0.188	2.439	0.28	0.37	115443
2	3.4	10.2	13.5	0.146	2.372	0.17	0.34	128251
3	3.0	10.3	12.5	0.151	2.564	0.22	0.37	115680
4	3.4	13.9	16.5	0.083	1.723	0.10	0.24	93285
5	4.9	10.6	13.2	0.129	2.635	0.16	0.61	117036
6	5.5	13.9	16.7	0.104	2.254	0.11	0.44	111651
7	3.2	6.8	9.5	0.156	2.760	0.36	0.49	129021
8	5.0	9.0	12.3	0.087	1.741	0.19	0.28	99751

Table 10 Heat evolution parameters

Mixture ID number	Parameters - Heat flow curve							Cumulative heat (mJ/g cementitious)
	tA (h)	tB (h)	tC (h)	(dQ/dt)A (mW/g)	(dQ/dt)C (mW/g)	KA–B (mW/(g·h))	KB–C (mW/(g·h))	
9	2.7	12.3	16.2	0.155	2.298	0.13	0.23	139346
10	2.5	12.6	16.4	0.093	1.617	0.09	0.16	101753
11	1.7	4.6	8.0	0.256	2.218	0.31	0.31	118526
12	2.3	6.7	10.3	0.160	2.286	0.26	0.28	128655
13	1.8	6.1	9.1	0.171	2.382	0.28	0.34	128728
14	4.1	13.3	16.4	0.067	2.209	0.13	0.31	120463
15	2.2	7.7	11.1	0.128	1.917	0.18	0.23	112157
16	2.9	8.7	11.8	0.134	2.311	0.22	0.29	130952
17	3.2	10.3	13.2	0.114	2.188	0.17	0.29	123712
18	3.5	11.9	14.7	0.107	2.268	0.16	0.29	127116
19	4.2	16.3	19.6	0.081	2.289	0.10	0.31	125461
20	3.6	12.1	15.3	0.092	1.774	0.11	0.24	104665
21	3.3	8.3	12.2	0.105	2.173	0.19	0.29	121505
22	4.3	14.2	17.3	0.101	2.803	0.12	0.49	146765
23	5.4	14.7	18.0	0.062	1.922	0.09	0.30	105418
24	3.4	7.4	11.3	0.161	2.839	0.23	0.44	164672
25	1.8	6.0	9.4	0.179	2.323	0.25	0.33	123993
26	3.6	10.5	13.4	0.139	2.316	0.18	0.32	125918
27	1.1	3.9	6.6	0.535	2.076	0.31	0.24	134780
28	1.2	3.6	7.1	0.469	2.507	0.31	0.36	135876
29	1.7	4.7	8.2	0.445	2.684	0.30	0.39	142004
30	2.3	7.4	10.3	0.329	2.460	0.23	0.33	135346
31	2.5	4.7	8.3	0.331	2.598	0.29	0.45	143331
32	1.4	3.8	7.4	0.340	2.111	0.30	0.30	121171
33	1.9	6.6	10.2	0.186	2.560	0.24	0.34	150325
34	3.5	10.5	14.0	0.133	2.491	0.19	0.29	154903

(cont.) Table 10 Heat evolution parameters

In the following sections, the effect of several factors on the hydration of cement paste samples will be analyzed. The heat flow and cumulative heat curves for all mixtures can be found in Appendix III.

4.3.3.1 Effect of type of HRWR

Heat flow curves showing the behavior of different types of HRWR are shown in Fig. 35 and Fig. 36. Two sets of mixtures, considering two cements (PC-III-A and PC-III-B) and the same w/cm ratio (0.33) are presented to analyze the effect of HRWR type on hydration. The corresponding cumulative heat curves can be found in Appendix III.

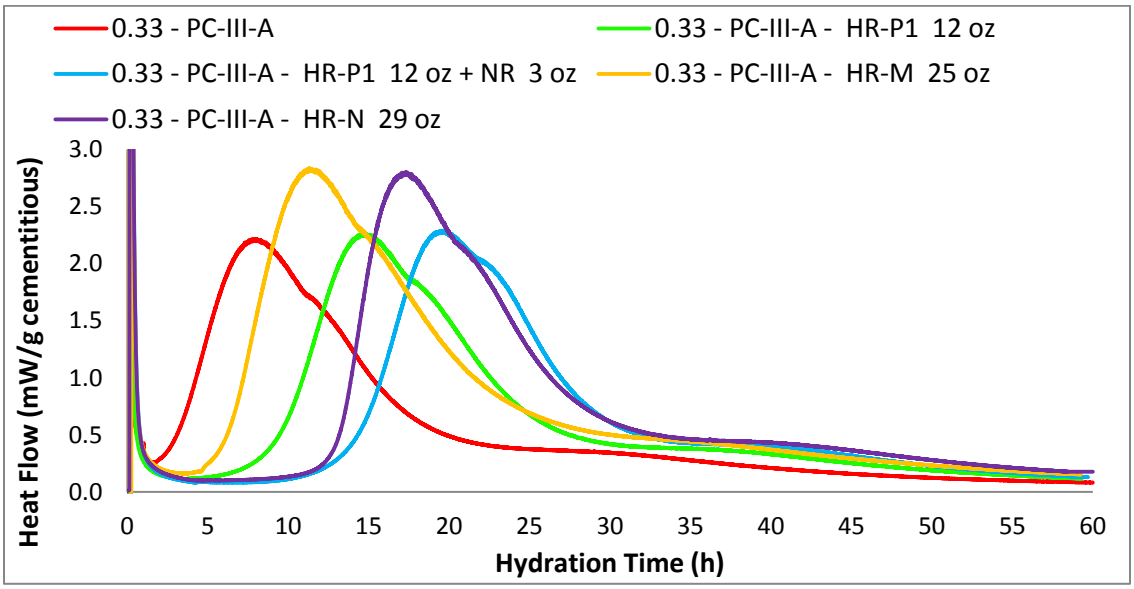

Fig. 35 Heat flow curves for cement paste with different HRWRs. PC-III-A

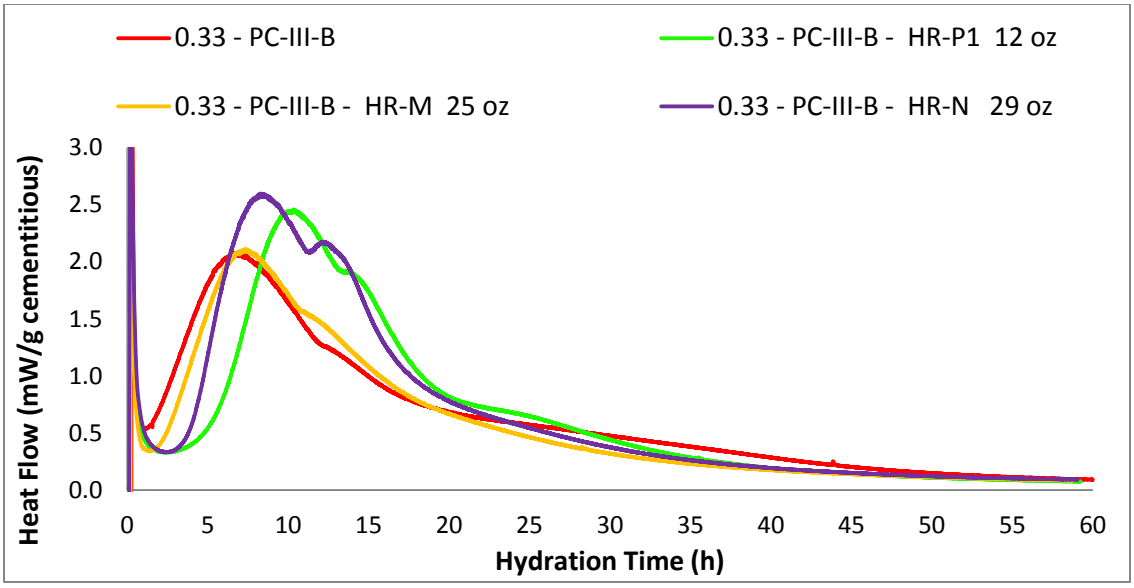

Fig. 36 Heat flow curves for cement paste with different HRWRs. PC-III-B

The dosage of each type of admixture was selected based on trial mixtures in concrete in order to obtain the adequate consistency for precast application.

Different trends were observed when comparing the effect of HRWR type on heat evolution in the set of mixtures with the same w/cm ratio (0.33) but different cement. Facts or trends that can be established base on the data presented in Table 10 are:

The addition of any HRWR delayed the onset of the acceleration period (this effect was relatively independent of w/cm ratio when the heat flow was normalized by grams of cement). The PC-III-A mixtures showed a greater delay in the onset of the acceleration period than PC-III-B mixtures for each superplasticizer considered. For both cements, the HR-N mixtures showed the longest induction period (comparing tA values). The HR-M mixtures showed the shortest induction period. The use of NR in combination with the polycarboxylate increased the delay in the onset of the acceleration period of the polycarboxylate mixture.

The heat evolution rates at point A were also reduced for all mixtures compared to the control mixtures with no admixture. The heat evolution rates at point A were lower for PC-III-A mixtures compared to the PC-III-B mixtures. Among different HRWRs, the differences were small.

In the acceleration period, heterogeneous nucleation and growth of C-S-H on alite and other mineral surfaces is the rate controlling mechanism (Bullard et al. 2011). The rate of hydration is proportional to the number of active sites from which C-S-H can grow. The incorporation of any HRWR decreased the secant slope KA–B of the heat flow curves compared to the control. This effect was more noticeable with PC-III-A than with PC-III-B. This indicates that the rate of C-S-H nucleation and growth at the beginning of the acceleration period was reduced with the use of any HRWR. Among the different HRWRs, HR-M mixtures showed the highest KA–B slope for both cements. The polycarboxylate combined with the normal range water reducer and the HR-N mixtures showed the lowest KA–B slope with PC-III-A. With PC-III-B cement, the polycarboxylate mixture showed the lowest slope and the naphthalene and melamine mixtures showed similar values only slightly lower than the control.

The slopes at point B were similar or higher than the control mixtures when the HRWRs were added. The mixtures with HR-N showed the highest slopes at point B with both cements, meaning that the naphthalene superplasticizer substantially increased the C-S-H nucleation and growth rates of the control mixtures. The KB–C value of the melamine mixtures was higher than the polycarboxylate mixtures for PC-III-A, but lower with PC-III-B. For PC-III-A, it seems that the polycarboxylate-based HRWR, with and without NR, does not significantly change the nucleation + growth kinetics since the behavior was similar to the control mixture in the acceleration period regarding the

acceleration rate. For PC-III-B, the HR-P1 mixture showed a higher KB–C slope than the control mixture, again indicating a higher C-S-H nucleation and growth rate.

The main peaks of heat flow corresponding to alite hydration (point C) are similar or greater in the mixtures with HRWRs compared to both control mixtures. For PC-III-A, among the different HRWRs, HR-N and HR-M mixtures presented the highest values, with very similar values. Both polycarboxylate mixtures showed values slightly greater than the control. For PC-III-B, the HR-N mixture showed again the highest value, followed by the HR-P1 mixture. The HR-M mixture showed a value slightly greater than the control.

Regarding the cumulative heat at the end of the test period, for PC-III-A the HR-M mixture exhibited the greatest value, followed by the HR-N. Both polycarboxylate mixtures (with and without NR addition) showed a cumulative heat value slightly greater than the control, but the relative difference was small. For PC-III-B, the HR-N mixture showed the greatest value. Again, the polycarboxylate mixture showed a value similar to the control. The melamine mixture showed the lowest cumulative heat at the end of the test, fact that contradicts the result obtained with PC-III-A.

4.3.3.2 Effect of polycarboxylate-based HRWR dosage

The exothermic heat flow curves of paste samples of w/cm 0.33 and increasing dosages of polycarboxylate-based HRWR (HR-P1) are shown in Fig. 37 for PC-III-A and Fig. 38 for PC-III-B. The respective cumulative heat curves can be found in Appendix III.

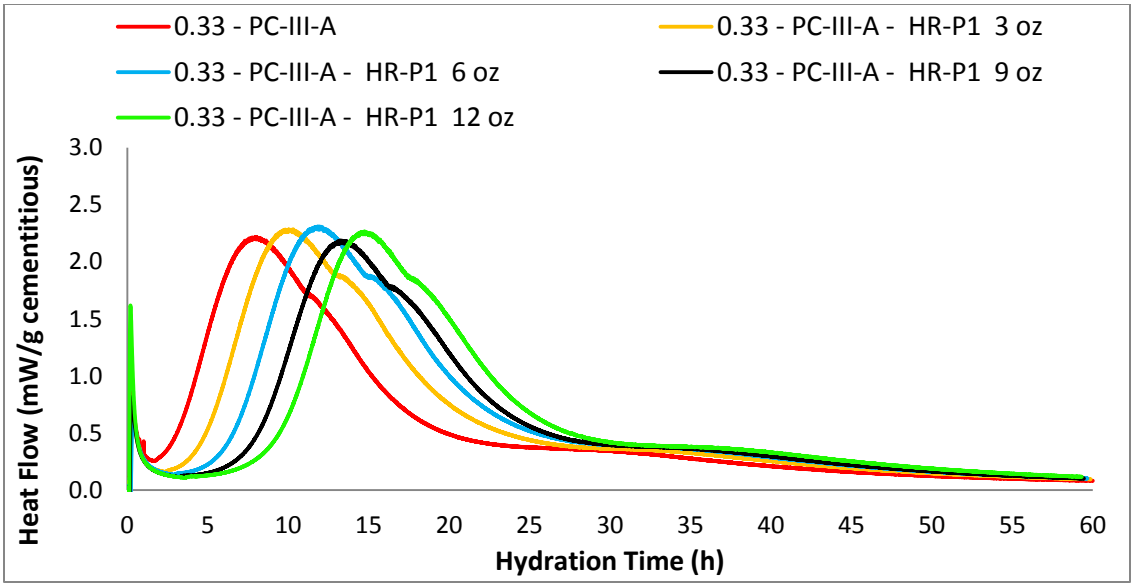

Fig. 37 Heat flow curves for cement paste with different HRWR dosage. PC-III-A

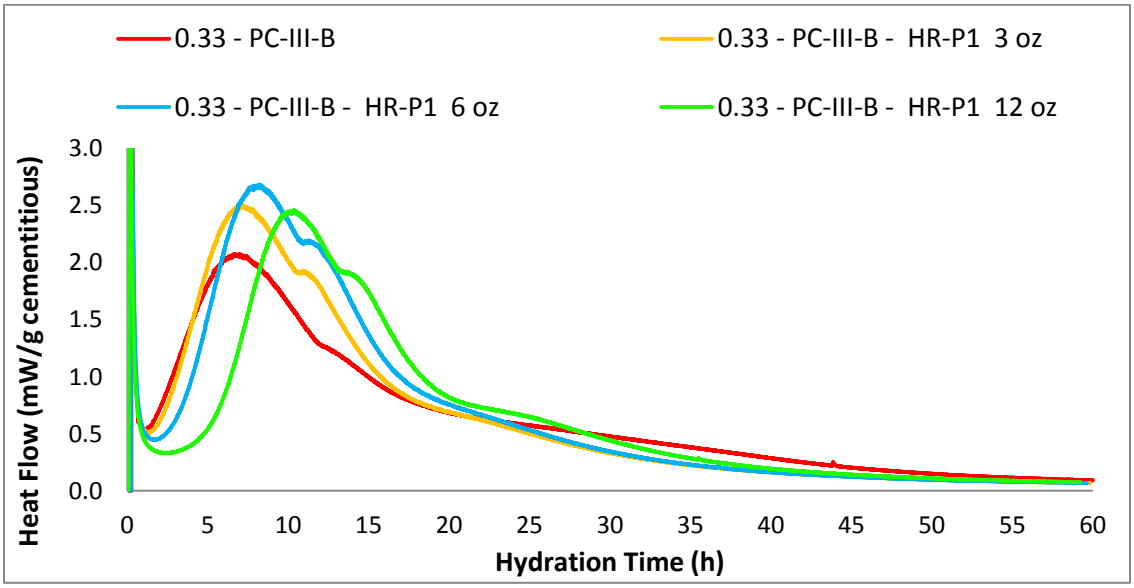

Fig. 38 Heat flow curves for cement paste with different HRWR dosage. PC-III-B

It is observed that the addition of the HRWR and its progressive increase in dosage delayed the onset of the acceleration period. The heat evolution rate at point A was also reduced with increasing dosage. The PC-III-A mixtures showed a greater delay in the onset of the acceleration period than PC-III-B mixtures for every dosage of superplasticizer considered. The heat evolution rates at point A were also lower for PC-III-A mixtures compared to the PC-III-B mixtures.

The secant slope KA–B of the heat flow curves, which is an indicator of the rate of C-S-H nucleation at the beginning of the acceleration period, was similar for both cements in the no-admixture mixtures. The data show that the increase in polycarboxylate-based HR-P1 dosage decreased the secant slope KA–B of the heat flow curves. This indicates that the rate of C-S-H nucleation at the beginning of the acceleration period is reduced with the increase in polycarboxylate dosage. When the HRWR was added and the dosage increased, the decrease in KA–B was more pronounced in the PC-III-A mixtures.

Fig 39 and Fig 40 present data from Table 10 in the form of graphs to better analyze the following results.

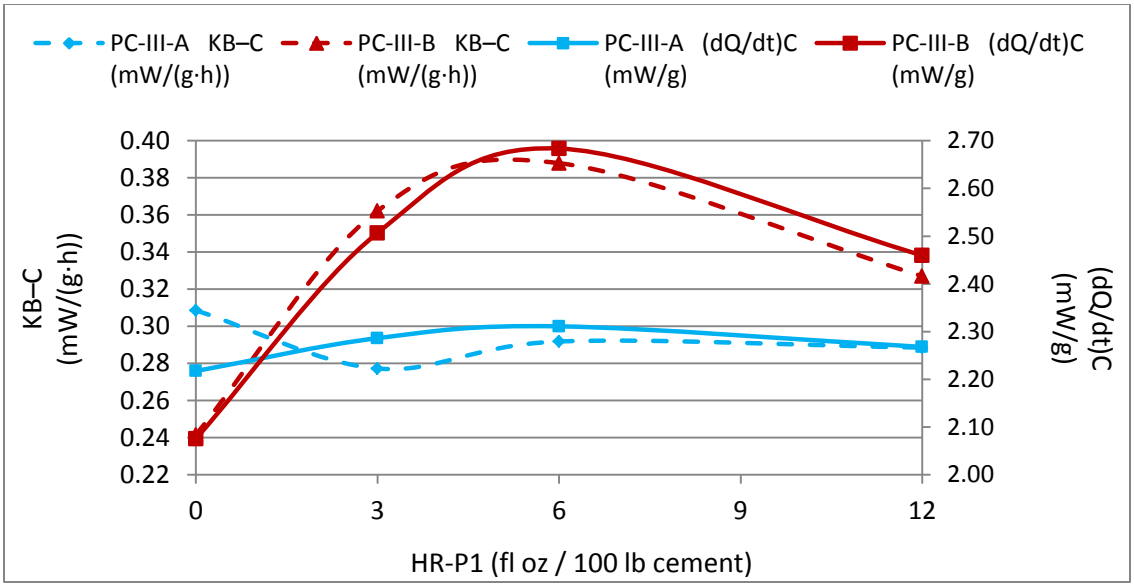

Fig. 39 Slope at point B and Heat flow peak due to alite hydration for cement paste as functions of HR-P1 dosage. w/cm 0.33 - PC-III-A and PC-III-B mixtures

In the case of PC-III-A the slopes at point B are similar for all dosages, indicating similar nucleation and growth rates. On the other hand, for PC-III-B mixtures the slopes at point B increased with the incorporation of the HRWR as compared to the control. This increase was not proportional to the increase in HR-P1 dosage: a peak was observed for the intermediate dosage of 6 fl oz/100 lb cement.

The main peaks of heat flow corresponding to alite hydration showed values greater than the control in the mixtures with polycarboxylate, for both cements. PC-III-B mixtures showed higher peaks of heat flow than PC-III-A mixtures when the HRWR was added. The relative differences in heat evolution peaks between different dosages are also more noticeable in the PC-III-B mixtures. Again, the greatest values of heat evolution peaks were obtained for the intermediate dosage of 6 fl oz/100 lb cement, for both cements. The curve corresponding to the sample with PC-III-A and 9 fl oz/100 lb cement

is not included in the analysis because does not follow this trend and may have to be repeated to confirm the result.

The cumulative heat curves also clearly show that the use of polycarboxylate-based HRWR delays the acceleration of the hydration reaction. This is evident by the shifting of the curves to the right with the increase in admixture dosage.

The cumulative heat of hydration at the end of the calorimetry test for the mixtures with HRWR is slightly greater than the control, for both cements. This may be attributable to a better dispersion of the cement particles, consequently enhancing their access to water and allowing a better distribution of the space for hydration products to grow, thus allowing greater degree of reaction. In the case of the tests performed in this study, the last fact was not proportional to the increase in admixture dosage. The greatest values of cumulative heat were obtained for the intermediate dosage of 6 fl oz/100 lb cement, for both cements. PC-III-B mixtures showed higher cumulative heat values than PC-III-A pastes.

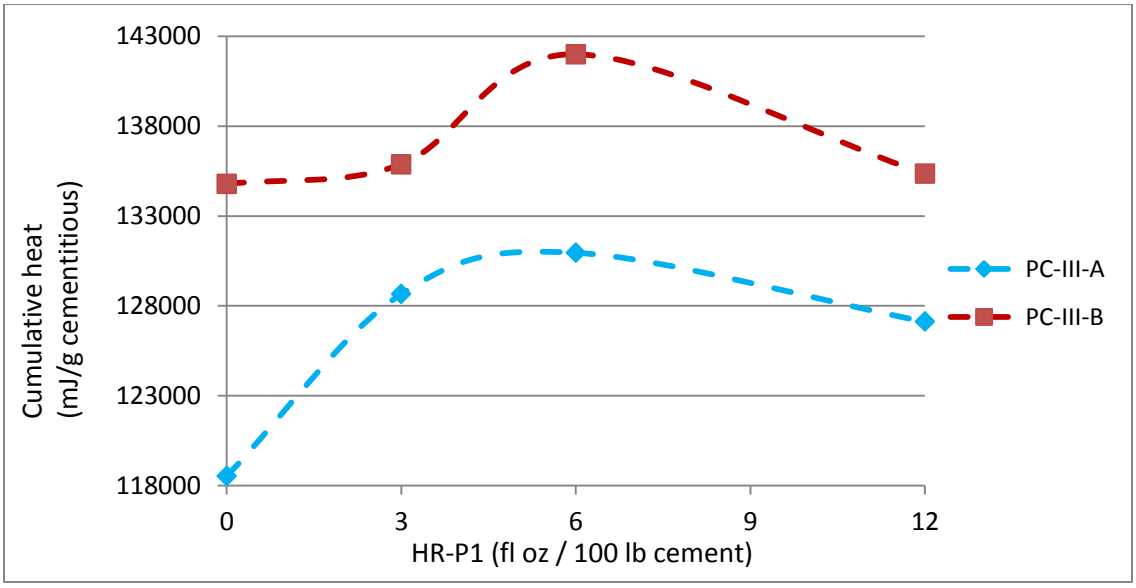

Fig. 40 Cumulative heat at 60 hours as a function of HR-P1 dosage, w/cm 0.33 - PC-III-A and PC-III-B mixtures

It is clear that the final cumulative values obtained with all dosages lie in the same small range, as in (Jansen et al. 2012), indicating that the progressive increase in polycarboxylate-based HRWR dosage in the range considered does not cause significant changes in the degree of hydration at this age. This is true for both cements tested.

PC-III-B cement seems to be more sensitive to the incorporation of the HRWR and its corresponding increase in dosage than PC-III-A. However, considering all the mixtures that incorporated the chemical admixture, there is no clear evidence of substantial modification of C-S-H nucleation + growth kinetics with the increase in polycarboxylate dosage from the minimum dosage (3 fl oz/100 lb cement) to the maximum (12 fl oz/100 lb cement) – the behavior is similar for all mixtures in the acceleration period regarding the acceleration rate.

The effect of the HRWR incorporation and dosage increase is more pronounced during the induction period, causing the delay in the onset of the acceleration period.

4.3.3.3 Effect of SRA

The exothermic heat flow curves showing the effect of SRA incorporation on hydration of cement paste samples are shown in Fig. 41. Cumulative heat curves for the cement paste mixtures with and without SRA are presented in Fig. 42.

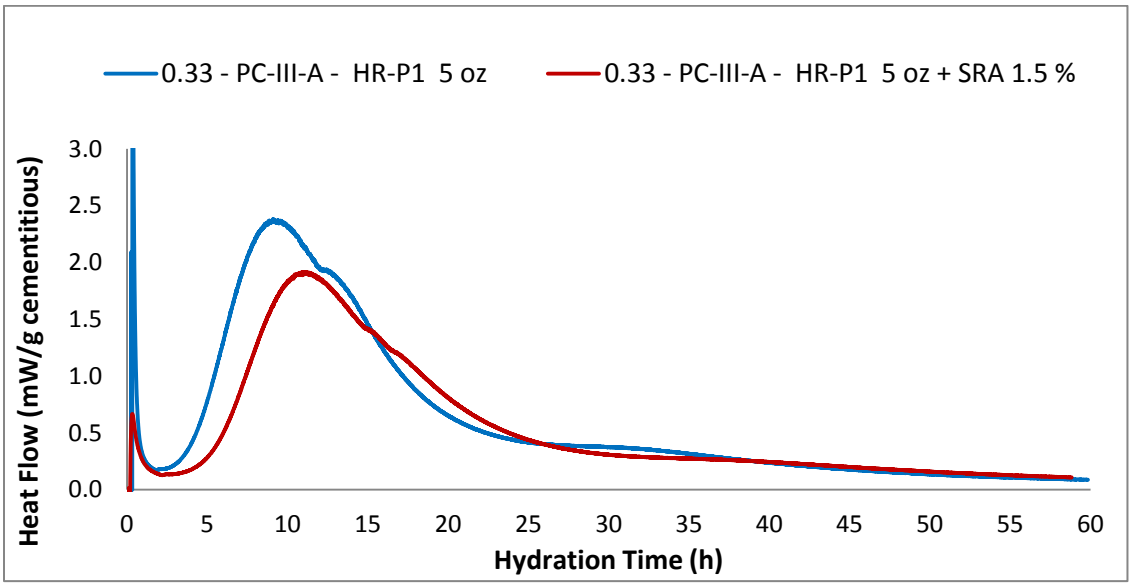

Fig. 41 Heat flow curves showing SRA incorporation effect

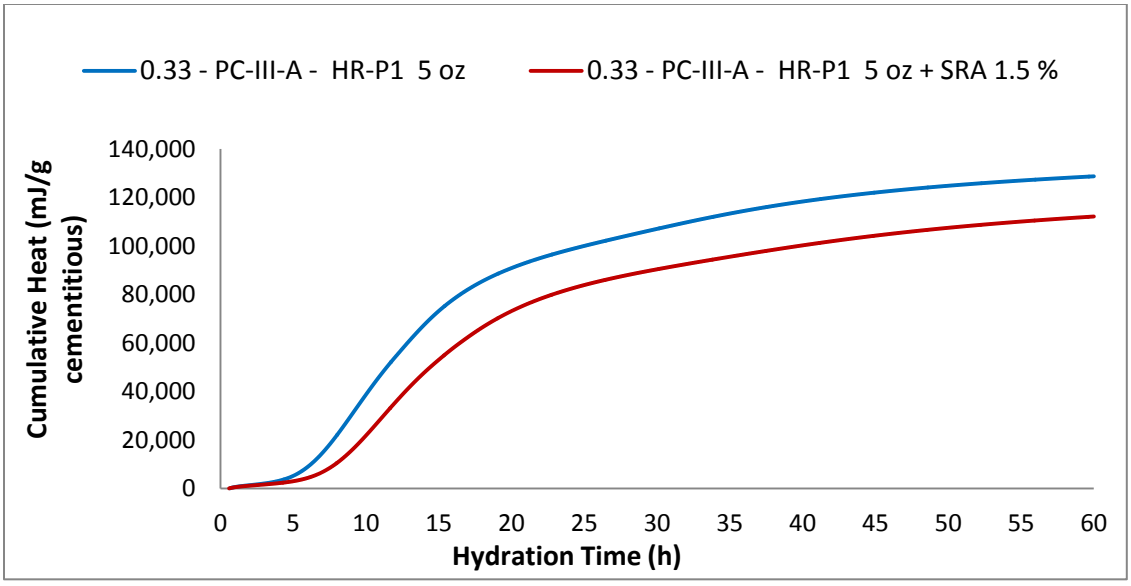

Fig. 42 Cumulative heat curves showing SRA effect

It is observed that the hydration of the SRA mixture is retarded with respect to the control mixture without SRA. This is again evident by the shift to the right of the SRA curves. The heat evolution rate at point A is reduced in the SRA mixture. The secant slope KA–B of the heat flow curve is lower with the addition of SRA, indicating a slower rate of C-S-H nucleation at the beginning of the acceleration period. The slope at point B is also reduced with SRA, which indicates a slower C-S-H nucleation and growth rate. The main peak of heat evolution (point C) is lower in the SRA mixture. Rajabipour et al. (Rajabipour et al. 2008) found that the polarity of the mixing water is reduced by the incorporation of the SRA. This produces a reduction in alkali dissolution and decreases the alkali ions concentration in the pore fluid. As a result of this phenomenon, cement hydration can be retarded in mixtures with SRA. As it can be seen in Fig. 42 and Table 10, the cumulative heat at the end of the test period is lower for the SRA mixture than the

non-SRA mixture. The results presented here agree with the results obtained by Sant et al. (Sant et al. 2011).

4.3.3.4 Effect of Fly ash incorporation

The exothermic heat flow curves showing the effect of Class F fly ash incorporation (25 % replacement for PC-III-A cement) on hydration of paste samples are shown in Fig. 43 for w/cm 0.28 and Fig. 44 for w/cm 0.33.

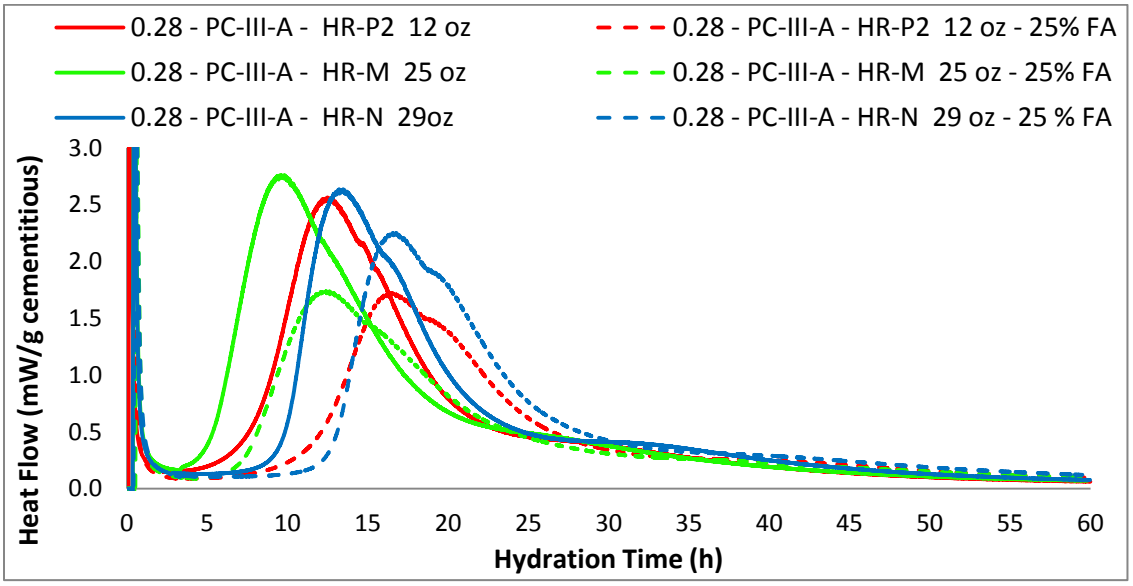

Fig. 43 Heat flow curves showing Fly ash incorporation effect. w/cm 0.28

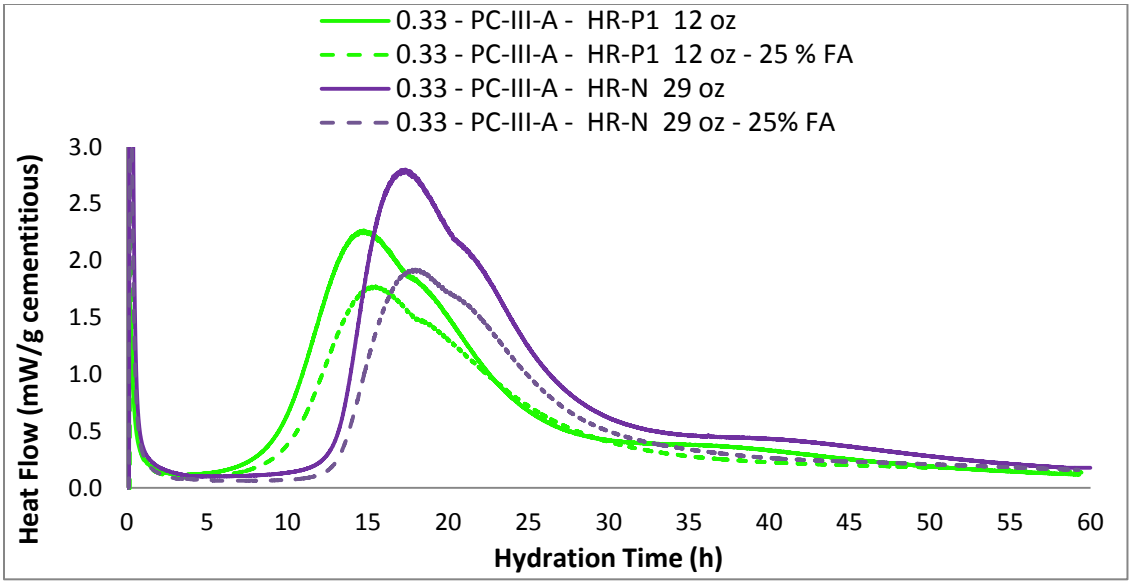

Fig. 44 Heat flow curves showing Fly ash incorporation effect. w/cm 0.33

In this set of mixtures, 25 % of the cement (PC-III-A) of the reference mixture was replaced by Class F fly ash. The same HRWR dosage (based on weight of total cementitious material) was used for both mixtures (control mixture and fly ash mixture).

It is observed that the onset of the acceleration period was delayed when a percentage of cement was replaced by fly ash. The heat evolution rates at point A were reduced in the FA mixtures compared to the control cement pastes.

The FA mixtures, showed lower slopes at the beginning of the acceleration period, which indicates a slower rate of C-S-H nucleation.

The slopes at point B are also reduced with the replacement of FA, which indicates a slower C-S-H nucleation and growth rate in the acceleration period.

The main peaks of heat evolution (point C) were lower for the FA mixtures.

These results were expected and they are thought to be related to the reactivity of the fly ash at early ages, which differs from the behavior at later ages, and the way the

data are presented. Although Class F Fly ash is highly pozzolanic, it was expected that its effects on early hydration were not significant (Poole 2007) (Xie 2014), therefore producing a "diluting effect". Because the curves were normalized by grams of cementitious material (cement + fly ash), and the heat released during the first hours of hydration is due to the hydration of cement, it was expected that the main peak of the fly ash system would be lower due to the lower cement content in the mixture. Fig. 45 shows the same heat flow curves for w/cm 0.33 mixtures, but normalized by grams of cement.

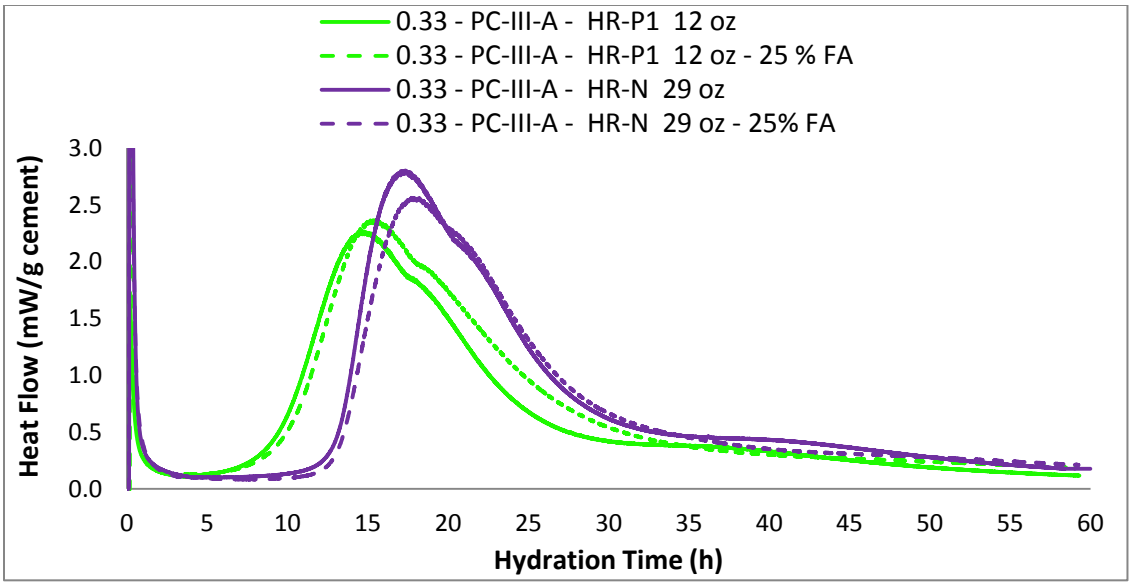

Fig. 45 Heat flow curves normalized by cement weight effect. w/cm 0.33

It can be observed that straight cement and fly ash systems have very similar behaviors, agreeing with the explanation presented above. This supports the idea that the effect of Class F fly ash on early cement hydration is not very significant. When normalized by paste or cementitious material content, however, the effect on heat released becomes evident. The same arguments cannot be fully established for the w/cm

0.28 system. Fig. 46 shows the heat flow curves for w/cm 0.28 mixtures normalized by cement content.

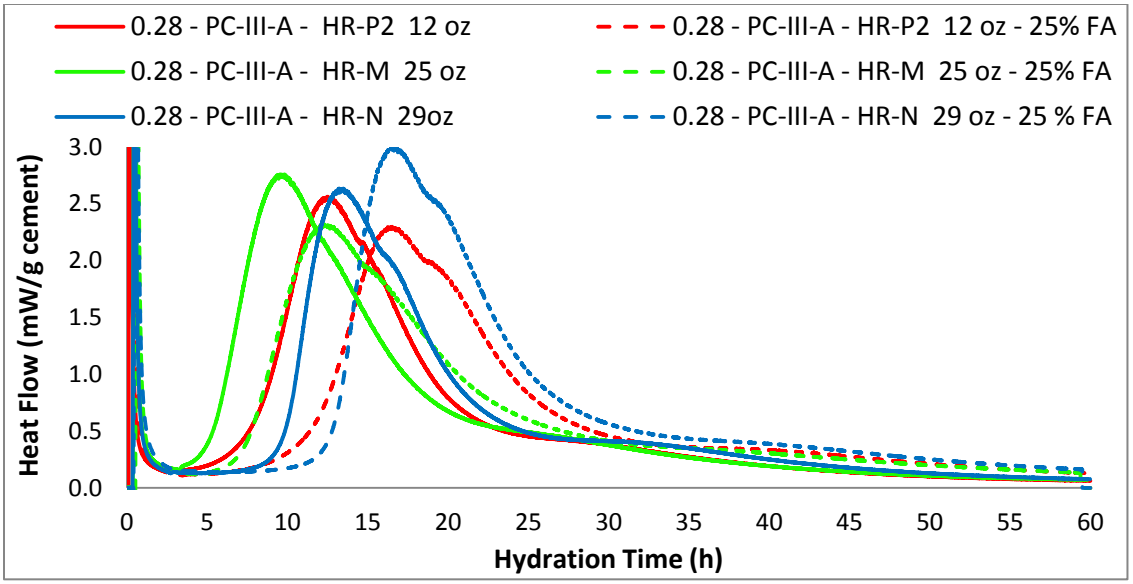

Fig. 46 Heat flow curves normalized by cement weight effect. w/cm 0.28

It is seen that, although the differences between main peaks decreased (except for the fly ash HR-N mixture, which exhibited a higher heat evolution at point C than the control), the fly ash mixtures' peaks (points C) are significantly shifted to the right. This fact may indicate that the effect of fly ash on these lower w/cm systems (compared to the w/cm 0.33) may be different. A deeper impact on the lengthening of the induction period is observed. These results can be a consequence of the variability of the test and more testing is needed to provide a full explanation or confirm the results.

4.3.4 Summary and conclusions

Based on the results presented, the following conclusions can be made:

- The addition of any HRWR extended the duration of the induction period and reduced the slopes of the heat flow curves at the beginning of the acceleration period. HR-M mixtures showed the shortest induction period. HR-N mixtures showed the longest induction period. The use of NR in combination with the polycarboxylate increased the delay in the onset of the acceleration period of the polycarboxylate mixture.
- The addition of any HRWR produced similar or higher slopes at point B (acceleration period) than the control mixtures. The mixtures with HR-N showed the highest slopes, meaning that the naphthalene superplasticizer substantially increased the C-S-H nucleation and growth rates. The relative effects of the melamine and polycarboxylates varied depending on the cement source.
- The main peaks of heat flow corresponding to alite hydration were similar or greater in the mixtures with HRWRs compared to plain control mixtures. HR-N mixtures showed the highest values. The relative values of the melamine and polycarboxylates varied depending on the cement source.
- There is no clear evidence of substantial modification of C-S-H nucleation + growth kinetics with the increase in polycarboxylate dosage from the minimum dosage (3 fl oz/100 lb cement) to the maximum (12 fl oz/100 lb cement) – the behavior was similar for all mixtures in the acceleration period regarding the acceleration rate. In addition, the final cumulative heat values obtained with all dosages lie in the same small range, indicating that the progressive increase in polycarboxylate dosage in the range considered does not cause significant changes in the degree of hydration at this age. The effect of increasing the

polycarboxylate dosage is more pronounced during the induction period, causing the delay in the onset of the acceleration period.

- The incorporation of a SRA caused the retardation of the cement hydration. A lower heat flow rate, main peak of heat evolution and cumulative heat at the end of the test were exhibited by the SRA mixture.
- The partial replacement of Class F fly ash did not have significant effects on early cement hydration in w/cm 0.33 mixtures. When normalized by paste or cementitious material content, however, the effects on the heat released became evident: longer induction period, lower rates of heat flow and lower main peak of heat evolution. The same arguments could not be fully established for the w/cm 0.28 systems, where a deeper impact on the lengthening of the induction period was observed.

4.4 CONCRETE

4.4.1 Introduction

This section refers to the set of tests performed on concrete specimens. Complementing the testing made on paste (chemical shrinkage, autogenous shrinkage and isothermal calorimetry) a battery of tests was conducted on concrete to capture the actual influence of mixture parameters on volume changes and cracking potential.

Volume change testing includes drying shrinkage on concrete prisms specimens and autogenous deformation using free shrinkage frames (FSF). In order to assess the development of stresses due to restrained deformation, rigid cracking frame (RCF) testing was used. As it was previously explained in Chapter 2, RCF tests were performed together with free shrinkage frames and the evaluation of mechanical property development. In addition for each mixture, a 2 cubic foot concrete block was cast in parallel with drying shrinkage prisms. These blocks were stored in an exposure site in order to provide the references for each mixture analyzed regarding the time and severity of cracking. The details of this last procedure are presented in Chapter 5.

4.4.2 Mixture proportions and testing matrix

A wide range of concrete mixtures were tested in this project. Table 11 provides the mixture proportions. Three w/cm ratios were evaluated (0.28, 0.33 and 0.42).Within each w/cm ratio group of mixtures several variables were tested, which include: cement type and content, fly ash replacement/addition, aggregates type, admixture type and dosage, and some mitigation measures such as the use of SRA, saturated lightweight fine aggregate and fibers.

The graphs for each test will be presented with the following codification for each mixture:

(w/cm) (Type of cement) (Type of admixture 1) (Dosage) + (Type of admixture 2) (dosage) - - (Other mixture parameters). The reference proportions for each w/cm are highlighted and it is assumed that CA-R and FA-R aggregates are used unless indicated.

	(lb/yd^3)							
w/cm	Cement	Class F Fly ash	Water	CA-R	FA-R	CA-L	FA-L	FA-LW
0.28	705		197	1722	1444			
	705		197	1722	1230			152
	705		197	1722	1016			304
0.33	705		233	1722	1352			
	611		202	1722	1511			
	846		279	1722	1113			
	529	176	233	1722	1352			
	705	176	291	1722	1053			
	705		233	1722	1138			152
	705		233	1722	924			304
	705		233			1766	1217	
0.42	705		296	1722	1186			
	705		296	1722	972			152
	705		296	1722	758			304
	705		296			1766	1056	

Table 11 Concrete mixture proportions

The admixture type and dosage and other variations considered are shown in Table 12, where all the mixtures and the corresponding tests performed on each one are presented. The details and results of each particular test are presented in the following sections.

w/cm	Cement type	Admixtures				Other mixture parameters	Drying shrinkage	F S F	R C F	Mech. Prop.	Exposure block
		Type	(floz/ 100 lb cement)	Type	(floz/ 100 lb cement)						
0.28	PC-III-A	HR-P1	12	NR	3	-	X	X	-	-	-
		HR-P2	12	-	-	-	X	-	-	-	1/16/2014
			12	NR	3	-	X	-	-	-	3/19/2014
			12		3	SRA 0.75 %	X	-	-	-	1/29/2014
			12		3	SRA 1.50 %	X	-	-	-	1/21/2014
			12		3	152 lb/yd^3 FA-LW	X	-	-	-	4/3/2014
			9		2.25	304 lb/yd^3 FA-LW	X	-	-	-	4/2/2014
0.29	PC-III-A	HR-P1	15	NR	3	-	X	-	-	-	2/4/2014
		HR-P3	15	NR	3	-	X	-	-	-	2/4/2014
	PC-I-A	HR-P2	13.5	NR	3	-	X	-	-	-	2/25/2014
	PC-III-B	HR-P2	13.5	NR	3	-	X	-	-	-	3/4/2014
0.30	PC-III-A	HR-P2	12	NR	3	-	X	-	-	-	1/21/2014

Table 12 Concrete mixture proportions and tests performed

w/cm	Cement type	Admixtures				Other mixture parameters	Drying shrinkage	FSF	RCF	Mech. Prop.	Exposure block
		Type	(floz/ 100 lb cement)	Type	(floz/ 100 lb cement)						
0.33	PC-III-A	HR-P2	12	NR	3	611 pcy cement	X	X	X	X	9/22/2014
		HR-P1	12	-	-	-	X	X	X	X	7/3/2014
			12	NR	3	-	X	X	X	X	-
			12	NR	3	SRA 0.75 %	X	-	X	-	6/19/2014
			12	NR	3	SRA 1.50 %	X	X	-	-	-
		HR-P2	12	-	-	-	X	X	-	-	2/13/2014
			12	NR	3	-	X	X	X	X	1/29/2014
			12	NR	3	SRA 1.50 %	X	X	X	X	6/5/2014
			3	NR	0.75	Limestone AGGs	-	X	-	-	-
			6	NR	1.5	152 lb/yd^3 LW	X	X	X	X	4/24/2014
			6	NR	1.5	304 lb/yd^3 LW	X	X	-	-	4/24/2014
			12	NR	3	Micro fiber 1lb pcy	X	-	-	-	2/10/2014
			12	NR	3	Macro fiber 6 lb pcy	X	-	-	-	2/10/2014
		HR-N	22.5	-	-	-	X	X	X	X	11/10/2014
		HR-M	25	-	-	-	X	X	X	X	12/17/2014
		HR-P2	12	NR	3	Fly Ash 25% repl.	X	X	X	X	2/13/2014
		HR-P2	12	NR	3	Fly Ash 25% add.	X	-	-	-	2/20/2014
		HR-P1	12	NR	3	846 pcy cement	X	X	-	-	5/1/2014
		HR-P2	12	NR	3	846 pcy cement	X	X	X	X	5/16/2014
	PC-I-A	HR-P2	12	NR	3	-	X	X	-	-	2/25/2014
	PC-III-B	HR-P1	12	NR	3	-	X	X	X	X	2/18/2015
		HR-P2	12	NR	3	-	X	X	X	X	10/17/2014

(cont.)Table 12 Concrete mixture proportions and tests performed

w/cm	Cement type	Admixtures				Other mixture parameters	Drying shrinkage	FSF	RCF	Mech. Prop.	Exposure block
		Type	(floz/ 100 lb cement)	Type	(floz/ 100 lb cement)						
0.42	PC-III-A	HR-P2	1.5	-	-	-	X	-	-	-	1/16/2014
				NR	1.5	-	X	-	-	-	1/31/2014
					1.5	SRA 0.75 %	X	-	-	-	1/31/2014
					1.5	SRA 1.50 %	X	-	-	-	2/4/2014
					0.375	152 lb/yd^3 FA-LW	X	-	-	-	5/1/2014
					0.375	304 lb/yd^3 FA-LW	X	-	-	-	4/3/2014
			3	NR	1.5	Limestone AGGs	X	-	-	-	3/11/2014
	PC-III-B	HR-P2	3	NR	1.5	-	X	-	-	-	3/4/2014
	PC-I-A	HR-P2	3	NR	1.5	-	X	-	-	-	2/20/2014

(cont.)Table 12 Concrete mixture proportions and tests performed

4.4.3 Drying shrinkage

4.4.3.1 Procedure and experimental setup

In order to determine the change in length of hardened concrete specimens due to drying shrinkage, ASTM C157 test method was followed. Three concrete prism specimens for each mixture were cast in rigid molds. A single batch was prepared to cast the drying specimens and a two cubic foot exposure block. After casting, the specimens were stored in a temperature-controlled room at 23 +/- 3 °C and covered with wet burlap and plastic film to prevent evaporation until the age of 24 hours. At that age, the specimens were removed from the molds and stored for 15-30 min covered with wet burlap in the same temperature-controlled room. Immediately, the initial comparator reading was taken. After this initial reading, the specimens were stored in a drying room at RH of 50% and 23°C. Successive readings were taken at the ages of 4, 7, 14, 28, 56, 112 and 224 days. Further measurements were taken at later ages when possible. Length change for each specimen, ΔLx (%), was calculated as follows:

$$\Delta Lx = \frac{CRD - CRDinitial}{G} \times 100$$

where CRD is the difference between the comparator reading of the specimen and the reference bar at any age and G is the gage length (250 mm).

4.4.3.2 Results

Table 13 shows the measured drying shrinkage values for the mixtures studied. Every value in Table 13 is the average of three samples. It must be noted that the values referenced here to as “drying shrinkage” represent the total shrinkage exhibited under

unsealed conditions. Therefore, the measured values are the sum of autogenous and drying shrinkage from 24 hours after casting. All drying shrinkage curves can be found in Appendix IV.

w/cm	Cement type	Admixtures				Other mixture parameters	Age (days)								
		Type	(fl oz/ 100 lb cement)	Type	(fl oz/ 100 lb cement)		Drying shrinkage (μm/m)								
0.28	PC-III-A	HR-P2	12	-	-	-	**0**	**3**	**8**	**13**	**28**	**56**	**111**	**224**	**458**
							0	93	173	203	243	283	307	317	320
			12	NR	3	-	**0**	**4**	**6**	**13**	**28**	**55**	**113**	**215**	**396**
							0	67	113	177	267	317	340	350	357
			12		3	SRA 0.75 %	**0**	**7**	**14**	**28**	**58**	**114**	**226**	**334**	
							0	120	173	213	280	305	325	330	-
			12		3	SRA 1.50 %	**0**	**3**	**8**	**14**	**29**	**57**	**112**	**226**	**453**
							0	43	107	153	200	240	280	304	307
			12		3	152 lb/yd^3 FA-LW	**0**	**5**	**14**	**28**	**56**	**115**	**224**	**381**	
							0	100	183	203	270	337	357	360	-
			9		2.25	304 lb/yd^3 FA-LW	**0**	**7**	**14**	**28**	**57**	**116**	**225**	**382**	
							0	190	263	307	390	463	477	487	-
0.29	PC-III-A	HR-P1	15	NR	3	-	**0**	**5**	**7**	**15**	**28**	**63**	**114**	**236**	**439**
							0	113	130	217	267	300	320	340	353
		HR-P3	15	NR	3	-	**0**	**5**	**7**	**15**	**28**	**63**	**114**	**236**	**439**
							0	95	115	180	225	260	275	305	315
	PC-I-A	HR-P2	13.5	NR	3	-	**0**	**7**	**14**	**28**	**58**	**112**	**227**	**418**	
							0	177	223	307	347	367	390	393	-
	PC-III-B	HR-P2	13.5	NR	3	-	**0**	**5**	**7**	**15**	**28**	**57**	**114**	**233**	**411**
							0	170	183	253	277	324	340	373	380
0.30	PC-III-A	HR-P2	12	NR	3	-	**0**	**3**	**8**	**14**	**29**	**57**	**112**	**226**	**453**
							0	123	187	207	270	313	353	370	373

Table 13 Drying shrinkage values for the mixtures studied

w/cm	Cement type	Admixtures				Other mixture parameters	Age (days)								
		Type	(floz/ 100 lb cement)	Type	(floz/ 100 lb cement)		Drying shrinkage (μm/m)								
0.33	PC-III-A	HR-P2	12	NR	3	611 pcy cement	**0**	**3**	**7**	**18**	**25**	**57**	**118**	**209**	
							0	120	180	230	257	317	353	367	-
		HR-P1	12	-	-	-	**0**	**7**	**14**	**28**	**56**	**112**	**224**	**290**	
							0	197	270	343	380	387	393	405	-
			12	NR	3	-	**0**	**1**	**7**	**18**	**57**	**113**	**225**	**529**	
							0	90	200	292	380	400	411	427	-
			12	NR	3	SRA 0.75 %	**0**	**7**	**14**	**28**	**56**	**113**	**234**	**304**	
							0	143	207	267	310	327	333	337	-
			12	NR	3	SRA 1.50 %	**0**	**4**	**7**	**14**	**28**	**63**	**88**	**223**	
							0	107	133	167	217	273	287	301	-
		HR-P2	12	-	-	-	**0**	**4**	**7**	**14**	**28**	**62**	**117**	**227**	**430**
							0	153	187	243	310	387	410	427	437
			12	NR	3	-	**0**	**7**	**11**	**14**	**29**	**56**	**113**	**225**	**445**
							0	126	170	240	320	390	420	431	433
			12	NR	3	SRA 1.50 %	**0**	**5**	**7**	**14**	**28**	**56**	**115**	**227**	**318**
							0	107	140	200	247	290	323	337	340
			6	NR	1.5	152 lb/yd^3 FA-LW	**0**	**6**	**7**	**13**	**28**	**56**	**112**	**234**	**360**
							0	223	270	313	413	503	580	583	587
			6	NR	1.5	304 lb/yd^3 FA-LW	**0**	**6**	**7**	**13**	**28**	**56**	**112**	**234**	**360**
							0	220	267	310	430	503	557	577	587
			12	NR	3	Micro fiber 1lb/yard	**0**	**3**	**7**	**14**	**28**	**57**	**120**	**230**	**433**
							0	100	180	223	297	383	417	430	433

(cont.) Table 13 Drying shrinkage values for the mixtures studied

w/cm	Cement type	Admixtures				Other mixture parameters	**Age (days)**								
		Type	(floz/ 100 lb cement)	Type	(floz/ 100 lb cement)		Drying shrinkage (μm/m)								
0.33	PC-III-A	HR-P2	12	NR	3	Macro fiber 6lb/yard	**0**	**3**	**7**	**14**	**28**	**57**	**120**	**230**	**433**
							0	63	116	197	263	333	360	383	390
		HR-N	22.5	-	-	-	**0**	**3**	**7**	**15**	**32**	**57**	**121**		
							0	90	160	253	353	383	438	-	-
		HR-M	25	-	-	-	**0**	**5**	**7**	**11**	**15**	**32**	**57**	**123**	
							0	193	233	277	303	400	433	467	-
		HR-P2	12	NR	3	Fly Ash 25% repl.	**0**	**4**	**7**	**14**	**28**	**62**	**117**	**227**	**430**
							0	140	170	250	338	399	428	446	454
		HR-P2	12	NR	3	Fly Ash 25% add.	**0**	**4**	**7**	**14**	**28**	**56**	**112**	**220**	**423**
							0	120	171	239	296	407	449	478	485
		HR-P1	12	NR	3	846 pcy cement	**0**	**7**	**14**	**28**	**56**	**112**	**227**	**353**	
							0	210	273	329	403	453	470	473	-
		HR-P2	12	NR	3	846 pcy cement	**0**	**3**	**7**	**13**	**27**	**55**	**121**	**230**	**338**
							0	147	184	217	317	397	452	460	465
	PC-I-A	HR-P2	12	NR	3	-	**0**	**7**	**14**	**28**	**58**	**112**	**227**	**418**	
							0	190	257	343	390	443	463	470	-
	PC-III-B	HR-P1	12	NR	3	-	**0**	**4**	**7**	**9**	**19**	**29**	**60**		
							0	187	253	280	353	370	420	-	-
		HR-P2	12	NR	3	-	**0**	**5**	**7**	**13**	**27**	**58**	**114**	**184**	
							0	193	257	300	357	380	397	410	-

(cont.) Table 13 Drying shrinkage values for the mixtures studied

w/cm	Cement type	Admixtures				Other mixture parameters	Age (days)								
		Type	(floz/ 100 lb cement)	Type	(floz/ 100 lb cement)		Drying shrinkage (μm/m)								
0.42	PC-III-A	HR-P2	1.5	-	-	-	**0**	**3**	**8**	**13**	**28**	**56**	**111**	**224**	**458**
							0	110	190	240	313	407	457	513	530
				NR	1.5	-	**0**	**4**	**9**	**13**	**27**	**58**	**111**	**223**	**443**
							0	137	220	270	357	467	520	587	607
					1.5	SRA 0.75 %	**0**	**4**	**9**	**13**	**27**	**58**	**111**	**223**	**443**
							0	63	157	207	280	383	467	503	523
					1.5	SRA 1.50 %	**0**	**5**	**7**	**15**	**28**	**56**	**114**	**236**	**439**
							0	67	80	147	200	283	333	407	427
					0.375	152 lb/yd^3 FA-LW	**0**	**6**	**14**	**28**	**56**	**112**	**227**	**353**	
							0	153	233	300	410	497	510	523	-
					0.375	304 lb/yd^3 FA-LW	**0**	**5**	**14**	**28**	**56**	**115**	**224**	**381**	
							0	90	227	313	407	537	557	567	-
			3	NR	1.5	Limestone AGGs	**0**	**5**	**8**	**14**	**28**	**57**	**121**	**226**	**404**
							0	203	260	333	410	435	495	525	535
	PC-I-A	HR-P2	3	NR	1.5	-	**0**	**4**	**7**	**14**	**28**	**56**	**112**	**220**	**423**
							0	120	187	290	377	507	557	587	593

(cont.) Table 13 Drying shrinkage values for the mixtures studied

The following sections will evaluate the effects of several parameters on the measured drying shrinkage of concrete specimens.

4.4.3.2.1 Effect of w/cm ratio

Fig. 47 shows the drying shrinkage curves for concrete mixtures with three different w/cm ratios (0.28, 0.33 and 0.42), PC-III-A cement and HR-P2 HRWR (alone and in combination with a NR water reducer).

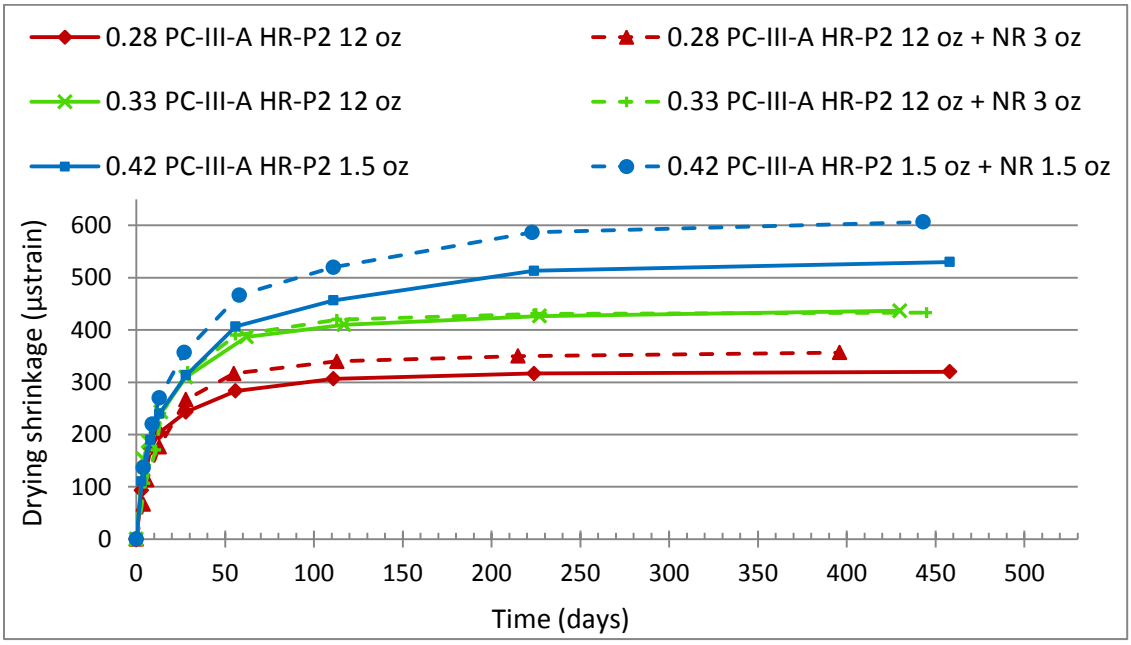

Fig. 47 Drying shrinkage curves showing the effect of w/cm ratio

As it was expected, it is seen that the increase in w/cm ratio produced an increase in the drying shrinkage measured. The difference between shrinkage values was more noticeable in the long term. As it is shown, the lower w/cm mixtures decreased the shrinkage rate and plateaued sooner than respective higher w/cm mixtures.

The mixtures that used a normal range water reducer in combination with the polycarboxylate showed the same trend. The 0.28 and 0.42 polycarboxylate + NR mixtures showed values higher than the polycarboxylate mixtures without NR. For the 0.33 mixture the difference was insignificant.

4.4.3.2.2 Effect of cement source

Fig. 48 and Fig. 49 show the drying shrinkage curves for concrete mixtures with two different Type III cements (PC-III-A and PC-III-B) for w/cm 0.28 and w/cm 0.33, respectively.

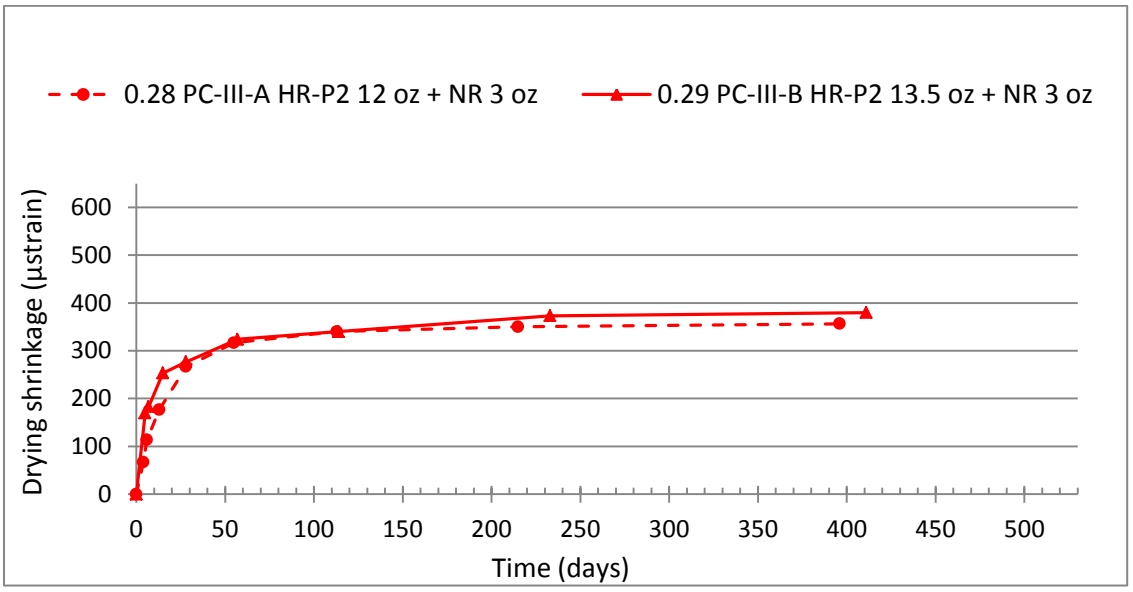

Fig. 48 Drying shrinkage curves for different Type III cements (PC-III-A and PC-III-B), w/cm 0.28

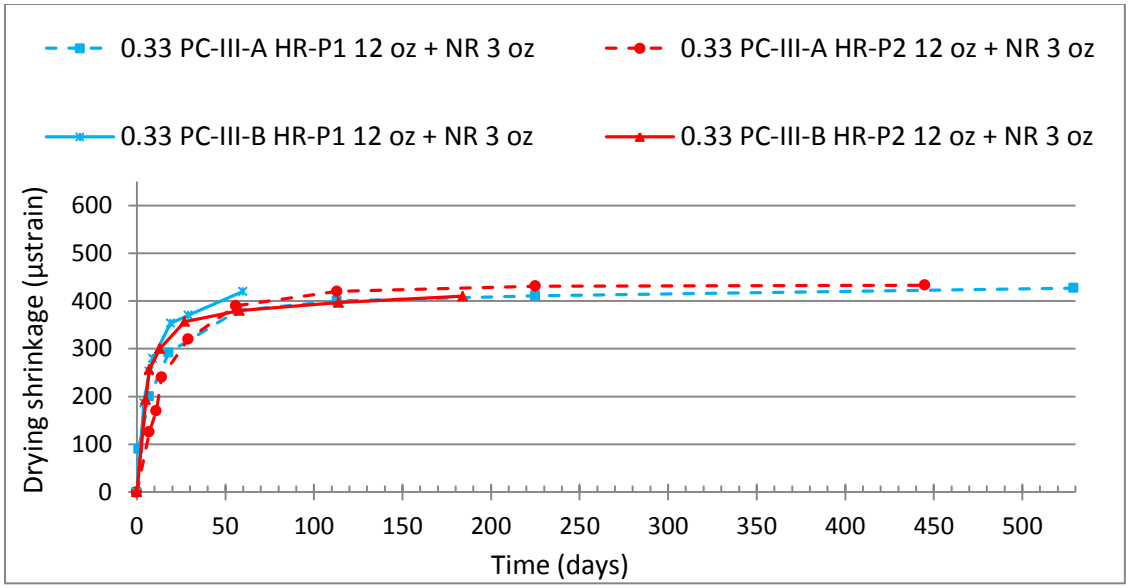

Fig. 49 Drying shrinkage curves for different Type III cements (PC-III-A and PC-III-B), w/cm 0.33

It is observed in both graphs that the total shrinkage values are very similar for both cements. The only difference that should be mentioned is the observed behavior at very early ages, where PC-III-B mixtures showed a higher rate of shrinkage than PC-III-A mixtures. This could be related to the rate of autogenous shrinkage experienced by the concrete mixtures, which occurs at the same time as drying shrinkage and has its maximum influence at this very early time.

4.4.3.2.3 Effect of HRWR type

Fig. 50 and Fig 51 show the drying shrinkage curves for PC-III-A concrete mixtures with different HRWRs, for w/cm 0.33 and w/cm 0.28 respectively.

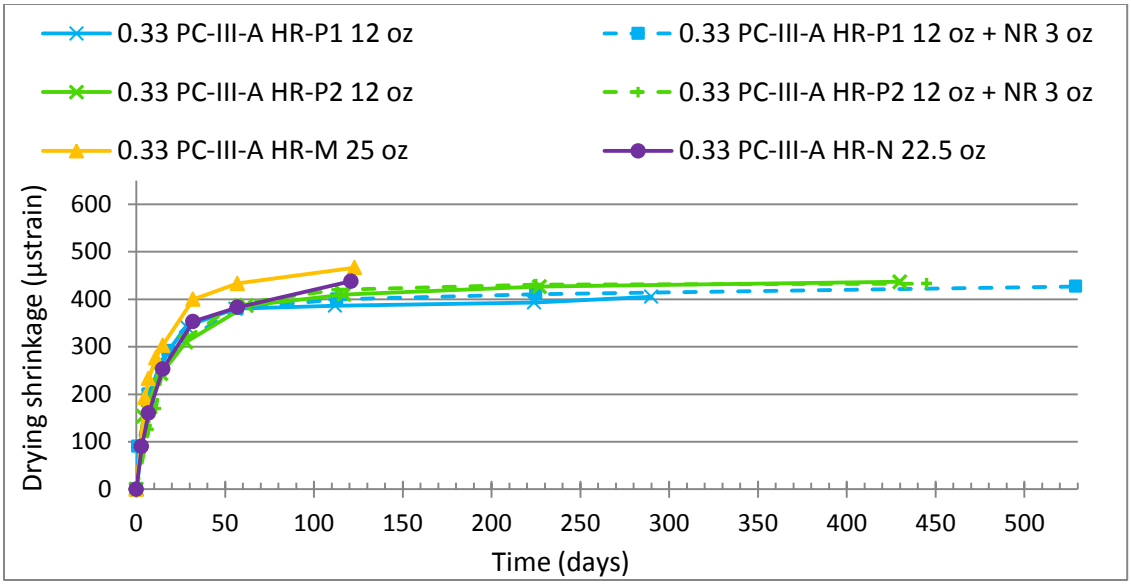

Fig. 50 Drying shrinkage curves showing the effect of HRWR type, w/cm 0.33

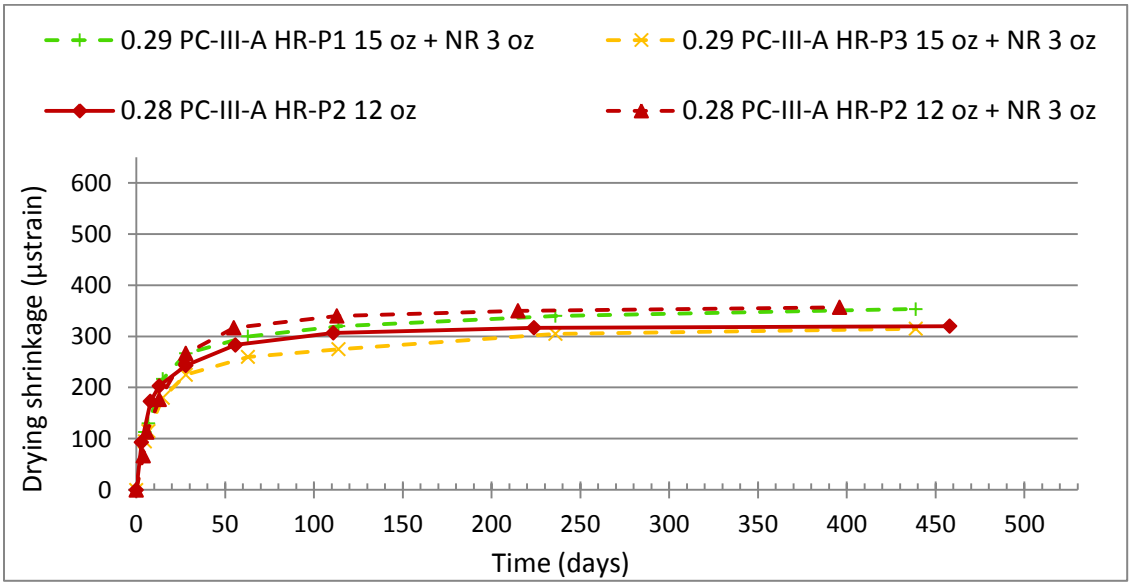

Fig. 51 Drying shrinkage curves showing the effect of HRWR (polycarboxylate) type, w/cm 0.28

Five different HRWRs were used: three polycarboxylate-based (HR-P1, HR-P2, HR-P3), a melamine-based (HR-M), and a naphthalene-based (HR-N) HRWRs. In addition, a normal range water reducing and retarding (Type D) admixture (NR) was used in conjunction with the polycarboxylate-based HRWRs, as it is a common practice in precast applications. The dosage of each type of admixture was selected based on trial mixtures in order to obtain the adequate consistency.

For w/cm 0.33 mixtures, it is observed that both polycarboxylate (HR-P1 and HR-P2) mixture showed very similar behaviors. This statement remains true for the mixtures that incorporated a NR. The plain HR-P2 mixture exhibited slightly higher shrinkage than the HR-P1 mixture, but the difference was small. The use of NR in combination with the polycarboxylates did not change significantly the drying shrinkage experienced in both cases.

Regarding the naphthalene and melamine mixtures, data were only available until 120 days, since those mixtures were cast later and are still being monitored. However, it is observed that their behavior did not differ substantially from the polycarboxylate mixtures until this time. Both mixtures show slightly higher shrinkage than the polycarboxylates. The HR-M mixture showed greater shrinkage than all other mixtures. Based on these preliminary results, it is expected that the final drying shrinkage values of HR-M and HR-N mixtures will be slightly higher than the polycarboxylate mixtures, but the difference should not be significant.

The w/cm 0.28 (and 0.29) mixtures presented in Fig. 51 showed a very similar behavior for all three polycarboxylates. All four mixtures presented very similar drying shrinkage values at ages greater than 1 year.

According to the results of this section, it does not seem that the type of HRWR has a strong influence on the drying shrinkage experienced by the concrete in the long

term. No significant difference was found between polycarboxylate-based HRWRs. The preliminary results of melamine and naphthalene HRWRs also indicate no substantial difference in the drying behavior compared to the polycarboxylates. The incorporation of the NR in combination with the polycarboxylates produced very small differences in shrinkage compared to the plain polycarboxylate mixtures.

4.4.3.2.4 Effect of cement content

Fig. 52 shows the drying shrinkage curves for w/cm 0.33, PC-III-A mixtures with different cement contents (611 lb/yd^3, 705 lb/yd^3, 846 lb/yd^3). Two polycarboxylates (HR-P1 and HR-P2) in combination with a normal range water reducer were used.

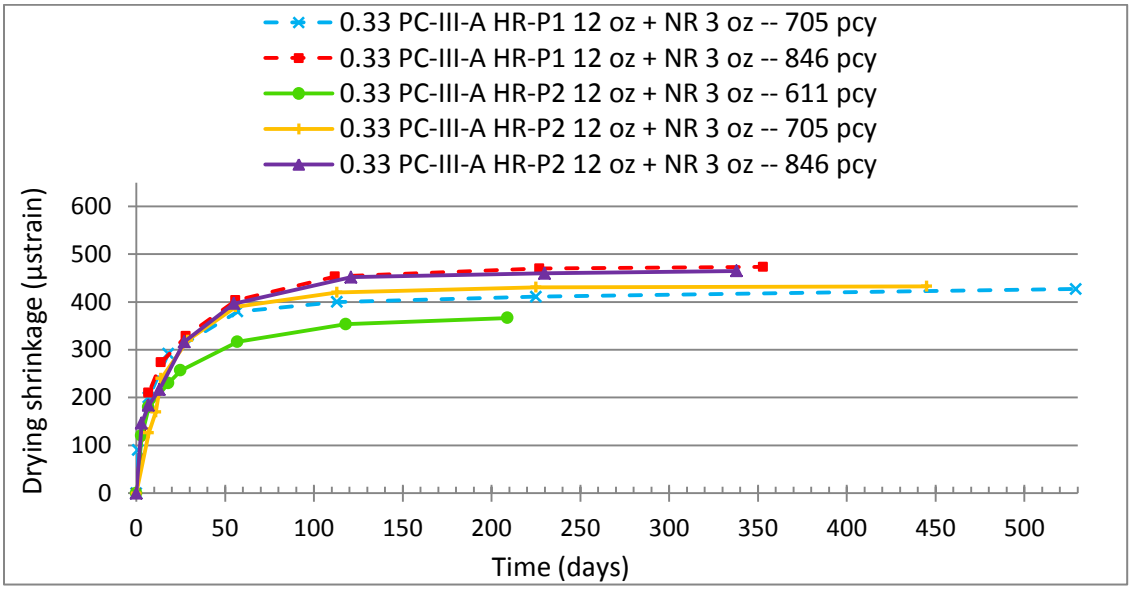

Fig. 52 Drying shrinkage curves showing the effect of cement content per cubic yard for a constant w/cm ratio (0.33)

As it was expected, the increase in cement content per cubic yard (for the same w/cm ratio) increased the drying shrinkage of the mixtures. This was observed for both polycarboxylates. The result is logical since higher cement content per cubic yard, while keeping a constant w/cm ratio, represent higher paste content in the concrete mixture. Because drying shrinkage is experienced by the cement paste, it is reasonable that the volume change of the concrete is greater as the paste content increases. In addition, higher paste contents means less total aggregate per cubic yard, which is considered volumetrically stable and provides restraint to the deformation.

4.4.3.2.5 Effect of Fly ash incorporation

Fig. 53 shows the effect of Class F fly ash incorporation on drying shrinkage for w/cm 0.33 mixtures. Fly ash was incorporated in one mixture as a replacement of 25 % of the cement and, in a second mixture, as an addition to the cement (25 % by mass of cement).

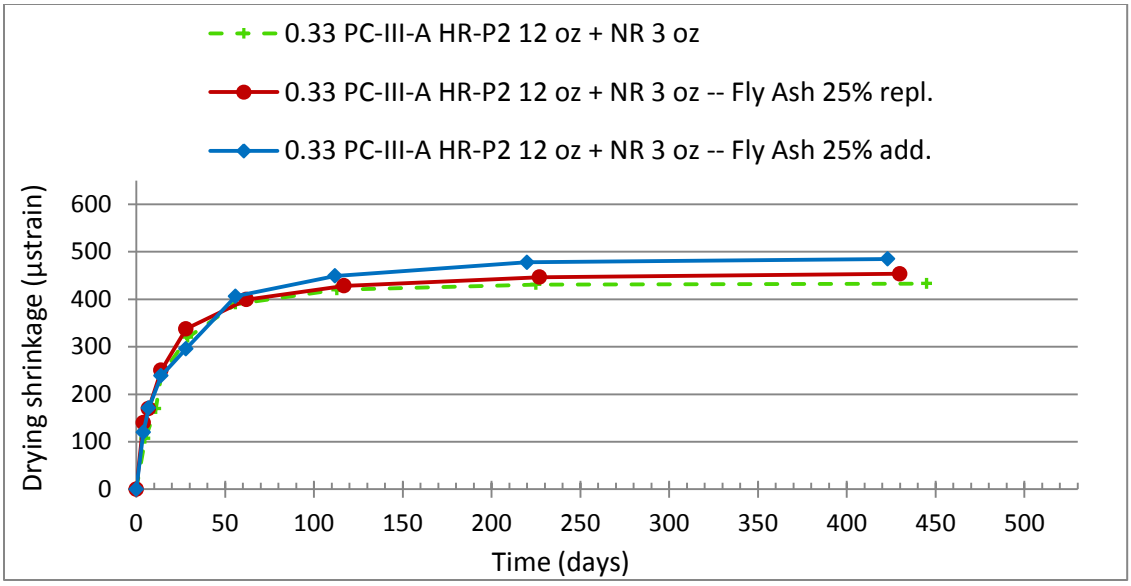

Fig. 53 Drying shrinkage curves showing the effect fly ash incorporation

As it is seen, the use of fly ash as partial replacement of cement (25 % by mass of cement) slightly increased the drying shrinkage compared to the control straight cement mixture. This result is explained by the fact that the same mixing water content was used for both mixtures, in order to maintain a constant water-to-cementitious material ratio. The slight increase in paste volume as a result of the fly ash inclusion is believed to have caused the slight increase in drying shrinkage (Brooks and Jiang 1999) (Joshi and Lohita 1997). If the mixing water of the concrete mixture were reduced (this could be done due to the reduced water demand of the fly ash system) the shrinkage exhibited by the fly ash mixture should be similar or lower than the straight cement concrete (Thomas 2007) (Brooks and Jiang 1999). This idea can explain the even higher shrinkage exhibited by the mixture that incorporated 25 % of fly ash (by mass of cement) in addition to the cement, which has the highest paste volume.

4.4.3.2.6 Effect of SRA incorporation

Fig. 54, Fig 55 and Fig 56 show the effect of SRA incorporation on drying shrinkage for w/cm 0.28, 0.33, and 0.42 mixtures, respectively. PC-III-A cement and two polycarboxylates (HR-P1 and HR-P2) in combination with a normal range water reducer were used.

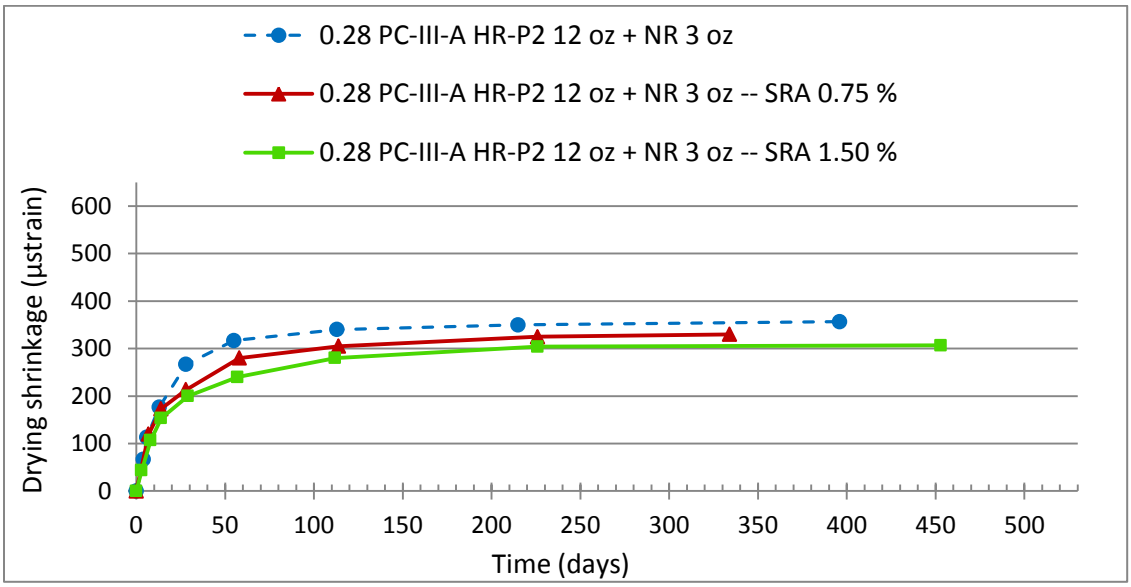

Fig. 54 Drying shrinkage curves showing the effect of SRA incorporation, w/cm 0.28

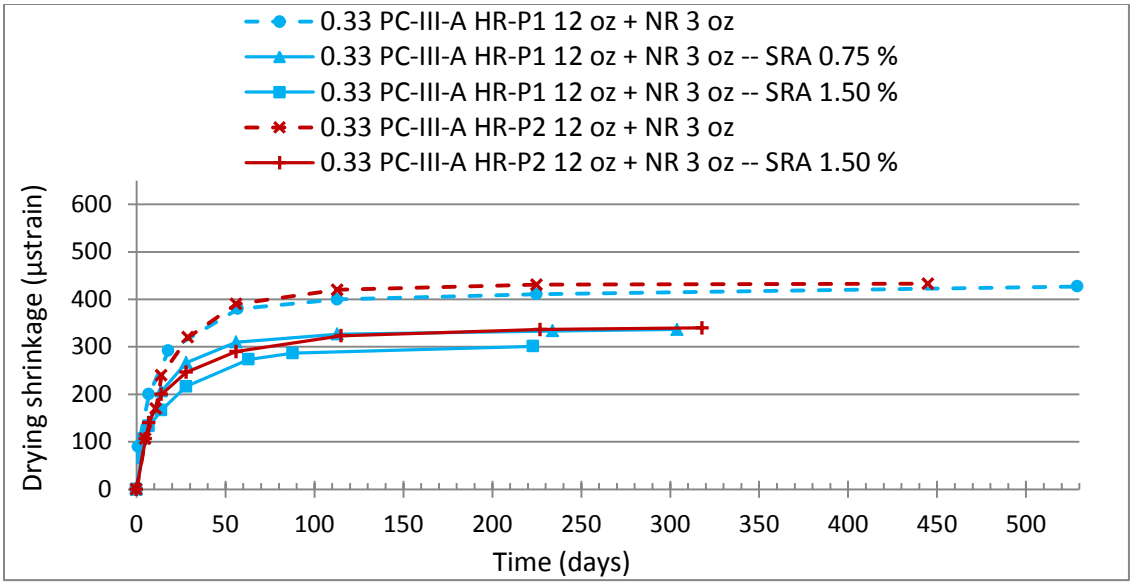

Fig. 55 Drying shrinkage curves showing the effect of SRA incorporation, w/cm 0.33

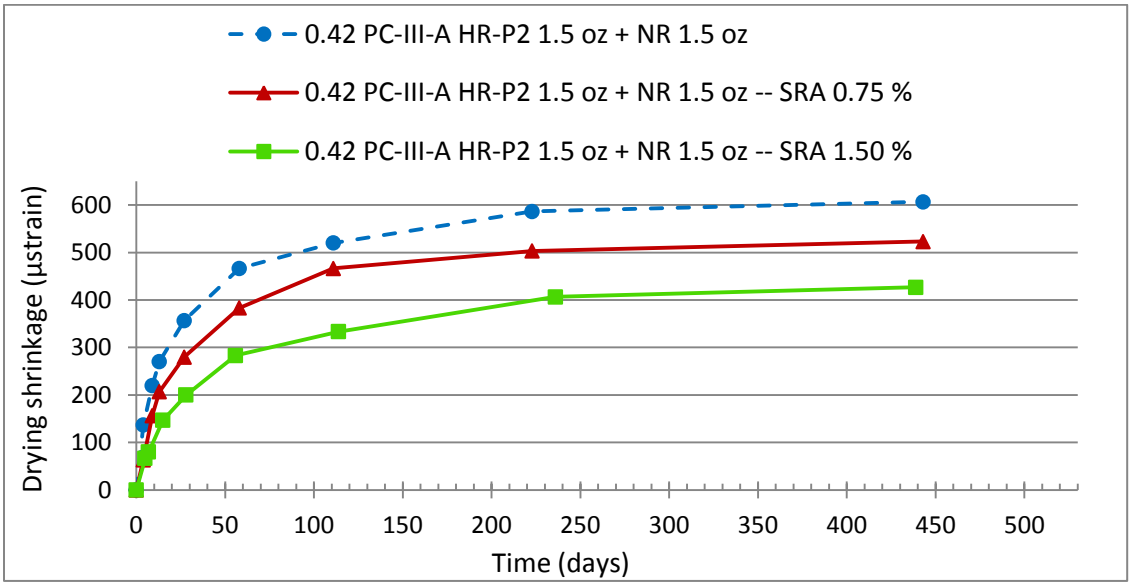

Fig. 56 Drying shrinkage curves showing the effect of SRA incorporation, w/cm 0.42

It is observed that the SRA incorporation reduced the drying shrinkage of the control mixtures. This result was consistently seen for the three w/cm ratios considered and, in the particular case of the w/cm 0.33 mixture, for both polycarboxylates. The % shrinkage reduction obtained increased as the dosage of SRA was increased from 0.75 to 1.5 %.

To better analyze the results, Table 14 shows the calculated % shrinkage reduction at the ages of 14 days and 224 days for all mixtures.

w/cm	HRWR	SRA (% cement)	Drying shrinkage 14 days (μstrain)	Shrinkage reduction 14 days %	Drying shrinkage 224 days (μstrain)	Shrinkage reduction 224 days %
0.28	HR-P2 + NR	Control	177	0	350	0
		0.75	173	2*	325	7*
		1.5	153	13	304	13
0.33	HR-P1 + NR	Control	269	0	411	0
		0.75	207	23	333	19
		1.5	167	38	301	27
	HR-P2 + NR	Control	240	0	431	0
		1.5	200	17*	337	22*
0.42	HR-P2 + NR	Control	270	0	587	0
		0.75	207	23	503	14
		1.5	147	46	407	31

Table 14 Shrinkage reduction % at the ages of 14 days and 224 days

It is shown that the reduction in shrinkage (%) compared to the control mixture was more significant as the w/cm increased. The w/cm 0.42 mixture showed a reduction in shrinkage considerably greater than the 0.28 and 0.33 mixtures.

The reduction in shrinkage (%) compared to the control was generally greater at 14 days than at 224 days. Two mixtures did not follow this trend (indicated with *) probably due to the variability of the measurements at this early age.

4.4.3.2.7 Effect of fiber reinforcement

Fig. 57 shows the effect of the incorporation of polypropylene fibers on drying shrinkage for w/cm 0.33 mixtures. Two types of polypropylene fibers were used, as described in chapter 3: micro fibers, with a dosage equal to 1 lb/yd^3, and macro fibers with a dosage equal to 3 lb/yd^3.

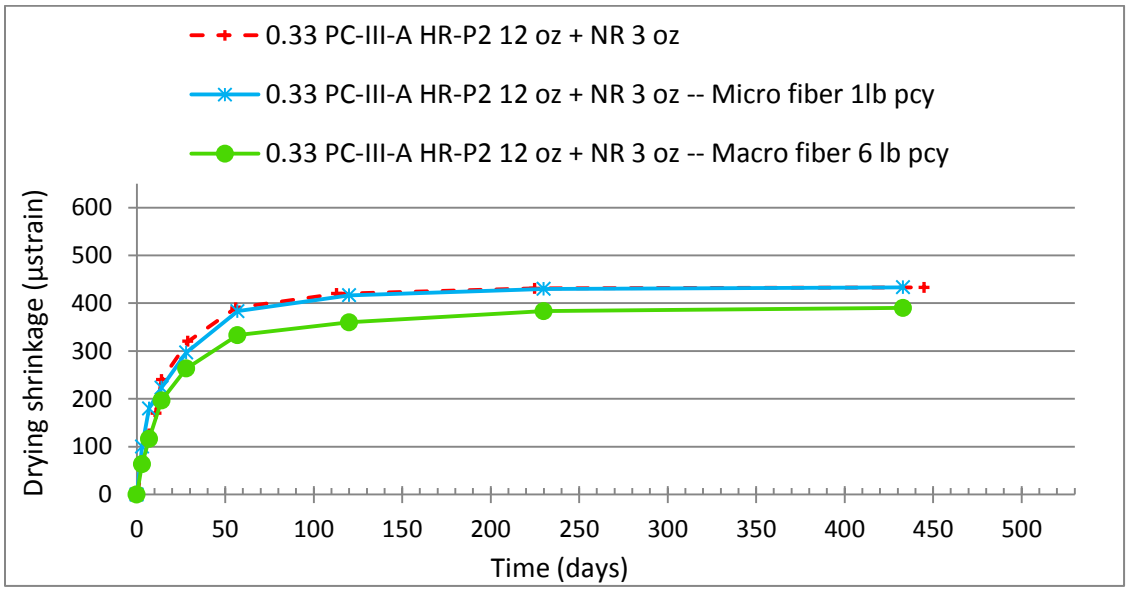

Fig. 57 Drying shrinkage curves showing the effect of polypropylene fiber reinforcement, w/cm 0.33

It is observed in the figure that the incorporation of micro fibers did not cause any change on the drying shrinkage behavior of the control mixture. It may be possible that

the effect of this type of fibers is more pronounced regarding the control of plastic shrinkage cracking than drying shrinkage. The macro fibers reduced the drying shrinkage of the control mixture 11 % at 224 days.

4.4.3.2.8 Effect of saturated lightweight fine aggregate incorporation

The effect of FA-LW incorporation on drying shrinkage for w/cm 0.28, 0.33, and 0.42 mixtures could not be analyzed due to the inconsistent results obtained. It was expected the partial replacement of saturated lightweight fine aggregate (FA-LW) for siliceous river sand (FA-R) would cause a reduction in the drying shrinkage experienced by the concrete mixtures. The reduction in shrinkage expected in the short and mid-term is a result of the decreased shrinkage rate of LWA concrete (Radlinska et al. 2008). It is believed that the conflicts with the expected behavior are related to the pre-saturation process of the FA-LW before mixing. In this project, the FA-LW was submerged in water and stored in a temperature-controlled room 24 hours before mixing the concrete. But the volume of water used to saturate the aggregate was not equal to the sum of the mixing water and the water that would be absorbed by the FA-LW (Radlinska et al. 2008), which would have provided with an accurate control of the w/cm ratio of the mixture. Before mixing, the FA-LW was strained to remove excess of free water. However, water in excess of the absorbed by the aggregate was still present and that moisture correction was not made. As a result, the w/cm ratio of the concrete mixtures is believed to have been different from the design, which may explain the contradictory results.

4.4.3.3 Summary and conclusions

Based on the results of this section the following conclusions can be made:

- The increase in w/cm ratio produced an increase in the drying shrinkage measured. This variable showed the deepest relative effect on drying shrinkage when compared to the other mixture parameters analyzed.
- No significant difference in total shrinkage was found with different sources of Type III cement. There was a slight difference in the observed behavior at very early ages, where PC-III-B mixtures showed a higher rate of shrinkage than PC-III-A mixtures. This could be related to the rate of autogenous shrinkage experienced by the concrete mixtures, which occurs at the same time as drying shrinkage and has its maximum influence at this very early time.
- The type of HRWR does not seem to have a strong influence on the drying shrinkage experienced by the concrete in the long term. No significant differences were found between polycarboxylate-based HRWRs. The incorporation of the NR in combination with the polycarboxylates produced very small differences in shrinkage compared to the plain polycarboxylate mixtures. The preliminary results of melamine and naphthalene HRWRs also indicate no substantial difference in the drying behavior compared to the polycarboxylates.
- The increase in cement content per cubic yard (for the same w/cm ratio) increased the drying shrinkage of the mixtures. This is a consequence of the higher paste content, less total aggregate in the concrete mixture.
- The use of fly ash as partial replacement of cement (25 % by mass of cement) slightly increased the drying shrinkage. This is believed to have been caused by the slight increase in the paste volume of the mixture as a result of keeping constant the mixing water content. This can explain the even higher shrinkage

exhibited by the mixture that incorporated 25 % of fly ash (by mass of cement) in addition to the cement, which has the highest paste volume.

- The SRA incorporation reduced the drying shrinkage of the control mixtures. The measured reduction in shrinkage (%) increased as the dosage of SRA was increased, as the w/cm increased, and was generally greater at 14 days than at 224 days.
- The incorporation of micro fibers did not cause any change on the drying shrinkage behavior of the control mixture. It may be possible that the effect of this type of fibers is more pronounced regarding the control of plastic shrinkage cracking than drying shrinkage. The macro fibers reduced the drying shrinkage of the control mixture by 11 % at 224 days.
- The effect of FA-LW incorporation on drying shrinkage could not be analyzed due to the inconsistent results obtained, which are believed to be related to the pre-saturation process of the FA-LW before mixing.

4.4.4 Concrete autogenous deformation

4.4.4.1 Procedure and experimental setup

As it was explained in Chapter 2, the free deformation frame method allows the tracking of autogenous deformation of concrete specimens. Fresh concrete specimens were cast in a temperature-controlled rigid formwork, shown in Fig. 58. Tests were performed in isothermal conditions at 23°C for 7 days.

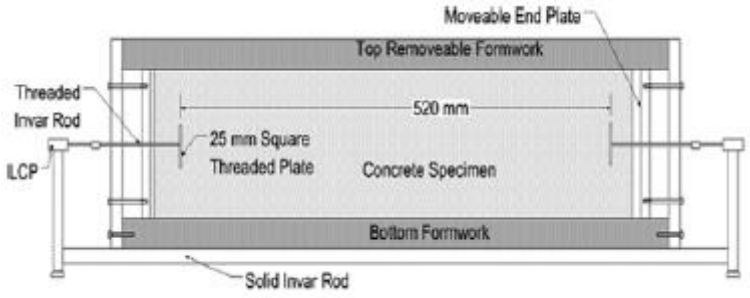

Fig. 58 Schematic Free deformation frame (Riding et al. 2008).

The dimensions of the concrete specimen are 150 x 150 x 520 mm (6” x 6” x 20.4”). The bottom bars of the frame are made of Invar, which has a very low coefficient of thermal expansion.

Before casting, the preparation of the frame included the placement of two layers of plastic on the formwork which were also lubricated with oil, in order to isolate the concrete and minimize the restraint. After placement and compaction of the concrete, a plastic layer was lubricated with oil and placed on the top surface of the sample. Aluminum tape was used to seal the specimen.

The frame is surrounded by a system of copper pipes connected to a programmable water bath. This allowed the active control of the temperature of the

specimen (isothermal) by the circulation of a fluid (mixture of water and coolant). Two thermocouples were lubricated with grease and inserted into the concrete. The thermocouples were connected to the data acquisition system, which continuously recorded and controlled the temperature of the water bath. The holes through which the thermocouples were inserted were sealed with grease to prevent evaporation.

Two Invar bars threaded onto 25 x 25 mm (1" x 1") plates were embedded into the concrete at each end of the specimen and connected to linear variable displacement transducers (LDVT) to capture the length change. An automatic data-logging system was used to record the data with a 5 minutes frequency.

The concrete was held in place with the end steel plates from the moment of casting until the time of initial setting. This point was determined as specified by ASTM C 403, measuring penetration resistance of mortar specimens obtained from the concrete by sieving, which were cured to match the temperature of the concrete in the frame. At the time of initial setting the specimen was released by backing away the two steel end plates. The strain was zeroed at this point.

4.4.4.2 Results

Table 15 shows the measured autogenous deformation for the concrete mixtures studied from the time of initial setting until the age of 7 days. Negative values indicate shrinkage (μm/m) and positive values indicate expansion (μm/m).

Table 15 also shows the autogenous fraction of the total shrinkage at the age of 7 days and 224 days. These values were calculated by dividing the autogenous shrinkage measured in the FSF (from initial setting until 7 days) by the total shrinkage (from initial setting until 7 days). The total shrinkage after initial setting was calculated by adding the autogenous shrinkage measured from initial setting until 24 hours after mixing to the total

shrinkage measured following ASTM C157 (ASTM C157 measurements started at 24 hours after mixing). Although this represents a very simplistic methodology and it is not completely accurate, values are presented as a first approach to evaluate the influence of autogenous shrinkage on early total shrinkage.

w/cm	Cement type	Admixtures				Other mixture parameters	Autogenous deformation 7 days (μm/m)	Autogenous/ Total Shrinkage 7 days (%)	Autogenous/ Total Shrinkage 224 days (%)
		Type	(floz/ 100 lb cement)	Type	(floz/ 100 lb cement)				
0.28	PC-III-A	HR-P1	12	NR	3	-	-48.0	35*	14*
0.33	PC-III-A	HR-P2	12	NR	3	611 pcy cement	-20.7	12	6
		HR-P1	12	-	-	-	-55.6	25	13
			12	NR	3	-	-51.2	25	12
			12		3	SRA 1.5 %	-19.1	14	6
		HR-P2	12	-	-	-	-29.4	17**	7**
			12	NR	3	-	-28.2	26**	7**
			12		3	SRA 1.5 %	-13.0	10	4
			6	NR	1.5	152 lb/yd^3 LW	12.0	-5**	-2**
			6		1.5	304 lb/yd^3 LW	31.3	-15**	-6**
			3	NR	0.75	Limestone AGGs	47.1	-	-
		HR-N	22.5	-	-	-	-16.3	10	-
		HR-M	25	-	-	-	-74.0	29	-
		HR-P1	12	NR	3	846 pcy cement	-45.7	22	10
		HR-P2	12	NR	3	846 pcy cement	-43.5	24	9
		HR-P2	12	NR	3	Fly Ash 25% repl.	-16.8	11	4
	PC-III-B	HR-P1	12	NR	3	-	-67.8	26	-
		HR-P2	12	NR	3	-	-65.8	25	16
	PC-I-A	HR-P2	12	NR	3	-	-22.8	13	5

(*) calculated using drying shrinkage values corresponding to the analogous mixture with w/cm 0.29.
(**) experimental-related inconsistencies

Table 15 Autogenous deformation for concrete mixtures from initial setting and autogenous fraction of the total shrinkage at the age of 7 days and 224 days

As can be observed in the table, the weight of autogenous shrinkage on early total shrinkage varied among different mixtures. For most mixtures autogenous shrinkage represented an average of 25 % of the total shrinkage during the first seven days. The percentage decreased at 224 days as drying shrinkage increased with time (autogenous measurements were stopped at 7 days). The autogenous fraction of total shrinkage was reduced when a mitigation measure was applied (incorporation of SRA, saturated lightweight fine aggregate), when the cement content was reduced or partially replaced by Class F fly ash, and with the use of a naphthalene-based superplasticizer. The values showed for the w/cm 0.28 mixture (*) were calculated using drying shrinkage values corresponding to the analogous mixture with w/cm 0.29 due to the unavailability of data for the 0.28 mixture. Some specific mixtures showed experimental-related inconsistencies and are indicated with **. The particular details will be presented in the following sections.

4.4.4.2.1 Effect of w/cm ratio

Fig. 59 shows the autogenous deformation curves for PC-III-A mixtures with the same admixture type and dosage and different w/cm ratio.

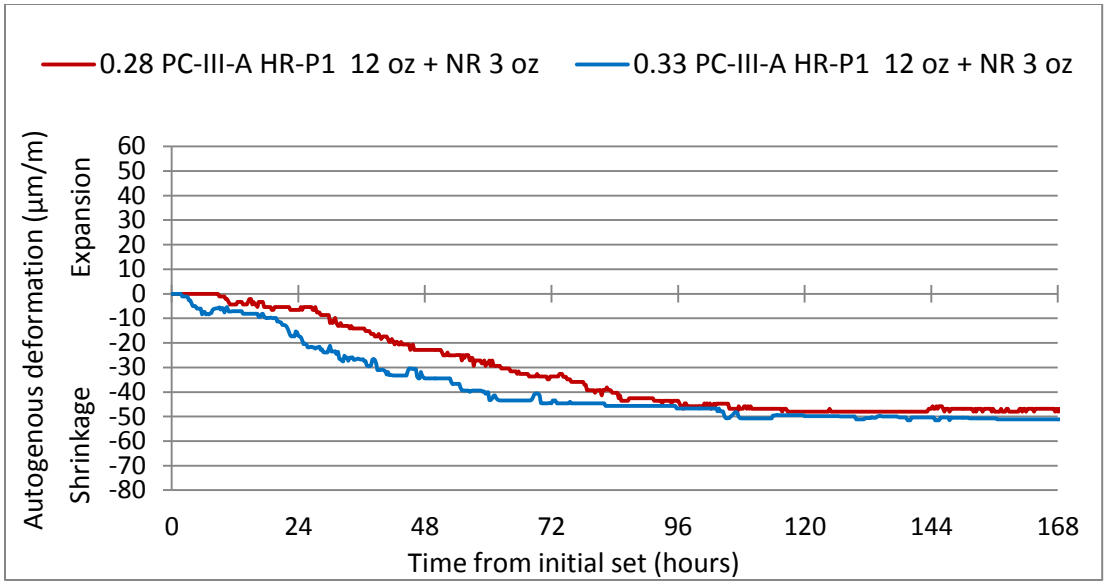

Fig. 59 Autogenous deformation curves showing the effect of w/cm ratio

As it is seen in Fig. 59, both concrete mixtures showed very similar behaviors. This is different from what we expected since lower w/cm mixtures often show higher autogenous shrinkage and, as a result, the 0.28 mixture should exhibit larger shrinkage at every age. It has to be mentioned that the mixture proportions used in this project keep constant cement and coarse aggregate contents per cubic yard (unless specified). As a result, the difference between the two w/cm mixtures considered in this case is the water and fine aggregate contents per cubic yard, resulting in different paste content. It may be possible that the measured volume change (experienced only in the cement paste phase) is lower in the 0.28 mixture as a result of the lower paste content compared to the 0.33 mixture, yet the relative difference in % paste contents is small. The results obtained could also be a mere consequence of the test sensitivity and additional testing should be conducted to confirm these outcomes.

4.4.4.2.2 Effect of cement source

Fig. 60 shows the autogenous deformation curves for PC-III-A and PC-III-B mixtures. The comparison is made on two set of mixtures with the same w/cm ratio and different type of polycarboxylate-based HRWR.

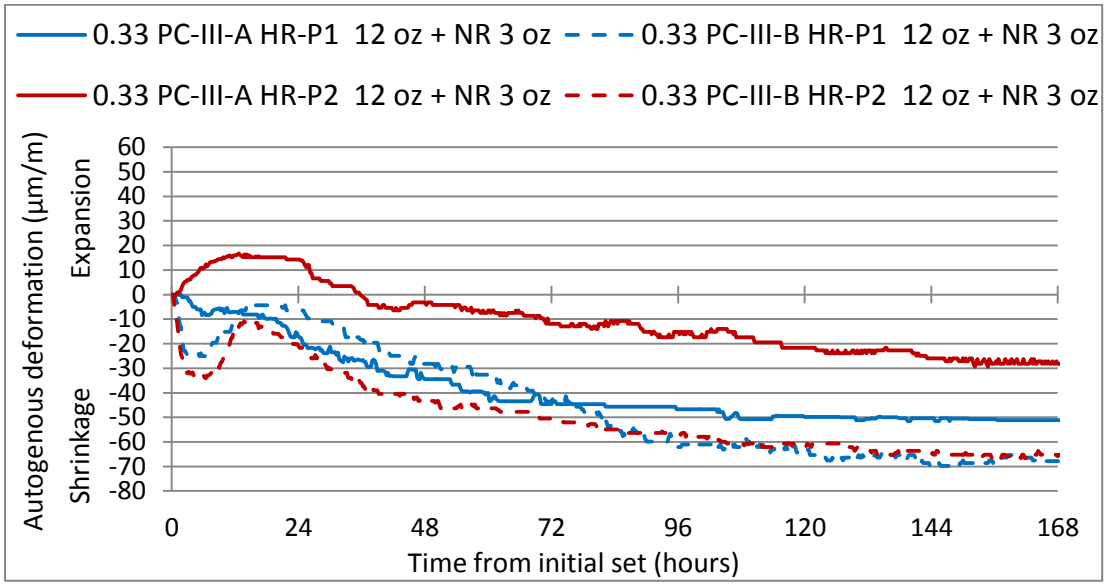

Fig. 60 Autogenous deformation curves showing the effect of cement source

It is observed that, as a general trend, mixtures with PC-III-B cement show greater autogenous shrinkage at the age of 7 days than the equivalent mixtures with cement PC-III-A. There is no apparent difference between the types of polycarboxylate-based HRWR used with PC-III-B cement, both mixtures showing the same strain value at the end of the test. On the other hand, PC-III-A mixtures showed a marked difference depending on the HRWR used. This last fact is in agreement with the results of autogenous shrinkage testing performed in cement paste, where the HR-P1 mixture also exhibited greater autogenous shrinkage than the HR-P2 mixture. However, it should be

noted that the HR-P2 concrete mixture showed an initial expansion period that lasted until 14 hours after initial set, which is principally responsible for the difference in the final shrinkage values observed between the two types of polycarboxylates. As it will be shown in the following sections, based on the information obtained from other tests, it is believed that this observed early expansion may be the consequence of particular tests conditions and may not represent the actual behavior of the mixture. It is probable that the final shrinkage of the reference PC-III-A HR-P2 mixture is somewhat higher, but still lower than the HR-P1 mixture.

One interesting observation about the PC-III-B mixtures is the behavior exhibited in the first 18 hours after initial set. It can be seen that both mixtures showed a strong shrinkage period immediately after initial setting until approximately 6 hours, followed by a strong expansion period until approximately 15 hours, finally followed by continuing shrinkage. As it will be shown in following sections, this behavior had a particular impact in the stress development.

4.4.4.2.3 Effect of cement content

Fig. 61 shows the autogenous deformation curves for w/cm 0.33, PC-III-A mixtures with different cement contents per cubic yard (611, 705 and 846 lb/yd^3).

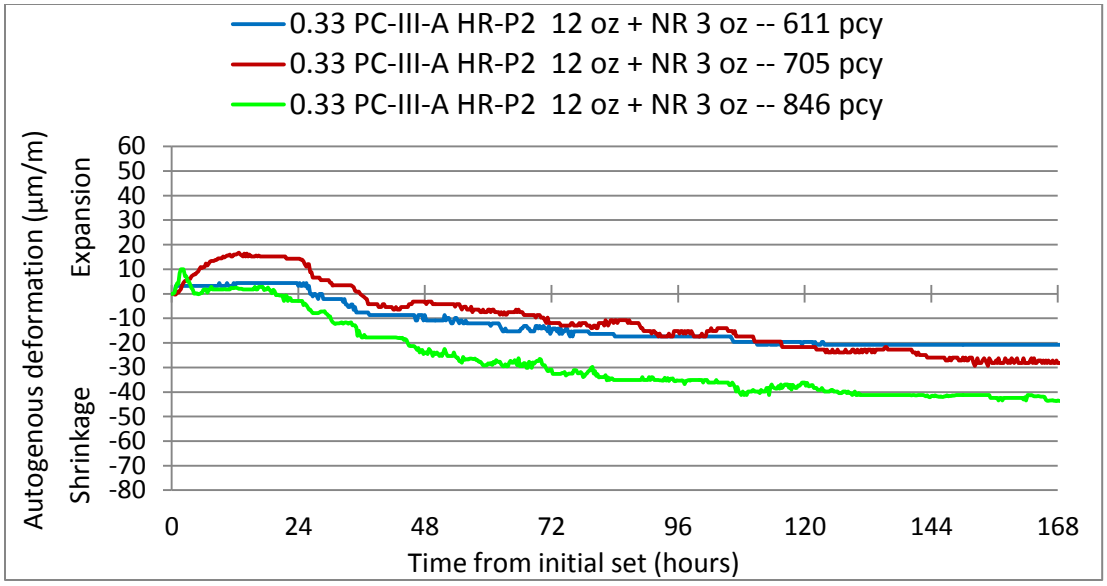

Fig. 61 Autogenous deformation curves showing the effect of cement content

It is observed that the increase in cement content per cubic yard, keeping a constant w/cm ratio, yielded a greater value of autogenous shrinkage measured at 7 days. This result was expected, since the paste content (the phase that changes volume) per cubic yard of the concrete mixture increases as the cement content is increased from 611 to 846 lb/yd^3, for the same w/cm. As the paste % of the mixture increases, less aggregate (considered to be volumetrically stable) is available to restraint the deformation.

In this comparison, it is clear that the 705 pcy mixture does not follow the trend during the first 120 hours of the test. This is a consequence of the observed high initial expansion, which is believed to be a measurement error. Following sections (FSF and RCF tests) will provide further evidence to support the fact that the measured deformation of the 705 pcy HR-P2 + NR mixture should lie closer to the 846 lb/yd^{3}curve. However, additional testing is needed to confirm this belief.

4.4.4.2.4 Effect of HRWR type

Fig. 62 shows the autogenous deformation curves for PC-III-A mixtures with different HRWR types.

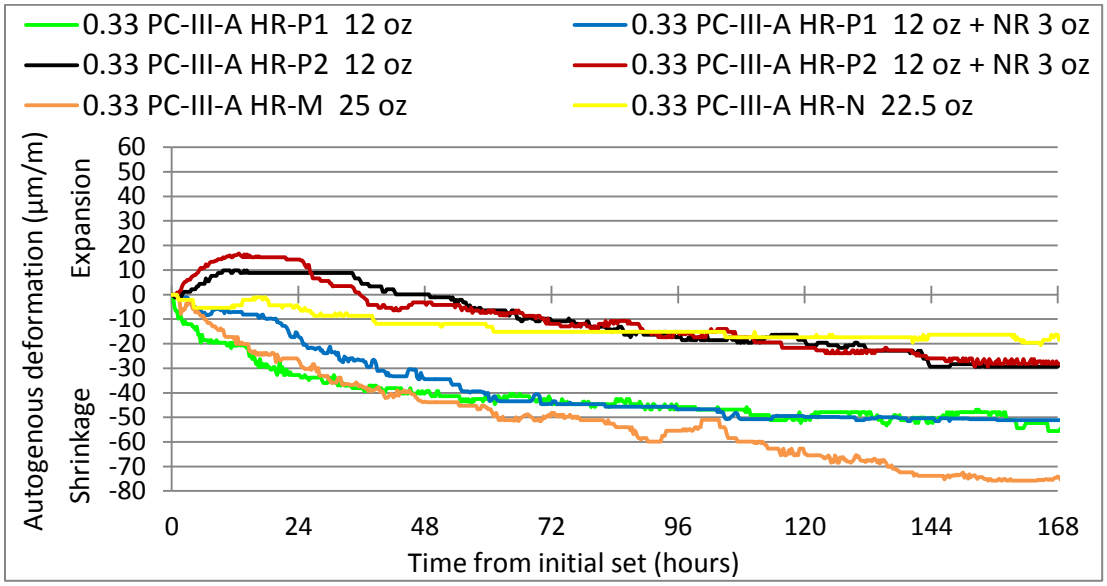

Fig. 62 Autogenous deformation curves for different HRWR types

Four different HRWRs were used: two polycarboxylate-based (HR-P1, HR-P2), a melamine-based (HR-M), and a naphthalene-based (HR-N) HRWRs. In addition, a normal range water reducing and retarding (Type D) admixture (NR) was used in conjunction with the polycarboxylate-based HRWRs, as it is a common practice in precast applications.

The HR-M mixture showed the greatest autogenous shrinkage value at the end of the test period. This agrees with the result obtained in cement paste samples, where the HR-M mixture also presented the highest autogenous strain.

Among the two polycarboxylate mixtures, HR-P1showed higher autogenous shrinkage than HR-P2, as it was mentioned before, also in agreement with cement paste test results. The simultaneous use of the NR water reducer with the polycarboxylates did not produce a difference in the final shrinkage measured, for both HR-P1 and HR-P2 mixtures. Both mixtures with HR-P2 (with and without the NR water reducer) showed an initial expansion that was not observed in the other mixtures. Based on the analysis of concrete temperature of both mixtures, it is believed that the observed expansions were caused by corresponding increases in concrete temperature that were measured during these initial hours of the test.

The HR-N mixture showed the lowest shrinkage compared to the other HRWRs. This result disagrees with the behavior observed in cement paste specimens, where the naphthalene mixture experienced more shrinkage than both polycarboxylate pastes.

4.4.4.2.5 Effect of mitigation strategies

Fig. 63 shows the autogenous deformation curves for two mitigation strategies applied to reference mixtures with 0.33 w/cm, PC-III-A cement and corresponding HR-P1+NR and HR-P2+NR water reducers. The parameters tested included the incorporation of a SRA (on both reference mixtures) and two different levels of saturated lightweight fine aggregate (FA-LW) replacement (on the HR-P2 mixture).

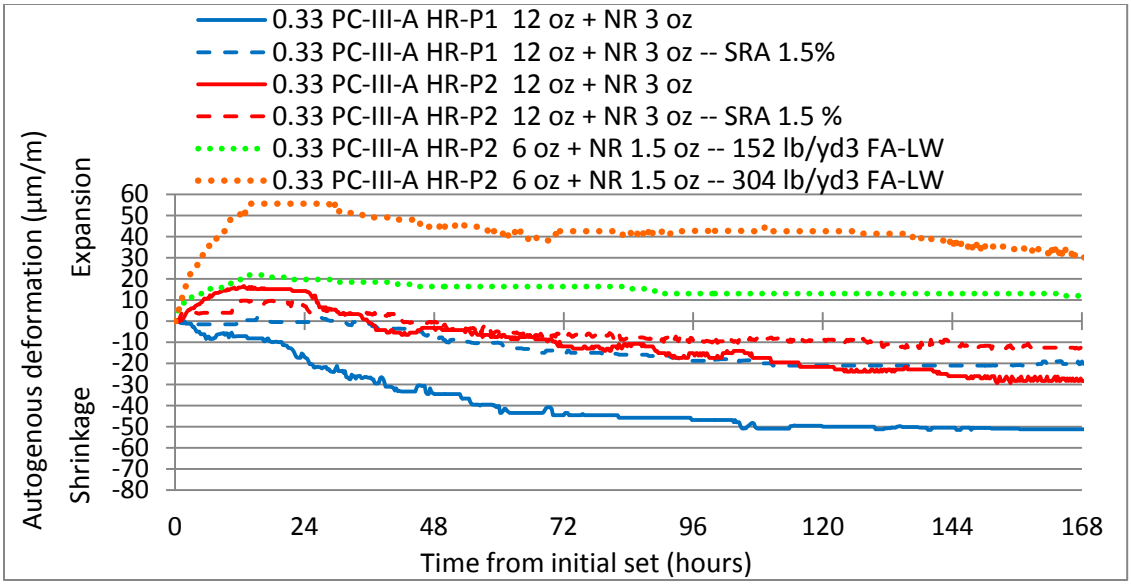

Fig. 63 Autogenous deformation curves showing the effect mitigation strategies

It is observed that both mitigation strategies reduced the autogenous shrinkage of the reference mixtures. In the case of the SRA incorporation, the reduction in shrinkage was more significant for the HR-P1 mixture than for the HR-P2 mixture. This could be a consequence of the relative position of the HR-P2 curve. As mentioned before, this mixture showed a particular initial expansion that may be related to the test variability and early sensitivity of the mixture to a change in temperature driven by the temperature control system. The fact that the initial expansion of the reference mixture without SRA was greater than the expansion measured for the SRA mixture further supports the possibility that the final shrinkage of the reference HR-P2 mixture could have been somewhat higher. Additional testing is necessary to answer this question. Nevertheless, the expected difference with respect to the presented curve should not be very significant.

The curves that incorporated the SRA (for HR-P1 and HR-P2) showed the same relative positions as the reference curves, i.e. the SRA-HR-P1 mixture exhibited greater

shrinkage than the SRA-HR-P2 mixture. The final lower shrinkage of both SRA mixtures was strongly influenced by the behavior shown immediately after initial setting. The SRA mixtures exhibited an initial period of either expansion, in the case of the SRA-HR-P2 mixture, or constant volume (with no shrinkage), in the case of the SRA-HR-P1 mixture, that was then followed by shrinkage.

The use of saturated lightweight fine aggregate caused the initial expansion of the concrete mixtures, which was followed by continuing shrinkage until the test was finished. As previously mentioned in Section 4.4.3.2.8, the pre-saturation process of the FA-LW before mixing may have affected the w/cm ratio of the LWA concrete mixtures. Both FA-LW mixtures showed net expansion at the end of the test. This effect was more substantial with the higher FA-LW replacement level (304 lb/yd^3).

4.4.4.2.6 Effect of Fly ash replacement

Fig. 64 shows the effect of the replacement of 25% fly ash for PC-III-A cement on autogenous shrinkage of concrete. A w/cm ratio of 0.33 and the same types of water reducers (HR-P2+ NR) were used. The dosage of both chemical admixtures was the same for both concrete mixtures and based on weight of cement. The fly ash mixture, having 25 % less cement per cubic yard, has therefore 25 % less total chemical admixtures per cubic yard.

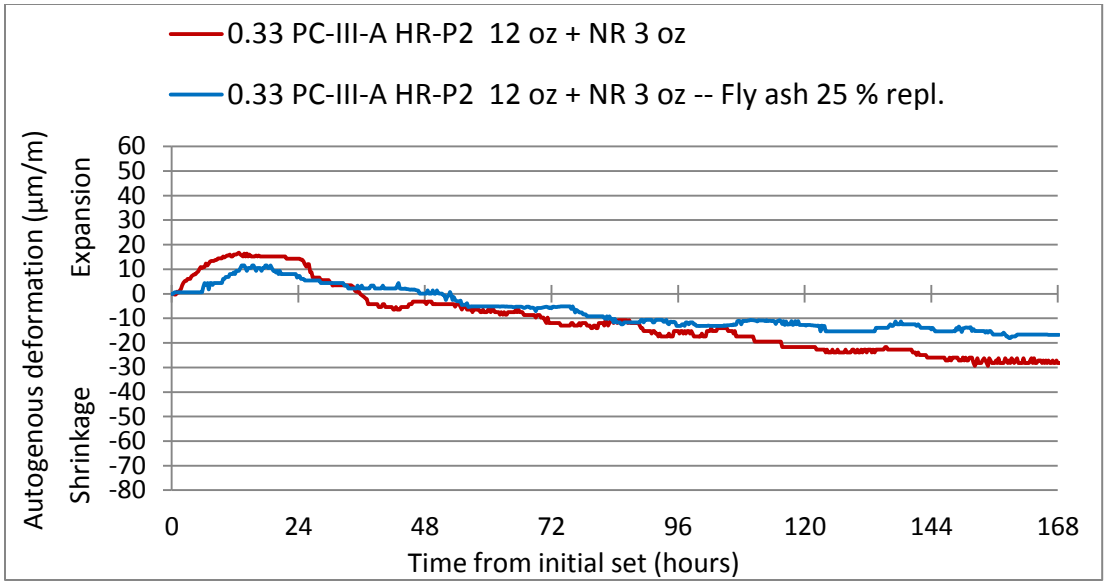

Fig. 64 Autogenous deformation curves showing the effect of fly ash replacement

It is observed that the replacement of 25 % of Class F fly ash for cement caused a reduction in the autogenous shrinkage measured until 7 days. This result was expected and it is thought to be related to the characteristics of the early hydration of the fly ash system, which differ considerably from the long-term behavior. As it was shown in the isothermal calorimetry section, the effect of Class F fly ash on early cement hydration was insignificant, resulting in lower heat evolution when normalized by cementitious material weight. The same "dilution" effect may be observed in this section, where, being the cementitious material content the same for both mixtures, the straight Portland cement mixture has a 100 % rather than 75 % of it contributing to early autogenous shrinkage. Although at later ages the fly ash will contribute to the increase in self-desiccation due to the pozzolanic reaction, it must be considered that the modulus of elasticity of the concrete will have increased also. The difference in the concrete mechanical properties may explain why, for a similar rate of self-desiccation, the

autogenous shrinkage driven by it may be lower at later ages than at early age. As a result, it may be possible that the expected long-term autogenous shrinkage of the fly ash system is lower than the straight cement concrete. However, measurements of autogenous deformation involved only the first 7 days after initial setting and more testing is needed to extrapolate these conclusions to the long term.

4.4.4.3 Summary and conclusions

Based on the results of this section the following conclusions can be made:

- No significant difference in autogenous shrinkage was found between the 0.28 and 0.33 w/cm ratio concrete mixtures. This result may be related to the lower paste (volumetrically unstable phase) content of the 0.28 mixture, consequence of keeping constant cement and coarse aggregate contents per cubic yard.
- Mixtures with PC-III-B cement showed greater autogenous shrinkage at the age of 7 days than the equivalent mixtures with cement PC-III-A. PC-III-B mixtures showed a particular behavior in the first 18 hours after initial set: both mixtures showed a strong shrinkage period immediately after initial setting until approximately 6 hours, followed by a strong expansion period until approximately 15 hours, finally followed by continuing shrinkage. As it will be shown in following sections, this behavior had a particular impact in the stress development.
- The increase in cement content per cubic yard, keeping a constant w/cm ratio, yielded a greater value of autogenous shrinkage measured at 7 days. This is

thought to be a result of the increase in the paste volume of the concrete with the increase in the cement content.

- Among the different HRWRs tested, the HR-M mixture showed the greatest autogenous shrinkage at 7 days. The HR-P1 mixture showed higher autogenous shrinkage than the HR-P2 mixture, although the difference between the two is believed to be smaller than presented. The simultaneous use of a NR water reducer with the polycarboxylates did not produce a difference in the final shrinkage measured. The HR-N mixture showed the lowest shrinkage compared to the other HRWRs, disagreeing with the results obtained in cement paste.
- The SRA incorporation effectively reduced the autogenous shrinkage of the reference mixtures. The final lower shrinkage exhibited by the SRA mixtures was strongly influenced by the non- net shrinkage behavior shown immediately after initial setting.
- The saturated lightweight fine aggregate mixtures showed net expansion at the end of the test. This effect was more significant with the higher FA-LW replacement level. These results may have been influenced by the pre-saturation process of the FA-LW before mixing.
- The replacement of 25 % of Class F fly ash for cement caused a reduction in the autogenous shrinkage measured at 7 days. This may be the result of a dilution of the cement content in the concrete mixture.

4.4.5 Restrained shrinkage tests

4.4.5.1 Procedure and experimental setup

As it was explained in Chapter 2, the testing approach selected in this research project consists in the use of a rigid cracking frame to measure the stresses in concrete due to restrained deformation, together with a free shrinkage frame to measure free autogenous deformation and the evaluation of mechanical property development.

The concrete free autogenous deformation procedure and results were presented before in Section 4.4.4. This section will focus on the restrained deformation testing and the measurement of the mechanical properties of the hardening concrete.

The procedure followed to measure the stress development by using rigid cracking frames was presented in Chapter 2. In this project, a small-scale version of the rigid frame was used for simplicity. Tests were performed in isothermal conditions at 23°C for 7 days.

Fresh concrete specimens were cast in the temperature-controlled rigid formwork. After placement and compaction of the concrete, a plastic layer was placed on the top surface of the sample. Aluminum tape was used to seal the specimen. Thermocouples were inserted into the fresh concrete in the middle section and in the crossheads and were connected to a software to control the temperature of the system. Measurements of the strain started immediately after casting.

In parallel with the RCF setup, 26 3 x 6" concrete cylinders were cast and cured following the same isothermal conditions as the rigid cracking frame specimen. The cylinders were tested at 16 hours, 1, 3, 7, and 28 days for compressive strength, splitting tensile strength and modulus of elasticity.

4.4.5.2 Testing matrix

Table 16 shows the testing matrix for the restrained shrinkage tests.

w/cm	Cement type	Admixtures				Other mixture parameters	RCF mixture ID
		Type	(floz/ 100 lb cement)	Type	(floz/ 100 lb cement)		
0.33	PC-III-A	HR-P1	12	-	-	-	1
			12	NR	3	-	2
		HR-P2	12	NR	3	-	3
			12	NR	3	SRA 1.5 %	4
			6	NR	1.5	152 lb/yd^3 LW	5
			12	NR	3	611 pcy cement	6
			12	NR	3	Fly Ash 25% repl.	7
			12	NR	3	846 pcy cement	8
		HR-N	22.5	-	-	-	9
		HR-M	25	-	-	-	10
	PC-III-B	HR-P1	12	NR	3	-	11
		HR-P2	12	NR	3	-	12

Table 16 Testing matrix for RCF tests

4.4.5.3 Results

The benefit of the methodology presented is that it allows one to know the actual stress state in the concrete throughout the duration of the test and combine it with the measured mechanical properties to evaluate cracking potential by means of the stress-to-strength ratio. In the following sections, the effect of different mixture parameters on the stress and mechanical properties developments will be analyzed.

Table 17 shows the measured mechanical properties at 16 hours, 1, 3, 7, and 28 days, the time of initial setting measured by penetration resistance (ASTM C403), the stress developed in the RCF at those specific times, and the calculated stress/strength

ratio for the concrete mixtures studied. Negative stress values indicate compression and positive values indicate tension.

RCF mixture ID	Initial setting (hr)	Age (days)	Compressive strength (psi)	Splitting Tensile strength (psi)	Modulus of elasticity (psi)	RCF Stress (psi)	Stress/ Splitting Tensile strength
1	4.4	0.68	5621	764	4451879	9	0.011
		1	6766	953	4888671	36	0.038
		3	8352	1101	5573266	162	0.147
		7	9212	1124	5836956	200	0.178
		28	9733	1180	-	-	-
2	7.0	0.67	4033	575	4066997	35	0.061
		1	6735	884	5292129	52	0.059
		3	9166	1002	6018940	129	0.129
		7	10113	1146	6097111	216	0.189
		28	10579	1346	6381222	-	-
3	8.0	0.67	3412	525	3581820	-46	-0.088
		1	6529	855	4820471	-29	-0.034
		3	9010	1045	5890877	112	0.107
		7	10204	1158	5916292	196	0.169
		28	10323	1290	6457981	-	-
4	11.0	0.67	1527	218	2788393	-23	-0.105
		1	4695	674	4771506	-45	-0.067
		3	7828	978	5948730	34	0.035
		7	8374	1037	6149249	96	0.093
		28	8876	1123	6345836	-	-
5	5.3	0.68	4162	638	3863154	-86	-0.135
		1	5682	798	4556892	-58	-0.072
		3	7238	881	5113693	74	0.084
		7	8291	1049	5318808	127	0.121
		28	8333	1065	5515676	-	-
6	8.0	0.75	4125	567	4670913	-40	-0.071
		1	6122	845	4867500	-43	-0.050
		3	7439	1112	5900763	72	0.065
		7	7975	1140	6004540	148	0.130
		28	8985	1212	6517710	-	-

Table 17 Initial setting, mechanical properties, stress developed in the RCF, and calculated stress/strength ratio for the concrete mixtures studied

RCF mixture ID	Initial setting (hr)	Age (days)	Compressive strength (psi)	Splitting Tensile strength (psi)	Modulus of elasticity (psi)	RCF Stress (psi)	Stress/ Splitting Tensile strength
7	7.3	0.69	2872	426	3617205	-23	-0.053
		1	4891	693	4761905	-12	-0.017
		3	6928	918	5241016	111	0.121
		7	7786	962	5524102	154	0.160
		28	9452	1224	6008830	-	-
8	8.8	0.90	5205	607	4793669	-5	-0.009
		1	5936	667	5008728	-4	-0.007
		2	8753	1005	6138730	117	0.116
		7	9860	1149	6480210	205	0.179
		28	11757	1175	6678144	-	-
9	4.3	0.68	5191	706	4463641	-61	-0.086
		1	6439	856	5040497	-20	-0.023
		3	7669	1008	5571844	149	0.148
		7	8464	1057	5695413	167	0.158
		28	10020	1196	6001610	-	-
10	3.9	0.69	4195	622	4464496	-17	-0.027
		1	5388	697	4966983	30	0.042
		3	6982	919	5548181	121	0.131
		7	7783	1042	5727451	242	0.232
		28	8196	1117	5991979	-	-
11	6.9	0.69	3443	523	3524467	13	0.026
		1	6410	834	4698435	-22	-0.027
		3	8781	1010	5593300	264	0.261
		7	9148	1152	5777418	265	0.230
		28	9703	1194	5931164	-	-
12	9.5	0.68	1925	341	3090351	-5	-0.015
		1	5703	718	4845482	-52	-0.073
		3	7990	1055	5754198	173	0.164
		7	8427	1104	5970074	175	0.158
		28	10032	1228	6308766	-	-

(cont.) Table 17 Initial setting, mechanical properties, stress developed in the RCF, and calculated stress/strength ratio for the concrete mixtures studied

4.4.5.3.1 Effect of HRWR type

Fig. 65 shows the stress development in the RCF for PC-III-A mixtures with different types of HRWRs.

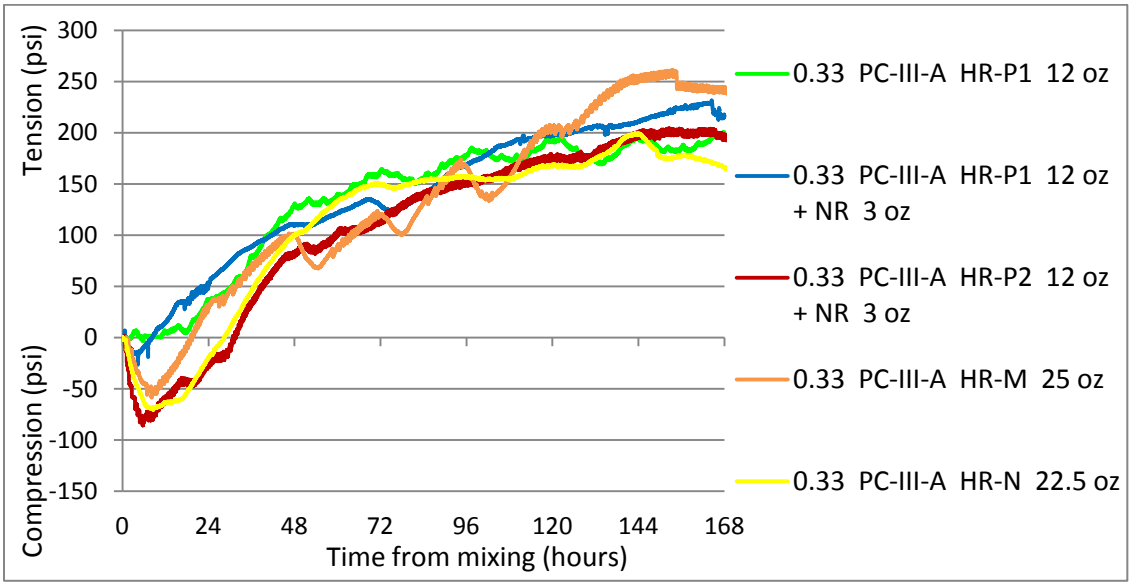

Fig. 65 Stress development for different HRWR mixtures. w/cm 0.33, PC-III-A

Four different HRWRs were used: two polycarboxylate-based (HR-P1, HR-P2), a melamine-based (HR-M), and a naphthalene-based (HR-N) HRWRs. In addition, a normal range water reducing and retarding (Type D) admixture (NR) was used in conjunction with the polycarboxylate-based HRWRs, as it is a common practice in precast applications.

It is observed that the stress development of each concrete mixture has a good correlation with the autogenous deformation measured in the FSF. When analyzing the data, it must be considered that FSF and RCF measurements start at different times. FSF measurements start at the time of initial set, while RCF start immediately after casting.

The HR-M, HR-N and HR-P2 mixtures showed significant compression at the beginning of the test. This compressive stress was much less noticeable in both HR-P1 mixtures. As self-desiccation proceeded, the subsequent restrained autogenous shrinkage caused the development of tensile stresses in all concrete mixtures. Following the same trend observed in the free shrinkage frames, the HR-M mixture developed the greatest tensile stress at the end of the test period. In further agreement with the FSF measurements, the HR-P1 mixtures showed a lower final stress than the HR-M mixture, followed by the HR-P2 and the HR-N concrete mixtures.

The analysis of the stress developed in the concrete as a result of restrained shrinkage provides a good starting point to compare the different mixtures. But in order to further evaluate the cracking potential, the development of mechanical properties (modulus of elasticity and tensile strength) must be considered, since these are the parameters that will determine the resistance to the buildup of tensile stresses. In this regard, a parameter that combines stress and strength developments needs to be determined. Fig. 66 presents graphically data showed in Table 17. The stress-to-splitting tensile strength ratio was calculated for the concrete mixtures and plotted as a function of time (from 16 hours up to 7 days). A higher stress-to-splitting tensile strength ratio indicates a higher cracking propensity.

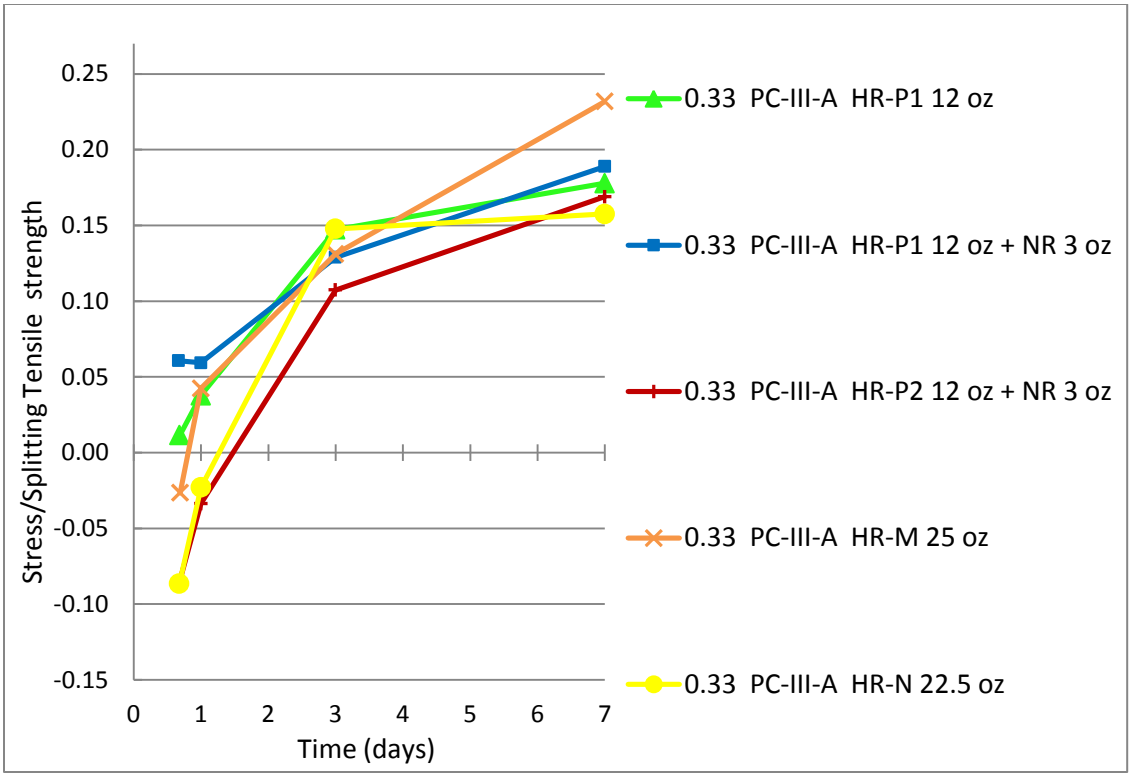

Fig. 66 Stress/Splitting tensile strength development for different HRWR mixtures

It is seen that the stress/strength ratio increased for all mixtures with time. In this case, the same trend as obtained by comparing the stress development in the RCF was observed: the melamine mixture showed the highest stress/strength ratio, followed by the HR-P1+NR mixture, the HR-P1 mixture, the HR-P2 mixture and the HR-N mixtures. The same relative behavior was observed in both analyses because the development of tensile strength was similar for all mixtures, which is equivalent to scaling all stress development curves by a similar factor.

4.4.5.3.2 Effect of different cement source

Fig. 67 shows the stress development in the RCF for equivalent mixtures prepared with PC-III-A and PC-III-B cements. The comparison is made on two set of mixtures with the same w/cm ratio and different type of polycarboxylate-based HRWR.

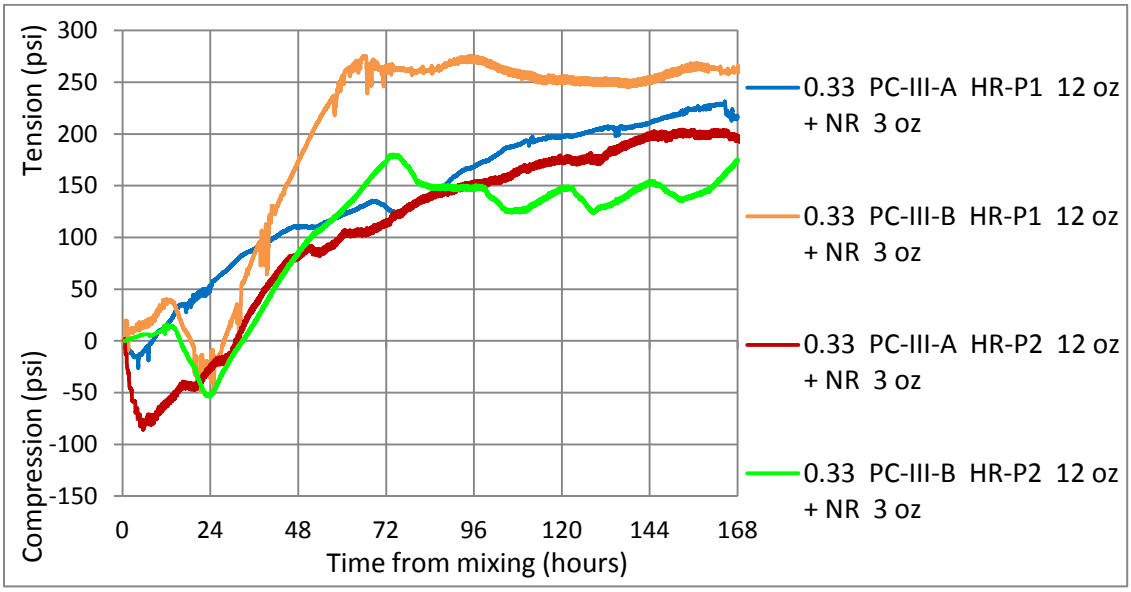

Fig. 67 Stress development for concrete prepared with different cements. w/cm 0.33, PC-III-A and PC-III-B

It is observed that the change of cement considerably changed the shape of the stress development curves. Both PC-III-B curves have the same particular shape. However, the difference between the final stresses developed by the two mixtures prepared with PC-III-B cement (HR-P1+NR and HR-P2+NR) is greater than between both PC-III-A mixtures. This does not correlate well with the final free deformation measured in the FSF at 7 days, where both PC-III-B mixtures showed very similar values. Considering that the PC-III-B HR-P2+NR mixture showed similar or slightly higher

modulus of elasticity than the PC-III-B HR-P1+NR mixture at 1, 3 and 7 days, and the fact that both mixtures experienced similar free deformation, it would be expected that the stress of the former mixture would be similar or slightly higher that the latter, without taking creep effects into account. Therefore, the difference between the two mixtures could be explained by a difference in the stress relaxation experienced by each mixture or by a simple test error. Based on the results of the other experiments performed in this project, it does not seem likely that such a significant difference between the two mixtures exists. Because of the uncertainty about the accuracy of this particular test, the PC-III-B HR-P2+NR mixture is consequently excluded from the analysis and needs to be repeated.

The PC-III-B HR-P1+NR mixture showed a higher tensile stress than both PC-III-A mixtures. This correlates well with the relative behavior in the FSF, where the PC-III-B mixture shrunk more than both PC-II-A mixtures. By looking at the modulus development, PC-III-A and PC-III-B mixtures exhibited similar values at every age.

In agreement with the behavior observed in the FSF test immediately after initial set (the PC-III-B HR-P1+NR mixture showed a strong shrinkage period immediately after initial setting that lasted 5 hours, followed by a strong expansion period for 10 hours, and then continuing shrinkage), the stress developed in the RCF shows the corresponding sharp changes in slope. Regarding this point, it must be mentioned that this mixture experienced tensile stresses since the very beginning, in contrast to most mixtures, which showed an initial pre-compression. Although the induced tensile stress is low, concrete's tensile strength is also extremely low at this time. The knowledge of the tensile strength at this very early age would have allowed us to calculate the stress/strength ratio and determine if the very low tensile strength makes it a critical point.

Fig. 68 presents the stress-to-splitting tensile strength ratio as a function of time (from 16 hours up to 7 days) for the concrete mixtures studied.

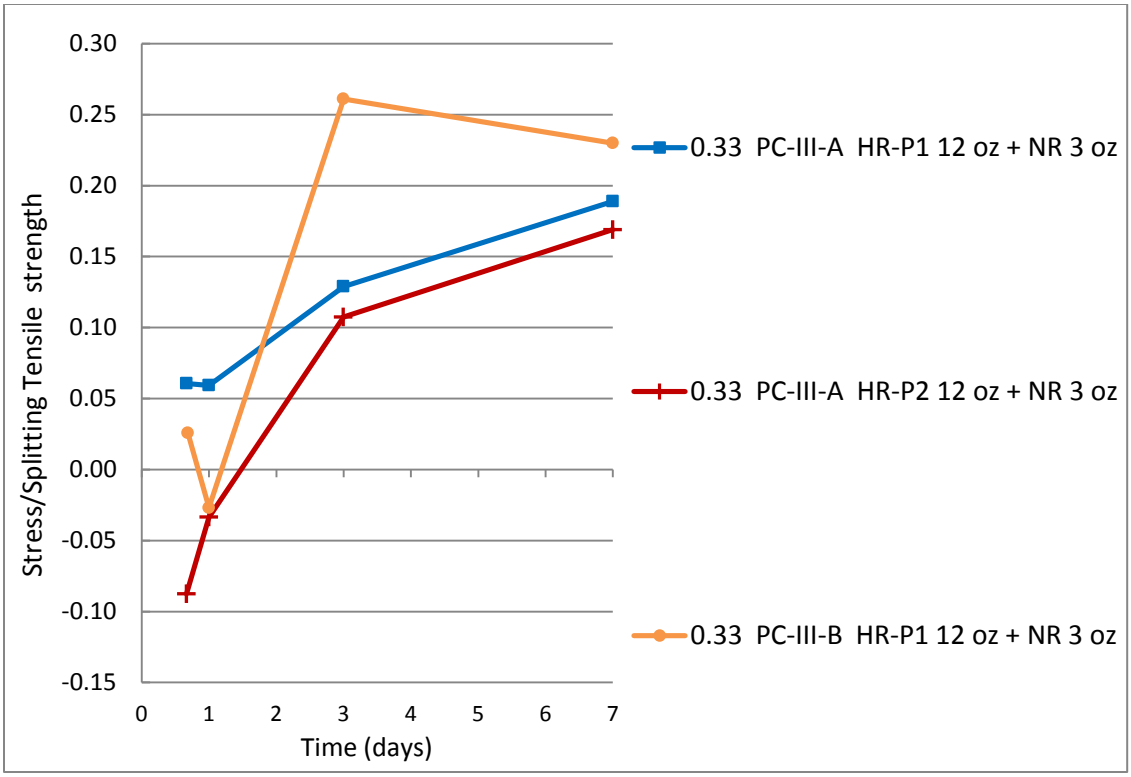

Fig. 68 Stress/Splitting tensile strength development for different cements

It is seen that the PC-III-B mixture exhibited a higher stress/strength ratio than the PC-III-A mixtures. As it was shown in the previous section, for PC-III-A mixtures the stress/strength ratio increased with time. On the other hand, the PC-III-B mixture showed a peak: the maximum stress/splitting tensile strength ratio was measured at the age of 3 days and then decreased. This was the result of the tensile stress reaching a maximum around 3 days and then remaining constant until the end of the test, and the splitting tensile strength increasing continuously with time. The same relative behavior was

observed in both analyses because the development of tensile strength was similar for all mixtures, which is equivalent to scaling all stress development curves by a similar factor.

4.4.5.3.3 Effect of cement content per cubic yard

Fig. 69 shows the stress development in the RCF for w/cm 0.33, PC-III-A mixtures with different cement contents per cubic yard (611, 705 and 846 lb/yd^3).

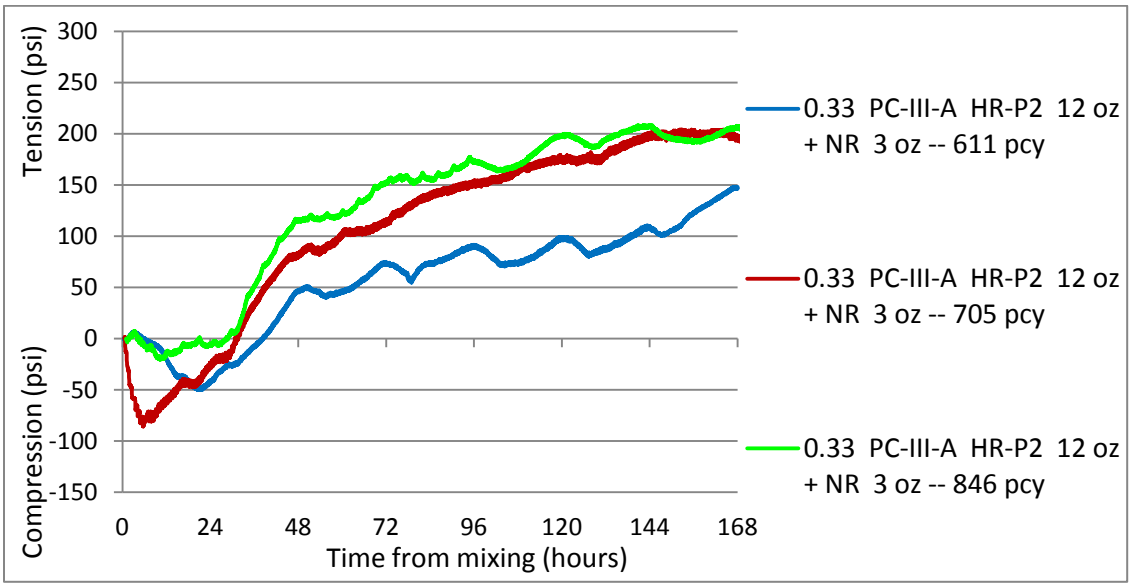

Fig. 69 Stress development for different cement content (per cubic yard) mixtures. w/cm 0.33, PC-III-A

The figure shows that the increase in cement content in the concrete mixture, keeping a constant w/cm ratio, increased the tensile stress developed. This is in good agreement with the results of autogenous deformation in the FSF, where higher autogenous shrinkage was measured as the cement content increased from 611 to 846

lb/yd^3. It is also observed that the difference was much more significant when the cement content increased from 611 to 705 lb/yd^3 than from 705 to 846 lb/yd^3.

Fig. 70 presents the stress-to-splitting tensile strength ratio as a function of time (from 16 hours up to 7 days) for the concrete mixtures studied.

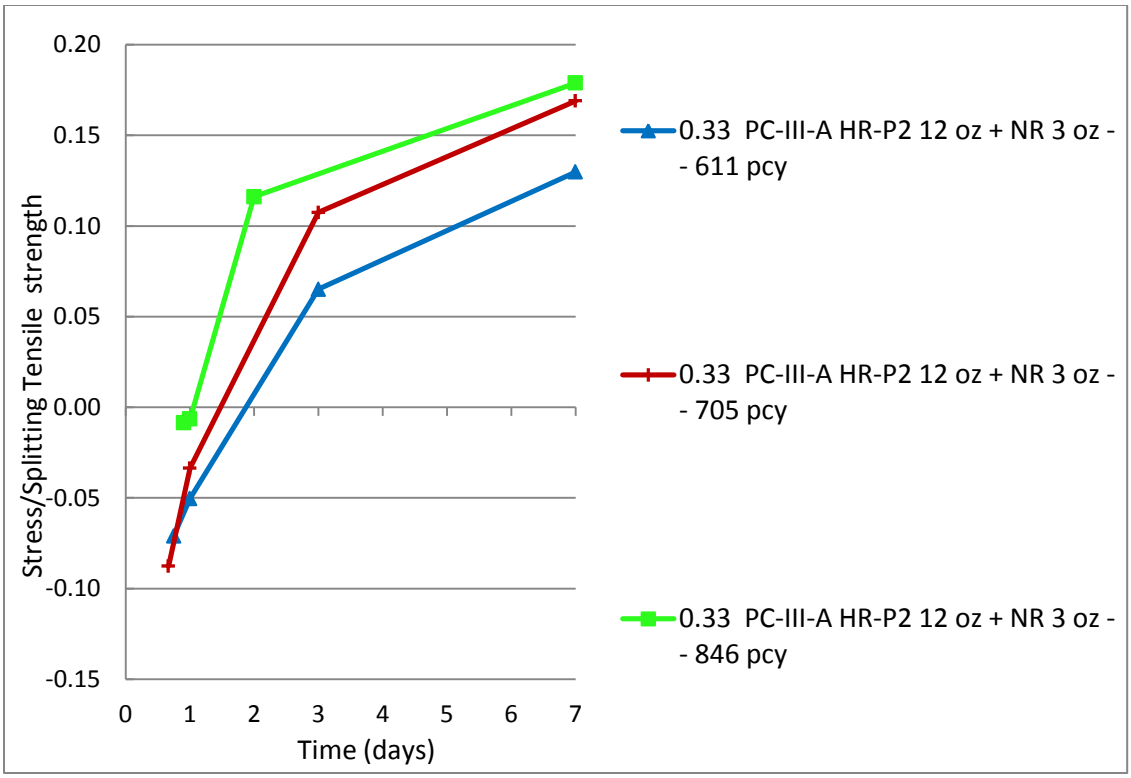

Fig. 70 Stress/Splitting tensile strength development for different cement contents

It can be clearly seen that the increase in cement content per cubic yard, keeping a constant w/cm ratio, resulted in higher tensile stress-to-splitting tensile strength ratios. The same relative behavior was observed in both analyses because the development of tensile strength was similar for all mixtures, which is equivalent to scaling all stress development curves by a similar factor.

4.4.5.3.4 Effect of mitigation strategies

Fig. 71 shows the stress development in the RCF for two mitigation strategies applied to a reference mixture with 0.33 w/cm, PC-III-A cement and HR-P2+NR water reducers. The parameters tested included the incorporation of a SRA and saturated lightweight fine aggregate (FA-LW) replacement.

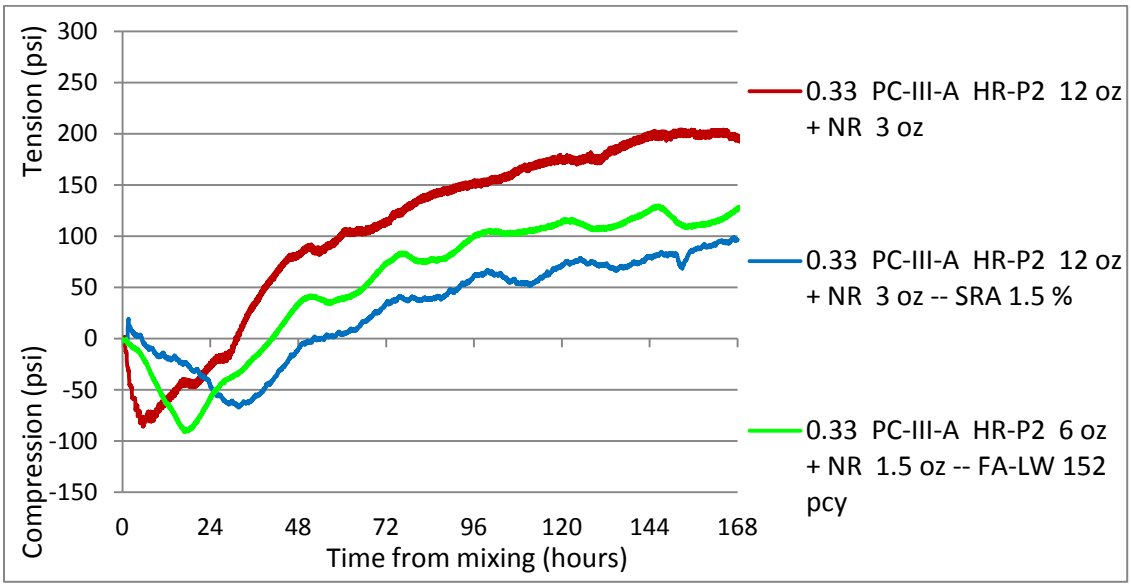

Fig. 71 Stress development for different mitigation mixtures. w/cm 0.33, PC-III-A

It is observed that both mitigation strategies reduced the stress developed by the reference mixture. For the SRA dosage and level of FA-LW replacement used in these tests, the reduction of the tensile stress was more significant in the SRA mixture than in the FA-LW mixture. Different relative behaviors may be obtained with different SRA dosages or FA-LW replacement levels. Both strategies extended the pre-compression

period experienced by the reference mixture. The SRA mixture exhibited a compression period longer than the FA-LW mixture. This fact mainly determined the difference between the final stresses of the mitigation mixtures, since the rate of tensile stress development was similar for both mixtures. As it was mentioned in previous sections, the FA-LW mixture behavior may be influenced by the pre-saturation process of the FA-LW before mixing.

Fig. 72 presents the stress-to-splitting tensile strength ratio as a function of time (from 16 hours up to 7 days) for the concrete mixtures studied.

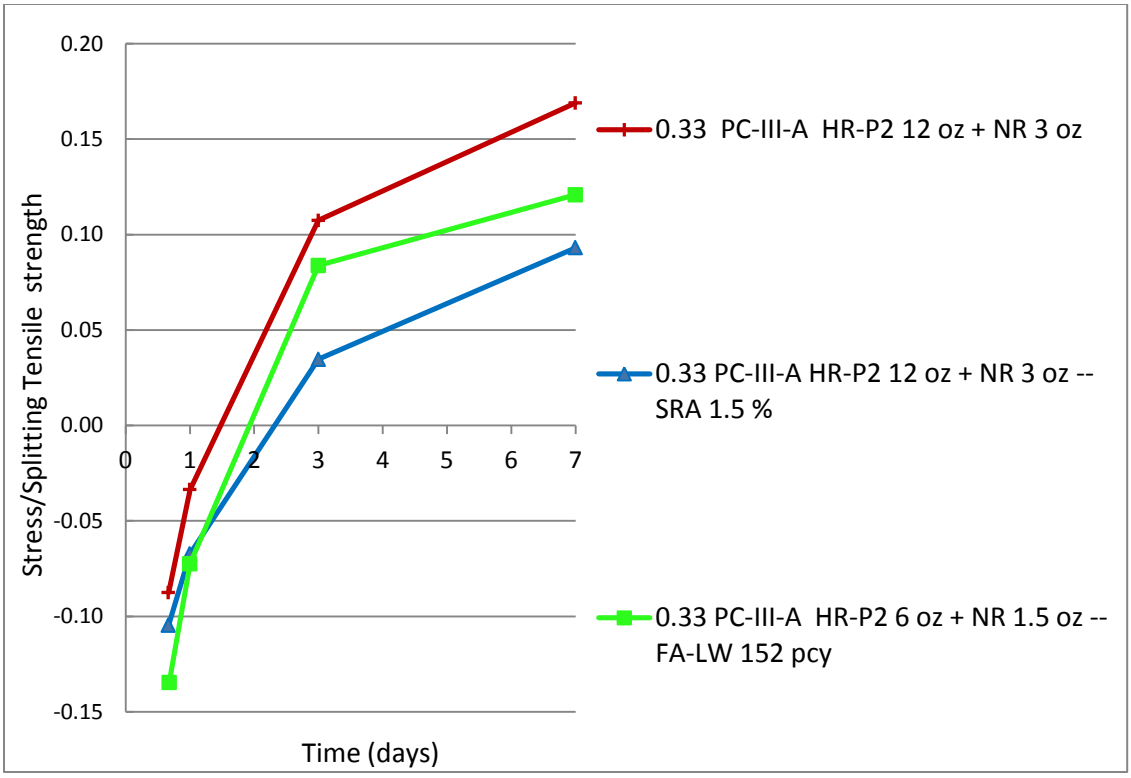

Fig. 72 Stress/Splitting tensile strength development for different mitigation mixtures

The lower splitting tensile strength of both mitigation mixtures compared to the control was more than compensated by the significant reduction in the tensile stresses developed. As a result, the same trend is observed in this figure: both mitigation mixtures showed lower stress-to-splitting tensile strength ratios, the SRA mixture being more efficient than the FA-LW mixture in reducing the tensile stress in the RCF (for the SRA dosage and FA-LW replacement level chosen in this study).

4.4.5.3.5 Effect of Fly ash replacement

Fig. 73 shows the effect of the replacement of 25% fly ash for PC-III-A cement on the stress development of concrete. A w/cm ratio of 0.33 and the same types of water reducers (HR-P2+ NR) were used. The dosage of both chemical admixtures was the same for both concrete mixtures and based on weight of cement. The fly ash mixture, having 25 % less cement per cubic yard, has therefore 25 % less total chemical admixtures per cubic yard.

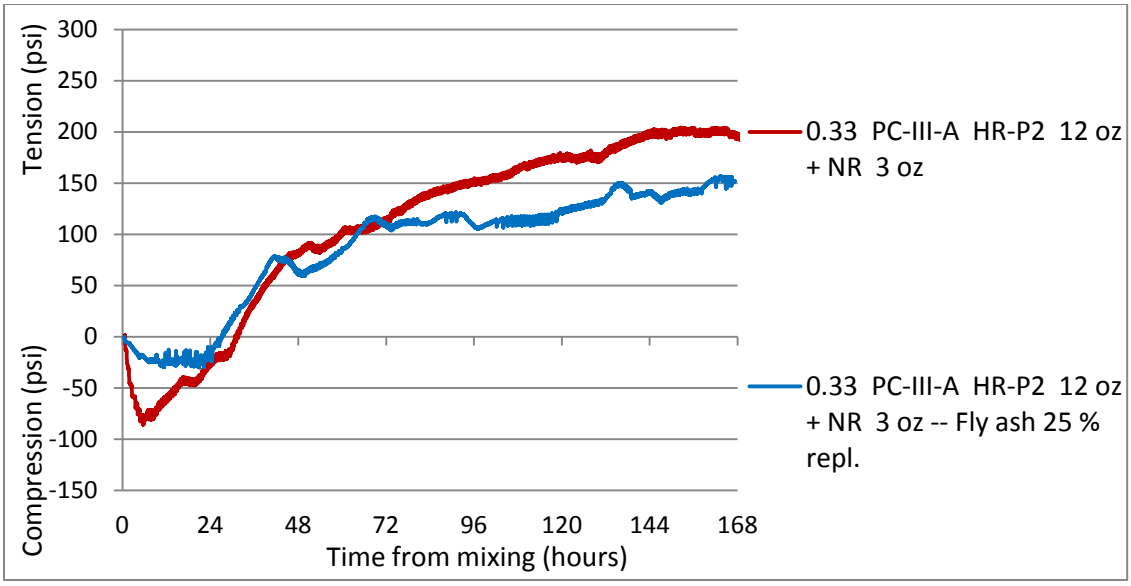

Fig. 73 Stress development curves showing the effect of 25 % fly ash replacement. w/cm 0.33, PC-III-A

In agreement with the behavior observed in the FSF tests, it is observed that the replacement of 25% fly ash for PC-III-A cement reduced the stress developed in the concrete measured until 7 days. As it was explained in the FSF section, the behavior at later ages may be different due to the pozzolanic reactivity of the fly ash.

Fig. 74 presents the stress-to-splitting tensile strength ratio as a function of time (from 16 hours up to 7 days) for the concrete mixtures studied.

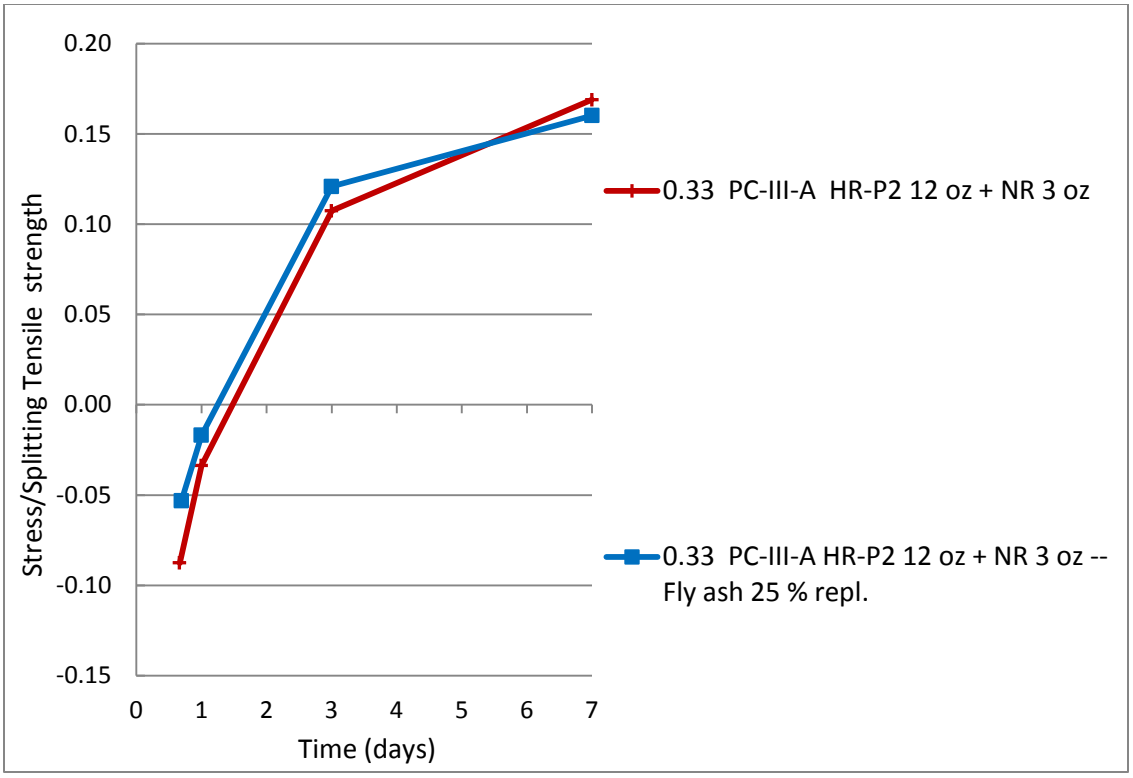

Fig. 74 Stress/Splitting tensile strength development showing the effect of 25 % fly ash replacement

Both mixtures presented similar stress-to-splitting tensile strength ratios at all ages until 7 days, which may indicate similar cracking potential in this time range. In the case where the stress was the same for both mixtures (3 days) the lower tensile strength of the fly ash mixture resulted in a higher stress/strength ratio than the control. At 7 days, the difference between the behaviors of the two mixtures observed in the RCF was less evident when comparing stress/strength ratios due to the lower tensile strength of the fly ash mixture.

4.4.5.4 Summary and conclusions:

Based on the results of this section the following conclusions can be made:

- The stress development as a result of restrained shrinkage was measured by means of RCF tests. The stress-to-splitting tensile strength ratio was calculated as an indicator of the cracking potential of the concrete mixtures.
- The stress development of each concrete mixture showed a good correlation with the autogenous deformation measured in the FSF.
- None of the mixtures tested showed cracking in the RCF during the test period of 7 days.
- Among the different HRWRs tested, the HR-M mixture developed the greatest tensile stress, followed by the HR-P1, HR-P2 and HR-N concrete mixtures. The stress/strength ratio increased for all mixtures with time. The same relative trends in stress/strength ratio were observed due to the similar splitting tensile strength development of all HRWR reference mixtures.
- The Type III cement source considerably changed the shape of the stress development curves. The PC-III-B mixtures showed tensile stresses immediately after casting, followed by a sharp change to an expansion period with compression stresses, and then another sharp transition to increasing tensile stresses until approximately the age of 3 days, when the stress plateaued. This result correlated well with the behavior observed in the FSF immediately after initial set. For PC-III-B concrete, the maximum stress/splitting tensile strength ratio was measured at the age of 3 days, in contrast to PC-III-A mixtures, which showed the maximum value at 7 days.

- The increase in cement content in the concrete mixture, keeping a constant w/cm ratio, increased the tensile stresses developed in the system and the tensile stress-to-splitting tensile strength ratio.
- Both the SRA and saturated lightweight fine aggregate incorporations reduced the stress developed in the concrete under restrained shrinkage and showed lower stress-to-splitting tensile strength ratios. Both strategies extended the pre-compression period experienced by the reference mixture. The lower splitting tensile strength of both mitigation mixtures compared to the control was more than compensated by the significant reduction in the tensile stresses developed. The reduction of the tensile stress was more significant in the SRA mixture than in the FA-LW mixture. This was related to the longer compression period experienced by the SRA mixture. The FA-LW mixture result may be influenced by the pre-saturation process of the FA-LW before mixing.
- The replacement of 25% fly ash for PC-III-A cement reduced the stress developed in the concrete measured until 7 days. Due to the lower tensile strength of the fly ash mixture, both mixtures presented similar stress-to-splitting tensile strength ratios at all ages.

Chapter 5: Field Work

5.1 INTRODUCTION

This section will focus on the field work performed in this project as a complement to the laboratory testing presented in the previous sections. As it was mentioned before, a wide set of mixtures was selected to cast exposure blocks. The objective was to have a reference for each concrete mixture subjected to outdoor conditions to analyze the time at which cracks become visible and their severity. Analogously, two visits to the TxDOT exposure site were made in order to perform a visual examination of similar concrete blocks cast between August 2010 and October 2012.

5.2 TXDOT EXPOSURE SITE VISITS

As a part of this project, two visits to the TxDOT exposure site were made. The objective was to perform a visual examination of concrete blocks cast at different precast plants in parallel with bridge girders between August 2010 and October 2012, in order to find trends and detect parameters that may have contributed to the observed distress.

5.2.1 Exposure Site description

The TxDOT Concrete Block Exposure Site is located in the Cedar Park Campus and stores more than 1500 concrete blocks, covering a broad spectrum of mixture parameters and curing conditions. The mixture designs used were based on three standard options to test for ASR and DEF. However, several parameters were modified and tested, including:

- w/cm ratio
- Cement source and type
- Cement content (lb/yd^3)
- Fly Ash replacement %
- Coarse Aggregate source
- Fine aggregate source
- Alkali Loading (Na2O eq - lb/yd^3)
- Chemical admixtures sources, types and dosages
- $LiNO_3$ incorporation and %
- Shrinkage reducing agent incorporation and dosages
- Curing time and temperature

Two different sizes of blocks were used. Blocks were instrumented to allow the monitoring of expansion. On the other hand, many no-instrumented blocks were also cast alone or in parallel with the instrumented ones.

5.2.2 Blocks examination

A total of 51 blocks were selected for visual examination. The variables considered for the selection included: w/c ratio, cement source, type and content (lb/yd^3), Class F fly ash incorporation, water-reducer source and type, aggregates sources, shrinkage reducing agent and expansive mineral additive incorporation (to produce ASTM C845 Type-K shrinkage-compensating cement).

To evaluate the condition of the blocks a rating system was established. The proposed system was based on the visual level of cracking. A 5-point scale, where 0 indicates no observable distress and 5 indicates the most severe cracking, was developed. The following pictures show examples of the different levels of cracking observed.

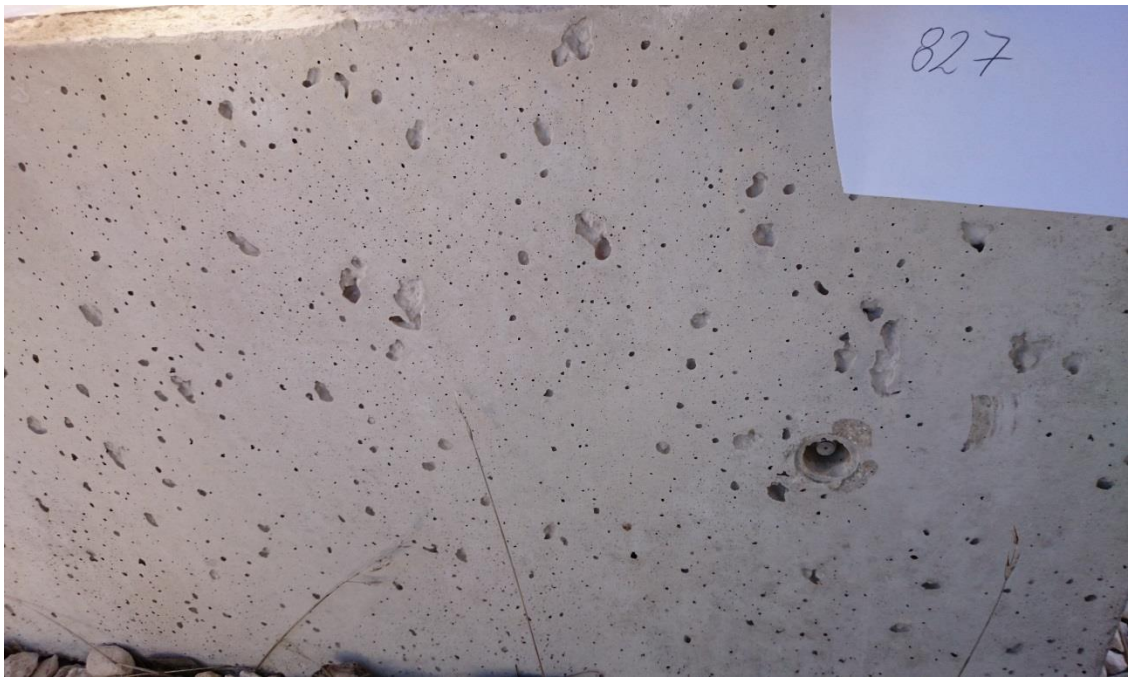

Fig. 75 Example Rating = 0

Fig. 76 Example Rating = 1

Fig. 77 Example Rating = 2

Fig. 78 Example Rating = 3

Fig. 79 Example Rating = 4

It was difficult to analyze the data and establish accurate trends due to the high number of variables in the TxDOT matrix and the limited number of samples that were examined. That fact made it hard to isolate the variable in analysis, keeping all other parameters constant. The comparisons that could be made consequently involved a very small number of mixtures and should be taken as general. A more detailed, statistical analysis with a bigger sample size should be performed in order to develop accurate conclusions.

The second visit took place 10 months after the initial visit. No substantial differences in the cracking ratings were observed between both visits. The table with the cracking rating for the blocks examined can be found in Appendix V.

Based on the observations and rating system proposed the following trends were found:

- Effect of w/c ratio: As the w/c decreased, higher distress was observed. This trend was observed for different aggregate sources and cement contents per cubic yard. An example of the determination of these conclusions is presented in Fig. 80. Each line represents a combination of mixtures where the only variable that changes is the one being analyzed, in this case, w/cm.

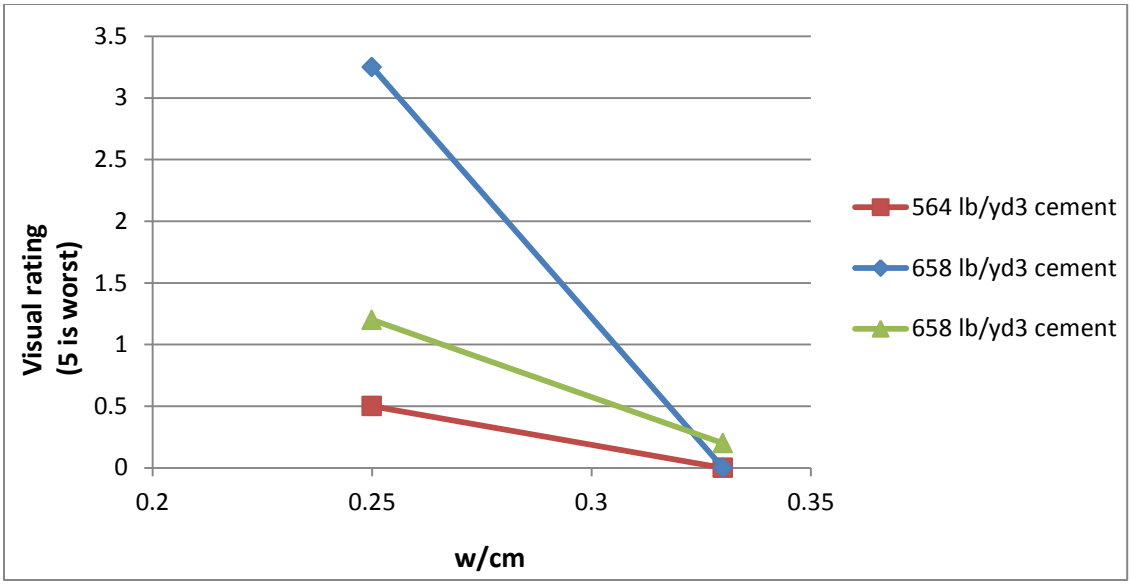

Fig. 80 w/cm effect on cracking rating

- *Effect of cement source and type:* No significant difference in cracking rating was found between PC-III-A and PC-III-B cements. PC-IP-B (Type I) cement showed better cracking rating than PC-IIIP-B (Type III).
- *Effect of cement content per cubic yard:* Higher cement content (lb/yd^3) showed worse cracking rating.
- *Effect of fly ash incorporation:* Mixtures that incorporated Class F fly ash showed better cracking rating.
- *Effect of shrinkage reducing agent + expansive mineral additive incorporation:*
    - For w/cm 0.33, 658 lb/yd^3 of PC-III-A cement, and HR-P2+NR water reducers the incorporation of a shrinkage reducing agent + expansive mineral additive resulted in a better cracking rating. Better rating was observed as the admixture dosage increased.

- For w/cm 0.33, 564 lb/yd^3 of PC-III-A cement, and HR-P2+NR water reducers the incorporation of a shrinkage reducing agent + expansive mineral additive caused the opposite effect: a worse cracking rating than the control was observed. The increase in the observed distress showed no relationship with the increase in admixture dosage.
- The mixtures that incorporated an additive to produce ASTM C845 Type-K shrinkage-compensating cement showed good cracking rating. However, the mixtures analyzed had a w/cm 0.46. One of the mixtures showed ASR cracking.

- The comparison between the cracking ratings of different water reducers was limited because most chemical admixtures had only one or two samples. A more detailed, statistical analysis with a bigger sample size should be performed in order to develop accurate conclusions.
- In the same way, a comparison between aggregate sources was not performed due to the limited number of data sets under the exact same conditions that would allow isolating the variable.

5.3 UT AUSTIN EXPOSURE SITE

As it was previously mentioned in Chapter 4, a wide set of 2 ft3 concrete blocks were cast and stored at the Construction Materials Research Group Exposure Site. Fig. 81 shows a picture of the concrete blocks cast for this project, stored at the exposure site at UT Austin.

Fig. 81 UT Austin block exposure site

The main objectives behind this idea were:

- To provide the reference for each mixture tested in the laboratory regarding the time and severity of cracking under real outdoor conditions. This will allow the research team to establish correlations between parameters measured through laboratory testing (autogenous free deformation, stress developed under restraint deformation, drying shrinkage, etc.) and cracking.
- To start building a collection of concrete specimens with mixture designs typically used in precast applications that provide cracking performance data for future projects.

5.3.1 Procedure

The exposure blocks were chosen to have a cubic shape and a volume of 2 ft3. Wood formworks were built and a protective layer of polyurethane was applied to the sides facing the concrete.

Concrete was mixed in a steel concrete mixer in a temperature-controlled room at 23 +/- 3 °C and then poured into the formwork. A single batch was prepared to cast the 2 ft3 exposure block and the drying shrinkage specimens, as mentioned before. After casting, the specimens were stored in the same temperature-controlled room at 23 +/- 3 °C covered with wet burlap and plastic film to prevent evaporation until the age of 24 hours. At that age, the block was striped and moved to the exposure site. The blocks cast during winter or when the outside temperature was very low were stored for an extra 24 hours inside the mixing room to avoid exposing them to a strong thermal gradient.

5.3.2 Mixture proportions and testing matrix

A wide set of mixtures was tested in this project. Three w/cm ratios were considered (0.28, 0.33 and 0.42).Within each w/cm ratio group of mixtures several variables were tested, which include: cement type and content, Class F fly ash replacement/addition, aggregates type, admixture type and dosage, and some mitigation measures such as the use of SRA, saturated lightweight fine aggregate and fibers. Table 11 and Table 12 in Chapter 4 presented the mixture proportions and testing matrix for concrete, showing the laboratory tests performed in parallel with each exposure block.

5.3.3 Results

Table 12 shows the date each block was cast. Until the present day only 5 mixtures have shown cracking. Table 18 shows the up-to-day data regarding the performance of the blocks.

w/cm	Cement type	Admixtures				Other mixture parameters	Cast date	Cracking rating
		Type	(floz/ 100 lb cement)	Type	(floz/ 100 lb cement)			
0.28	PC-III-A	HR-P2	12	-	-	-	1/16/2014	0.5
			12	NR	3	-	3/19/2014	0.25
0.29	PC-III-A	HR-P1	15	NR	3	-	2/4/2014	0.4
		HR-P3	15	NR	3	-	2/4/2014	0.4
0.30	PC-III-A	HR-P2	12	NR	3	-	1/21/2014	0.5

Table 18 Blocks showing cracking at UT Austin exposure site

It should be noted that the first blocks that showed cracking were all low w/cm mixtures in the range of 0.28 to 0.3. It should be mentioned that any comparison or conclusion must be made considering the age of blocks. All blocks will continue to be regularly monitored for cracking as a part of an ongoing project and the information will be updated.

5.4 SUMMARY AND CONCLUSIONS:

Based on the results of this section the following conclusions can be made:

- Two visits to the TxDOT exposure site were made to perform a visual examination of concrete blocks cast at different precast plants in parallel with

bridge girders between August 2010 and October 2012. A total of 51 blocks were selected for visual examination.

- In order to evaluate the condition of the blocks a cracking rating system was established.
- It was difficult to establish accurate trends due to the high number of variables in the TxDOT matrix and the limited number of samples that were examined. The comparisons that could be made consequently involved a very small number of mixtures and should be taken as general. A more detailed, statistical analysis with a bigger sample size should be performed in order to develop accurate conclusions.
- Based on the observations at the TxDOT exposure site and rating system proposed the following trends were found:
    - As the w/cm decreased, higher distress was observed.
    - No significant difference in cracking rating was found between PC-III-A and PC-III-B cements. PC-IP-B (Type I) cement showed better cracking rating than PC-IIIP-B (Type III).
    - Higher cement content (lb/yd^3) mixtures showed worse cracking rating.
    - Mixtures that incorporated Class F fly ash showed better cracking rating.
    - The incorporation of shrinkage reducing agent / expansive mineral additive showed inconsistent/unsystematic results.
    - Comparison between the cracking ratings of different water reducers and between different aggregate sources were not performed due to the limited number of data sets under the exact same conditions that would allow isolating the variable.

- A wide set of 2 ft3 concrete blocks were cast and stored at the Construction Materials Research Group Exposure Site starting in January, 2014. Until the present day only 5 mixtures have shown cracking.

Chapter 6: Conclusions

This thesis has presented the experimental approach followed to evaluate the influence of different mixture parameters on sources of volume changes of precast prestressed concrete mixtures. In addition, a smaller set of tests was performed to assess the cracking potential of the same concrete mixtures used for bridge girders production.

Chemical shrinkage of cement paste was determined using an automated version of ASTM C1608. Autogenous deformation of cement paste specimens was measured using the volumetric (membrane) method. The heat of hydration of cement pastes was determined by isothermal calorimetry. In addition, drying shrinkage of 1 day-cured concrete specimens was measured as indicated by ASTM C157. Autogenous free deformation of concrete was determined using a Free Shrinkage Frame. This last experimental procedure was executed for a smaller group of mixtures in parallel with a Rigid Cracking Frame that measured the stress development due to restrained deformation, and the determination of mechanical properties development.

As a complement to the laboratory testing, field work was performed in this project. A wide set of mixtures was selected to cast exposure blocks in order to have a reference concrete member for each mixture subjected to real outdoor conditions. The time at which cracks become visible and their severity were and are currently being analyzed. Analogously, two visits to the TxDOT exposure site were made in order to perform a visual examination of similar concrete blocks cast between August 2010 and October 2012. A cracking rating was defined.

Based on the results presented, the following conclusions can be extracted:

- The influences of different mixture proportions and materials on sources of volume changes have been analyzed and presented. It was observed that different mixture parameters affect each mechanism of volume change in different ways. In particular, no clear correlations could be found between the three types of tests performed in paste samples. In addition, the relative weights of the parameters evaluated were different when the same property was tested in paste or in concrete specimens.
- By the time cracking has been observed the mechanisms studied in this project, which contribute to the volume change, have already reached a steady-state. This means that we can compare the measured values of long-term total shrinkage. The mixtures that have exhibited the earliest and worst cracking are not the ones that have shown the highest total shrinkage. This result clearly shows that the evaluation of the cracking potential of the concrete mixtures cannot be based only on strain measurements.
- It is clear that none of the particular tests on volume changes (either at early ages or in the long term) by itself has provided a definite answer regarding the cracking occurrence. The consequent cracking seems to be the sum of the different mechanisms driving the volume change. In this regard, the combination of early age and long term analysis is critical.
- The relative weight of autogenous to total shrinkage seems to be a very important parameter among the mixtures considered in this study. The mixtures that showed the lowest autogenous/total shrinkage ratios have also shown the best cracking performance based on the observation of exposure blocks. This indicates that autogenous shrinkage may play a major role in the distress observed. The autogenous fraction of total shrinkage was reduced when a mitigation measure

was applied (incorporation of SRA, saturated lightweight fine aggregate), when the cement content was reduced or partially replaced by Class F fly ash, and with the use of a naphthalene-based superplasticizer.

- The analysis of the stress developed in the concrete as a result of restrained shrinkage coupled with the development of mechanical properties (modulus of elasticity and tensile strength) provided direct quantitative data regarding cracking potential. A parameter that combined stress and strength developments was determined. Although no cracking was observed in the restrained tests for any concrete mixture, they provided with valuable data about the relative behavior of mixtures that incorporated different parameters. The stress development of each concrete mixture showed a good correlation with the autogenous deformation measured in the FSF. The mixtures that showed the highest autogenous shrinkage also showed the highest stress developments. It should be remembered that the cracking frame tests were performed in autogenous conditions. These tests did not capture thermal or external drying effects.
- A next step in the investigation would be to run similar restrained shrinkage tests under time-temperature histories simulating different environmental and boundary conditions. It is desirable to link the early age and long term behaviors. The measurement of stress and strength developments for longer periods of time and under unsealed conditions would provide valuable data.
- Carbonation shrinkage should be also analyzed as it may represent an extra contributing factor in the long term.

Appendix I: Chemical Shrinkage curves

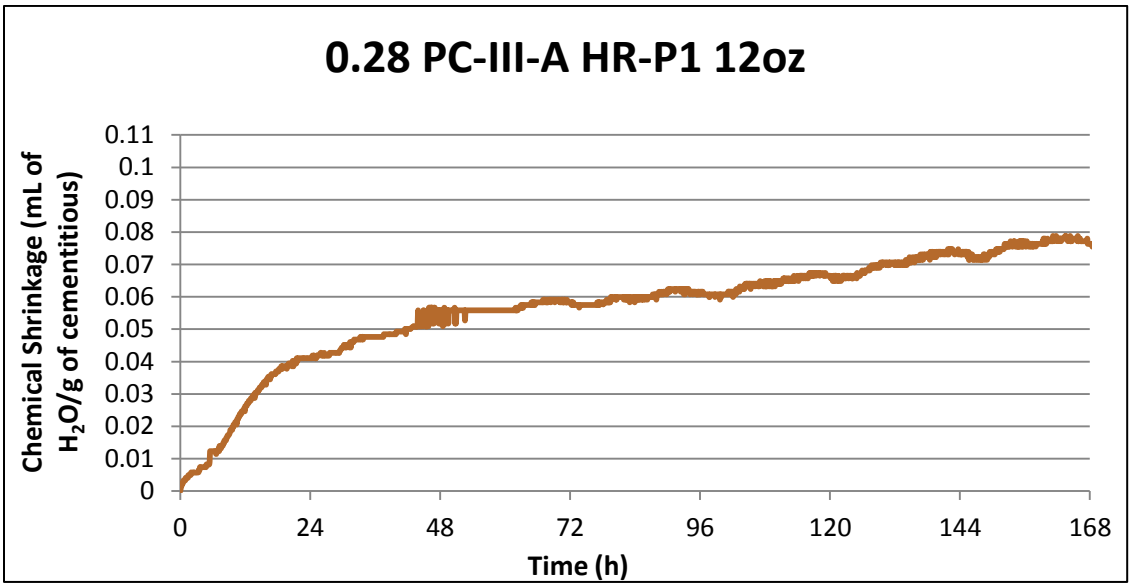

Fig. 82 Chemical Shrinkage 0.28 PC-III-A HR-P1 12oz

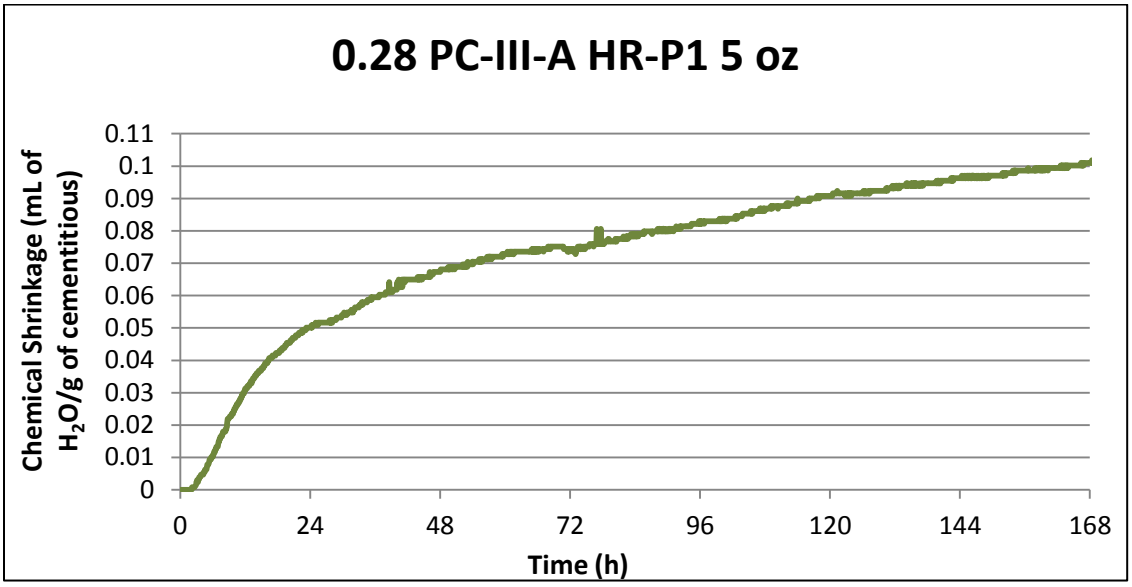

Fig. 83 Chemical Shrinkage 0.28 PC-III-A HR-P1 5 oz

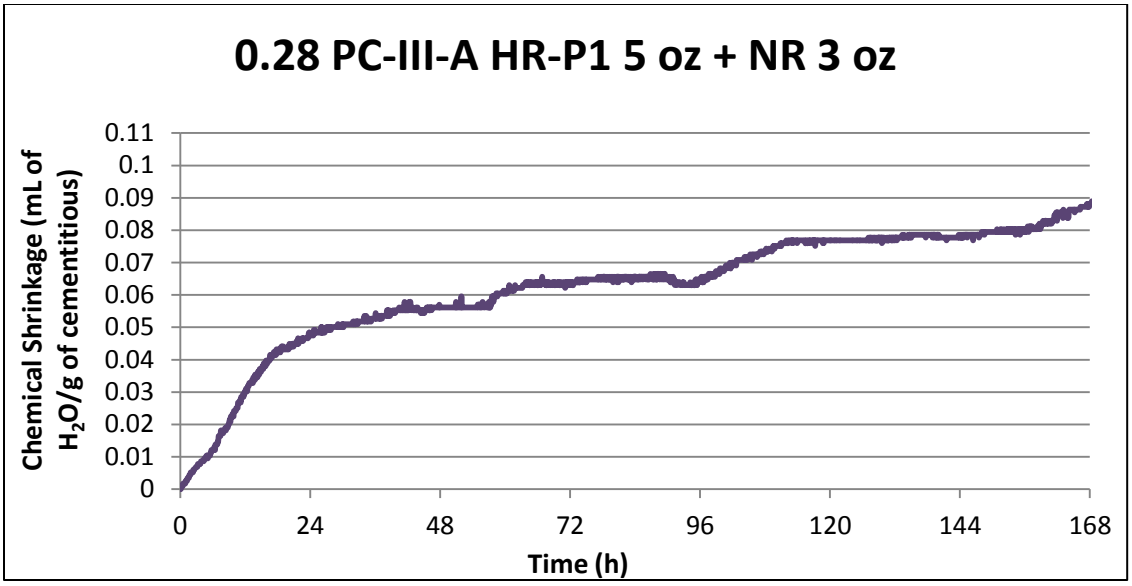

Fig. 84 Chemical Shrinkage 0.28 PC-III-A HR-P1 5 oz + NR 3 oz

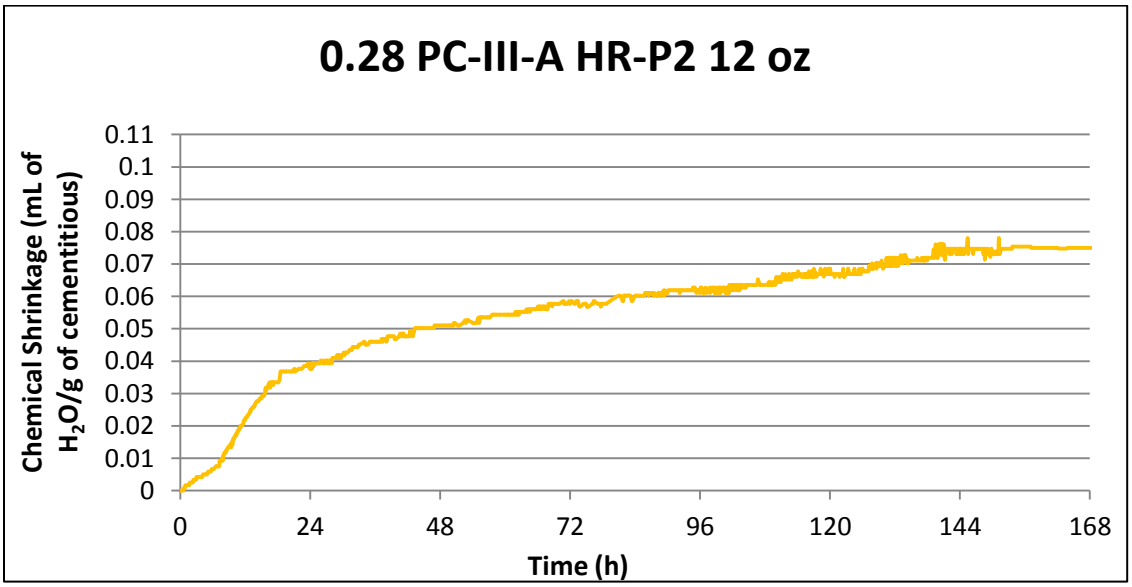

Fig. 85 Chemical Shrinkage 0.28 PC-III-A HR-P2 12 oz

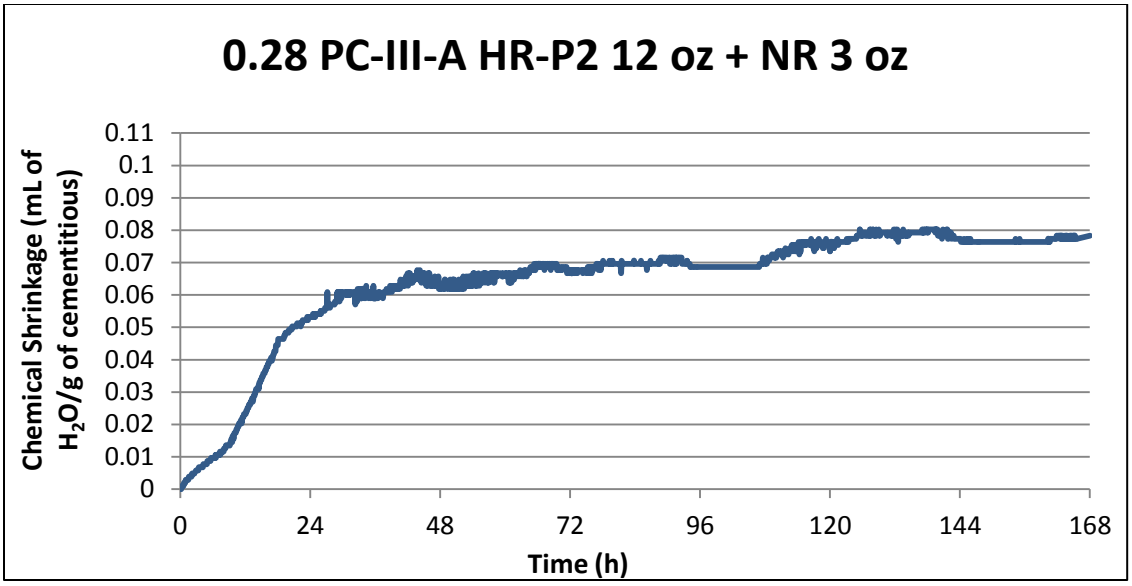

Fig. 86 Chemical Shrinkage 0.28 PC-III-A HR-P2 12 oz + NR 3 oz

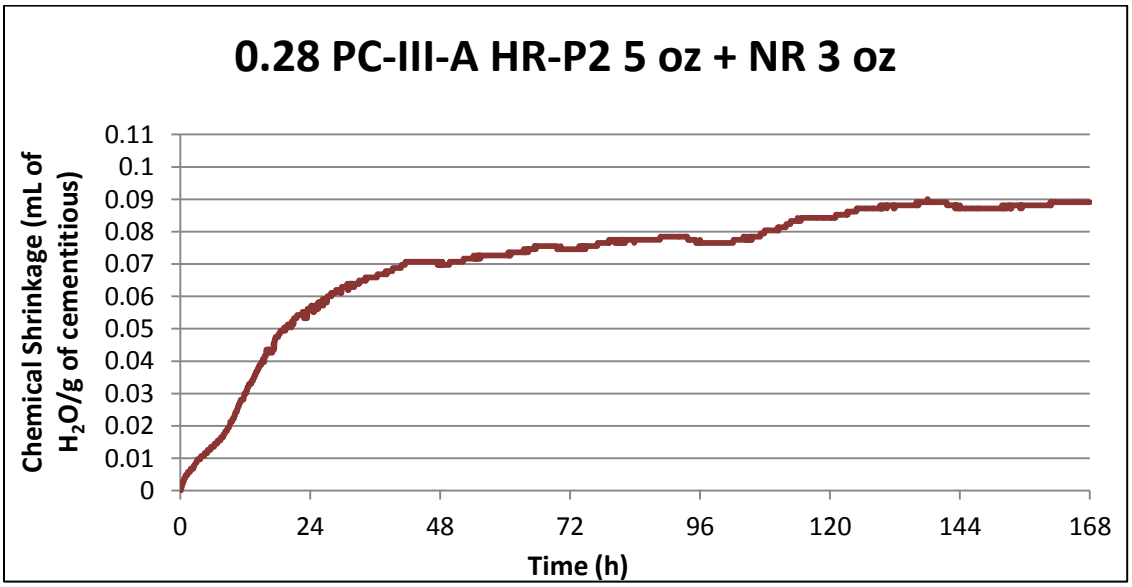

Fig. 87 Chemical Shrinkage 0.28 PC-III-A HR-P2 5 oz + NR 3 oz

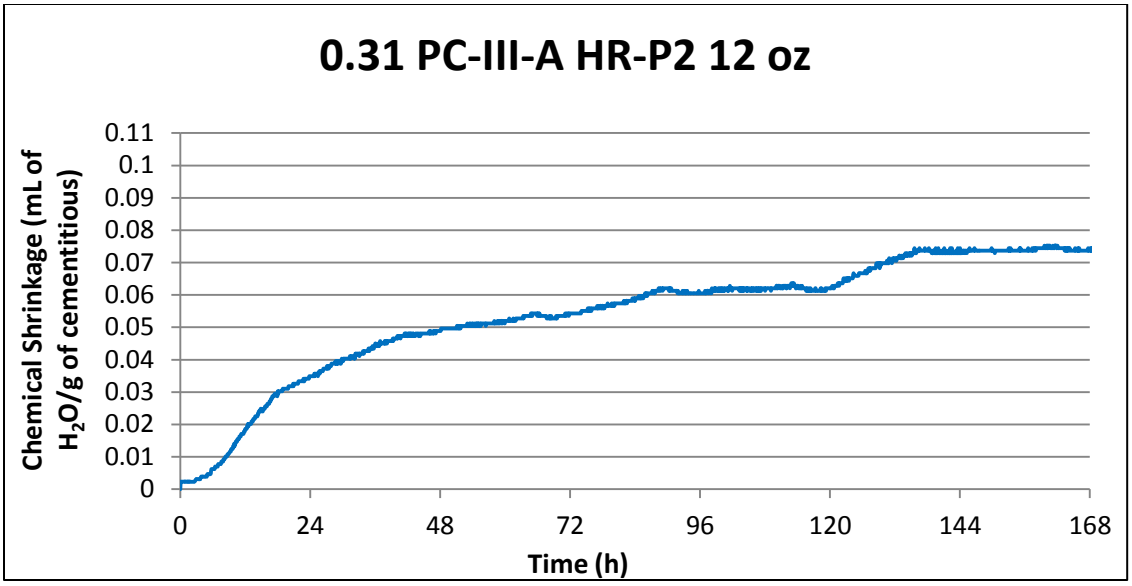

Fig. 88 Chemical Shrinkage 0.31 PC-III-A HR-P2 12 oz

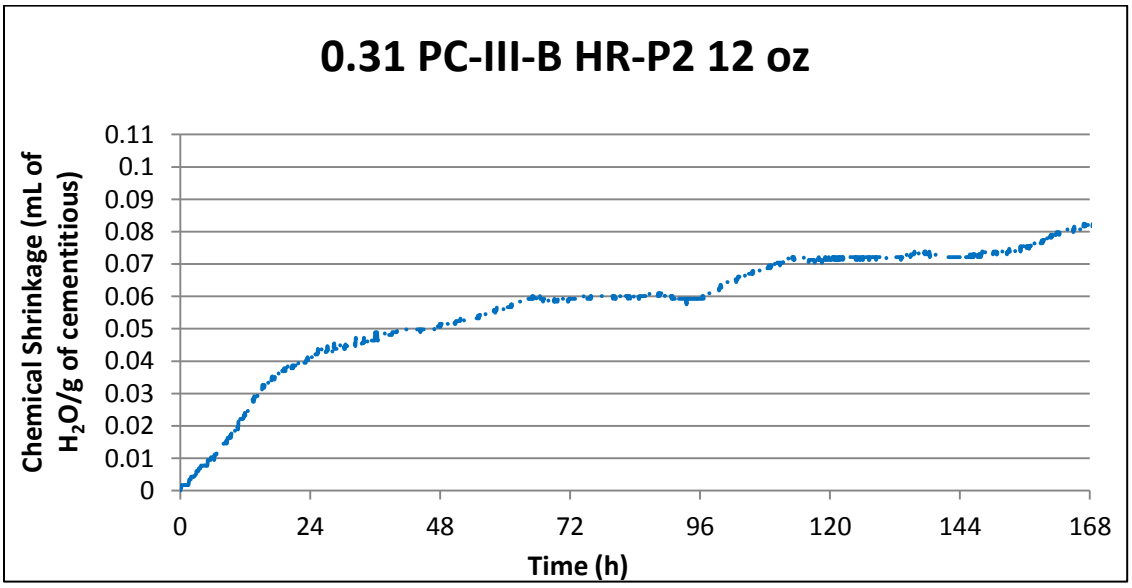

Fig. 89 Chemical Shrinkage 0.31 PC-III-B HR-P2 12 oz

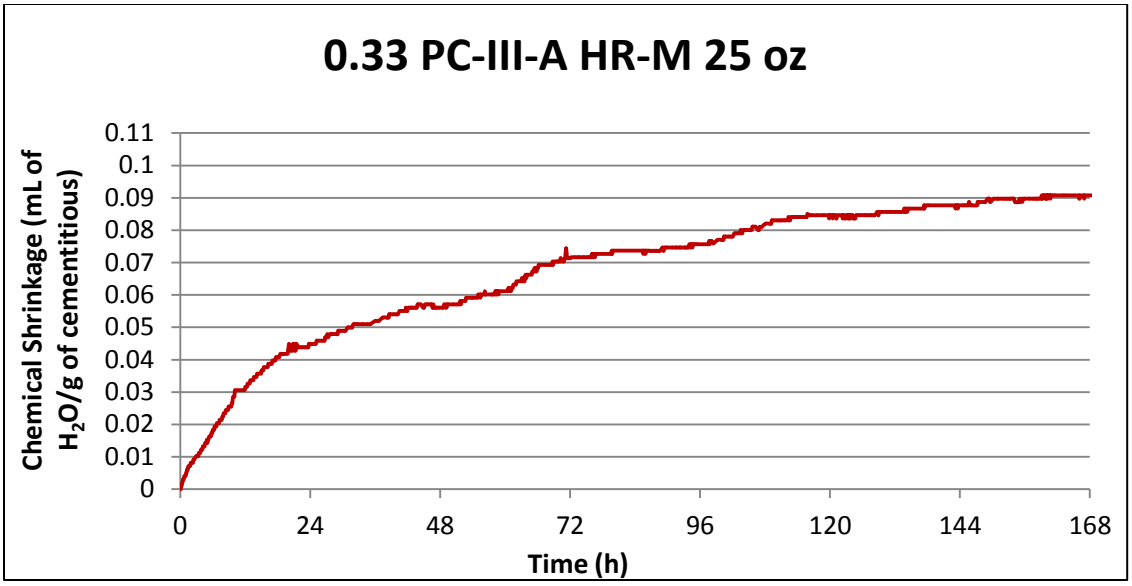

Fig. 90 Chemical Shrinkage 0.33 PC-III-A HR-M 25 oz

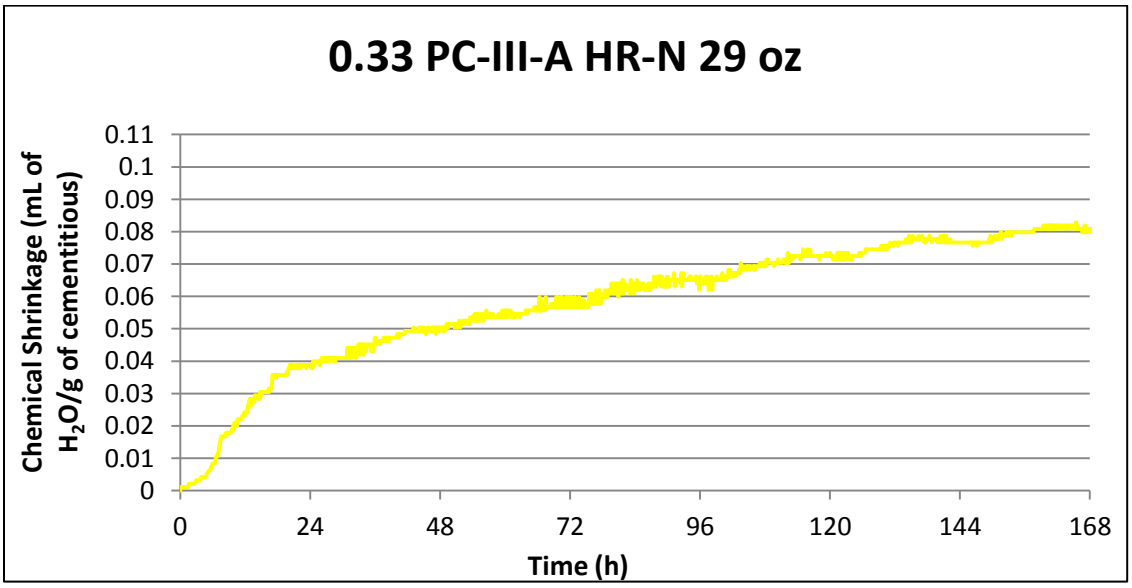

Fig. 91 Chemical Shrinkage 0.33 PC-III-A HR-N 29 oz

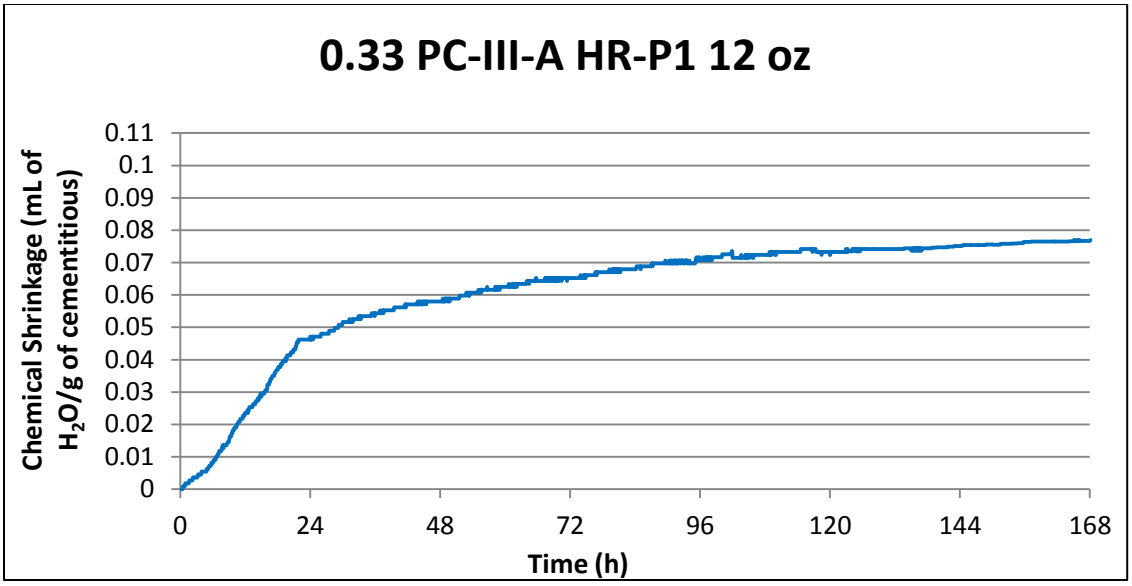

Fig. 92 Chemical Shrinkage 0.33 PC-III-A HR-P1 12 oz

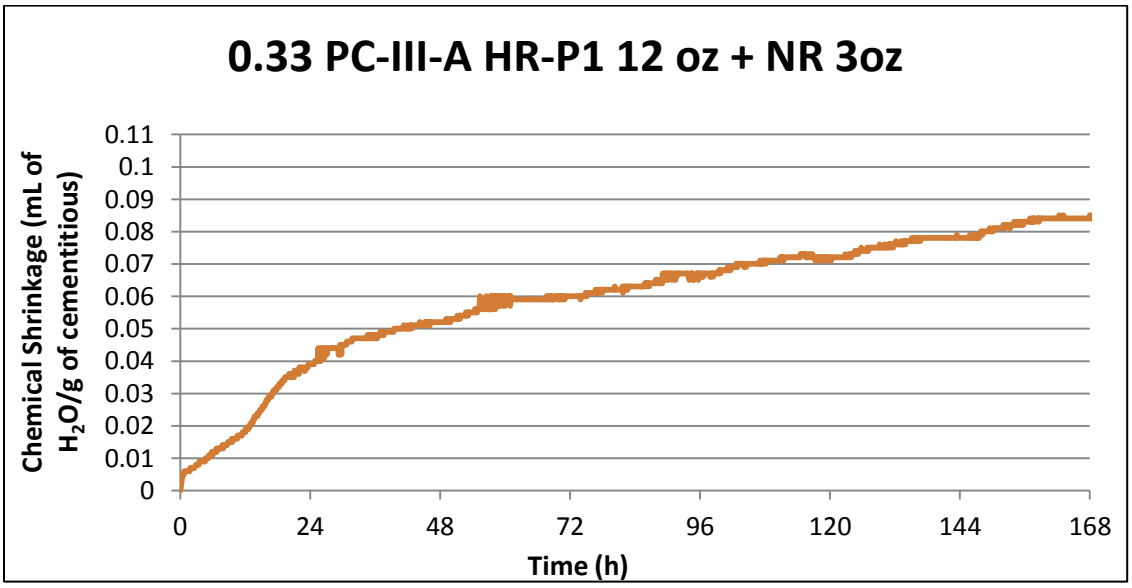

Fig. 93 Chemical Shrinkage 0.33 PC-III-A HR-P1 12 oz + NR 3oz

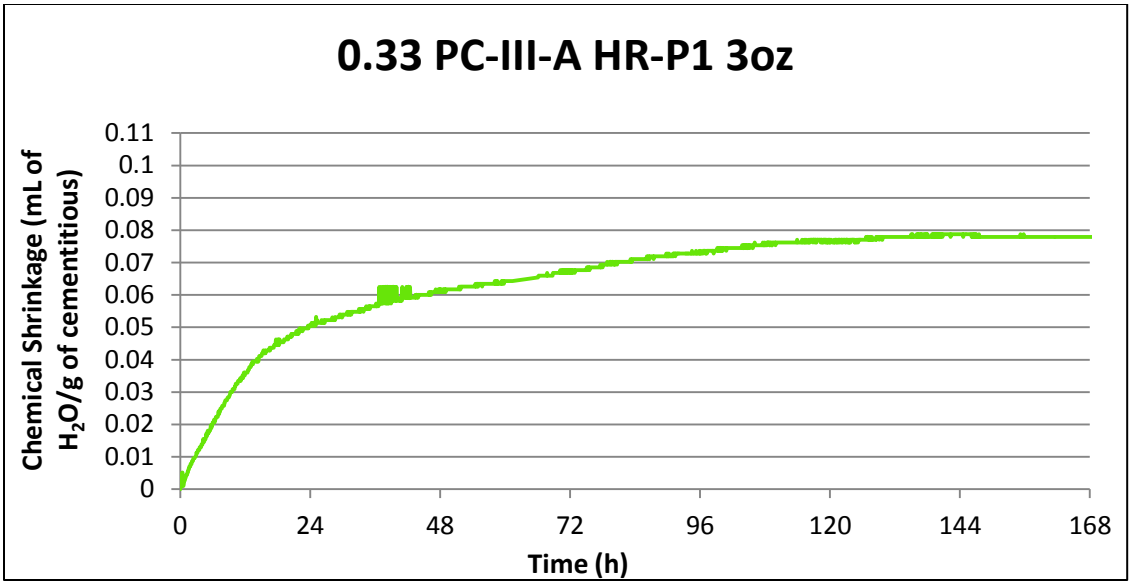

Fig. 94 Chemical Shrinkage 0.33 PC-III-A HR-P1 3oz

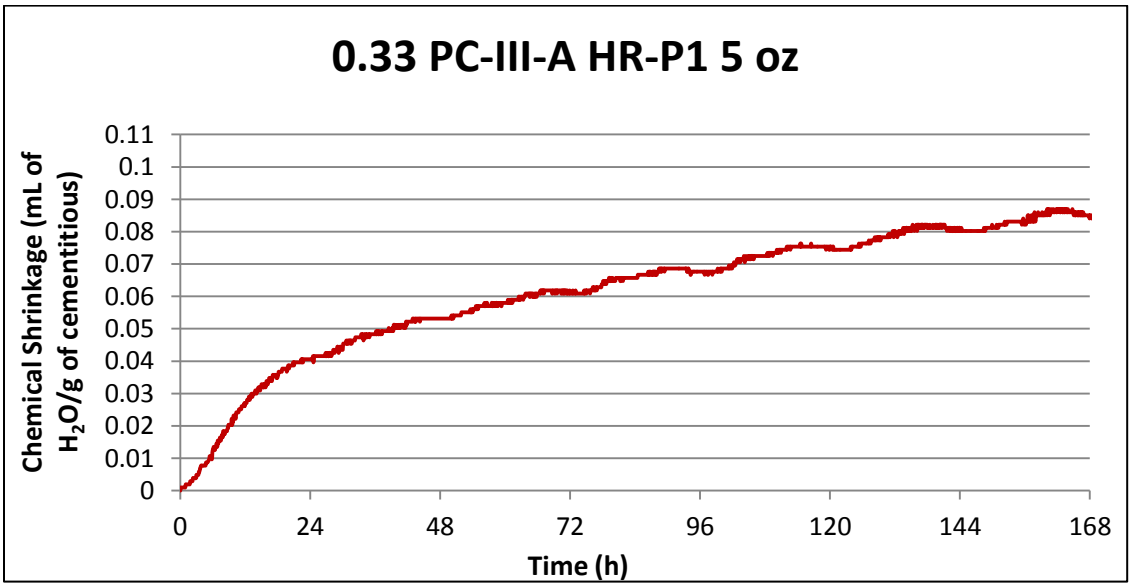

Fig. 95 Chemical Shrinkage 0.33 PC-III-A HR-P1 5 oz

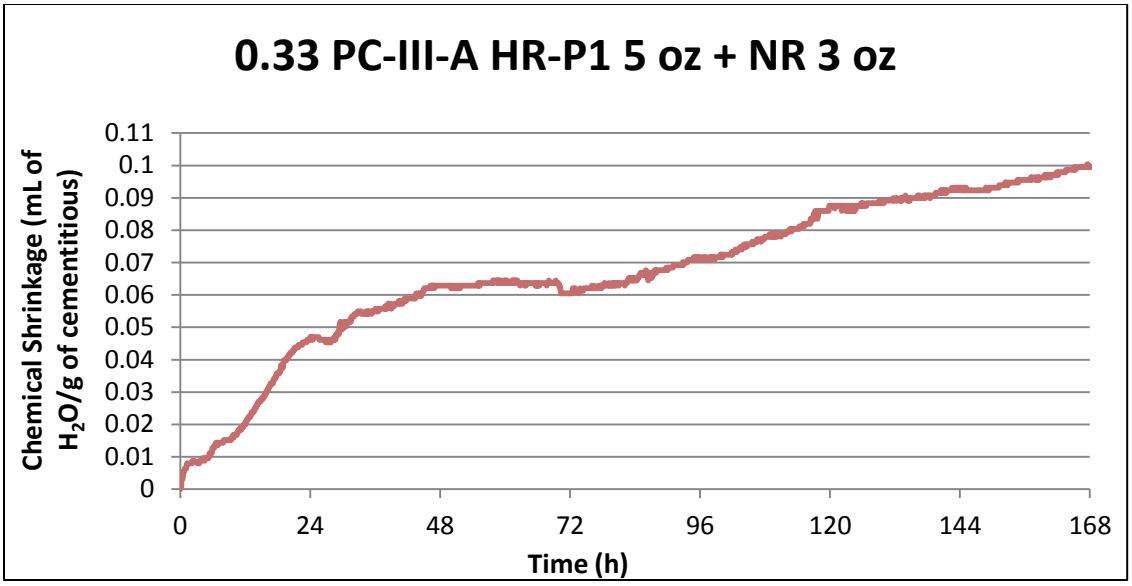

Fig. 96 Chemical Shrinkage 0.33 PC-III-A HR-P1 5 oz + NR 3 oz

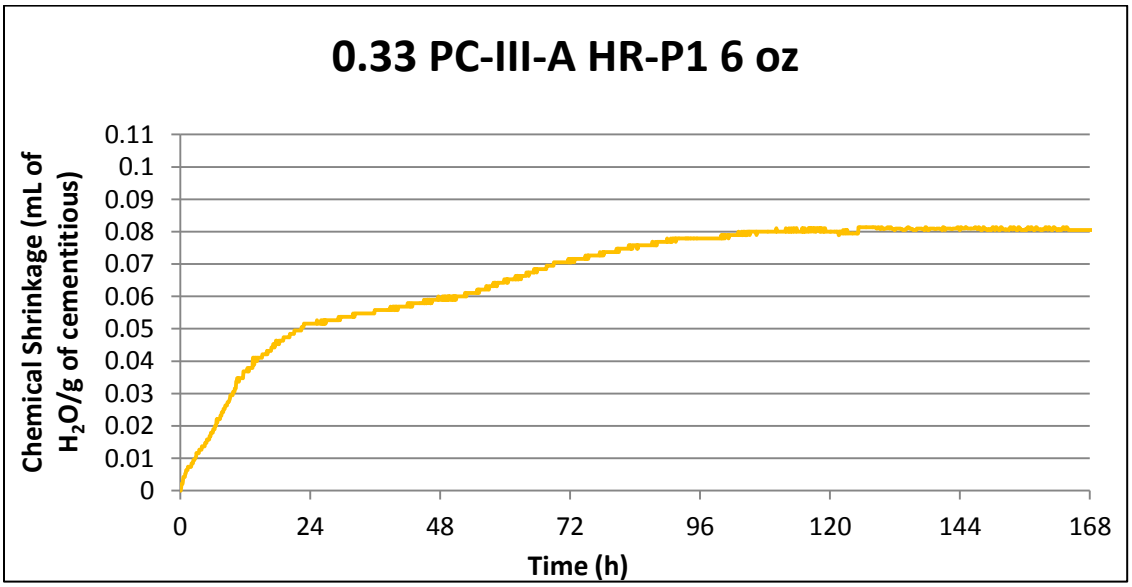

Fig. 97 Chemical Shrinkage 0.33 PC-III-A HR-P1 6 oz

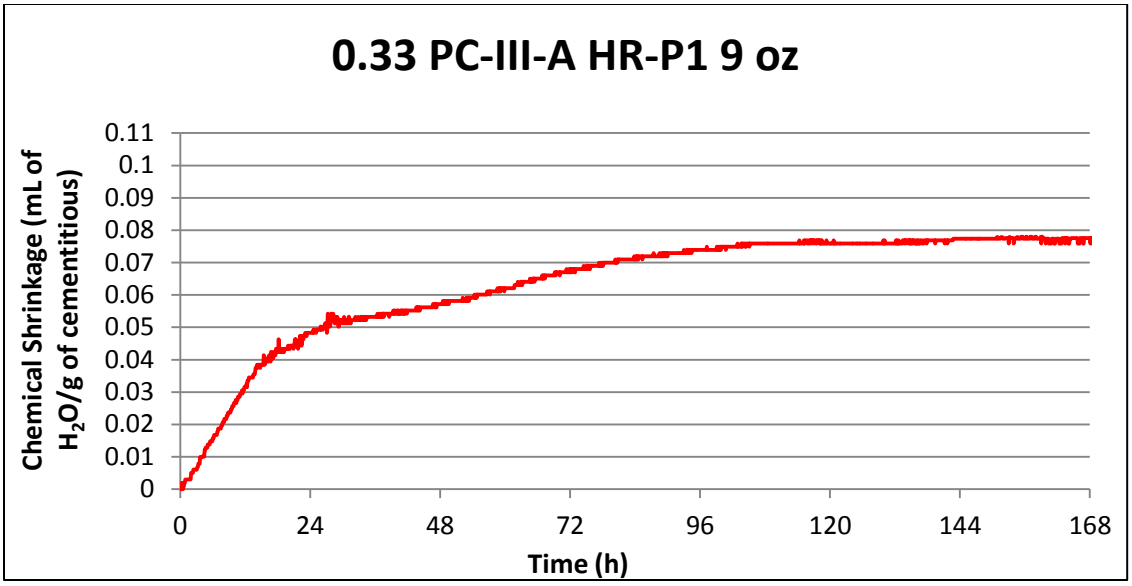

Fig. 98 Chemical Shrinkage 0.33 PC-III-A HR-P1 9 oz

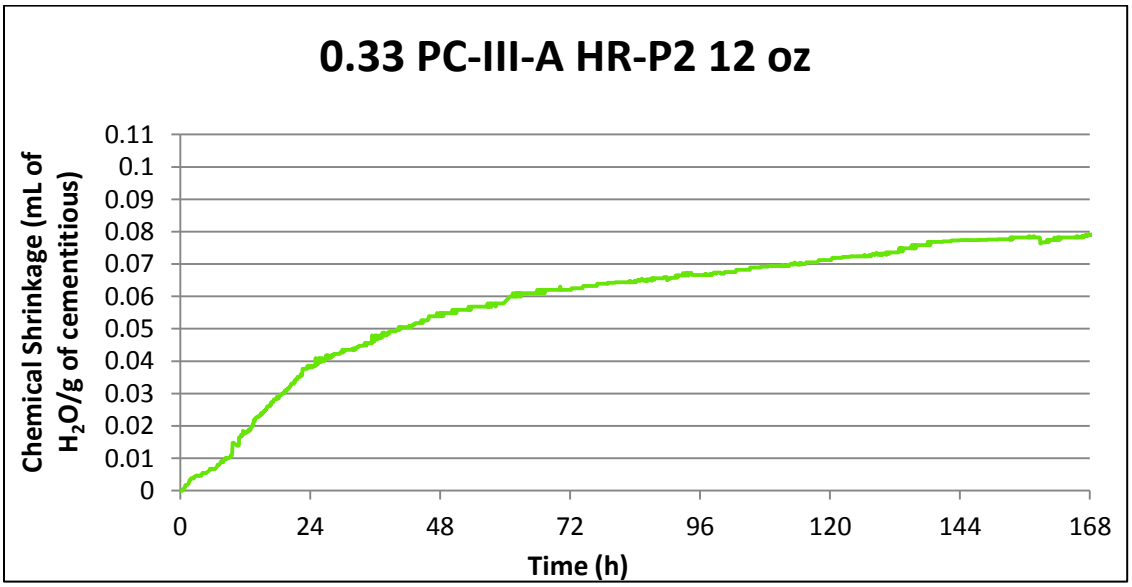

Fig. 99 Chemical Shrinkage 0.33 PC-III-A HR-P2 12 oz

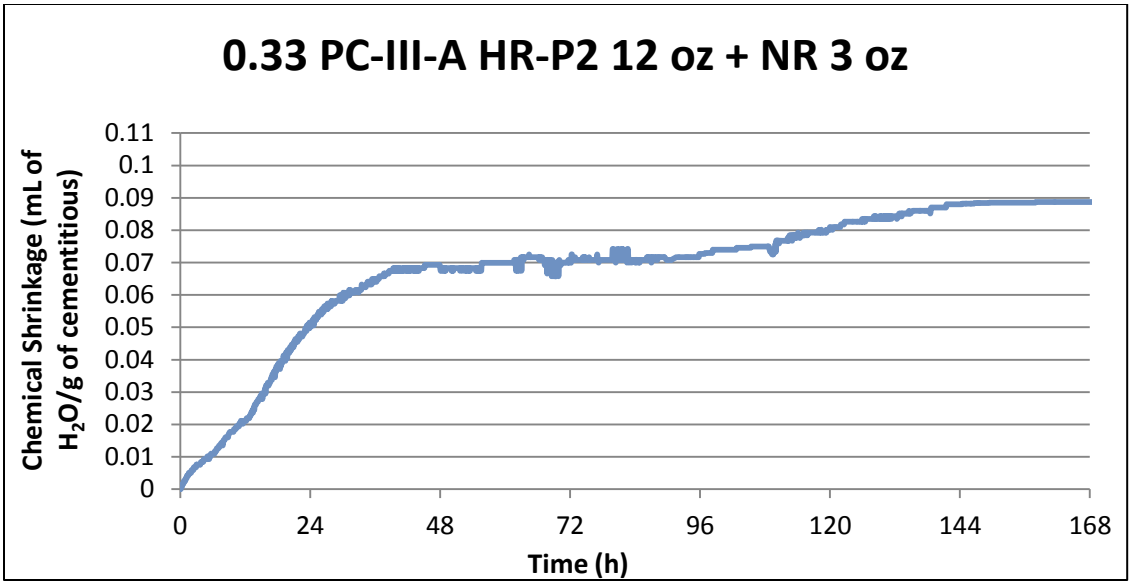

Fig. 100 Chemical Shrinkage 0.33 PC-III-A HR-P2 12 oz + NR 3 oz

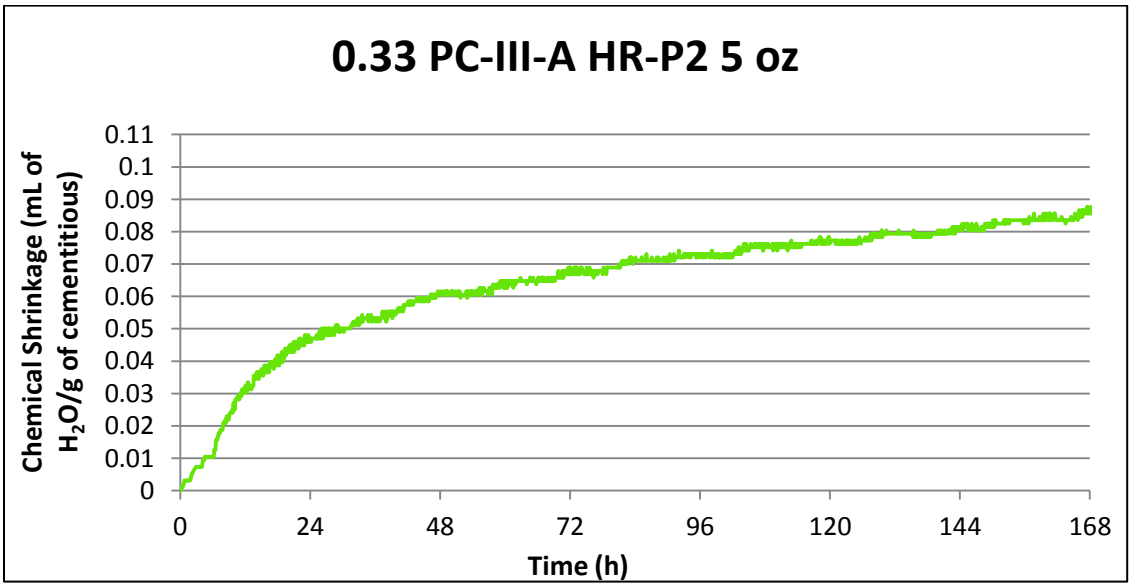

Fig. 101 Chemical Shrinkage 0.33 PC-III-A HR-P2 5 oz

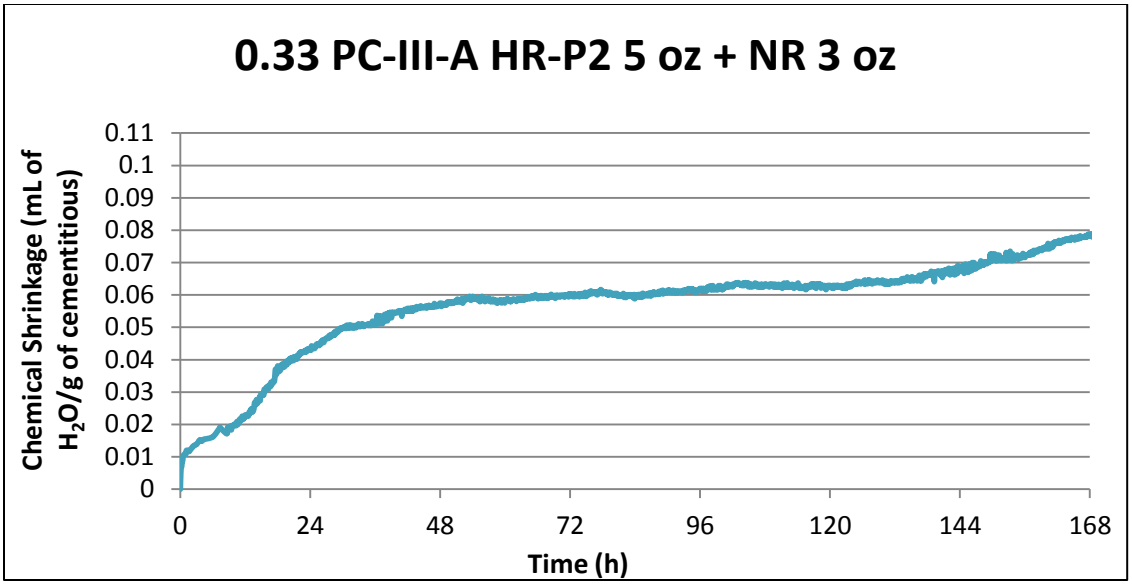

Fig. 102 Chemical Shrinkage 0.33 PC-III-A HR-P2 5 oz + NR 3 oz

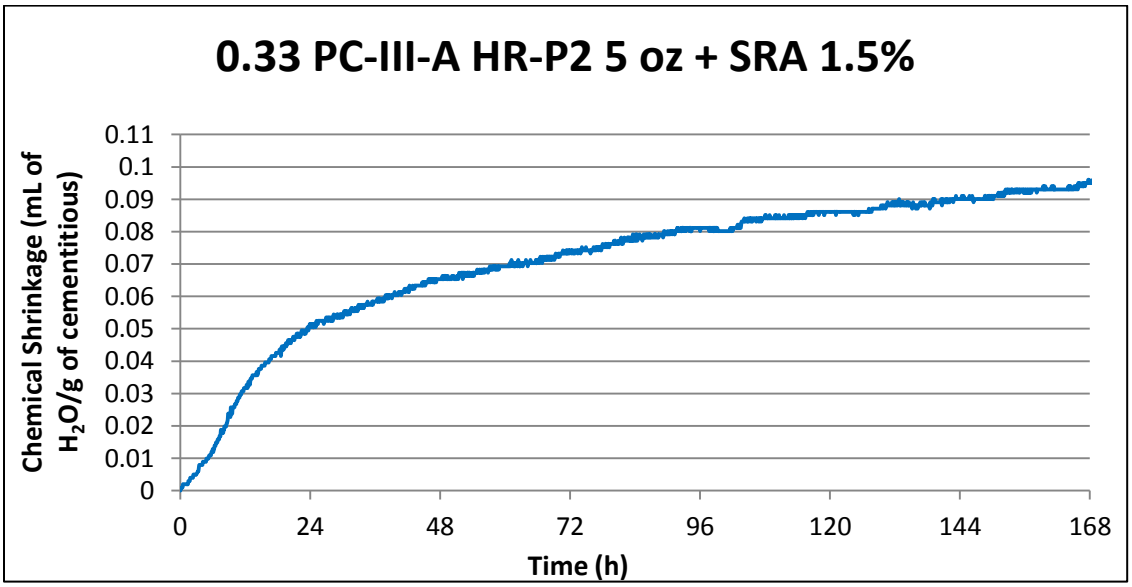

Fig. 103 Chemical Shrinkage 0.33 PC-III-A HR-P2 5 oz + SRA 1.5%

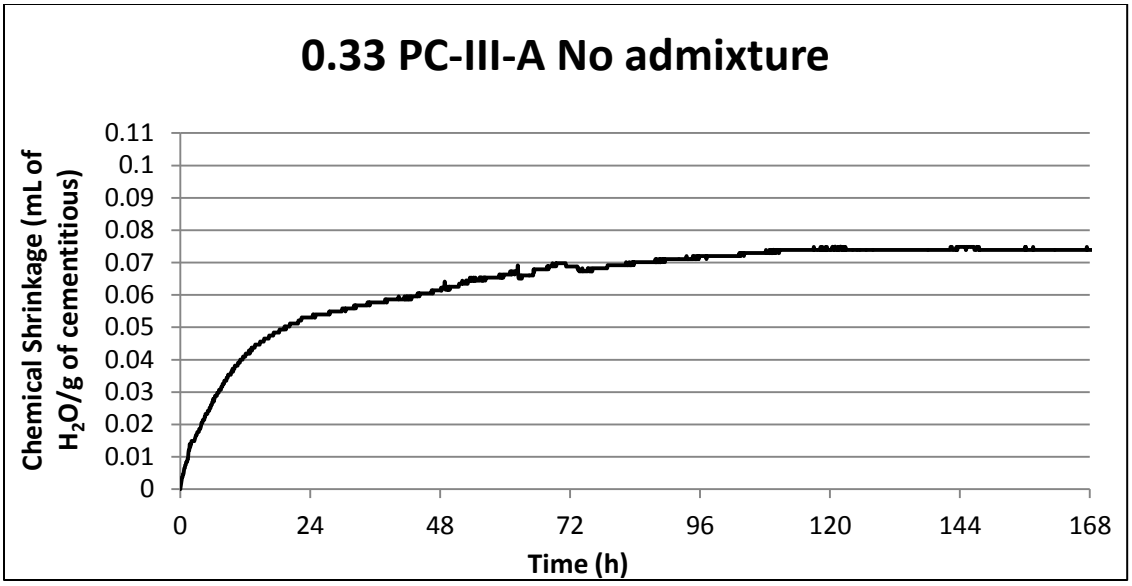

Fig. 104 Chemical Shrinkage 0.33 PC-III-A No admixture

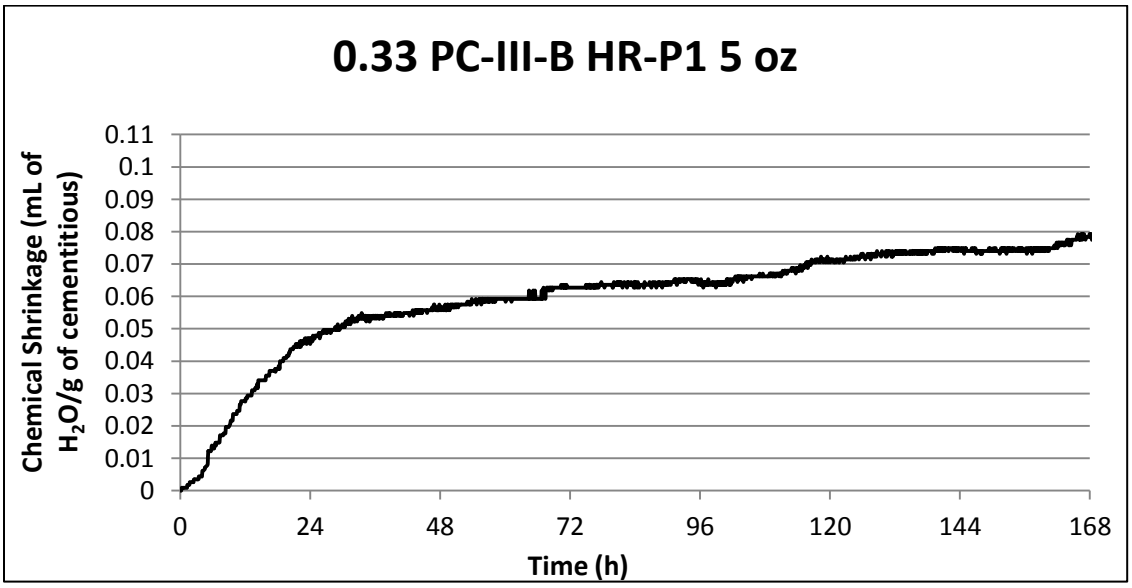

Fig. 105 Chemical Shrinkage 0.33 PC-III-B HR-P1 5 oz

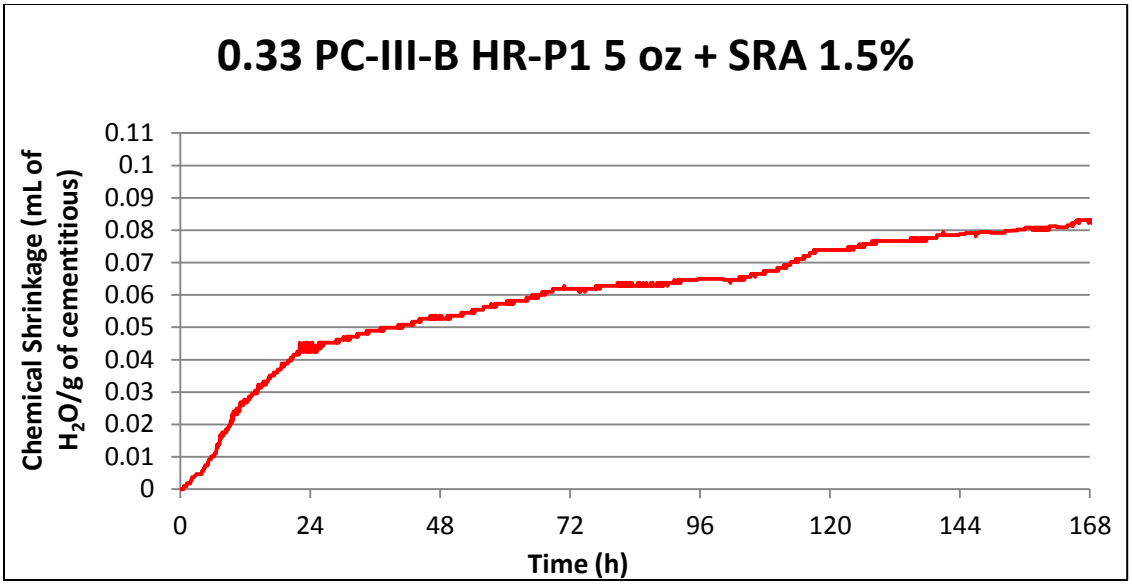

Fig. 106 Chemical Shrinkage 0.33 PC-III-B HR-P1 5 oz + SRA 1.5%

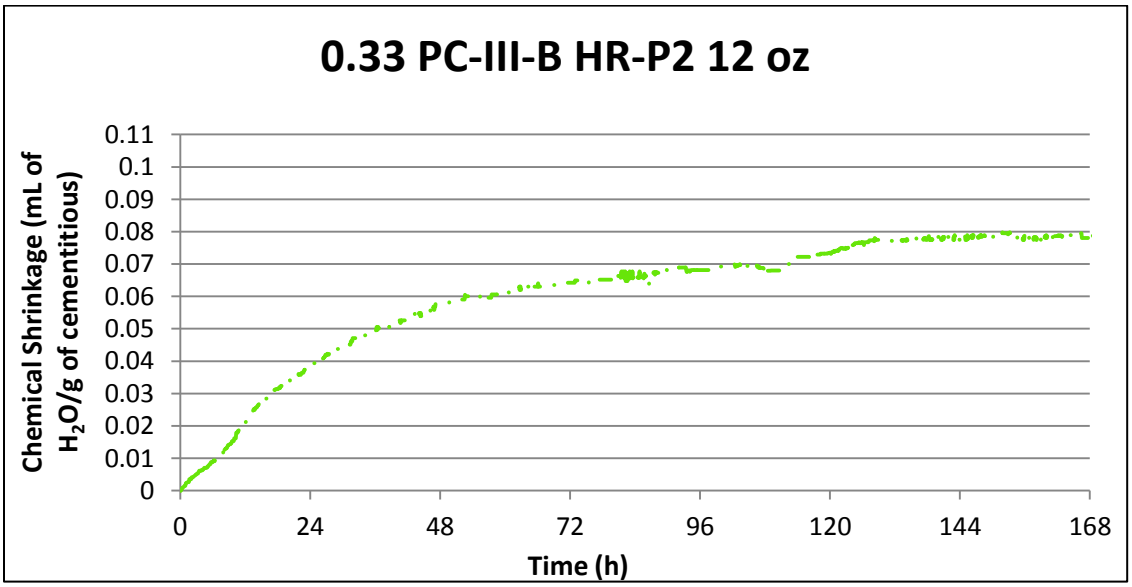

Fig. 107 Chemical Shrinkage 0.33 PC-III-B HR-P2 12 oz

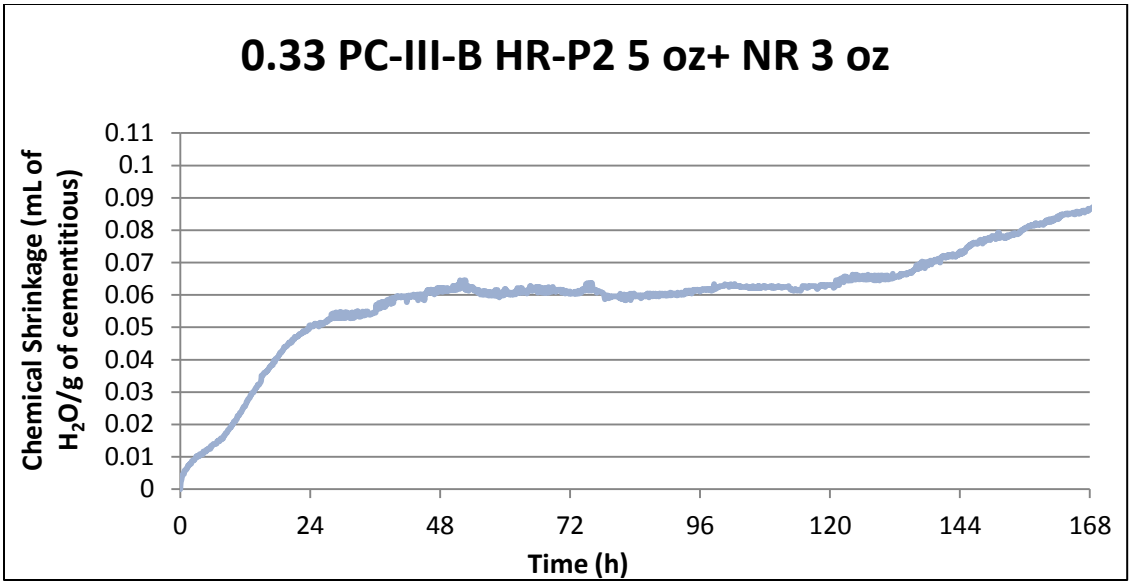

Fig. 108 Chemical Shrinkage 0.33 PC-III-B HR-P2 5 oz+ NR 3 oz

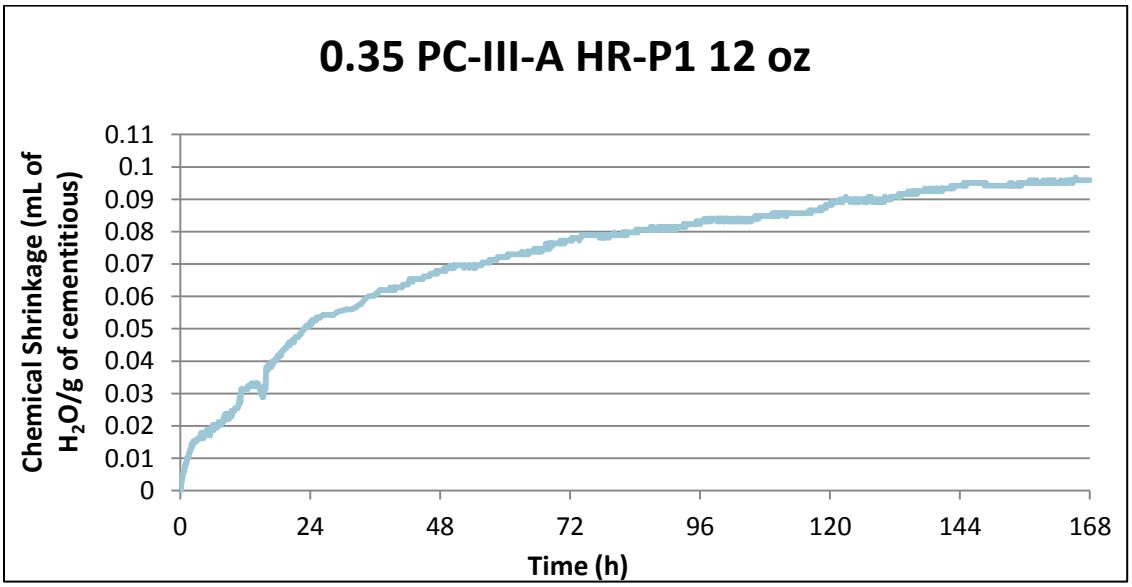

Fig. 109 Chemical Shrinkage 0.35 PC-III-A HR-P1 12 oz

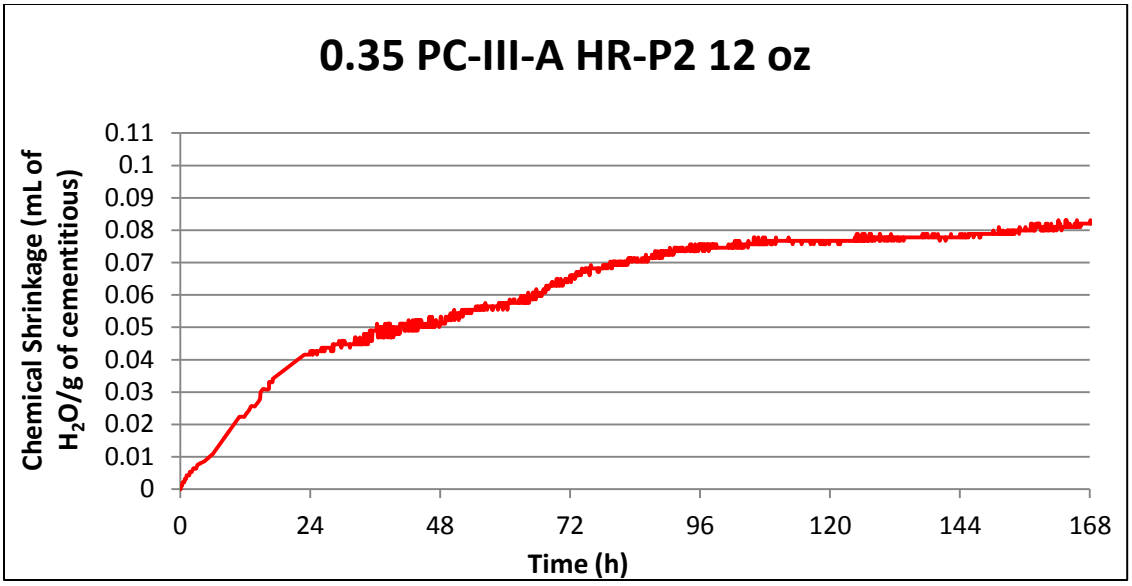

Fig. 110 Chemical Shrinkage 0.35 PC-III-A HR-P2 12 oz

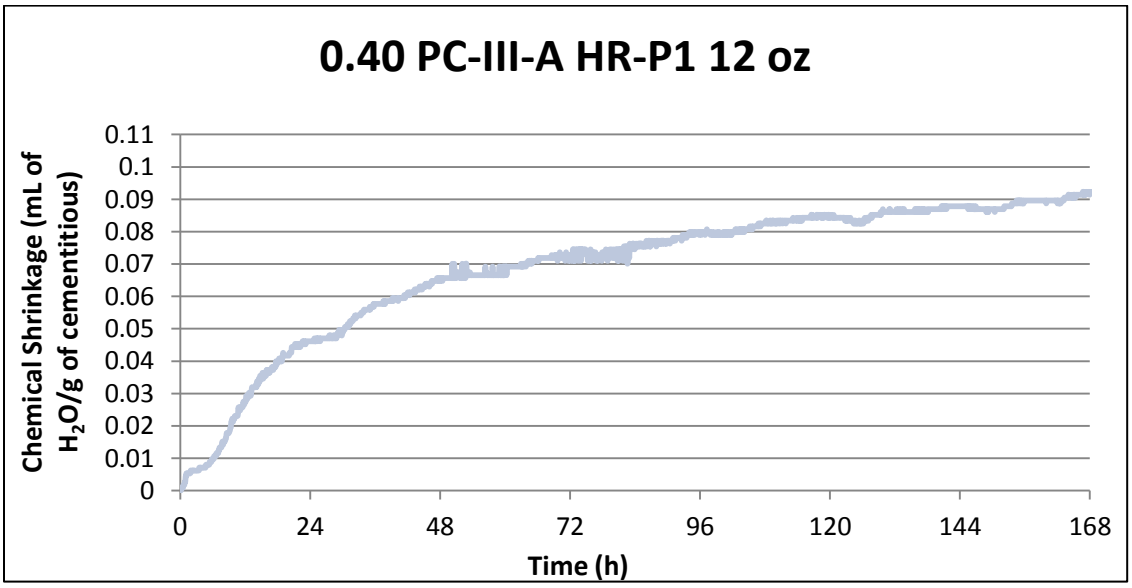

Fig. 111 Chemical Shrinkage 0.40 PC-III-A HR-P1 12 oz

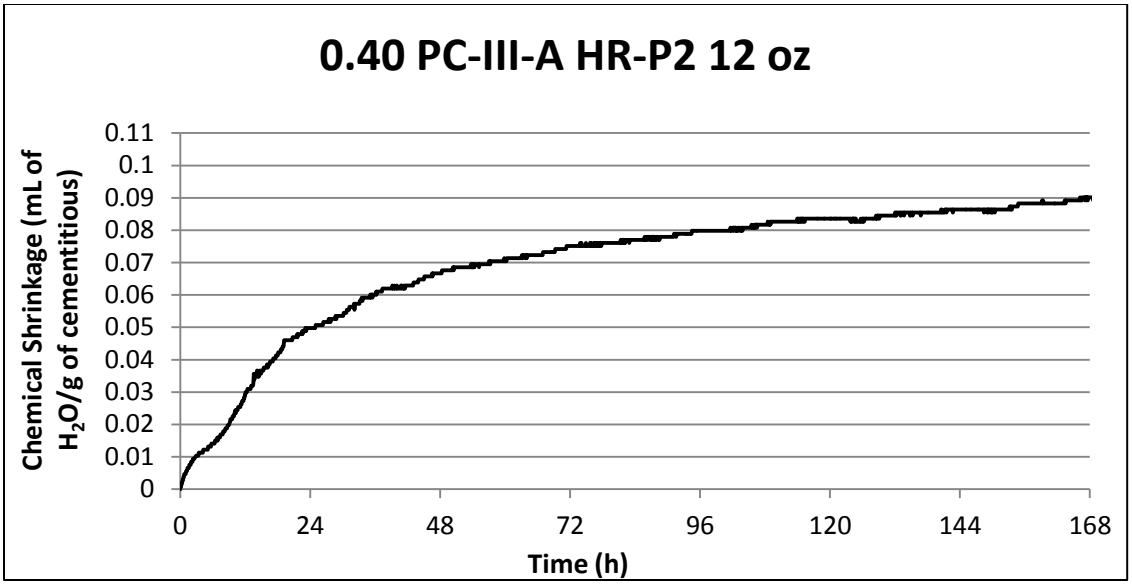

Fig. 112 Chemical Shrinkage 0.40 PC-III-A HR-P2 12 oz

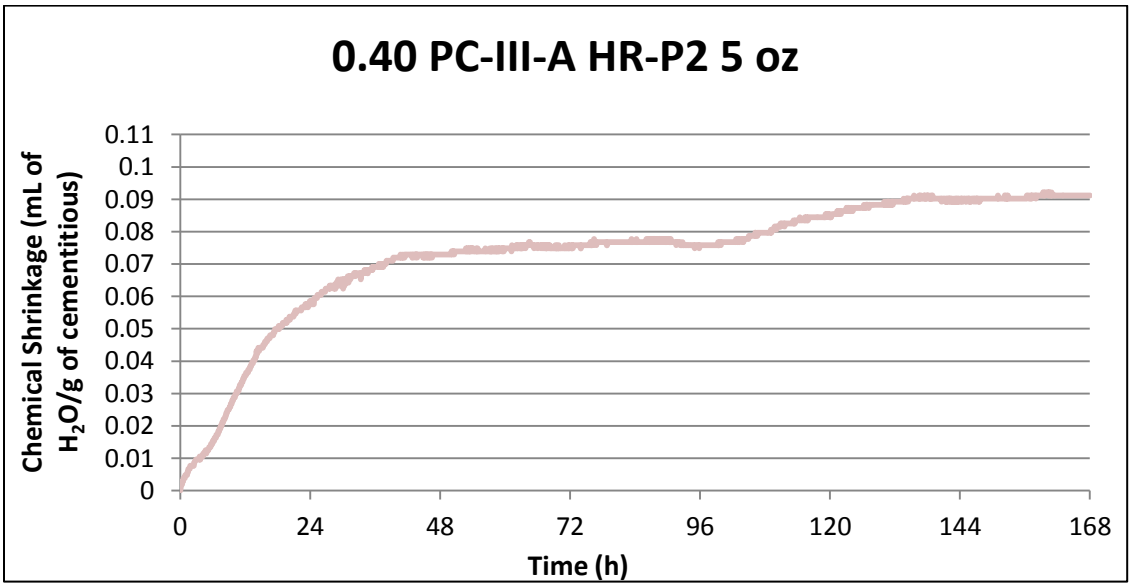

Fig. 113 Chemical Shrinkage 0.40 PC-III-A HR-P2 5 oz

Appendix II: Autogenous Shrinkage curves

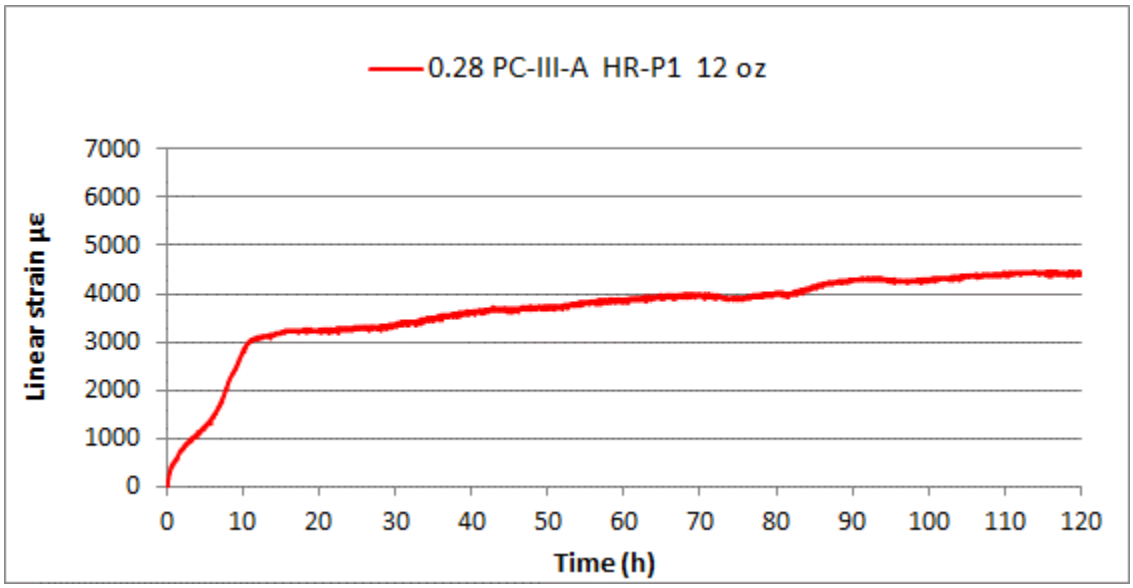

Fig. 114 Autogenous Shrinkage 0.28 PC-III-A HR-P1 12 oz

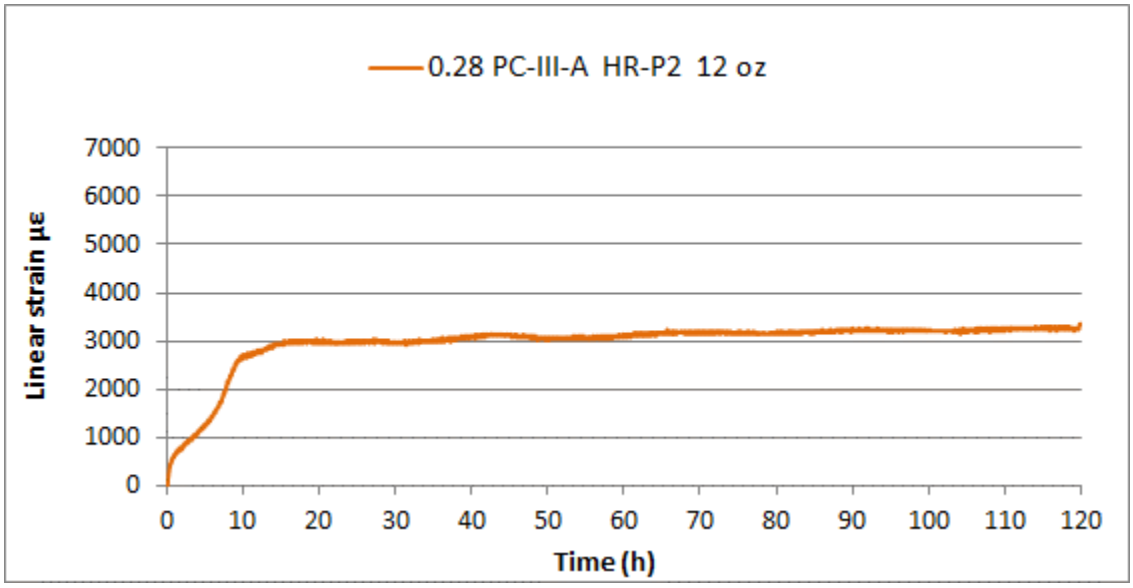

Fig. 115 Autogenous Shrinkage 0.28 PC-III-A HR-P2 12 oz

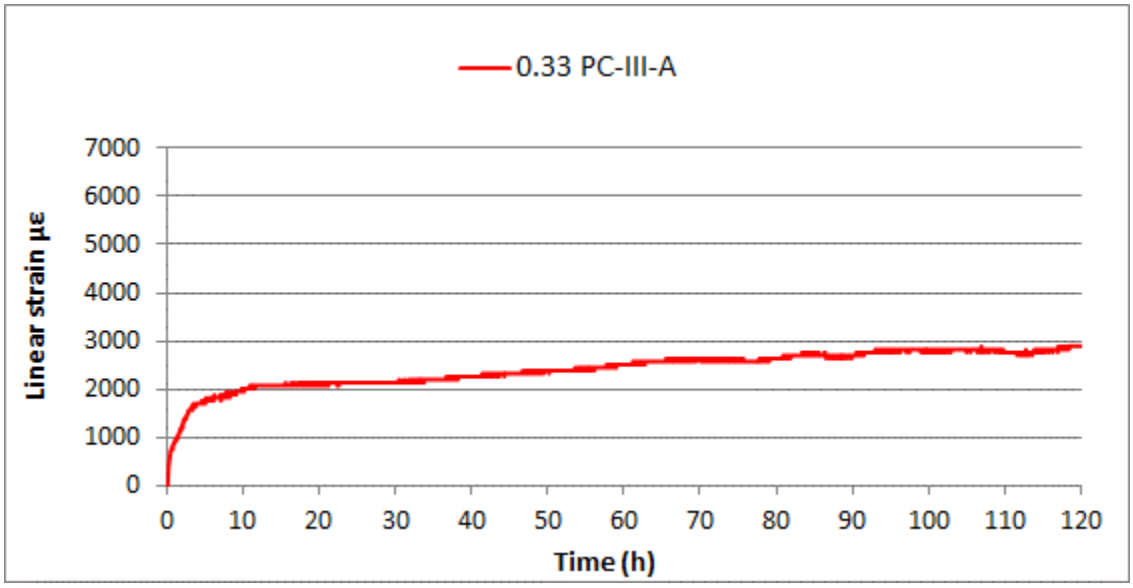

Fig. 116 Autogenous Shrinkage 0.33 PC-III-A

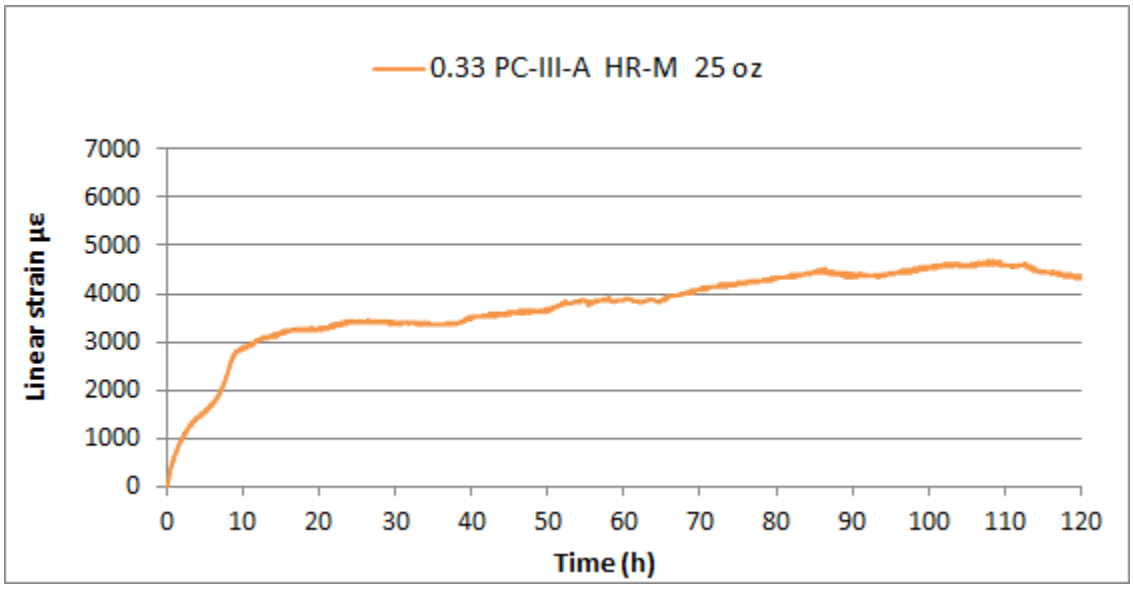

Fig. 117 Autogenous Shrinkage 0.33 PC-III-A HR-M 25 oz

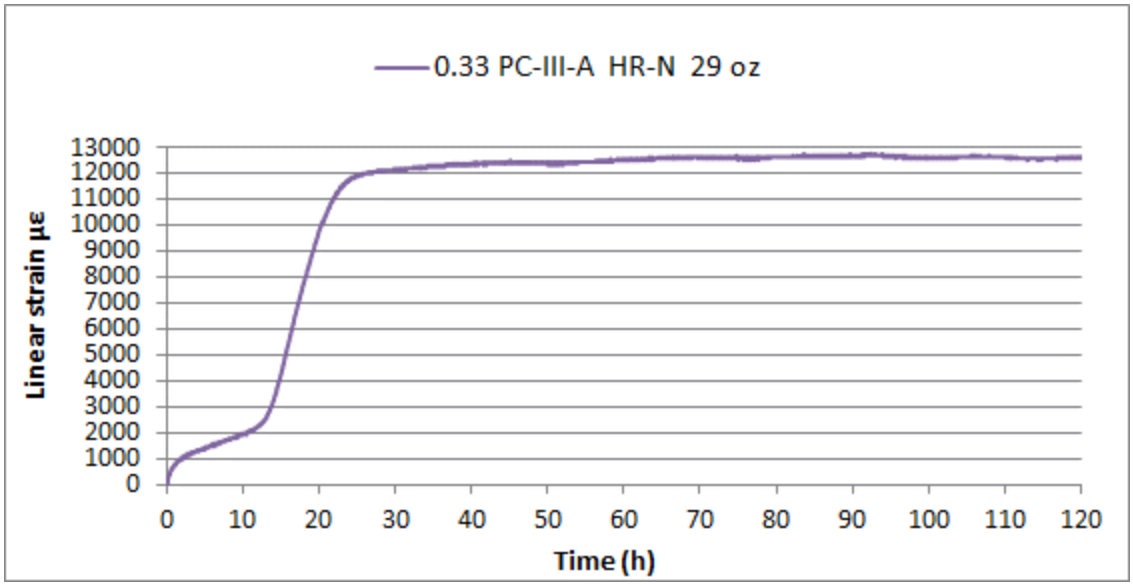

Fig. 118 Autogenous Shrinkage 0.33 PC-III-A HR-N 29 oz

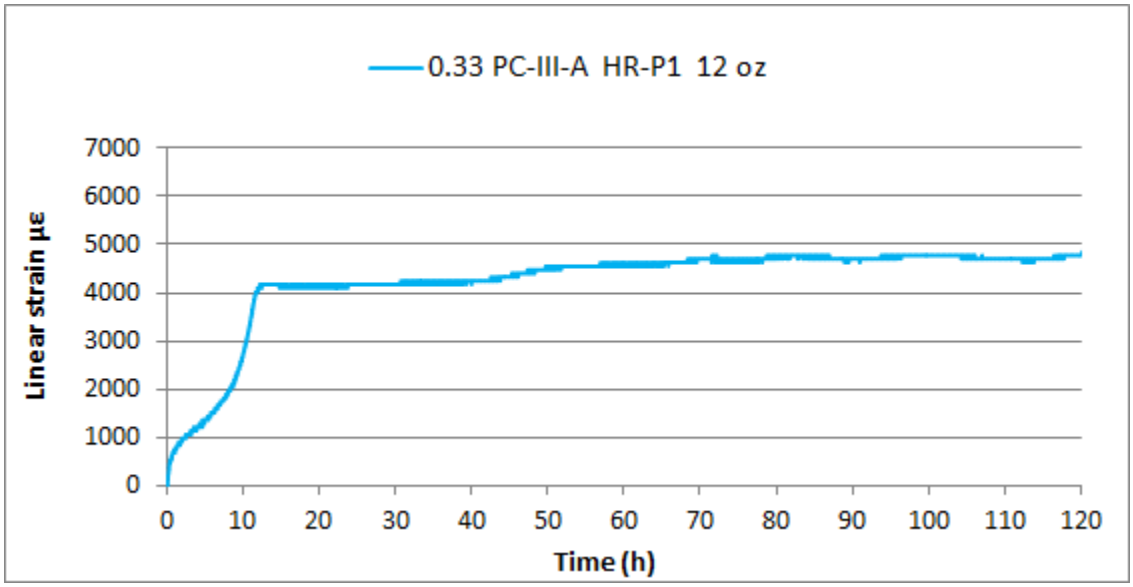

Fig. 119 Autogenous Shrinkage 0.33 PC-III-A HR-P1 12 oz

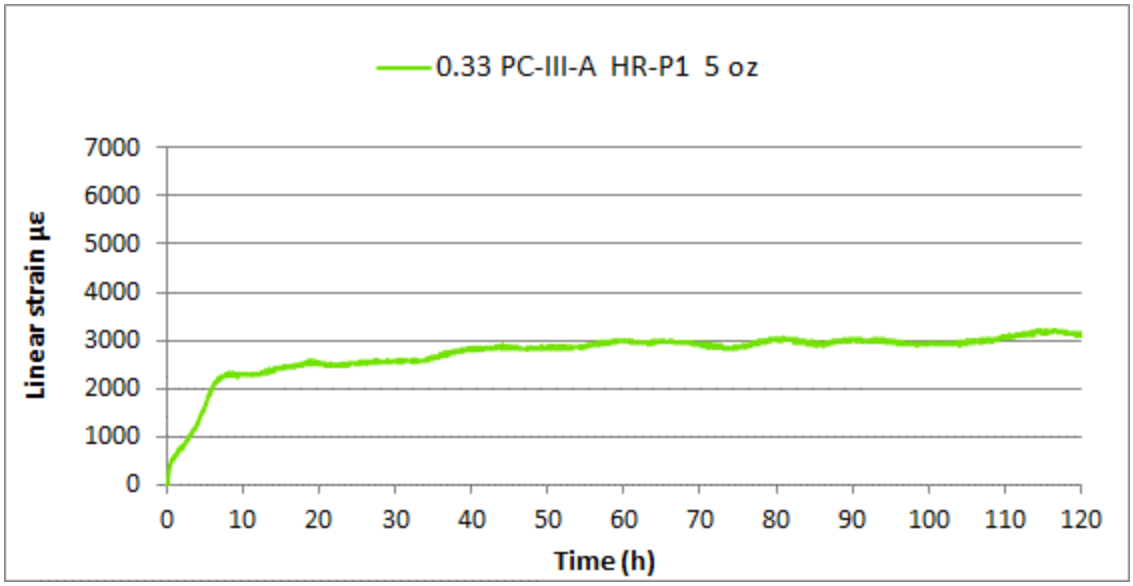

Fig. 120 Autogenous Shrinkage 0.33 PC-III-A HR-P1 5 oz

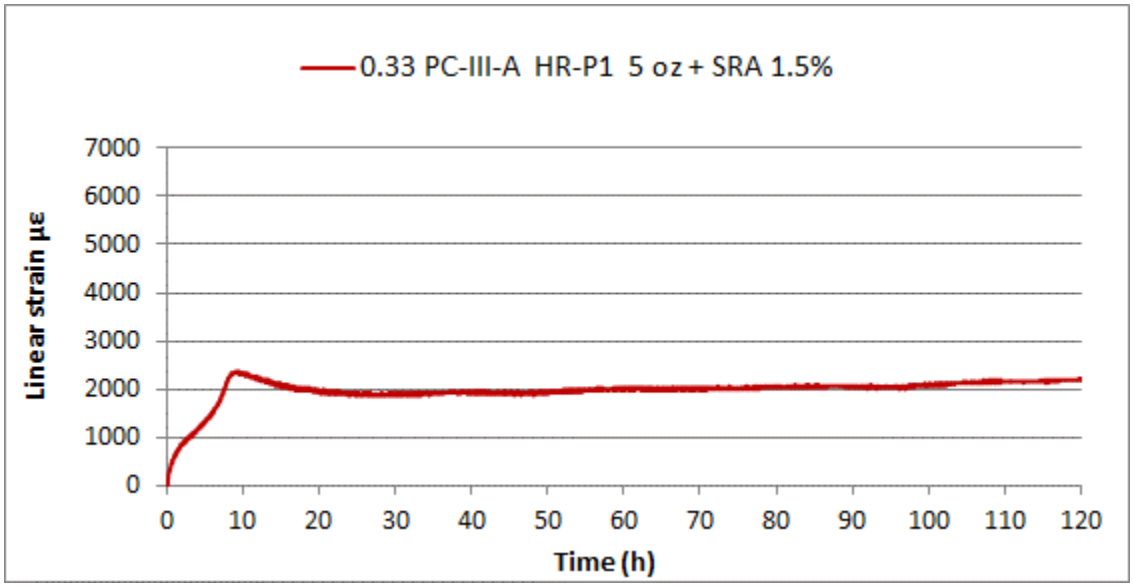

Fig. 121 Autogenous Shrinkage 0.33 PC-III-A HR-P1 5 oz + SRA 1.5%

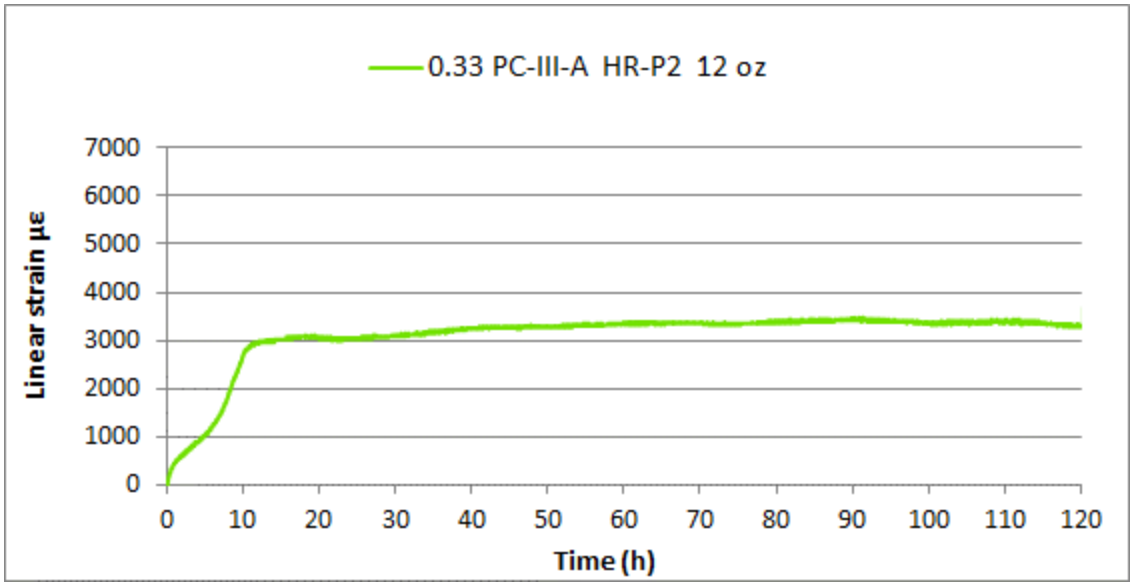

Fig. 122 Autogenous Shrinkage 0.33 PC-III-A HR-P2 12 oz

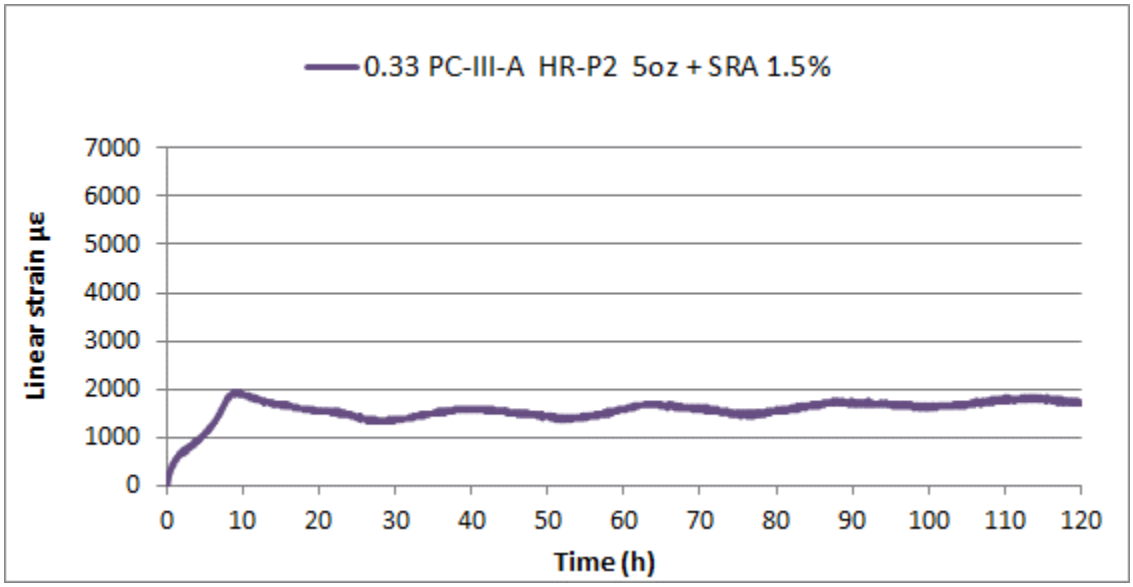

Fig. 123 Autogenous Shrinkage 0.33 PC-III-A HR-P2 5oz + SRA 1.5%

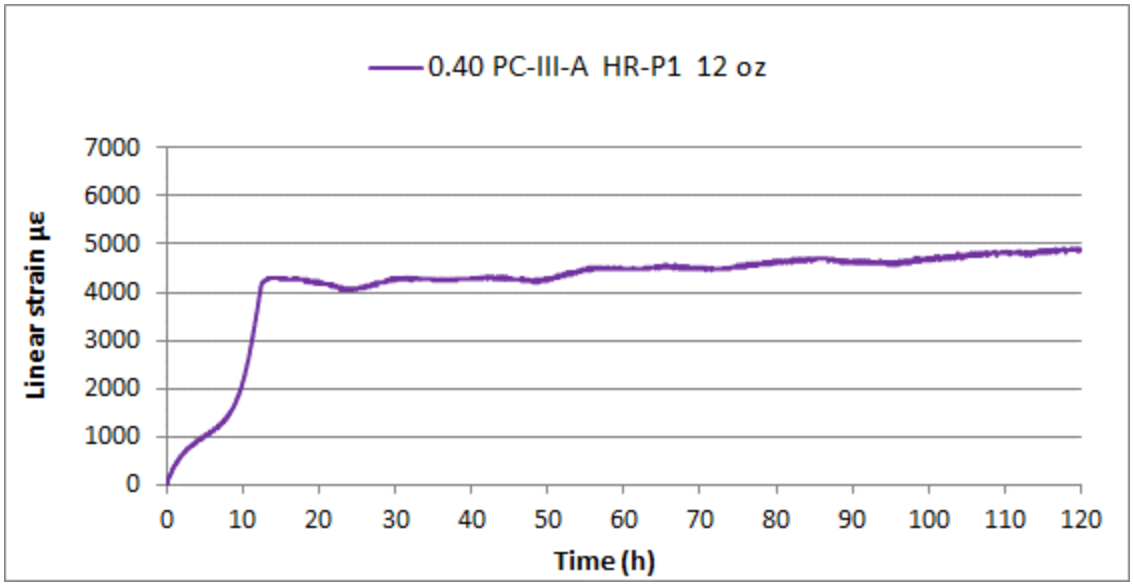

Fig. 124 Autogenous Shrinkage 0.40 PC-III-A HR-P1 12 oz

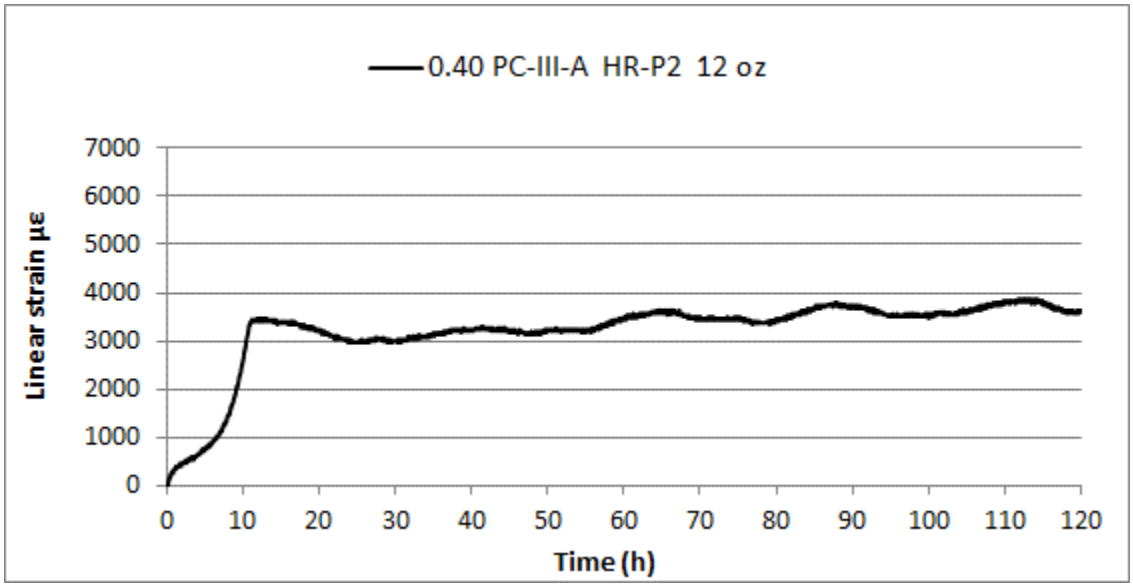

Fig. 125 Autogenous Shrinkage 0.40 PC-III-A HR-P2 12 oz

Appendix III: Isothermal calorimetry curves

III.1 HEAT FLOW CURVES

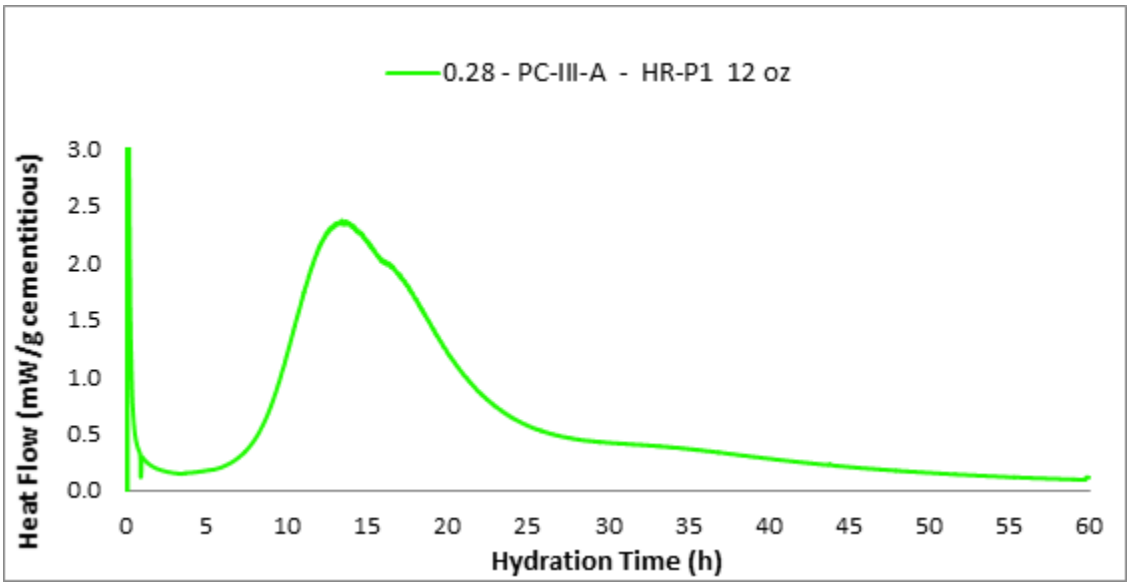

Fig. 126 Heat Flow 0.28 - PC-III-A - HR-P1 12 oz

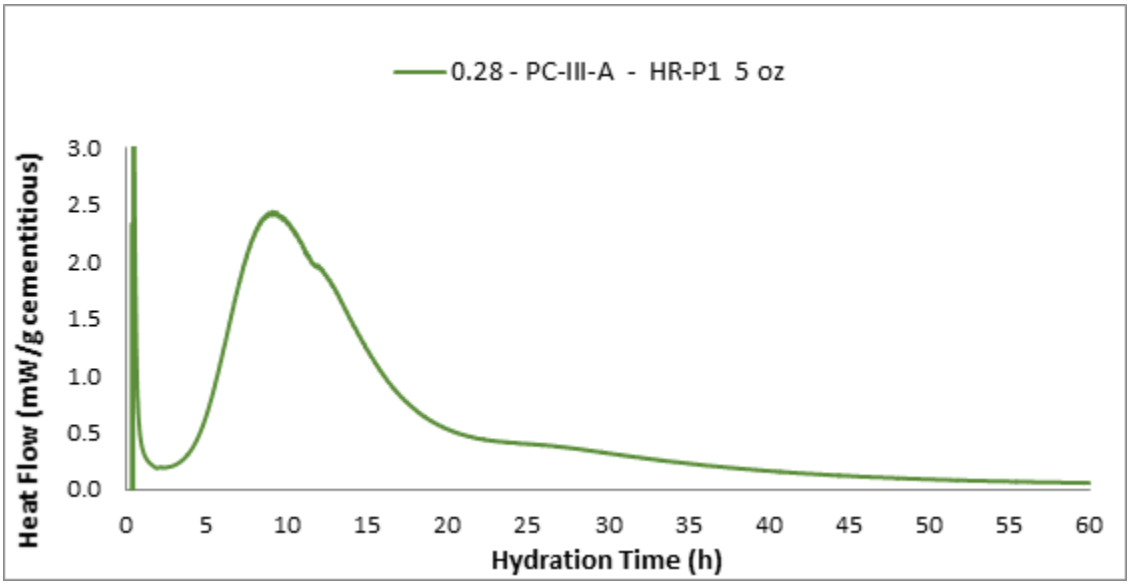

Fig. 127 Heat Flow 0.28 - PC-III-A - HR-P1 12 oz

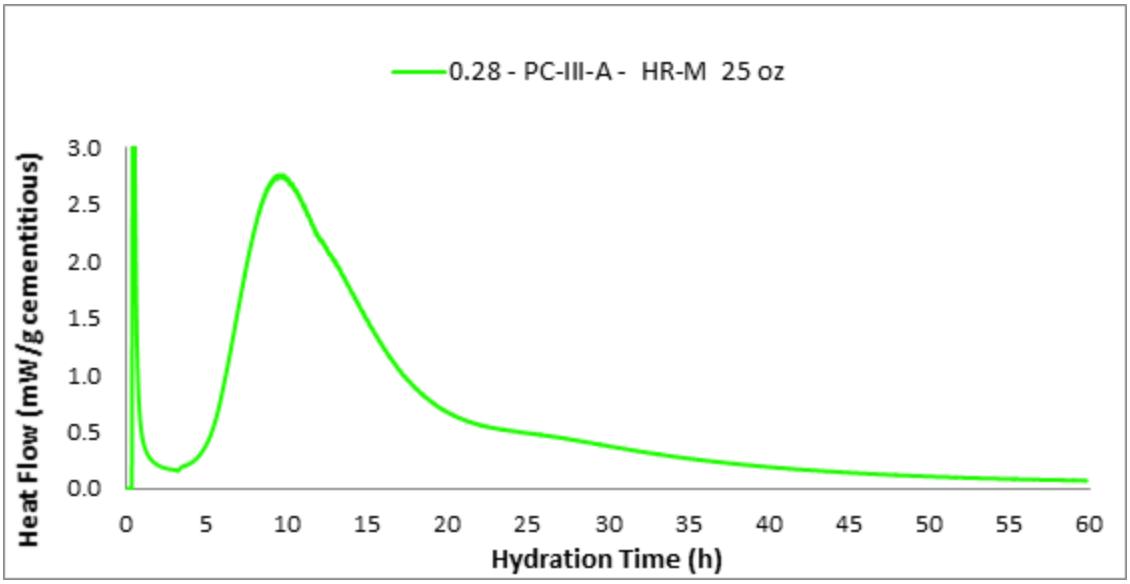

Fig. 128 Heat Flow 0.28 - PC-III-A - HR-M 25 oz

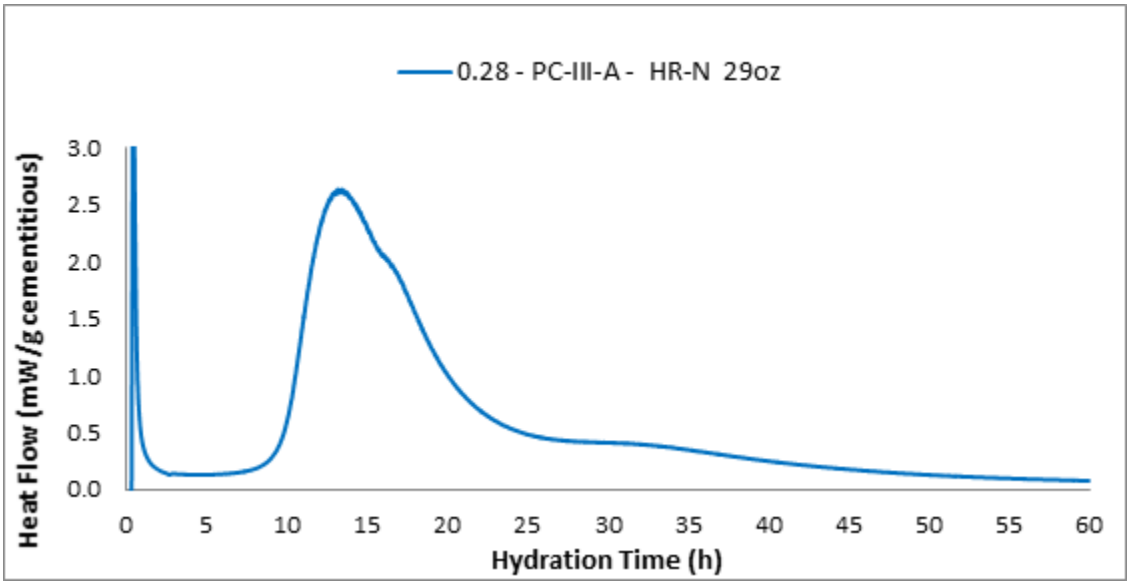

Fig. 129 Heat Flow 0.28 - PC-III-A - HR-N 29oz

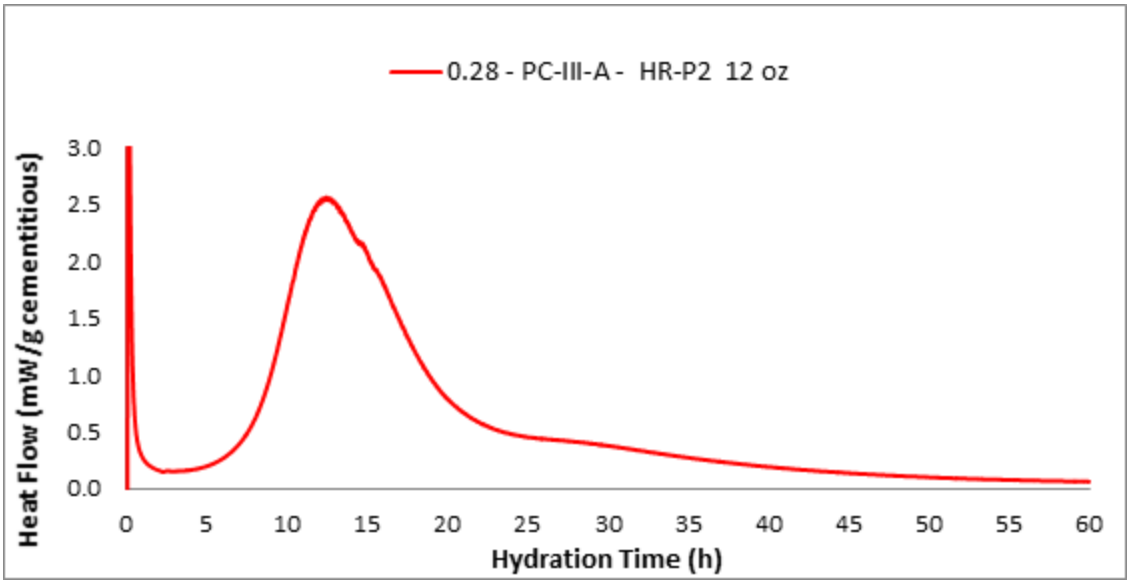

Fig. 130 Heat Flow 0.28 - PC-III-A - HR-P2 12 oz

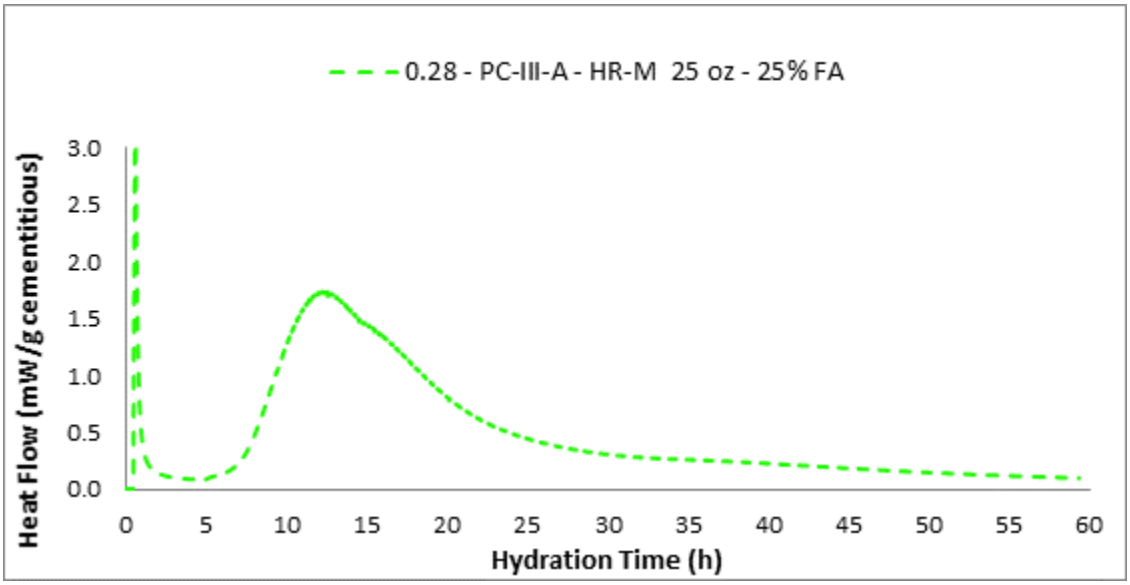

Fig .131 Heat Flow 0.28 - PC-III-A - HR-M 25 oz - 25% FA

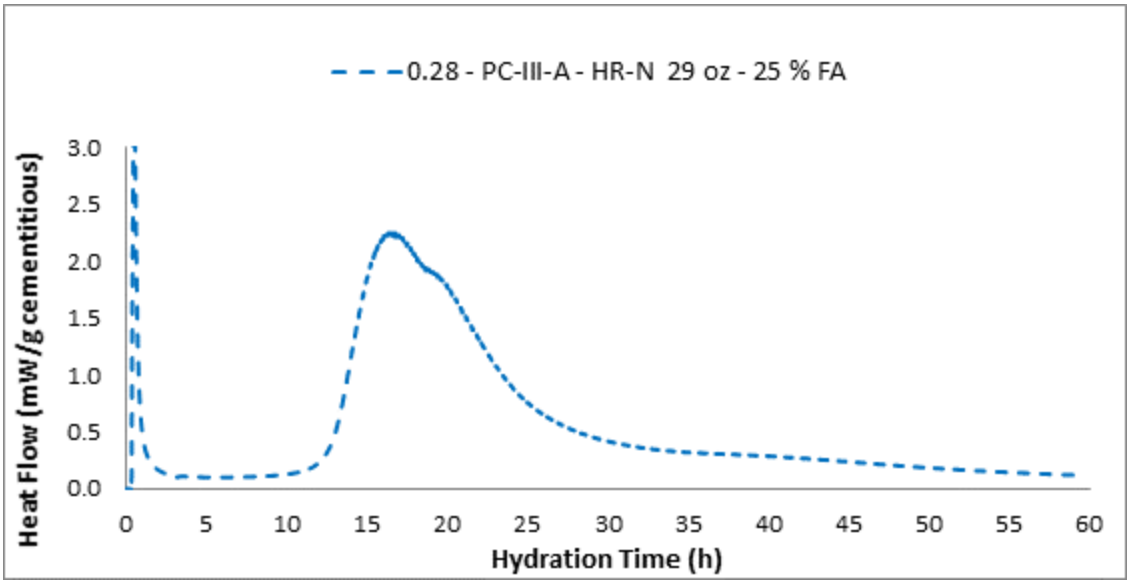

Fig. 132 Heat Flow 0.28 - PC-III-A - HR-N 29 oz - 25 % FA

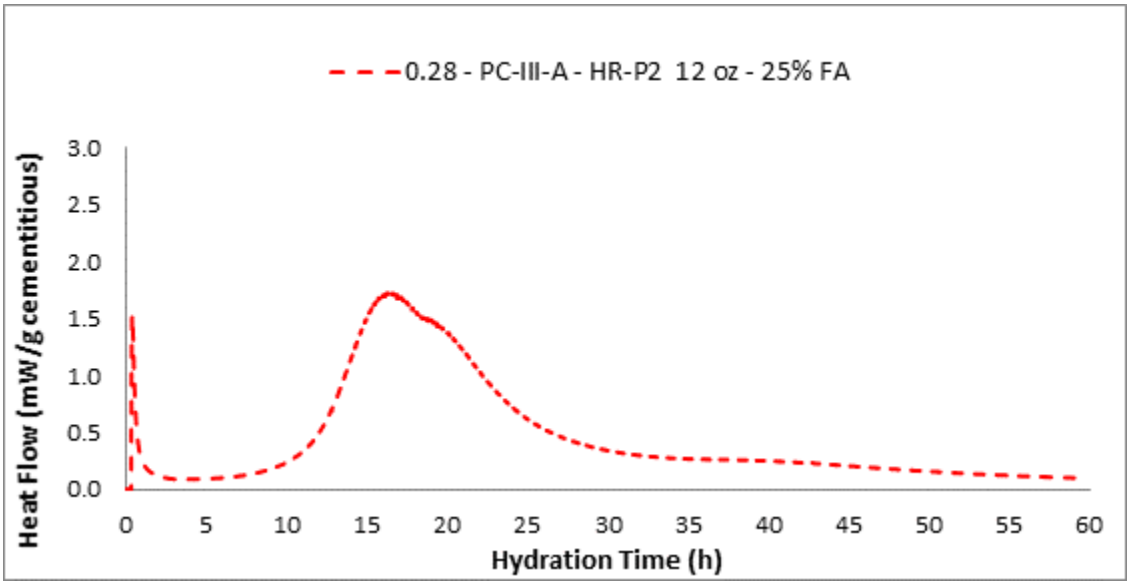

Fig. 133 Heat Flow 0.28 - PC-III-A - HR-P2 12 oz - 25% FA

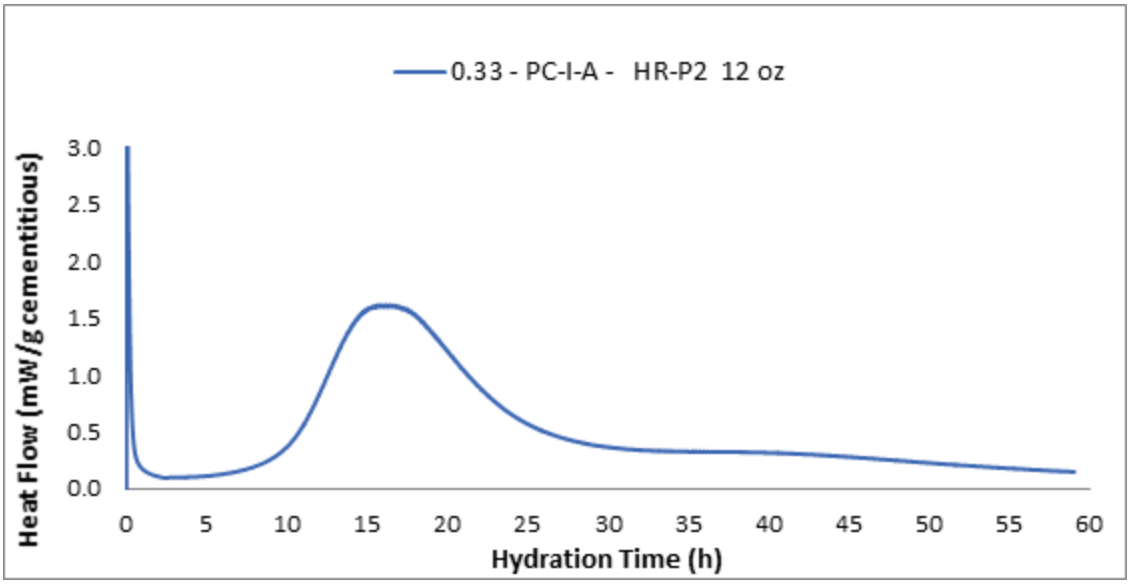

Fig. 134 Heat Flow 0.33 - PC-I-A - HR-P2 12 oz

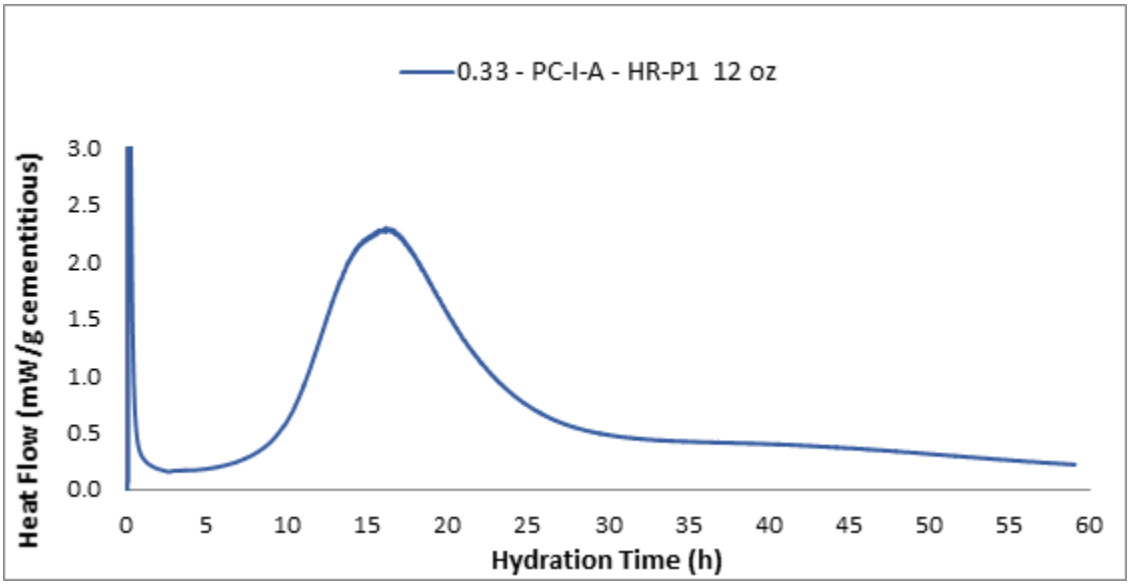

Fig. 135 Heat Flow 0.33 - PC-I-A - HR-P1 12 oz

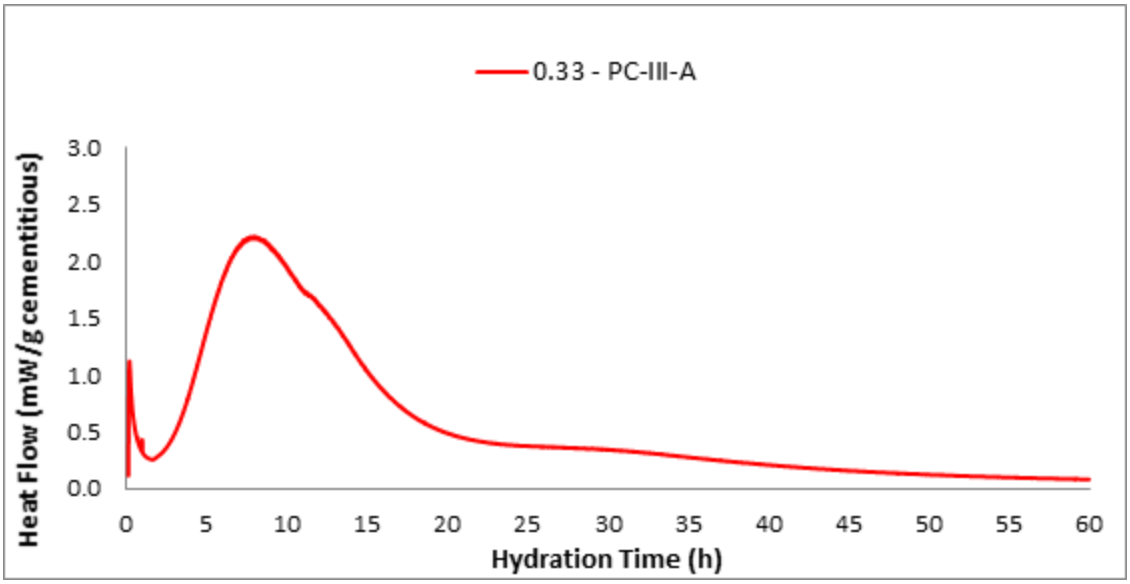

Fig. 136 Heat Flow 0.33 - PC-III-A

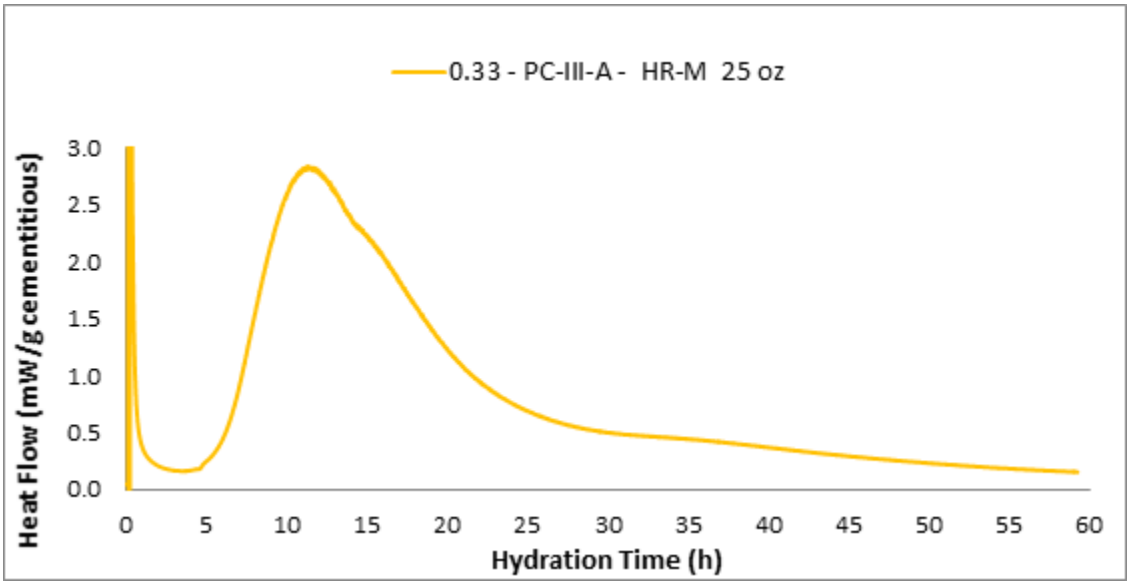

Fig. 137 Heat Flow 0.33 - PC-III-A - HR-M 25 oz

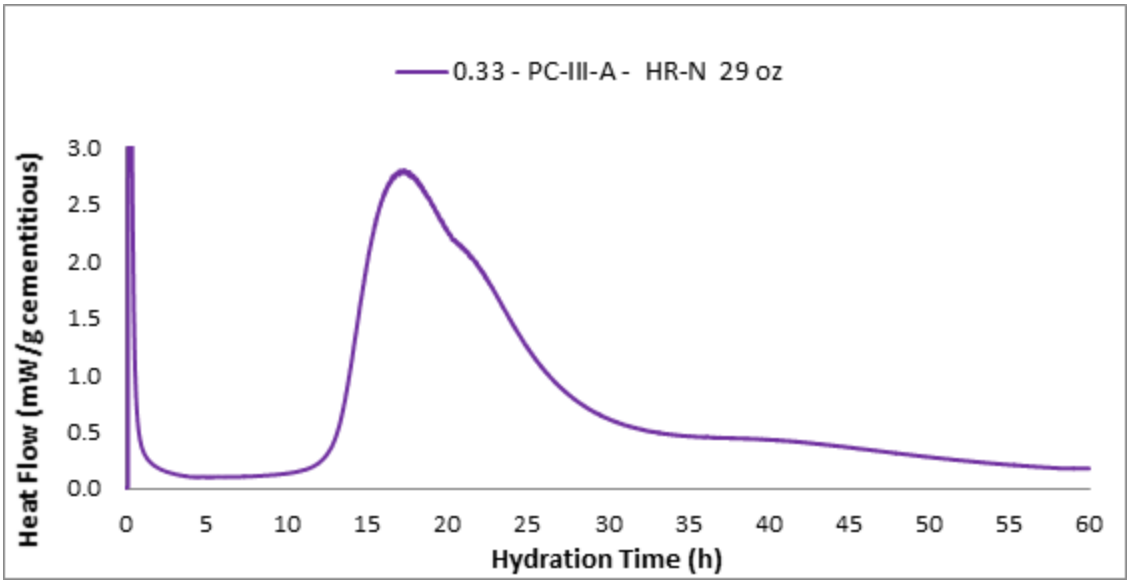

Fig. 138 Heat Flow 0.33 - PC-III-A - HR-N 29 oz

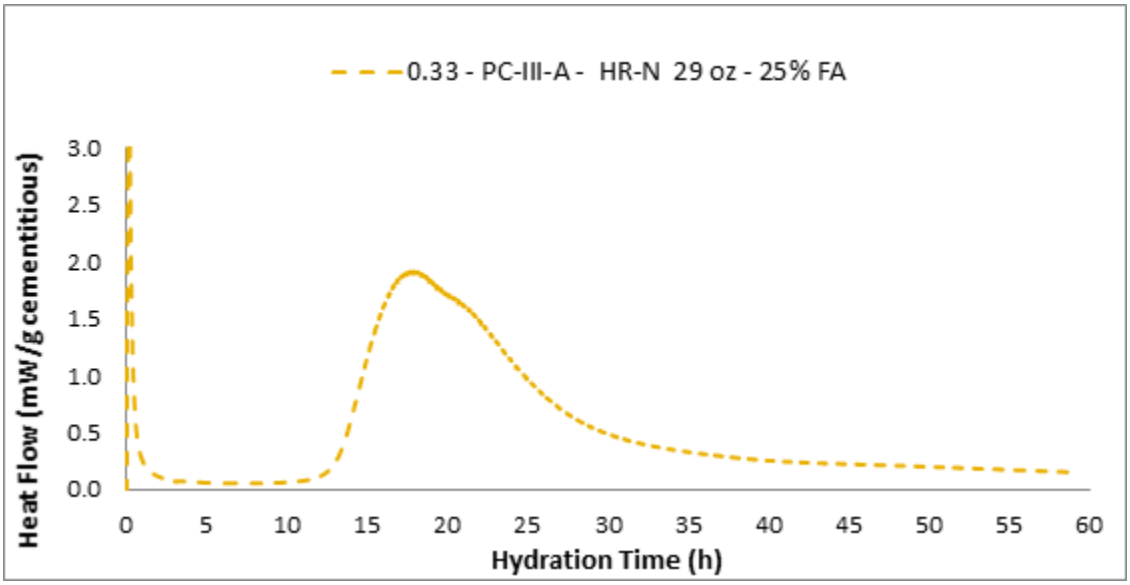

Fig. 139 Heat Flow 0.33 - PC-III-A - HR-N 29 oz - 25% FA

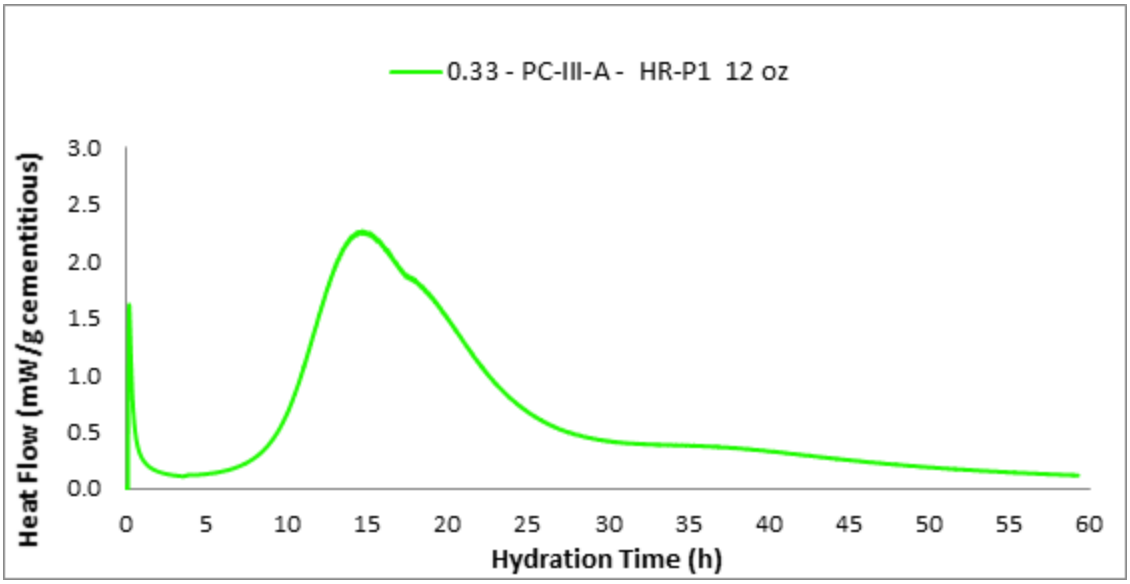

Fig. 140 Heat Flow 0.33 - PC-III-A - HR-P1 12 oz

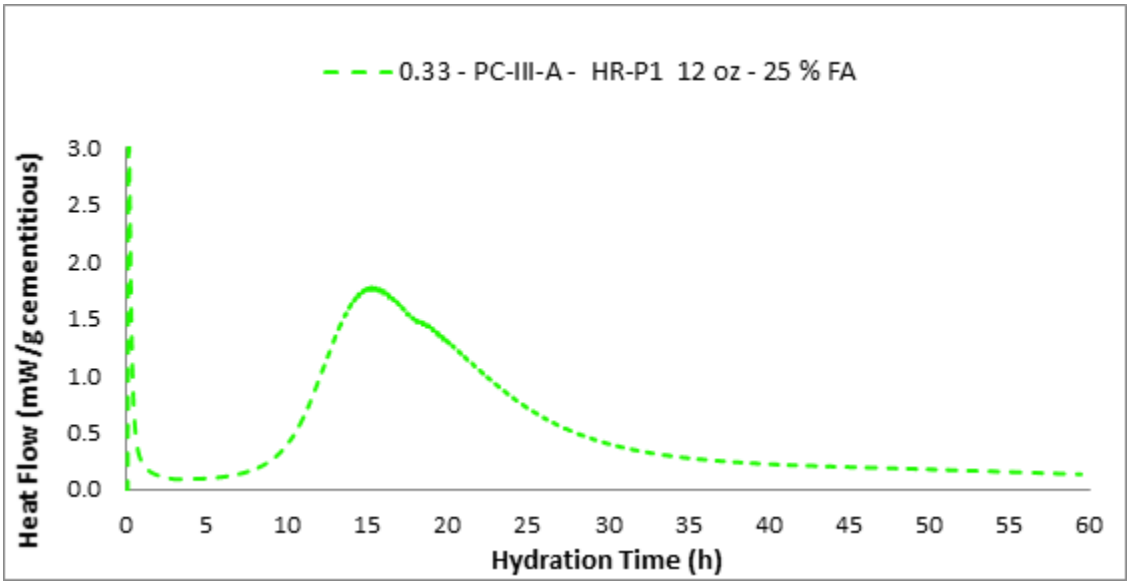

Fig. 141 Heat Flow 0.33 - PC-III-A - HR-P1 12 oz - 25 % FA

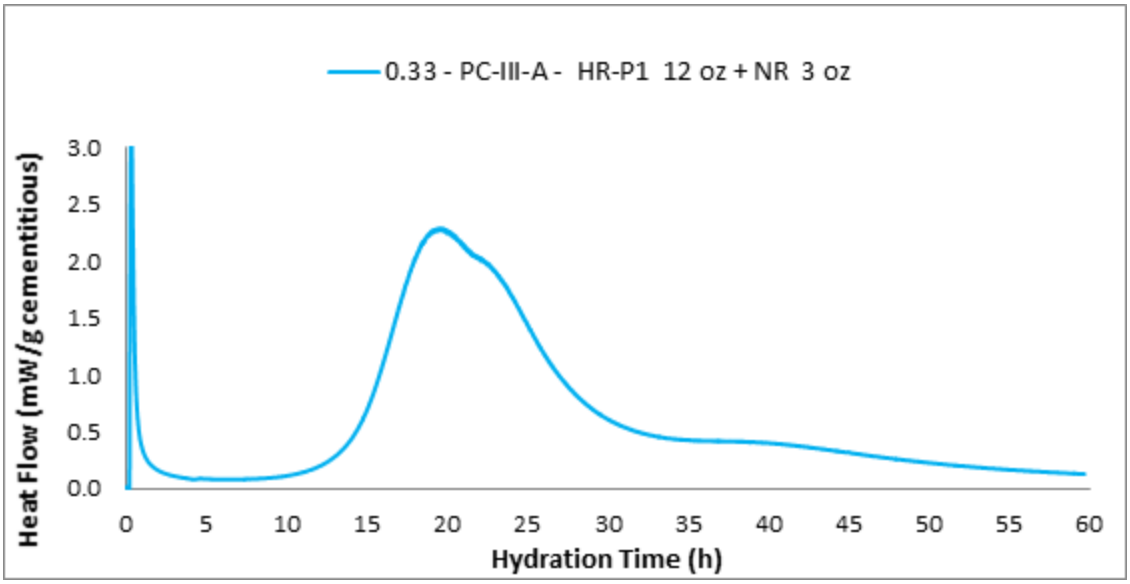

Fig. 142 Heat Flow 0.33 - PC-III-A - HR-P1 12 oz + NR 3 oz

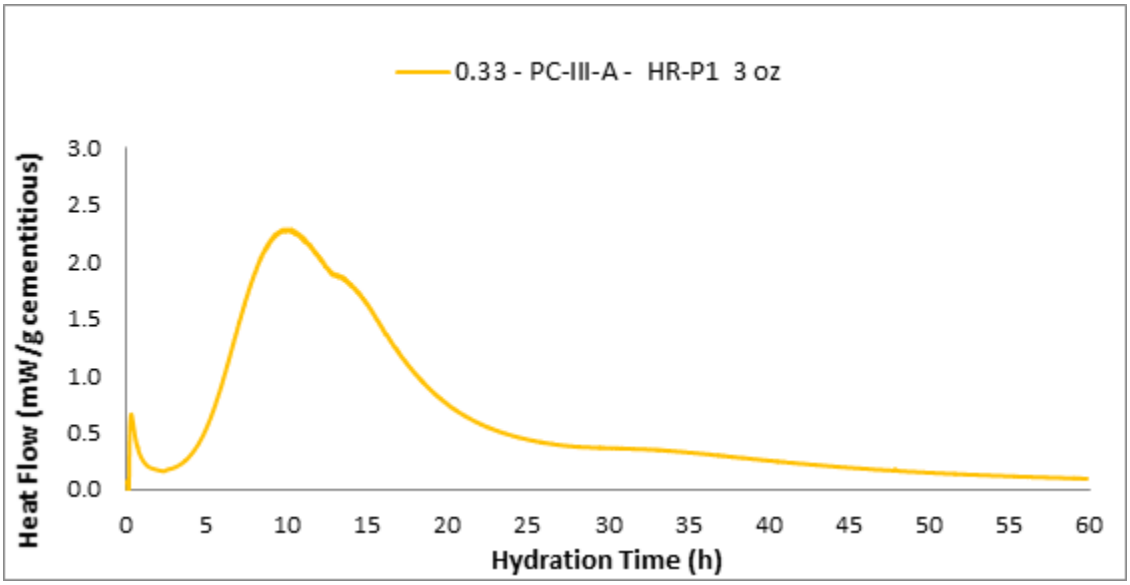

Fig. 143 Heat Flow 0.33 - PC-III-A - HR-P1 3 oz

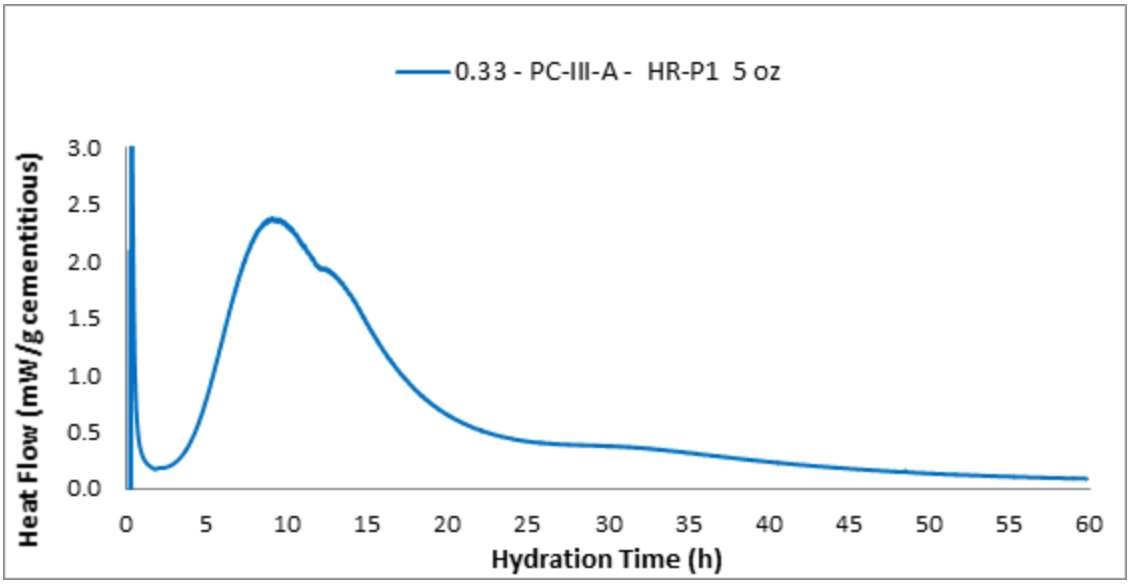

Fig. 144 Heat Flow 0.33 - PC-III-A - HR-P1 5 oz

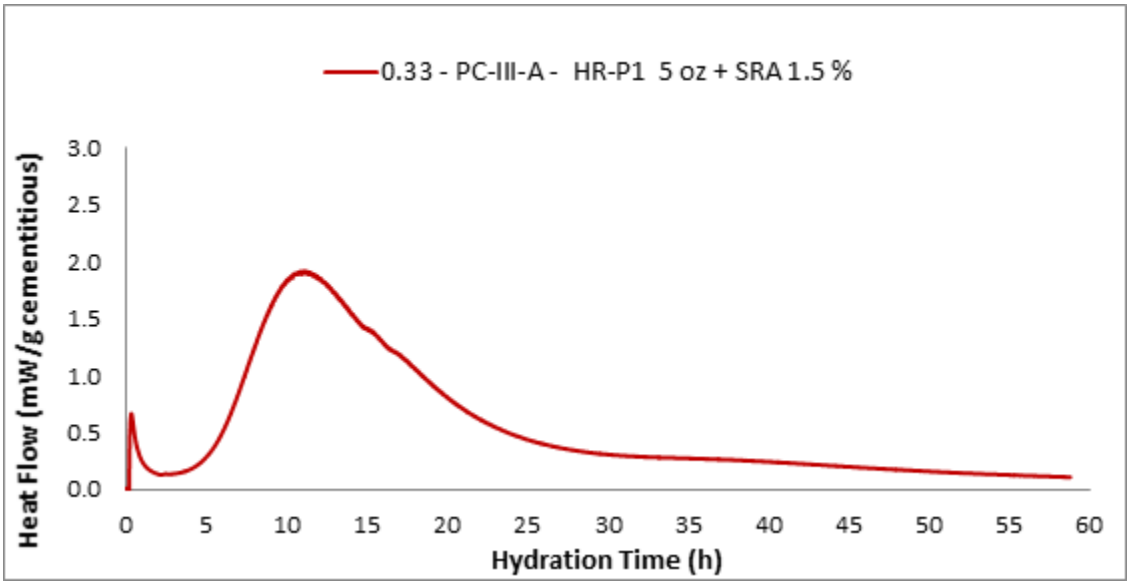

Fig. 145 Heat Flow 0.33 - PC-III-A - HR-P1 5 oz + SRA 1.5 %

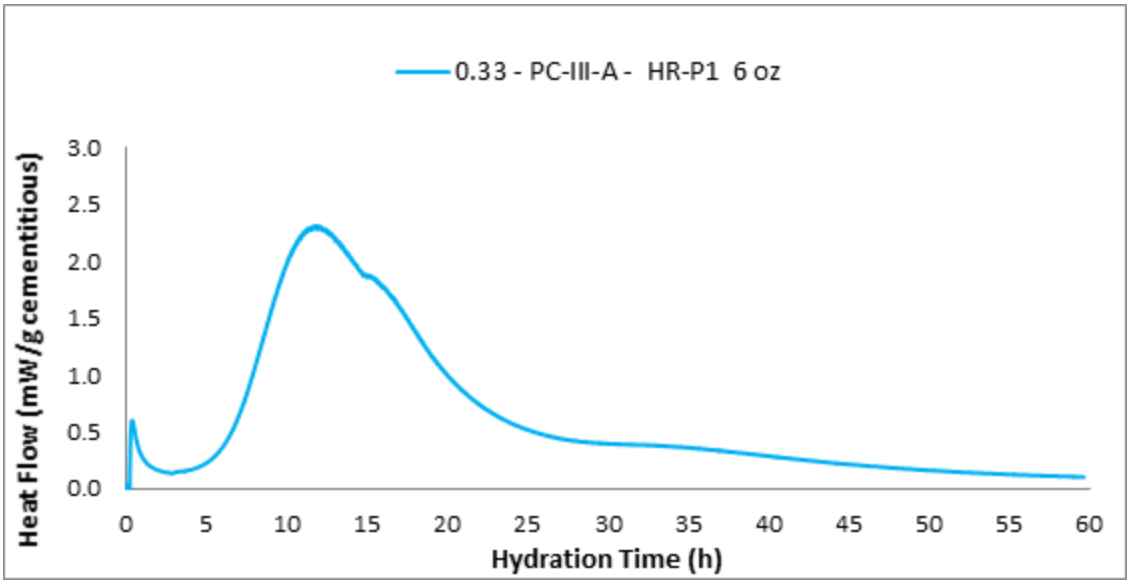

Fig. 146 Heat Flow 0.33 - PC-III-A - HR-P1 6 oz

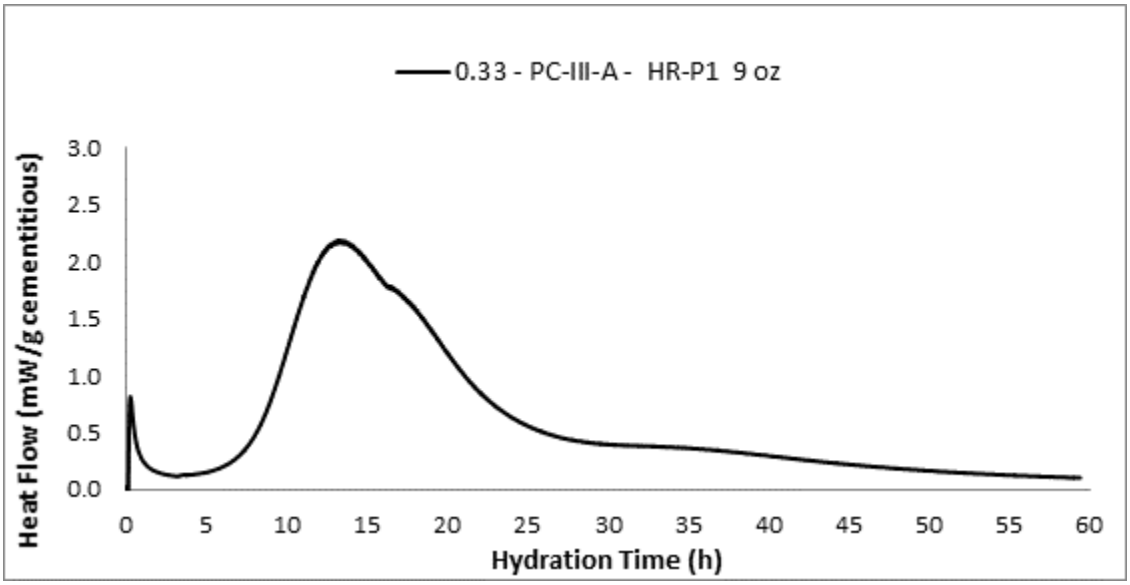

Fig. 147 Heat Flow 0.33 - PC-III-A - HR-P1 9 oz

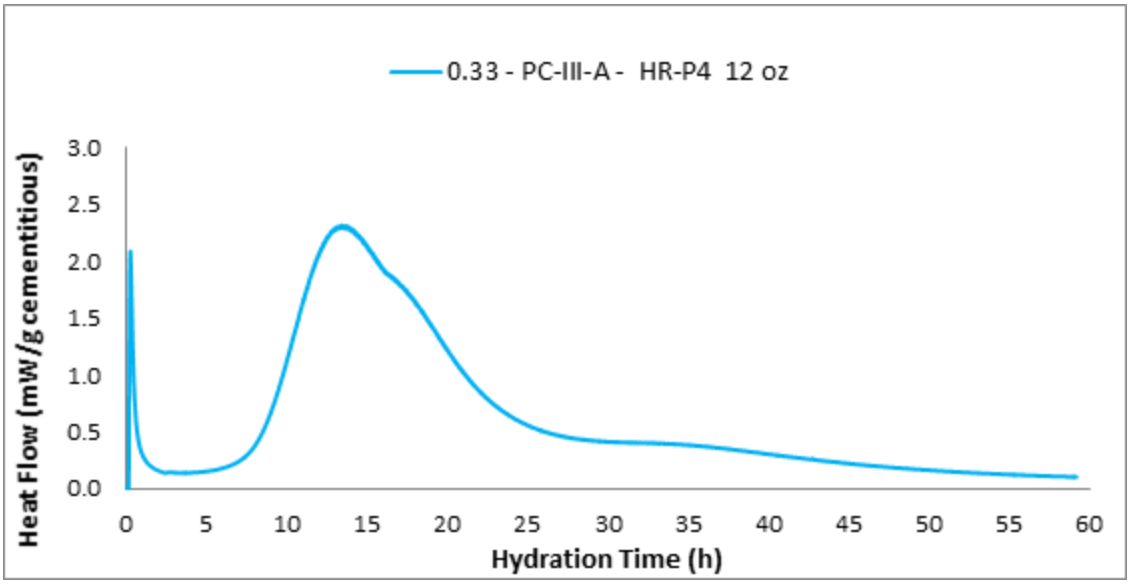

Fig. 148 Heat Flow 0.33 - PC-III-A - HR-P4 12 oz

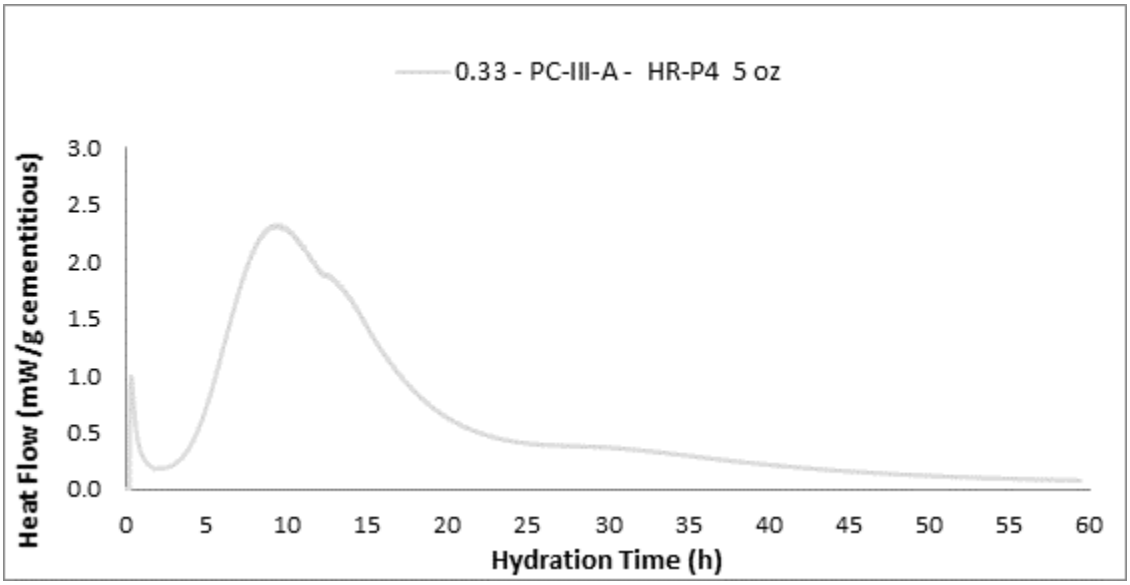

Fig. 149 Heat Flow 0.33 - PC-III-A - HR-P4 5 oz

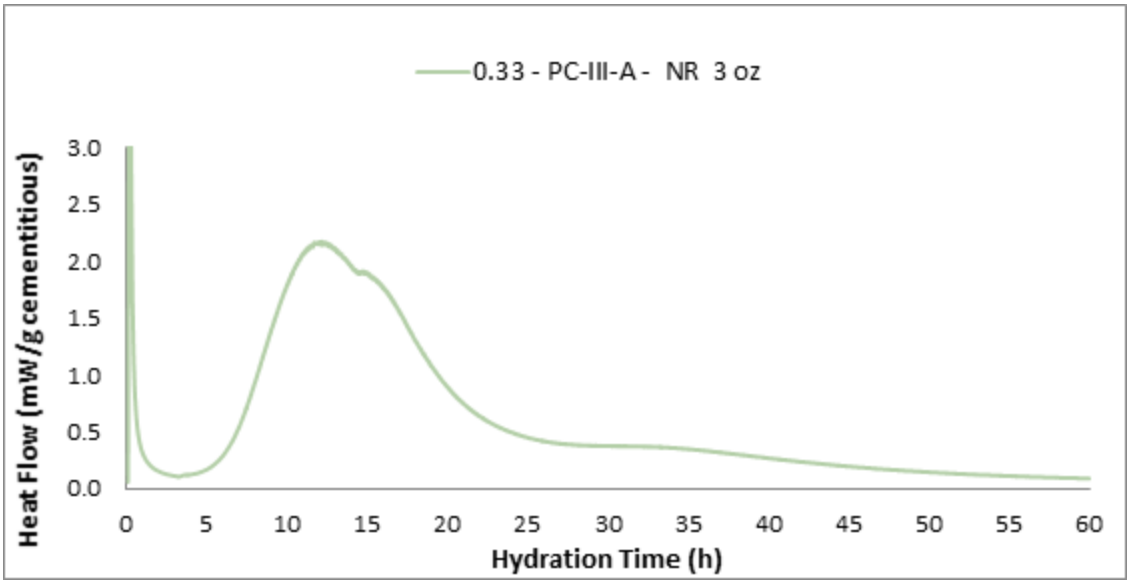

Fig. 150 Heat Flow 0.33 - PC-III-A - NR 3 oz

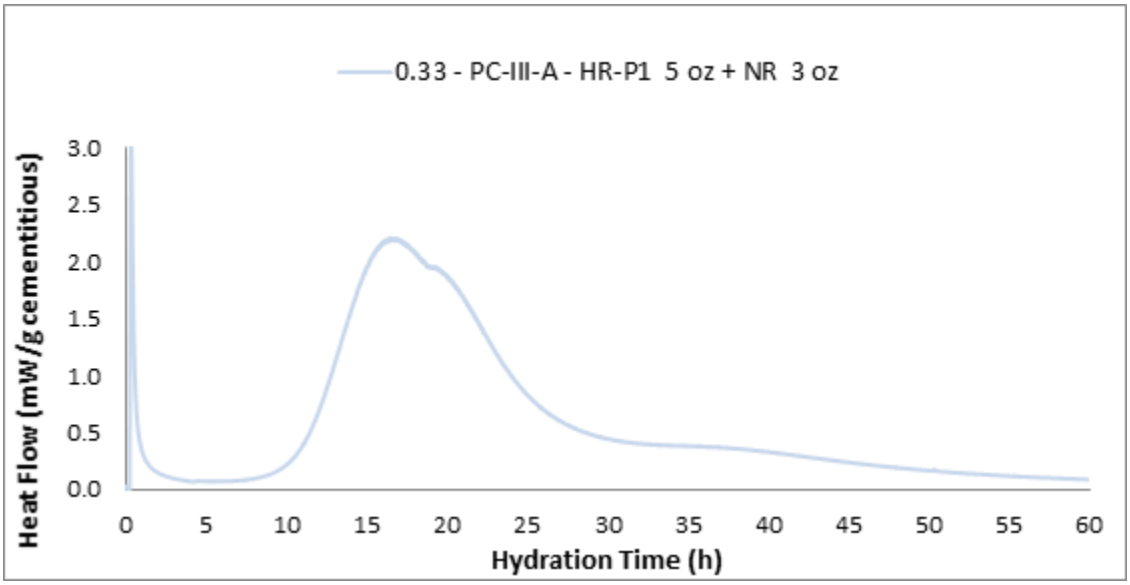

Fig. 151 Heat Flow 0.33 - PC-III-A - HR-P1 5 oz + NR 3 oz

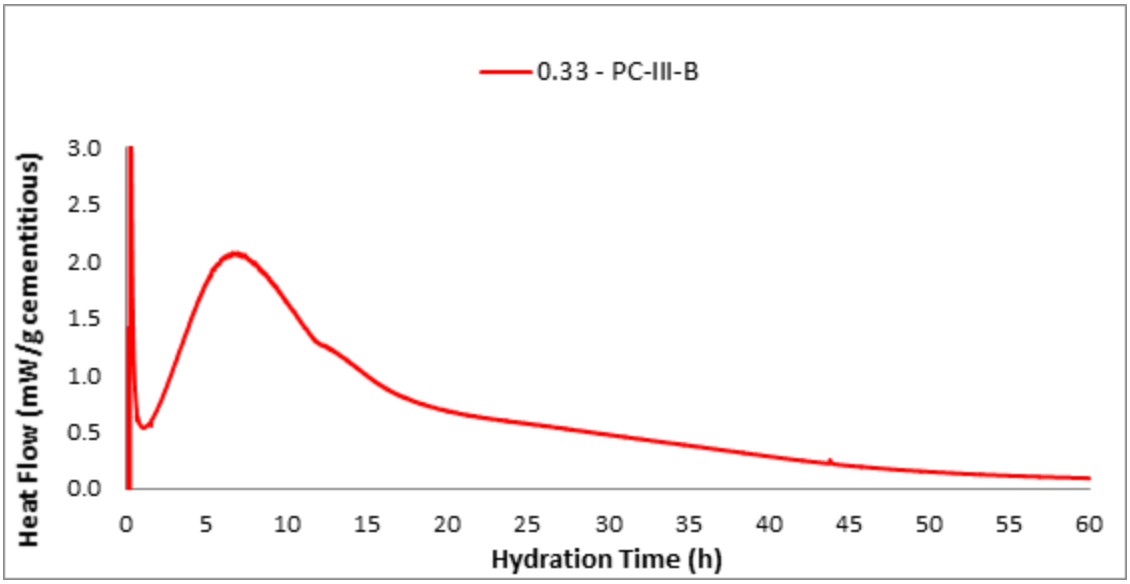

Fig. 152 Heat Flow 0.33 – PC-III-B

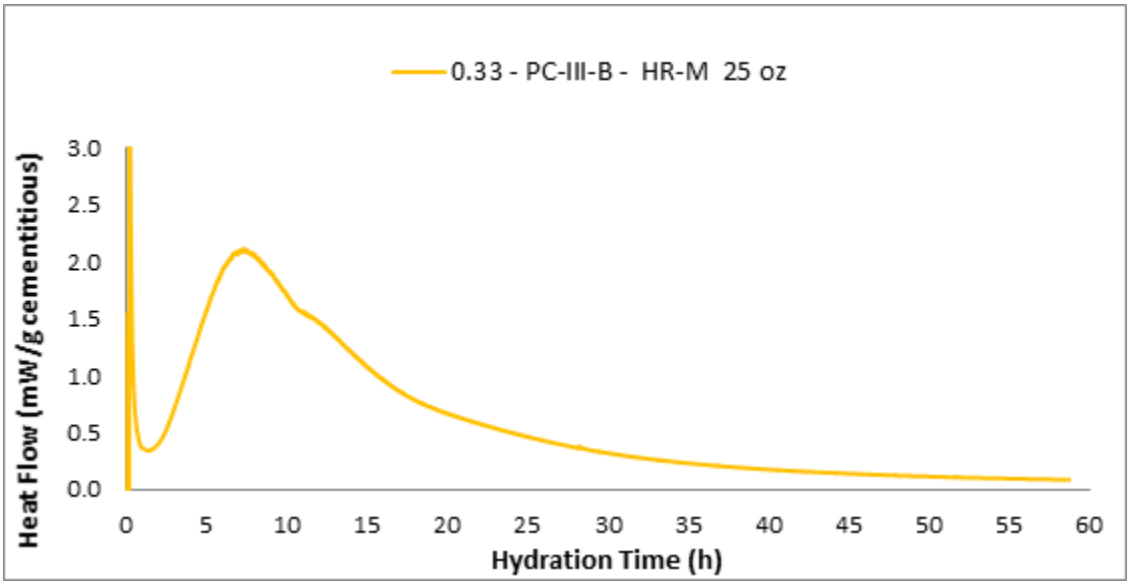

Fig. 153 Heat Flow 0.33 - PC-III-B - HR-M 25 oz

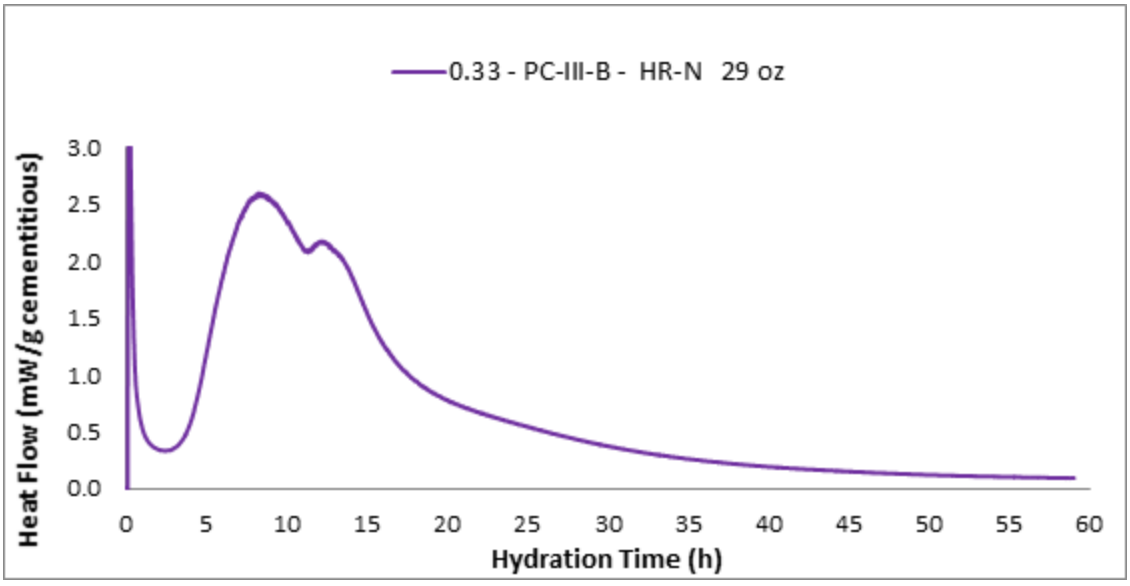

Fig. 154 Heat Flow 0.33 - PC-III-B - HR-N 29 oz

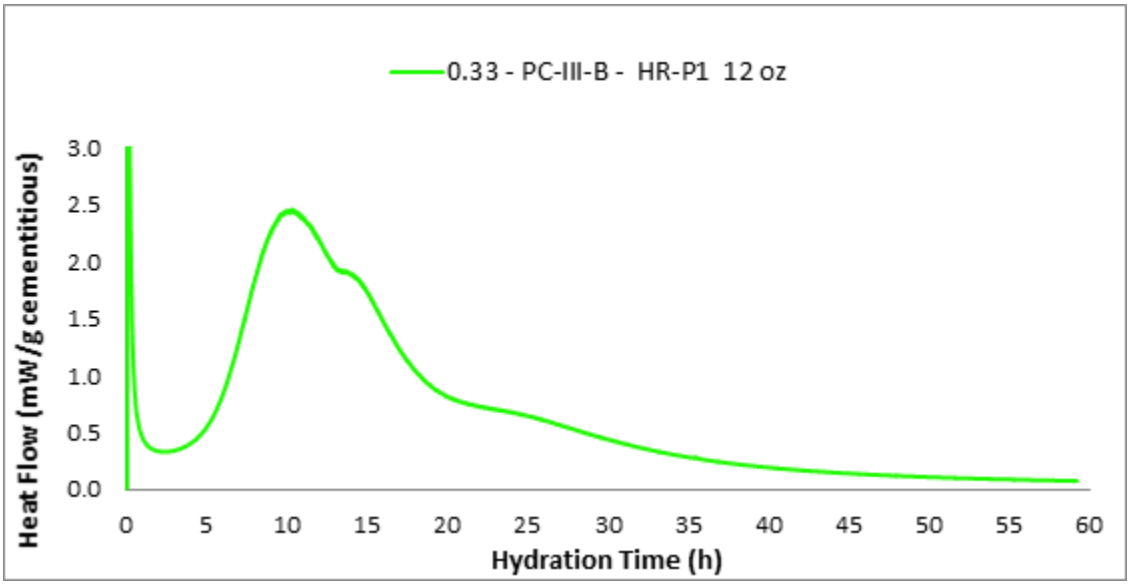

Fig. 155 Heat Flow 0.33 - PC-III-B - HR-P1 12 oz

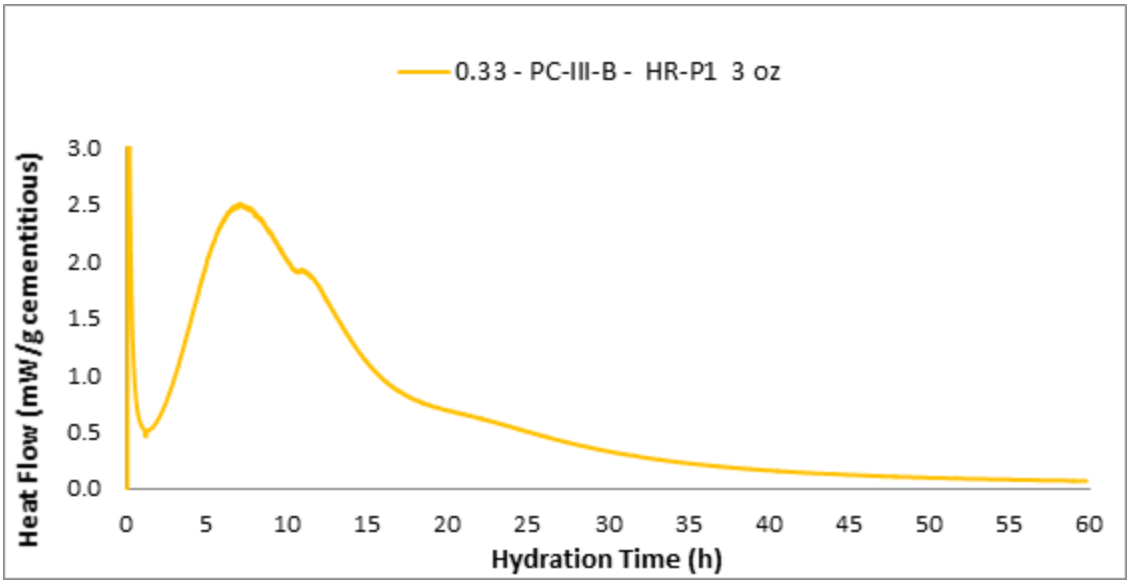

Fig. 156 Heat Flow 0.33 - PC-III-B - HR-P1 3 oz

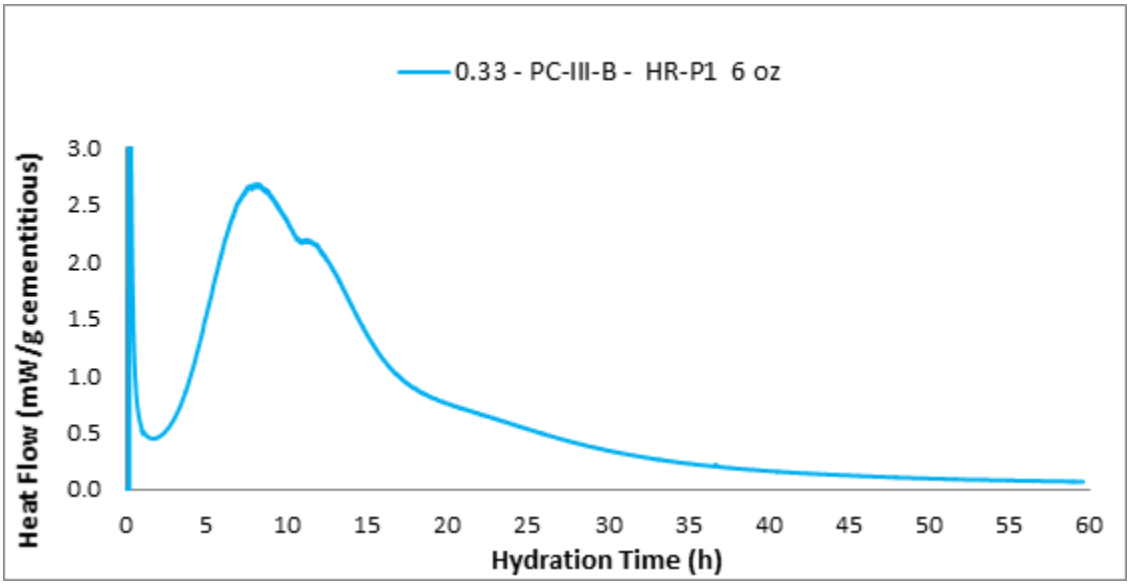

Fig. 157 Heat Flow 0.33 - PC-III-B - HR-P1 6 oz

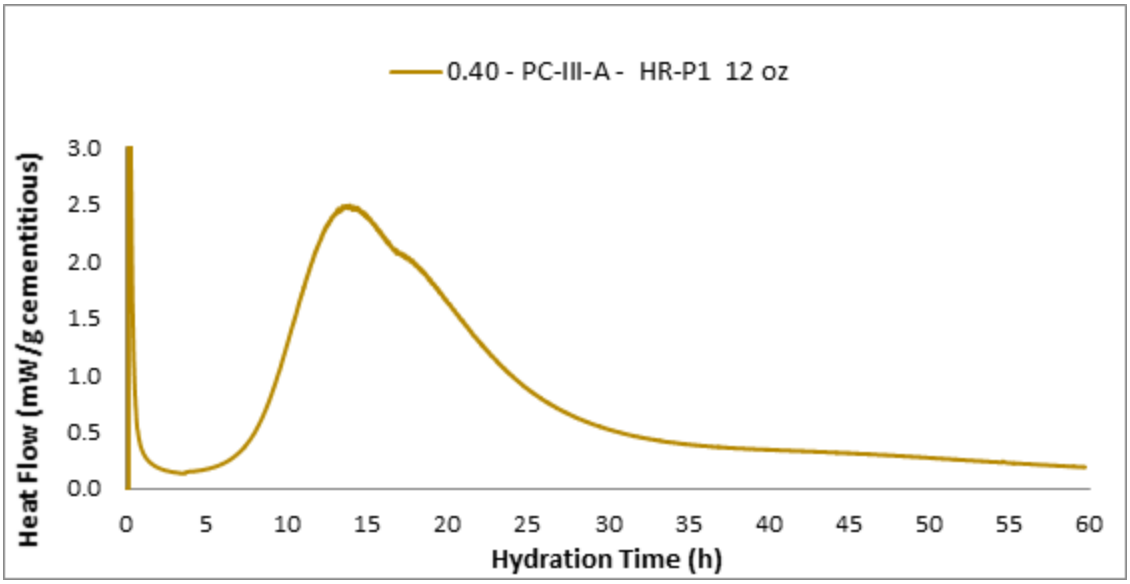

Fig. 158 Heat Flow 0.40 - PC-III-A - HR-P1 12 oz

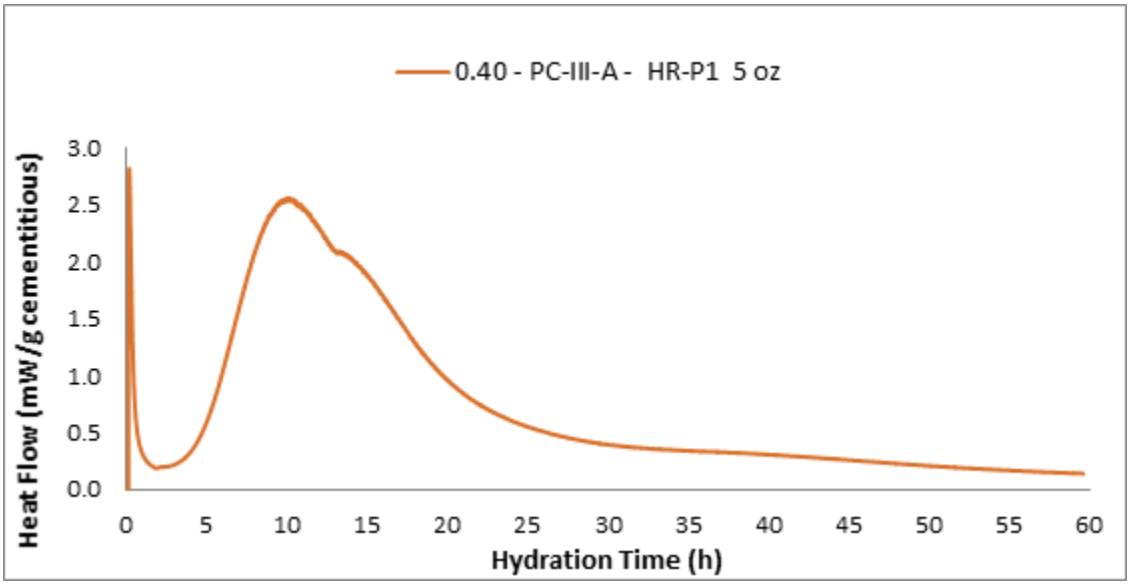

Fig. 159 Heat Flow 0.40 - PC-III-A - HR-P1 5 oz

III.2 CUMULATIVE HEAT CURVES

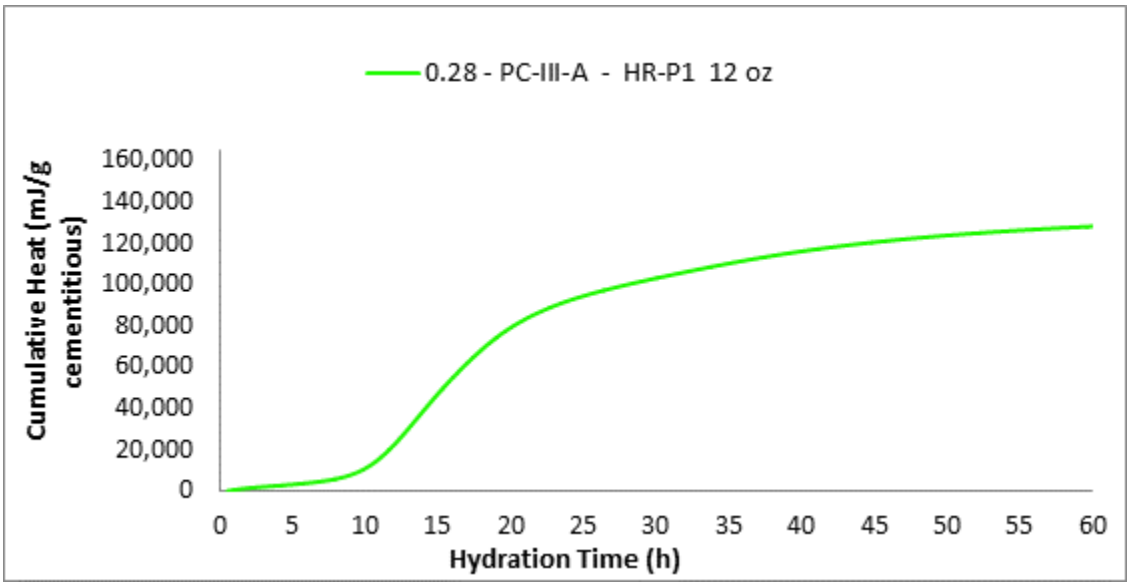

Fig.160 Cumulative Heat 0.28 - PC-III-A - HR-P1 12 oz

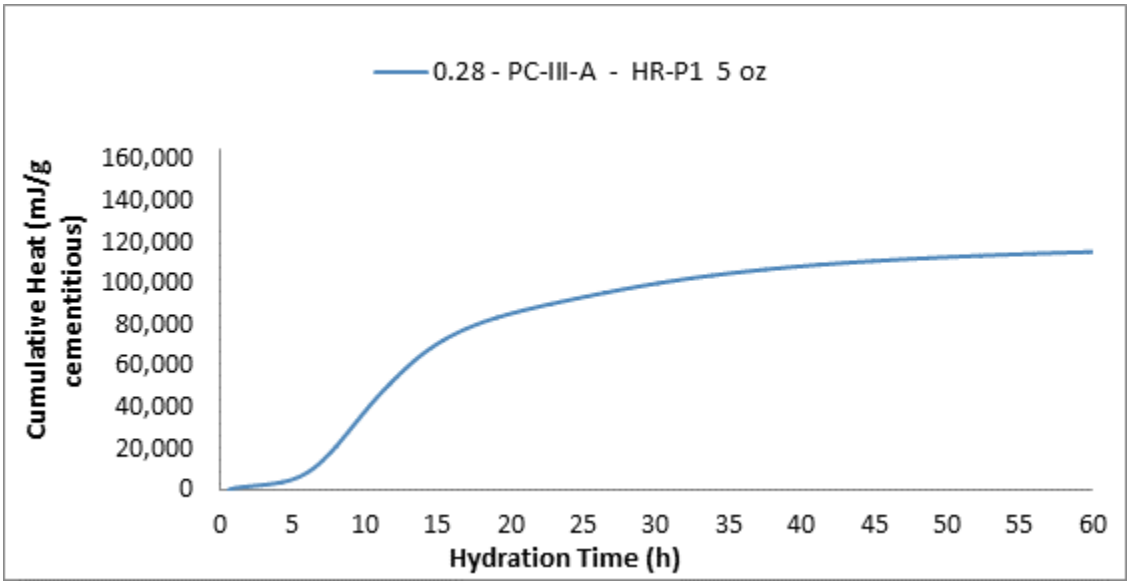

Fig.161 Cumulative Heat 0.28 - PC-III-A - HR-P1 5 oz

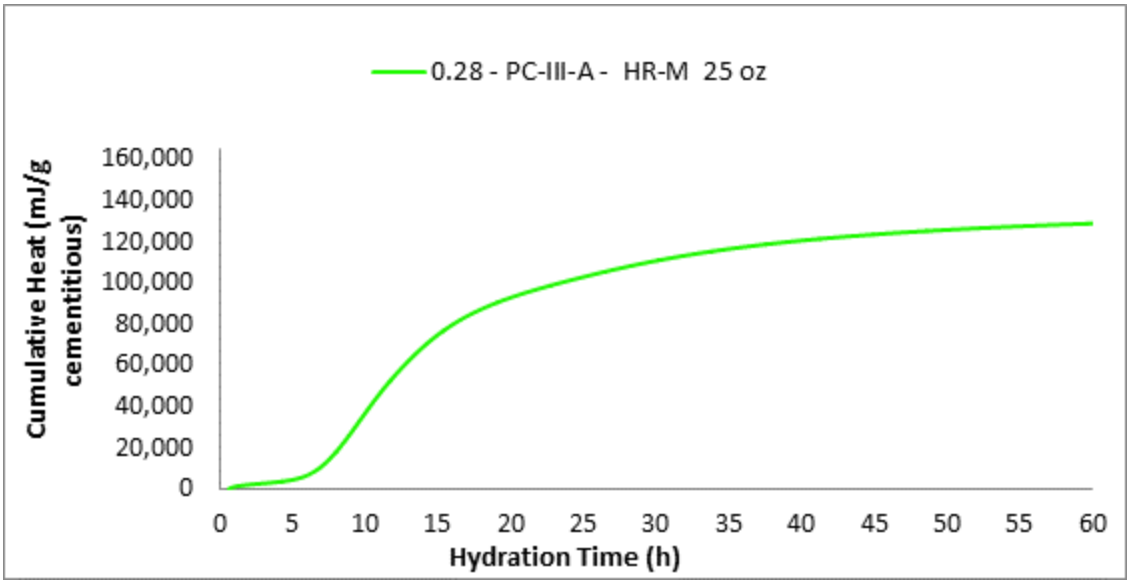

Fig.162 Cumulative Heat 0.28 - PC-III-A - HR-M 25 oz

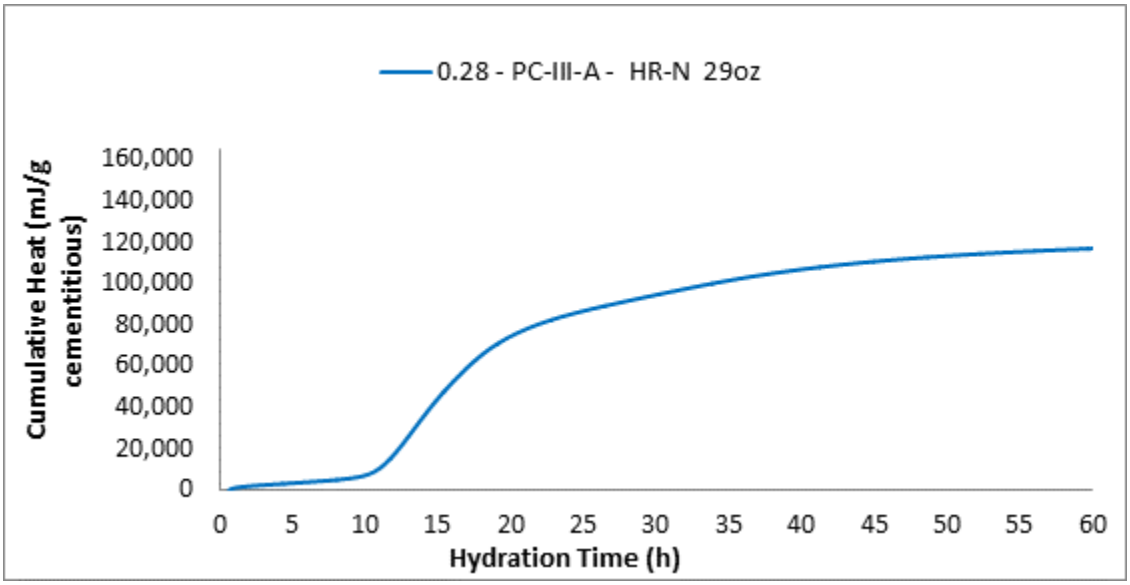

Fig.163 Cumulative Heat 0.28 - PC-III-A - HR-N 29oz

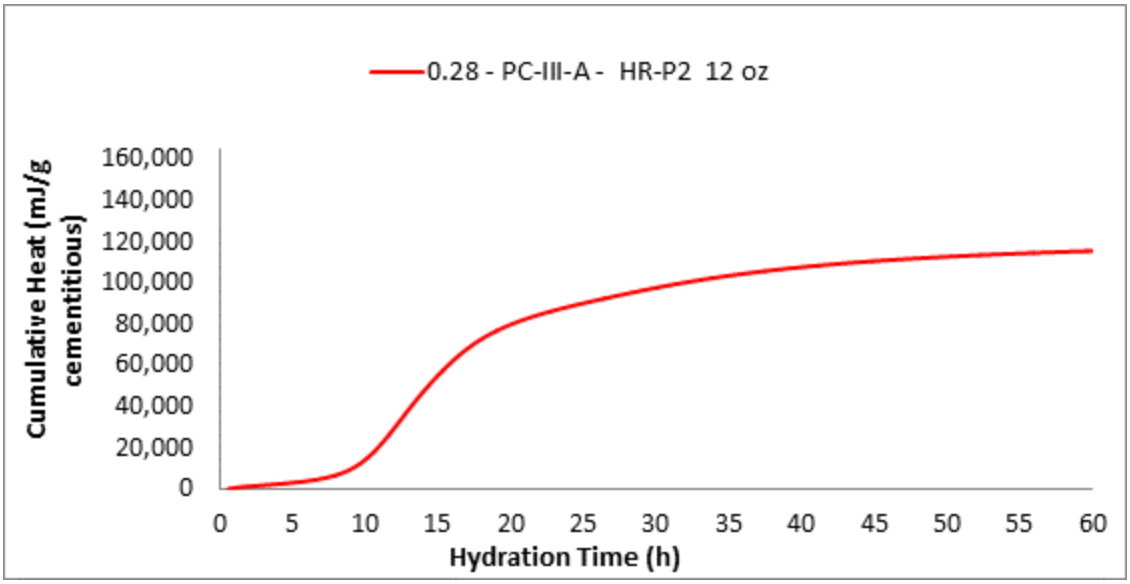

Fig.164 Cumulative Heat 0.28 - PC-III-A - HR-P2 12 oz

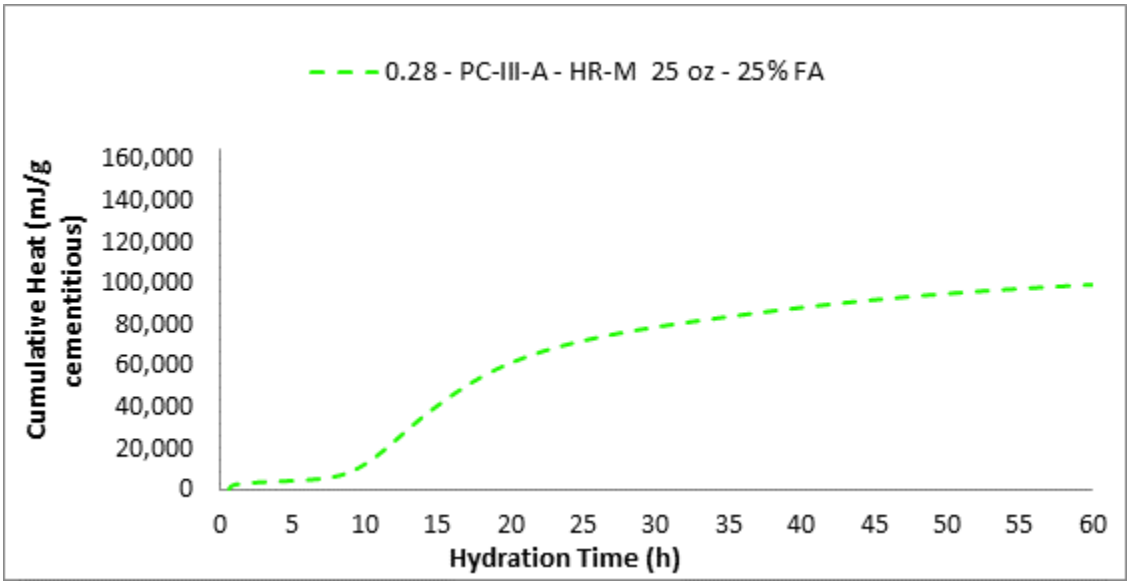

Fig.165 Cumulative Heat 0.28 - PC-III-A - HR-M 25 oz - 25% FA

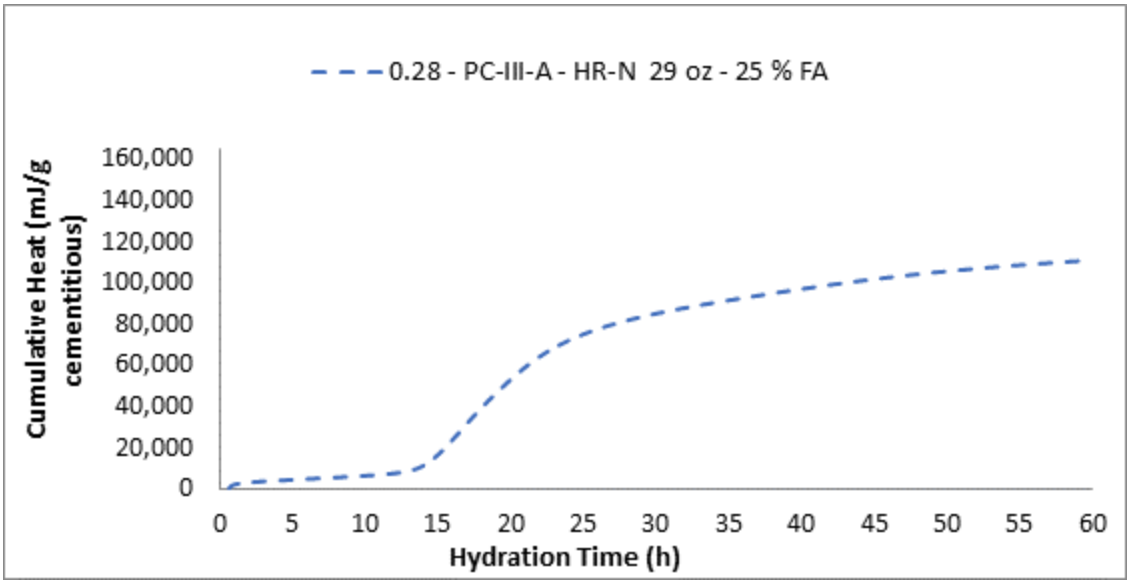

Fig.166 Cumulative Heat 0.28 - PC-III-A - HR-N 29 oz - 25 % FA

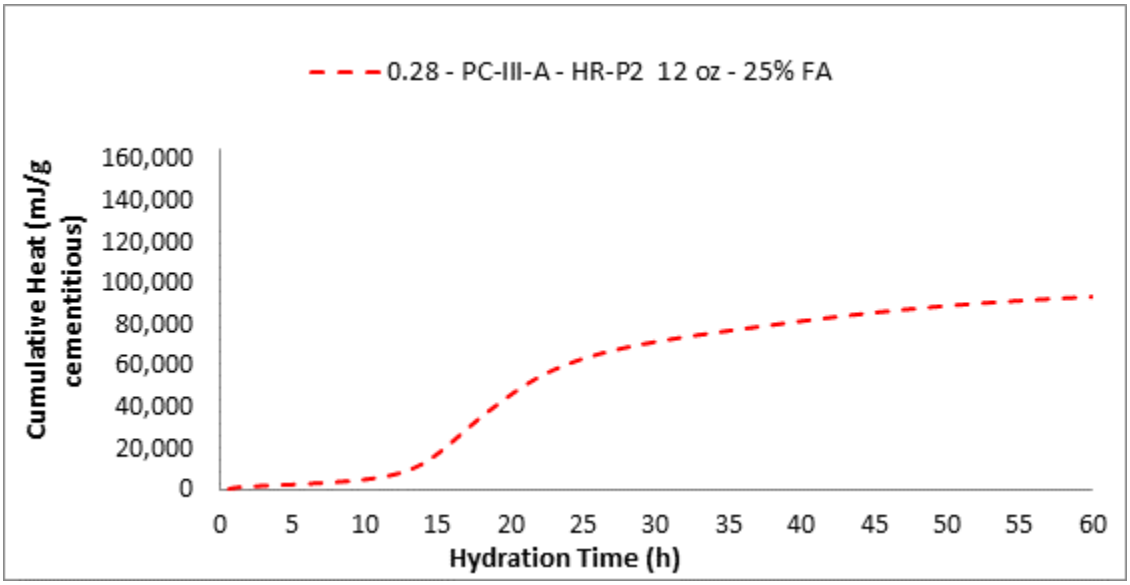

Fig.167 Cumulative Heat 0.28 - PC-III-A - HR-P2 12 oz - 25% FA

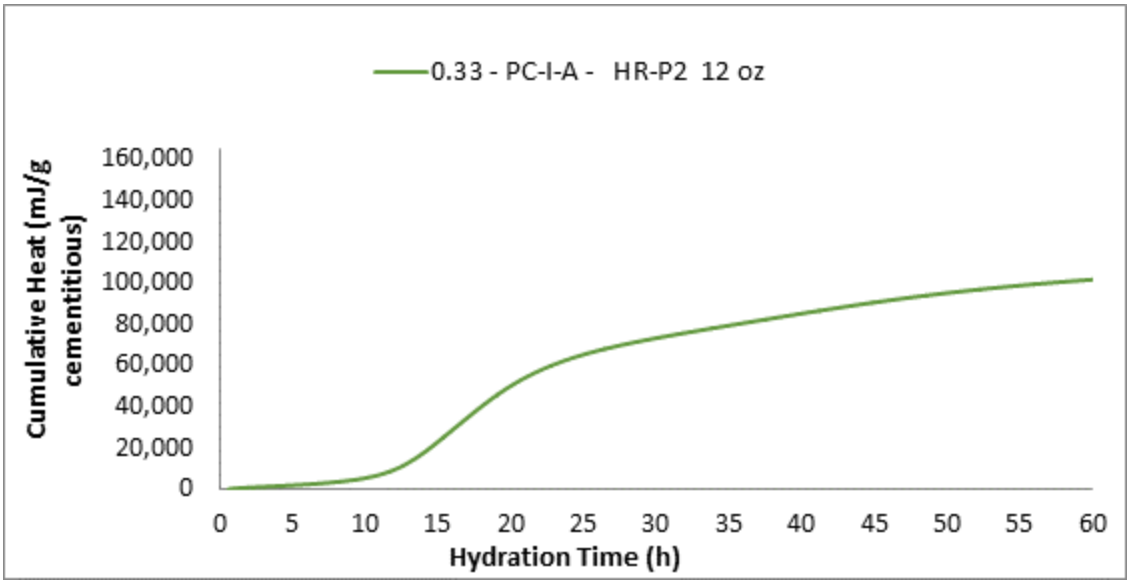

Fig.168 Cumulative Heat 0.33 - PC-I-A - HR-P2 12 oz

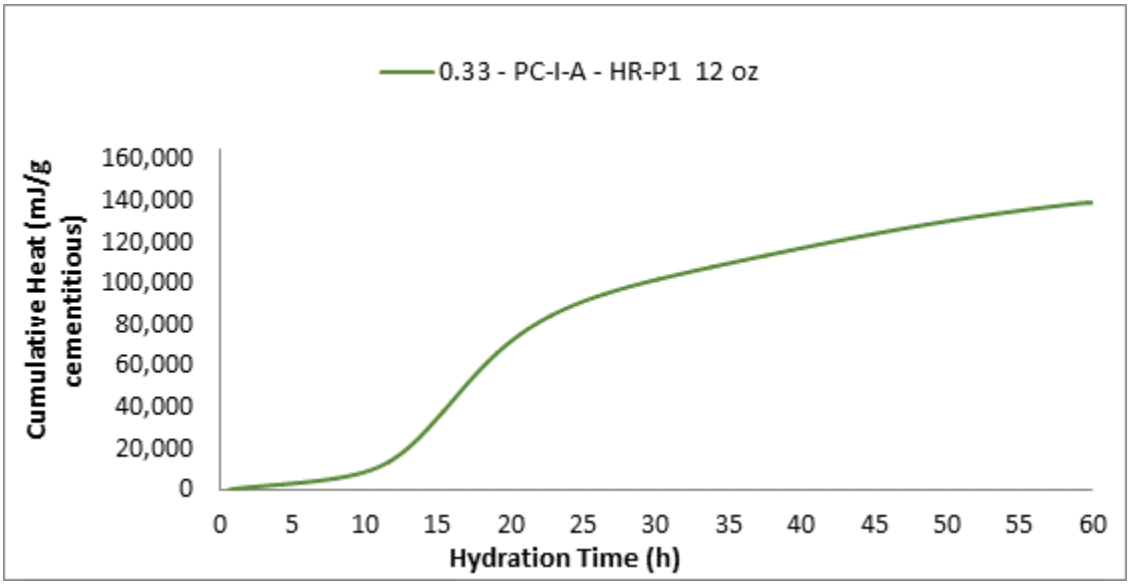

Fig.169 Cumulative Heat 0.33 - PC-I-A - HR-P1 12 oz

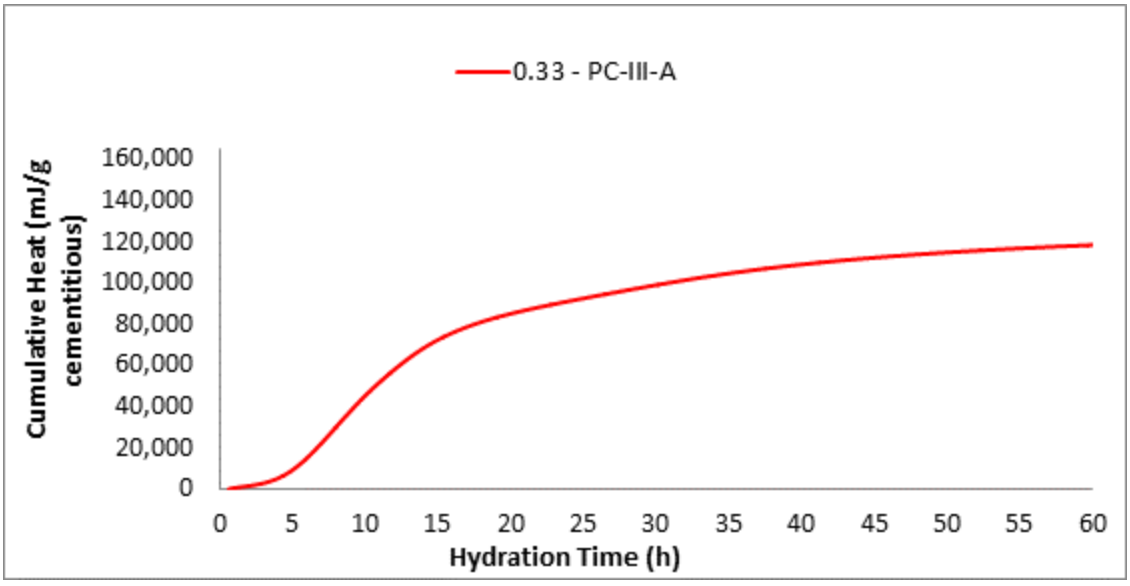

Fig.170 Cumulative Heat 0.33 - PC-III-A

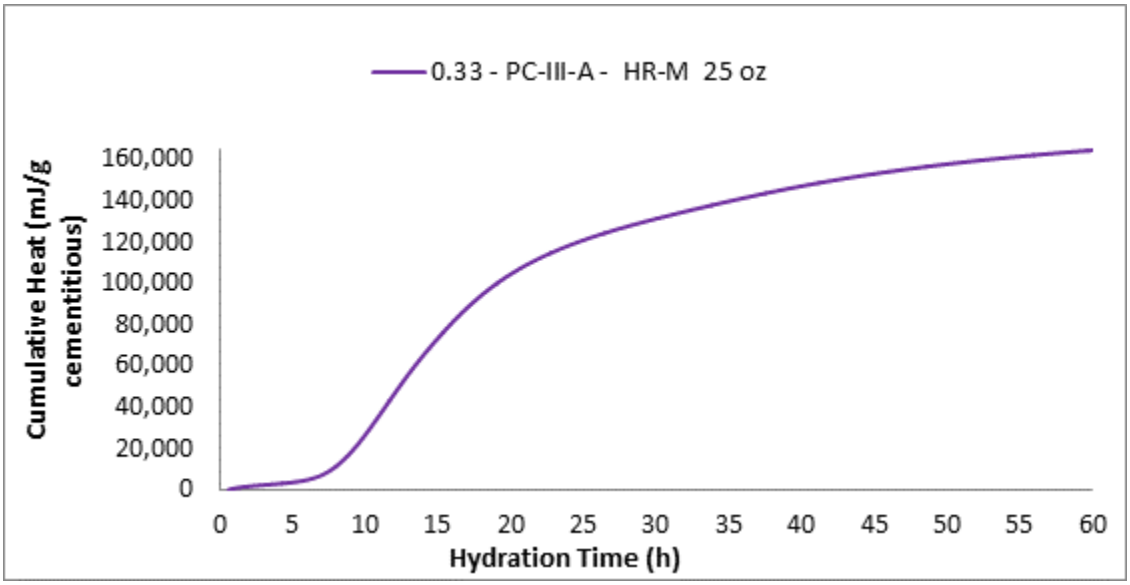

Fig.171 Cumulative Heat 0.33 - PC-III-A - HR-M 25 oz

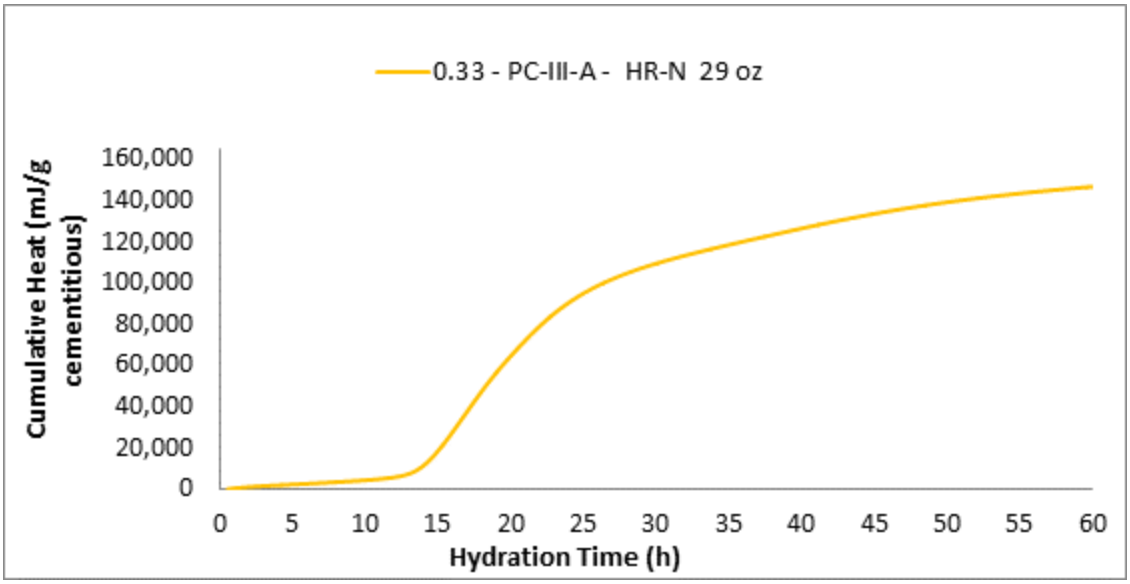

Fig.172 Cumulative Heat 0.33 - PC-III-A - HR-N 29 oz

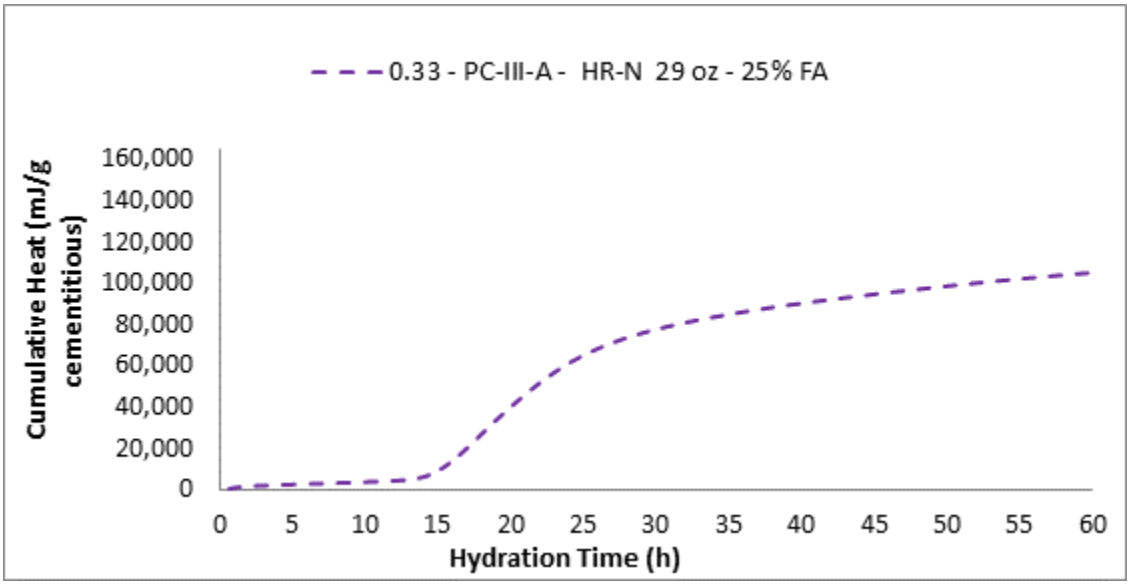

Fig.173 Cumulative Heat 0.33 - PC-III-A - HR-N 29 oz - 25% FA

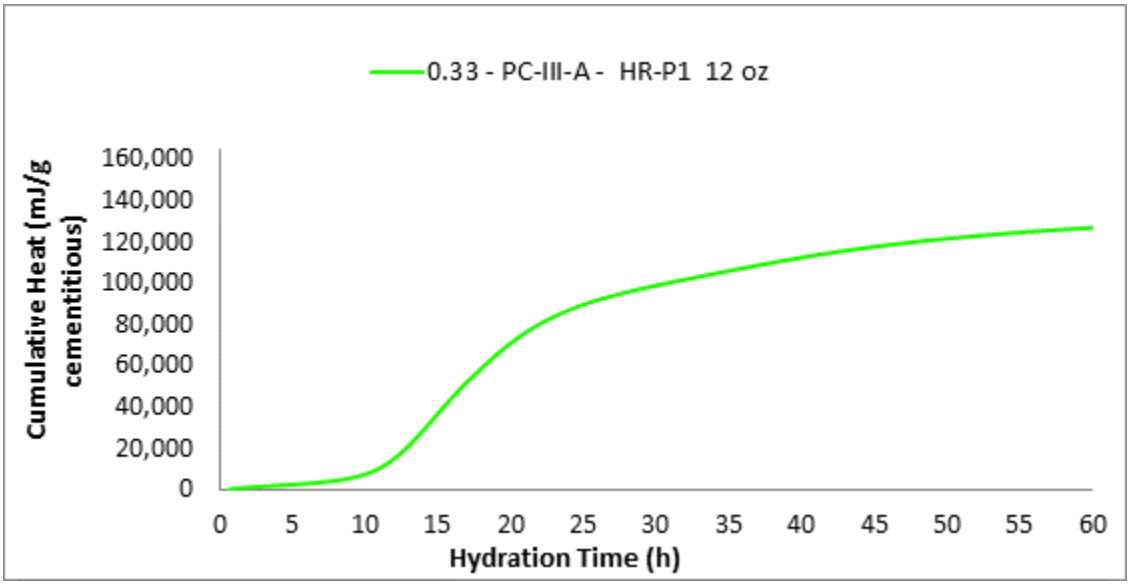

Fig.174 Cumulative Heat 0.33 - PC-III-A - HR-P1 12 oz

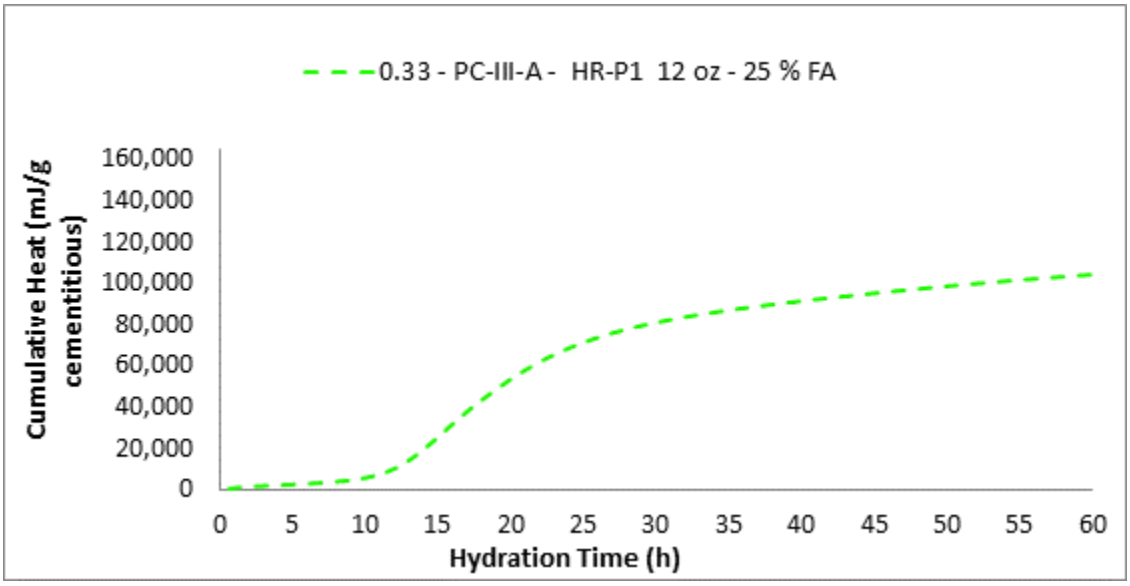

Fig.175 Cumulative Heat 0.33 - PC-III-A - HR-P1 12 oz - 25 % FA

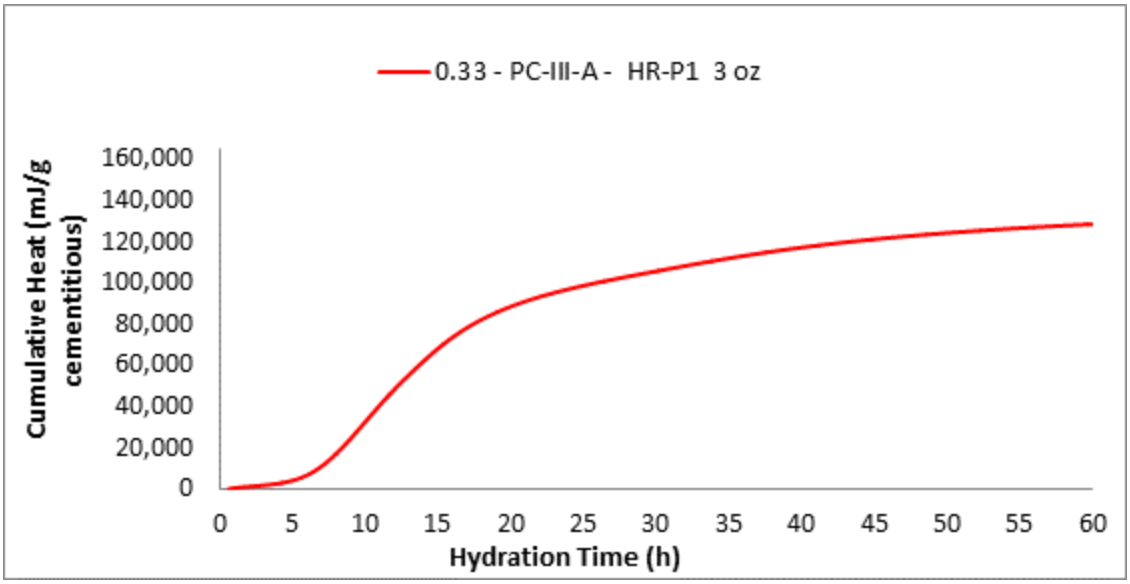

Fig.176 Cumulative Heat 0.33 - PC-III-A - HR-P1 3 oz

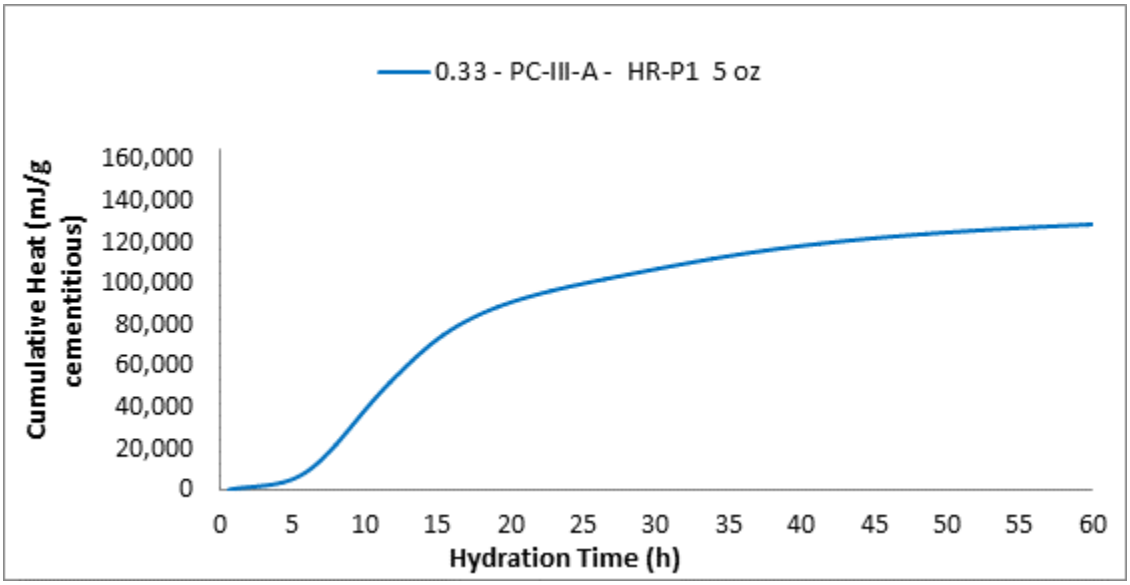

Fig.177 Cumulative Heat 0.33 - PC-III-A - HR-P1 5 oz

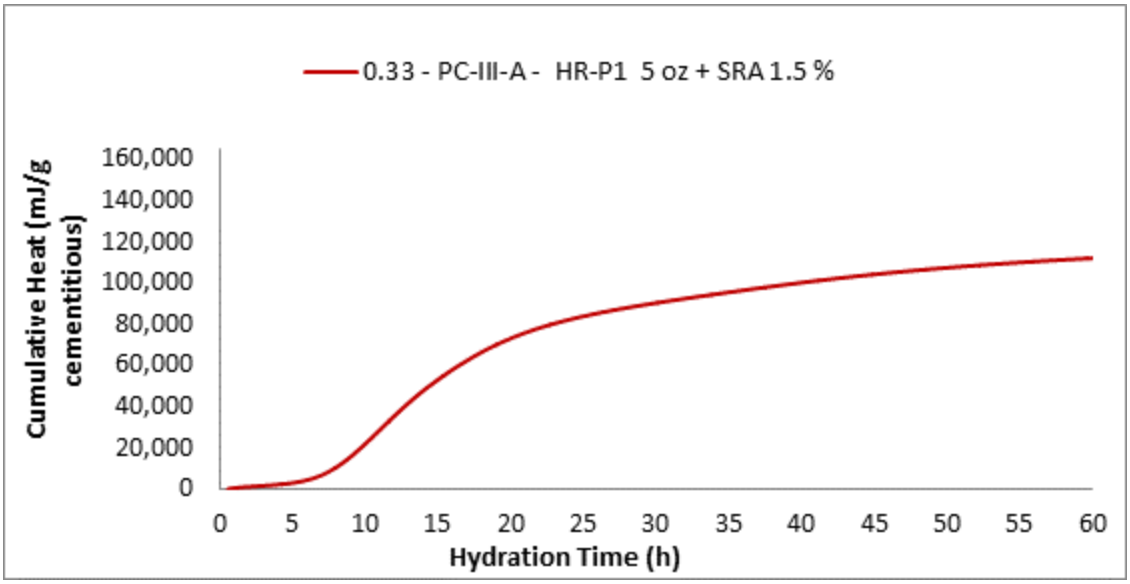

Fig.178 Cumulative Heat 0.33 - PC-III-A - HR-P1 5 oz + SRA 1.5 %

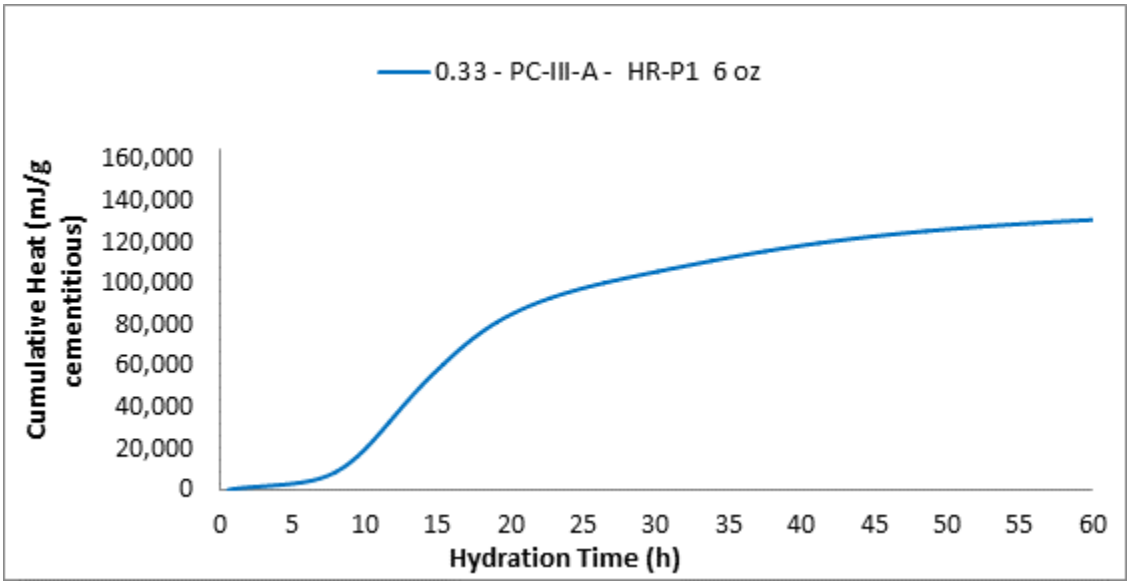

Fig.179 Cumulative Heat 0.33 - PC-III-A - HR-P1 6 oz

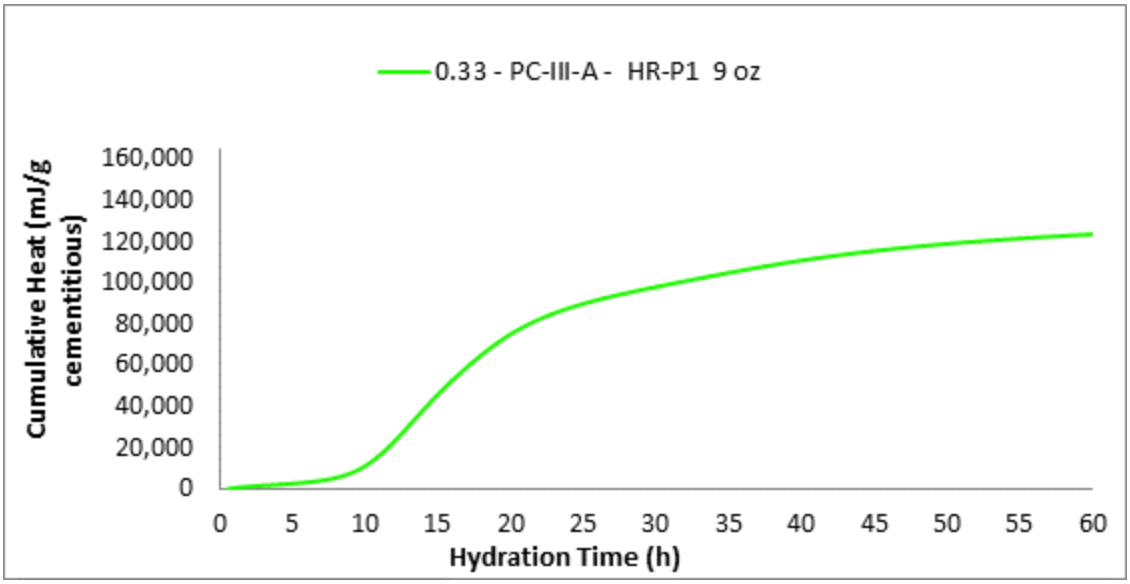

Fig.180 Cumulative Heat 0.33 - PC-III-A - HR-P1 9 oz

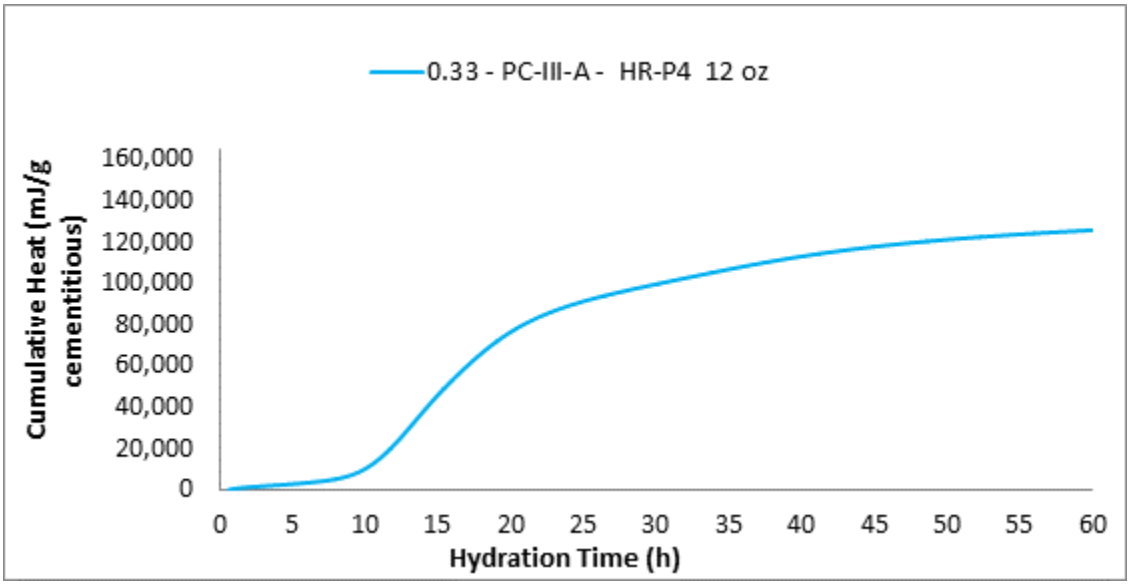

Fig.181 Cumulative Heat 0.33 - PC-III-A - HR-P4 12 oz

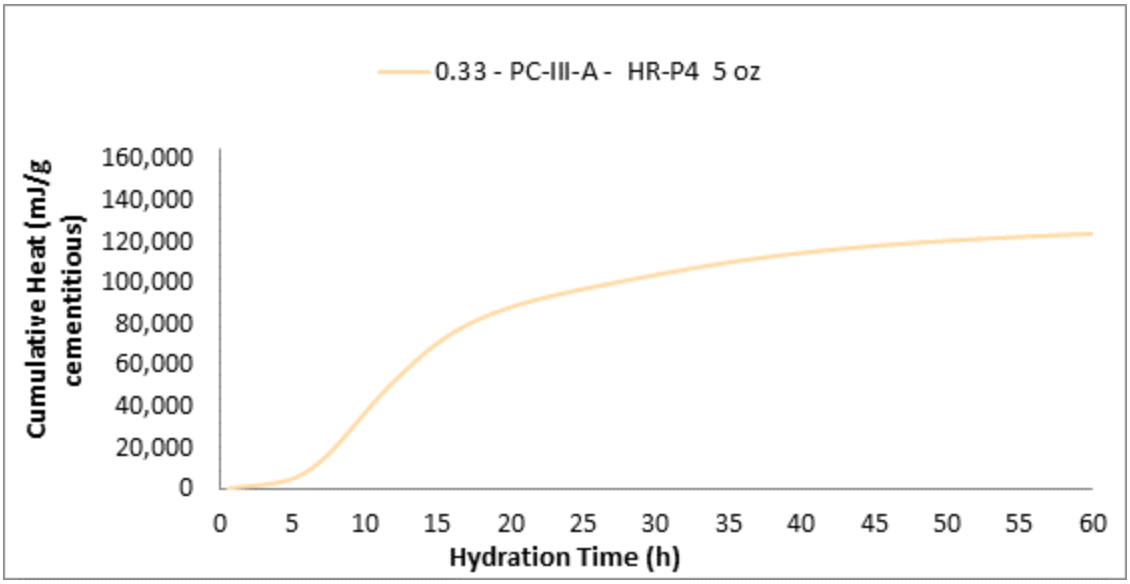

Fig.182 Cumulative Heat 0.33 - PC-III-A - HR-P4 5 oz

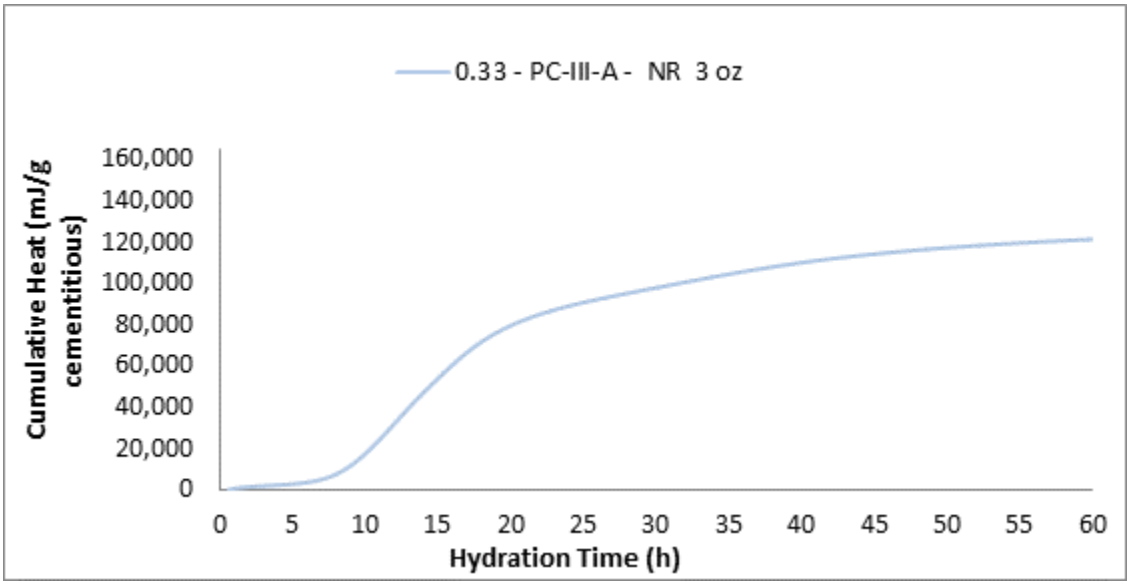

Fig.183 Cumulative Heat 0.33 - PC-III-A - NR 3 oz

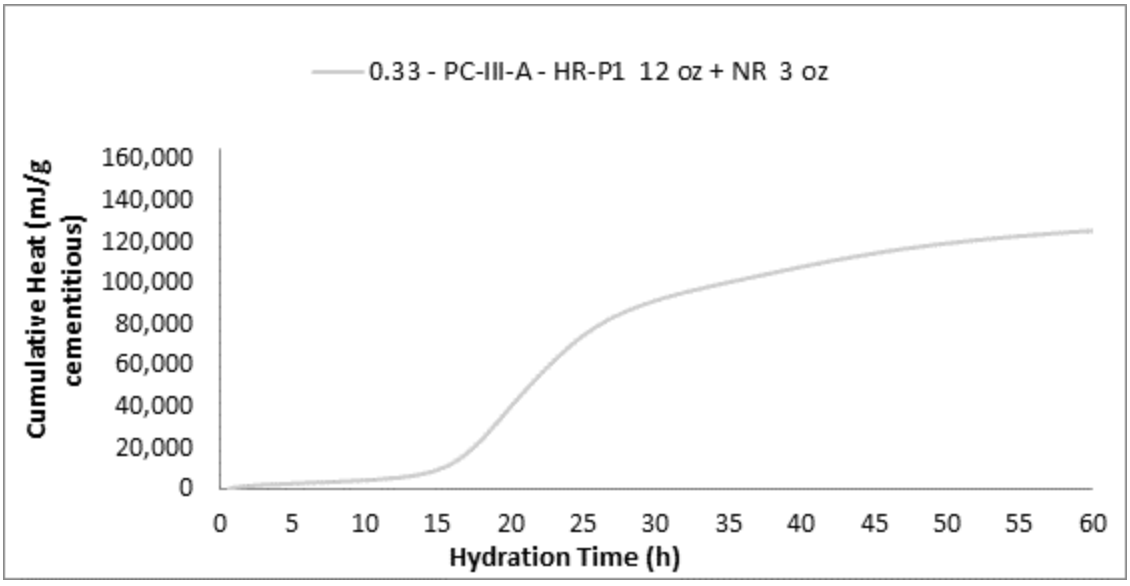

Fig.184 Cumulative Heat 0.33 - PC-III-A - HR-P1 12 oz + NR 3 oz

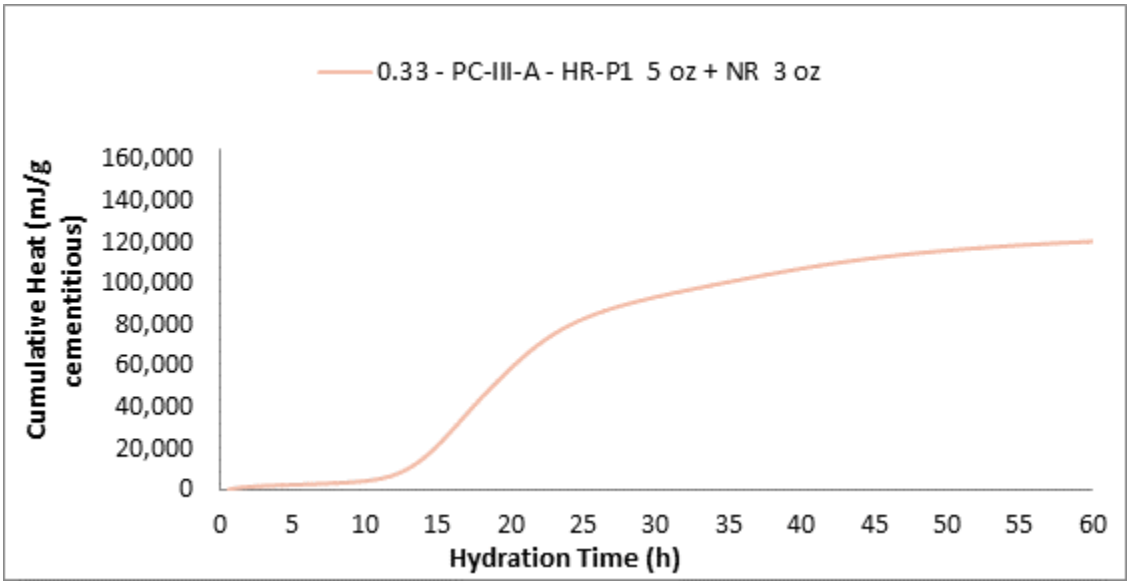

Fig.185 Cumulative Heat 0.33 - PC-III-A - HR-P1 5 oz + NR 3 oz

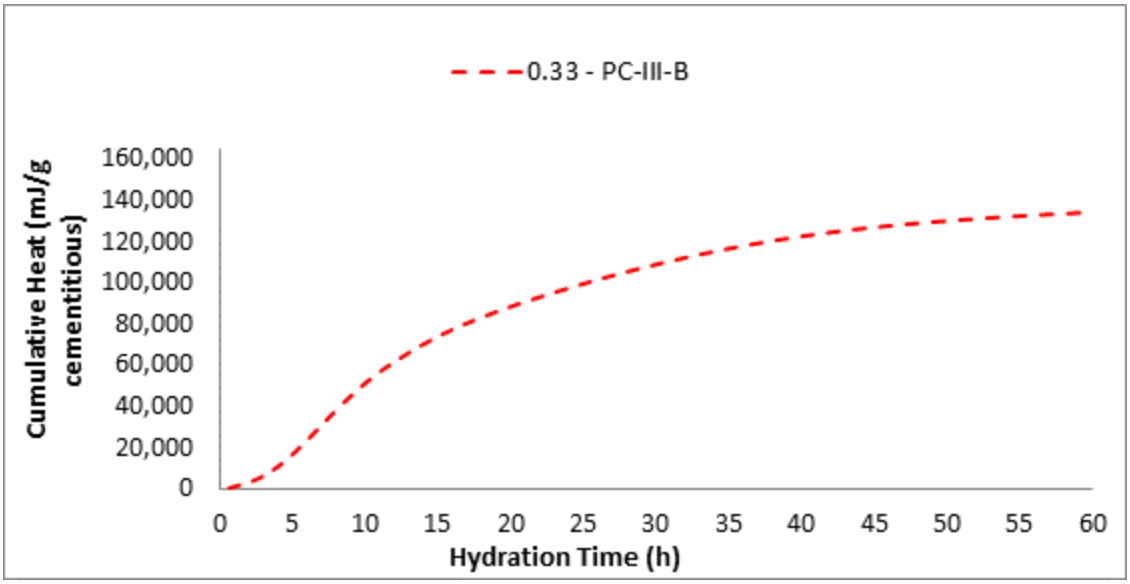

Fig.186 Cumulative Heat 0.33 - PC-III-B

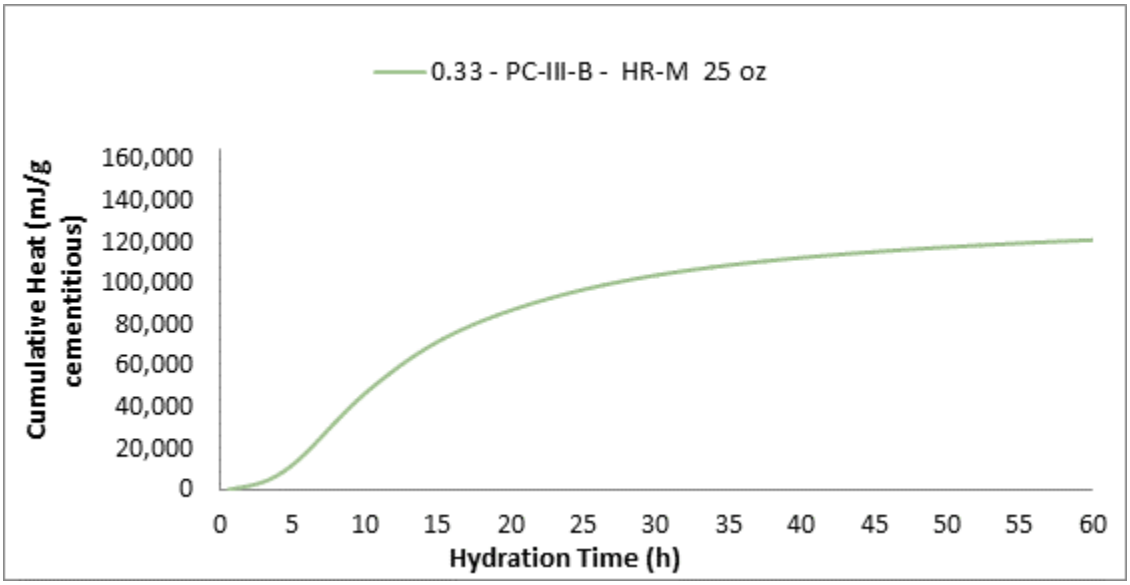

Fig.187 Cumulative Heat 0.33 - PC-III-B - HR-M 25 oz

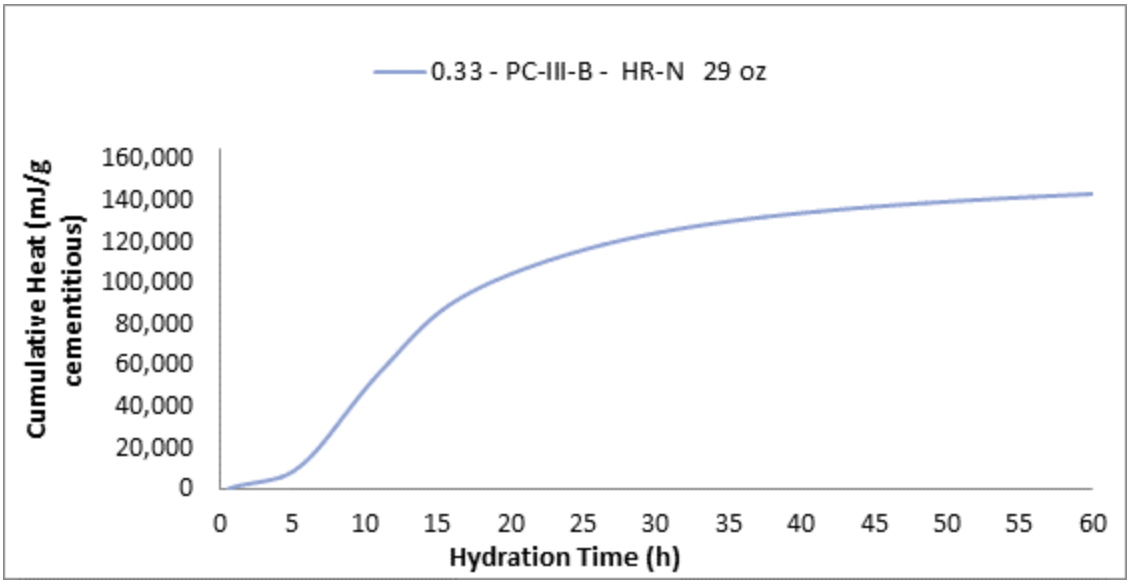

Fig.188 Cumulative Heat 0.33 - PC-III-B - HR-N 29 oz

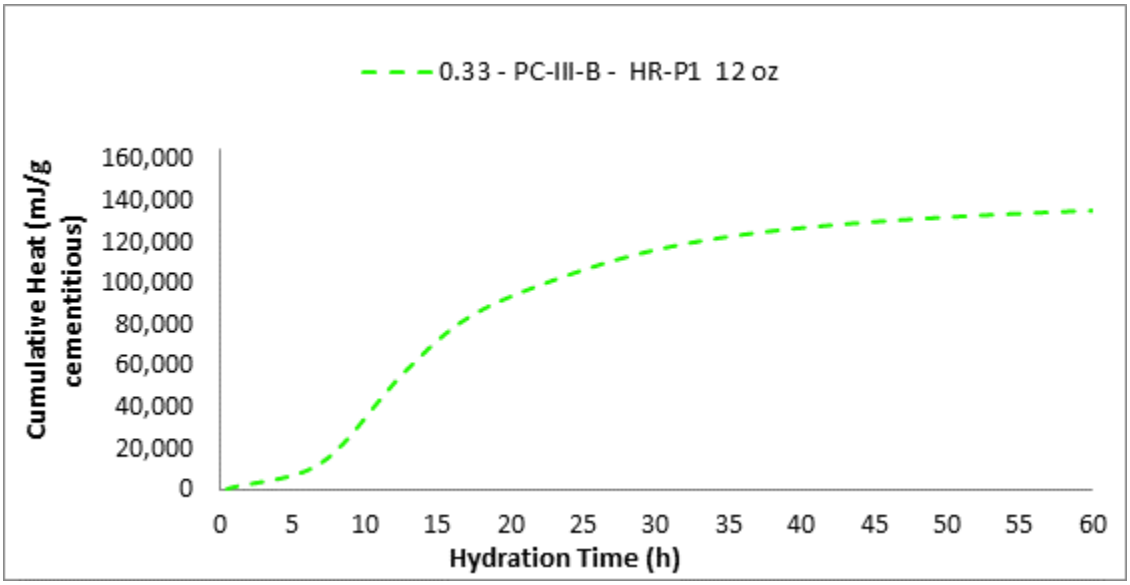

Fig.189 Cumulative Heat 0.33 - PC-III-B - HR-P1 12 oz

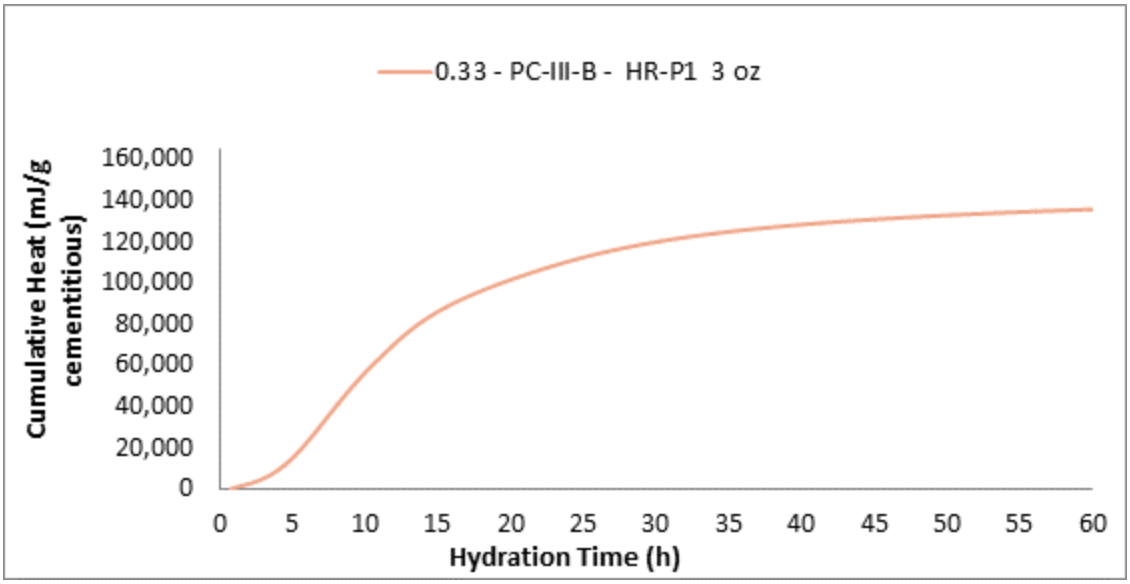

Fig.190 Cumulative Heat 0.33 - PC-III-B - HR-P1 3 oz

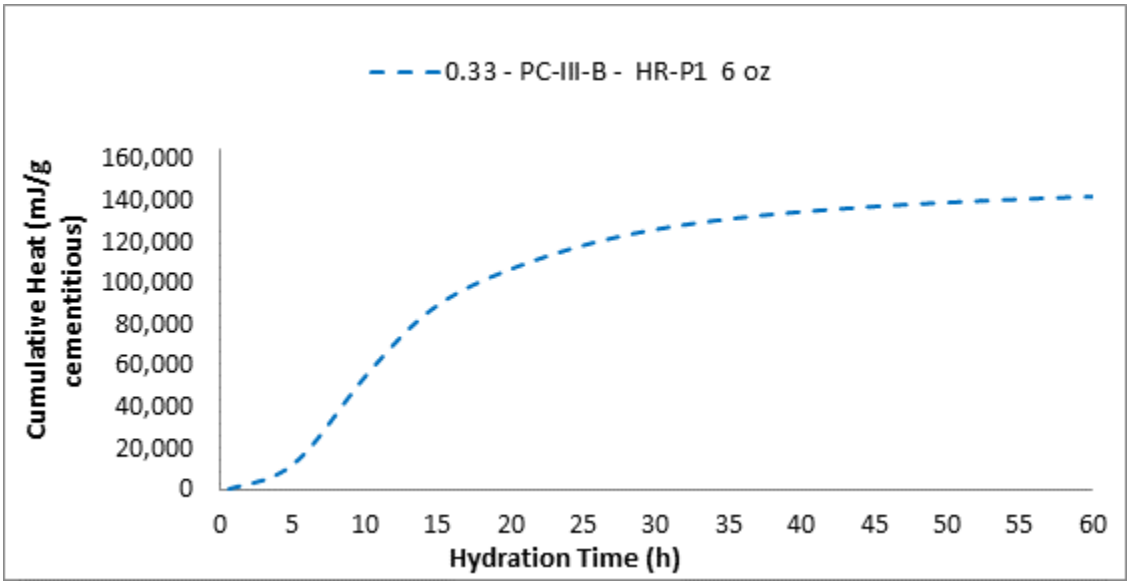

Fig.191 Cumulative Heat 0.33 - PC-III-B - HR-P1 6 oz

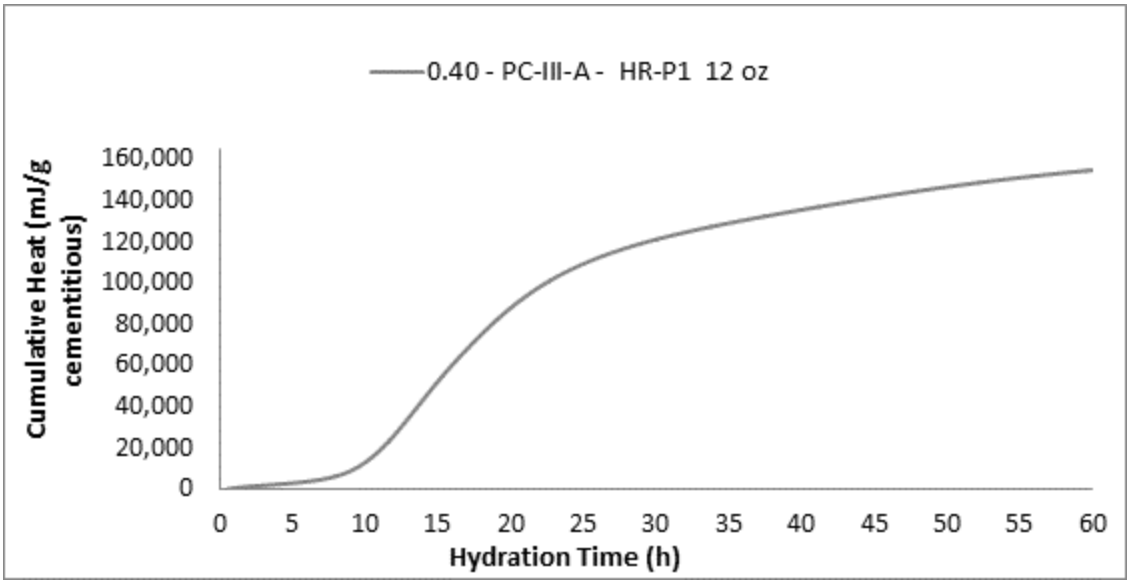

Fig.192 Cumulative Heat 0.40 - PC-III-A - HR-P1 12 oz

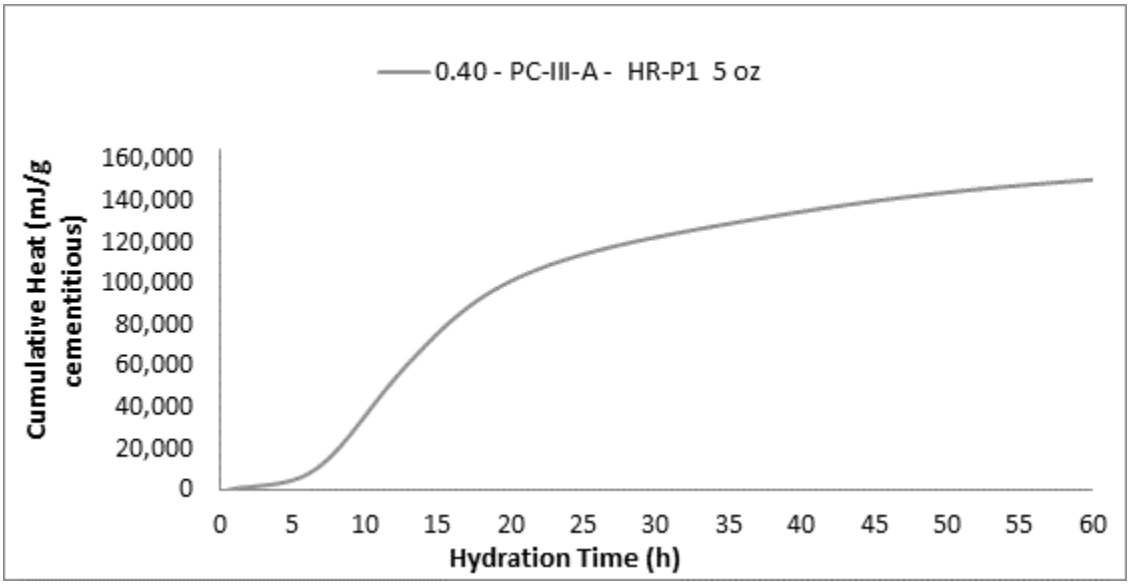

Fig.193 Cumulative Heat 0.40 - PC-III-A - HR-P1 5 oz

Appendix IV: Drying Shrinkage curves

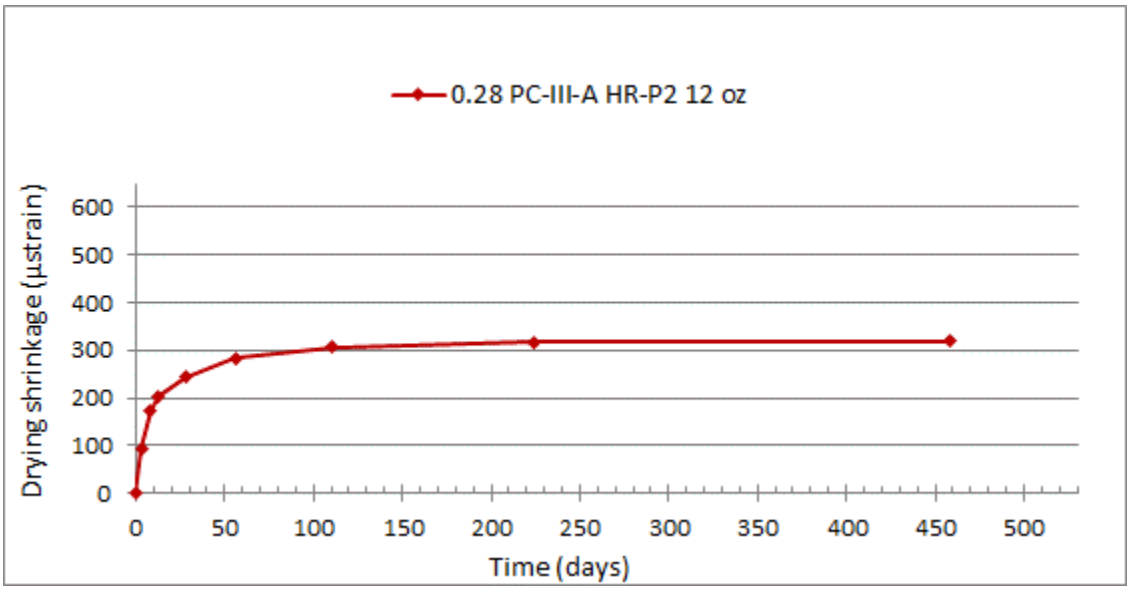

Fig.194 Drying Shrinkage 0.28 PC-III-A HR-P2 12 oz

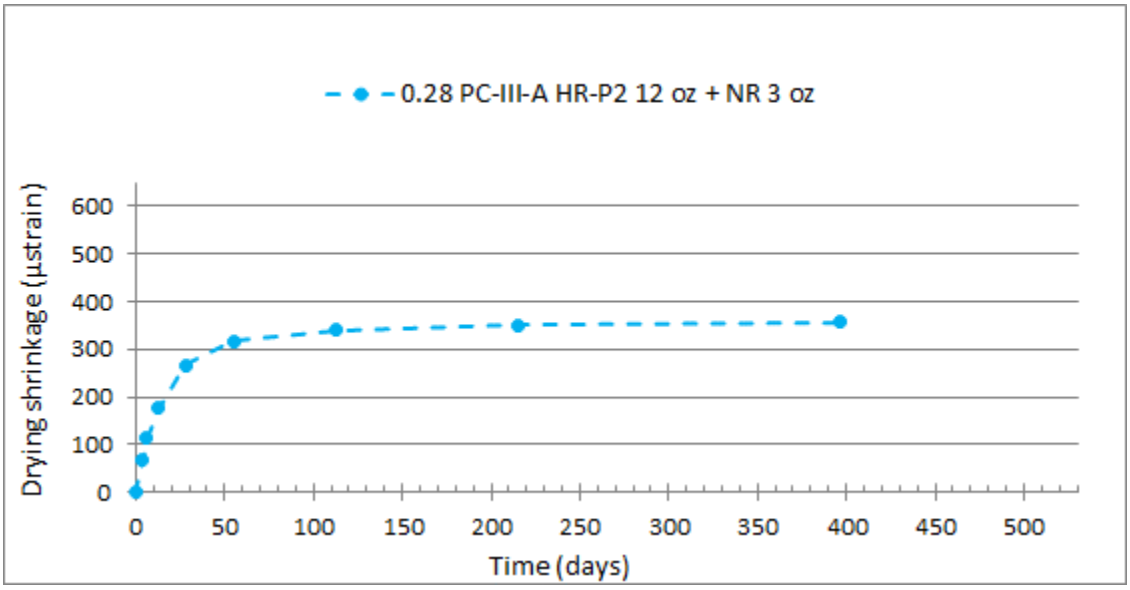

Fig.195 Drying Shrinkage 0.28 PC-III-A HR-P2 12 oz + NR 3 oz

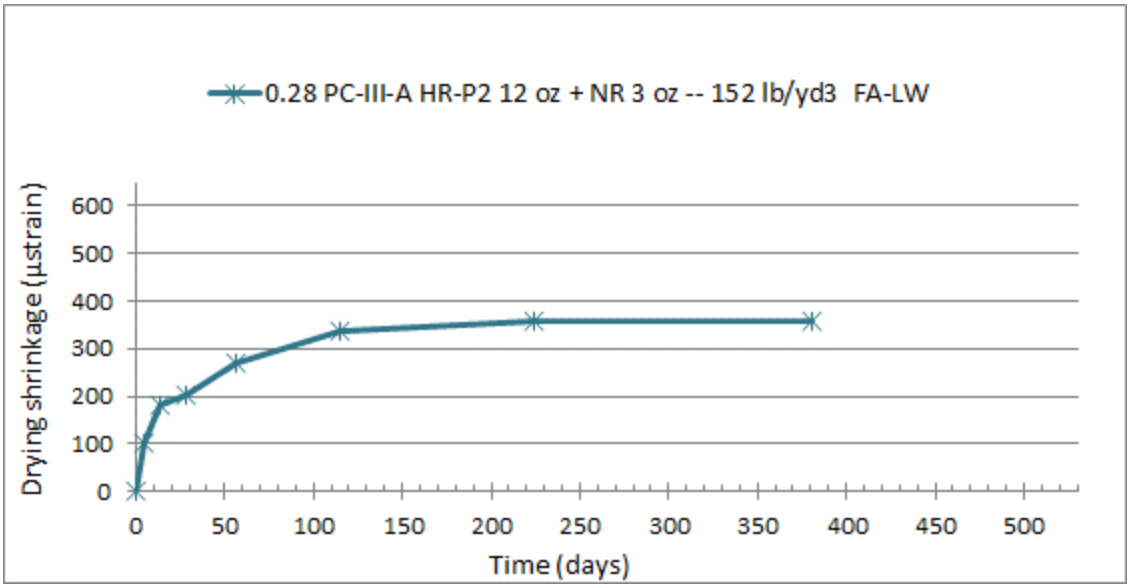

Fig.196 Drying Shrinkage 0.28 PC-III-A HR-P2 12 oz + NR 3 oz -- 152 lb/yd3 FA-LW

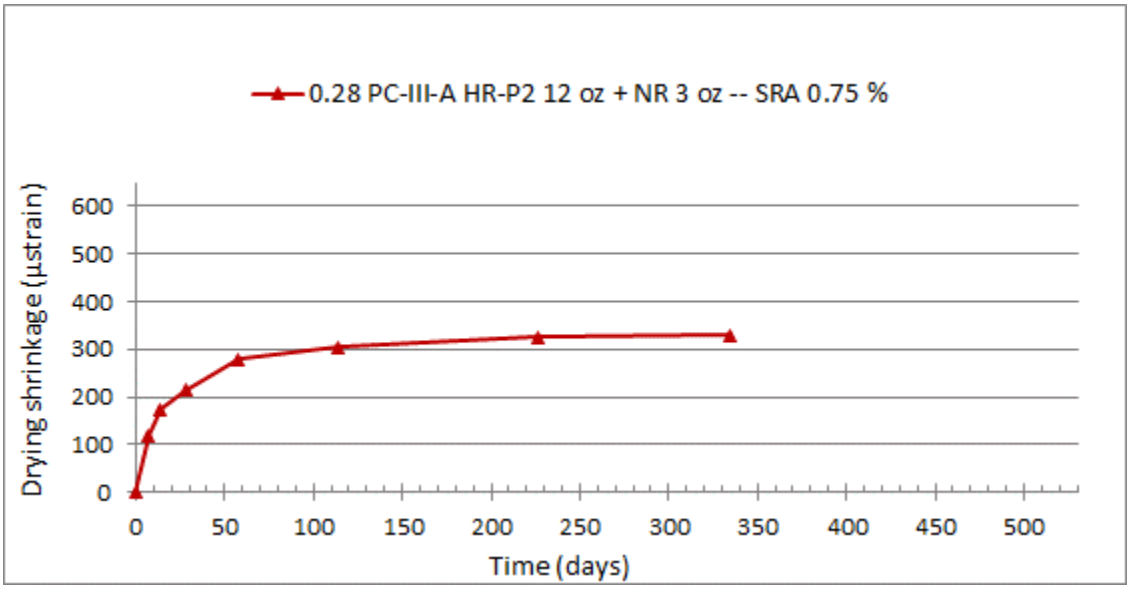

Fig.197 Drying Shrinkage 0.28 PC-III-A HR-P2 12 oz + NR 3 oz -- SRA 0.75 %

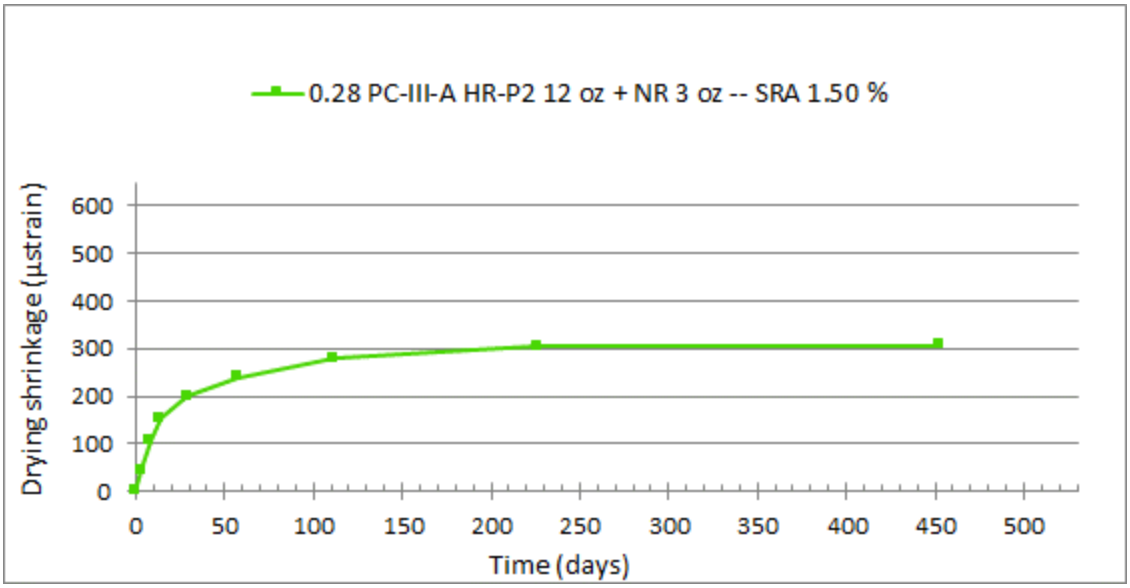

Fig.198 Drying Shrinkage 0.28 PC-III-A HR-P2 12 oz + NR 3 oz -- SRA 1.50 %

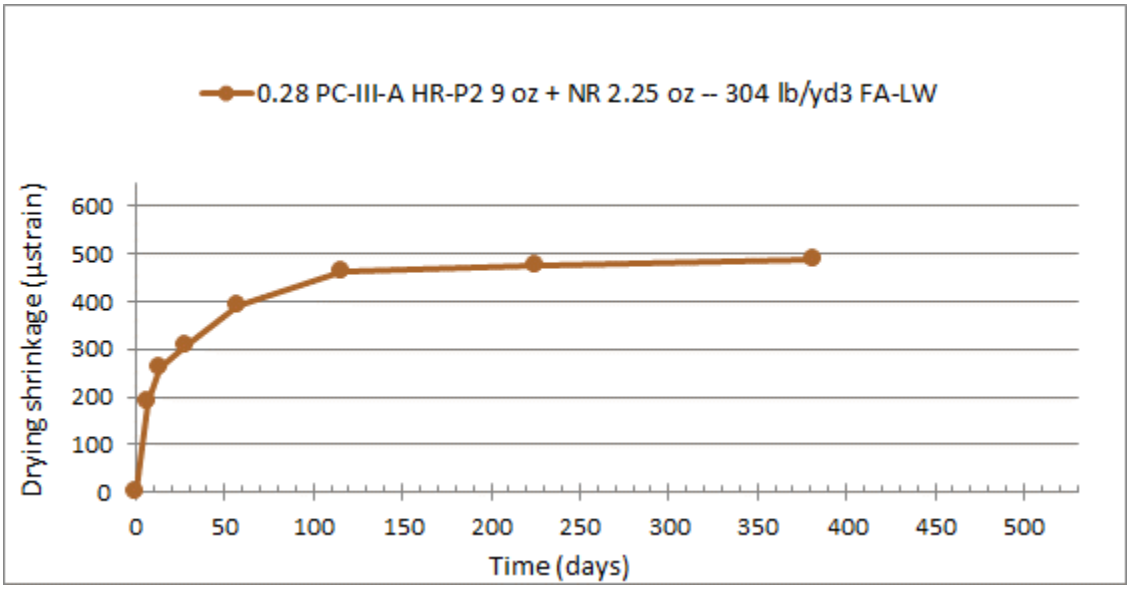

Fig.199 Drying Shrinkage 0.28 PC-III-A HR-P2 9 oz + NR 2.25 oz -- 304 lb/yd3 FA-LW

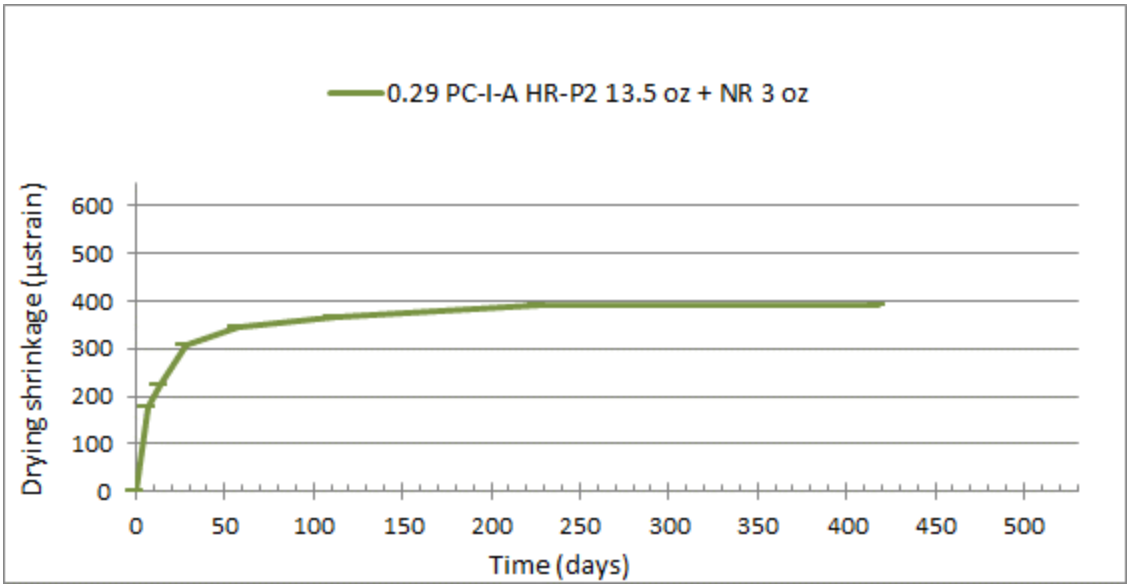

Fig.200 Drying Shrinkage 0.29 PC-I-A HR-P2 13.5 oz + NR 3 oz

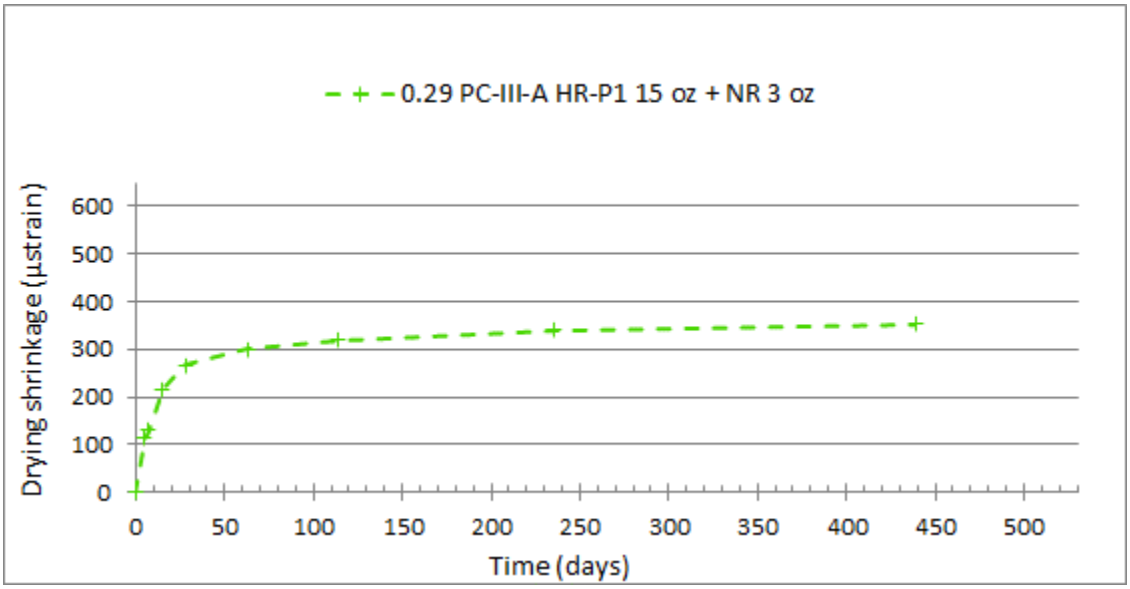

Fig.201 Drying Shrinkage 0.29 PC-III-A HR-P1 15 oz + NR 3 oz

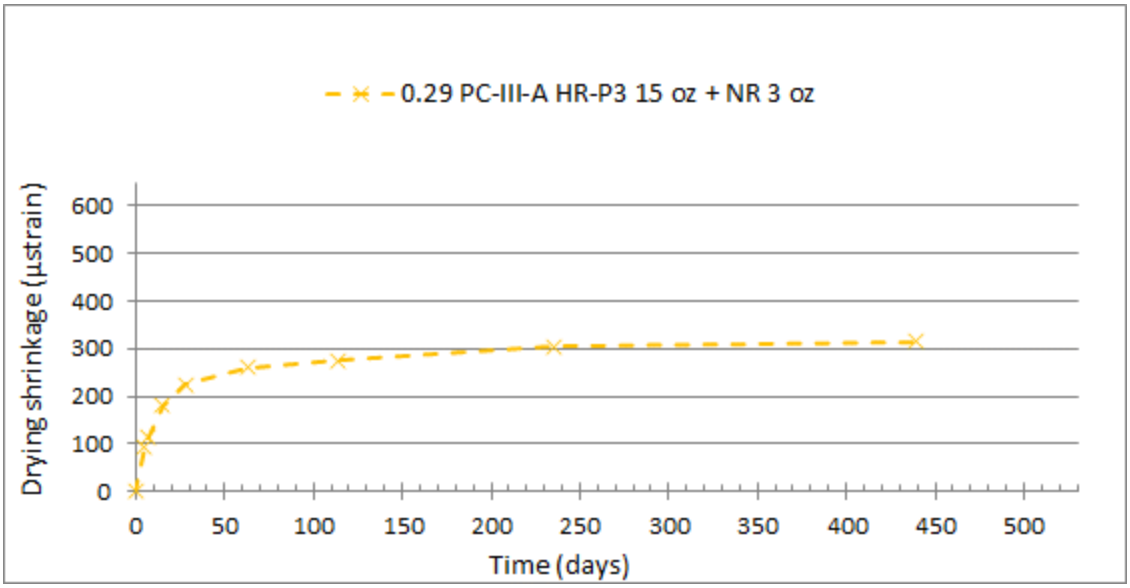

Fig.202 Drying Shrinkage 0.29 PC-III-A HR-P3 15 oz + NR 3 oz

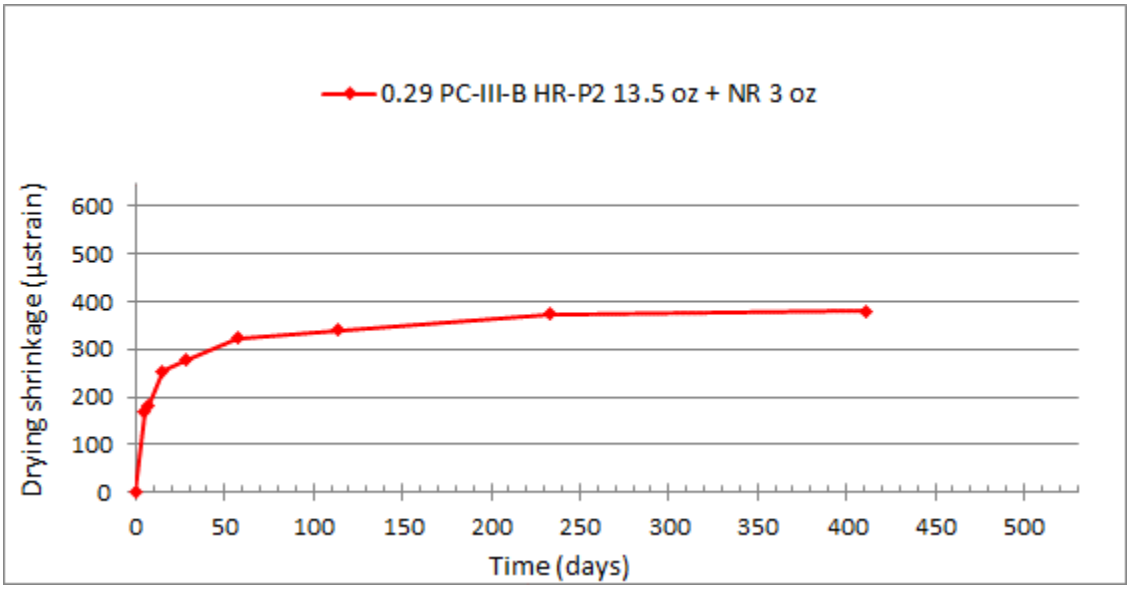

Fig.203 Drying Shrinkage 0.29 PC-III-B HR-P2 13.5 oz + NR 3 oz

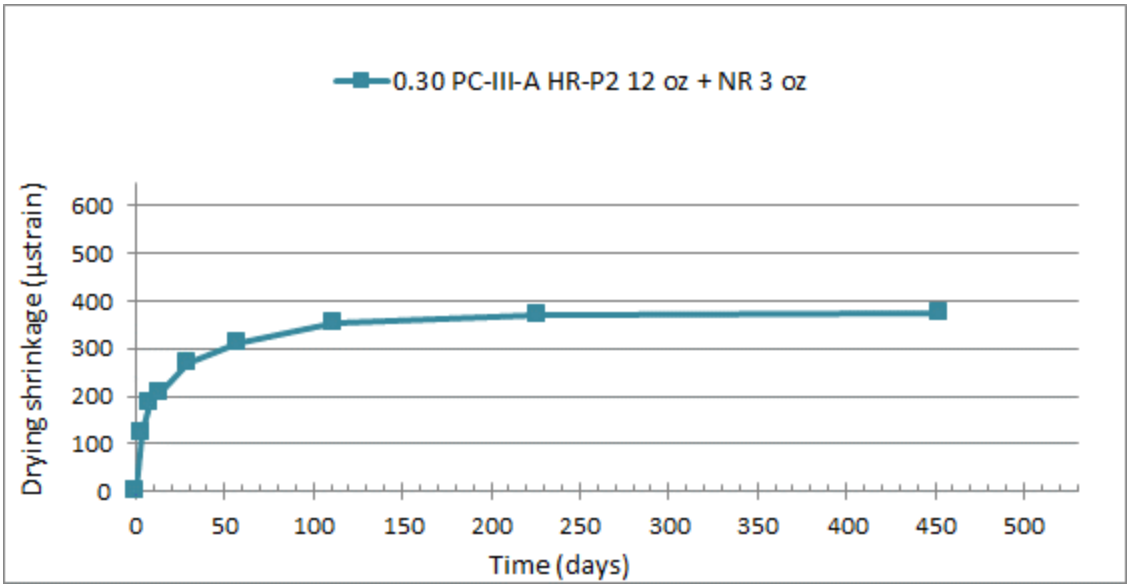

Fig.204 Drying Shrinkage 0.30 PC-III-A HR-P2 12 oz + NR 3 oz

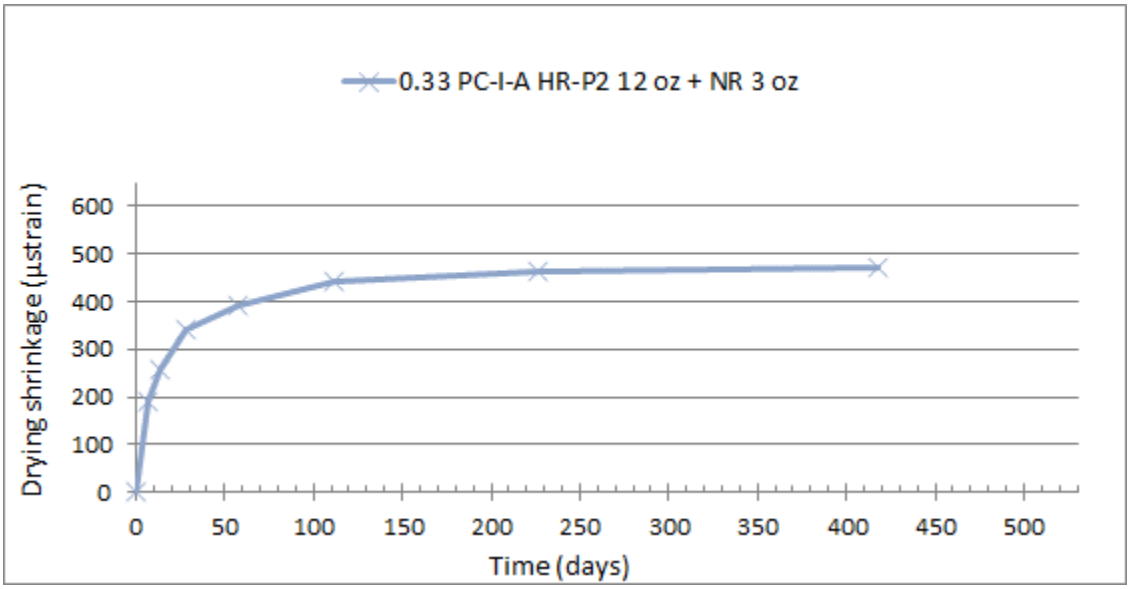

Fig.205 Drying Shrinkage 0.33 PC-I-A HR-P2 12 oz + NR 3 oz

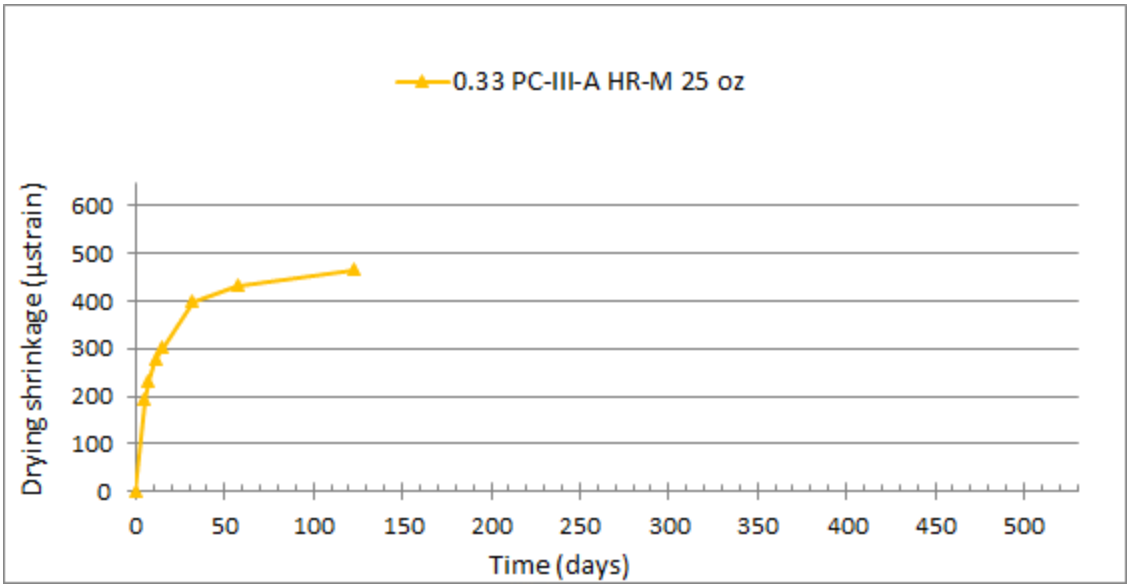

Fig.206 Drying Shrinkage 0.33 PC-III-A HR-M 25 oz

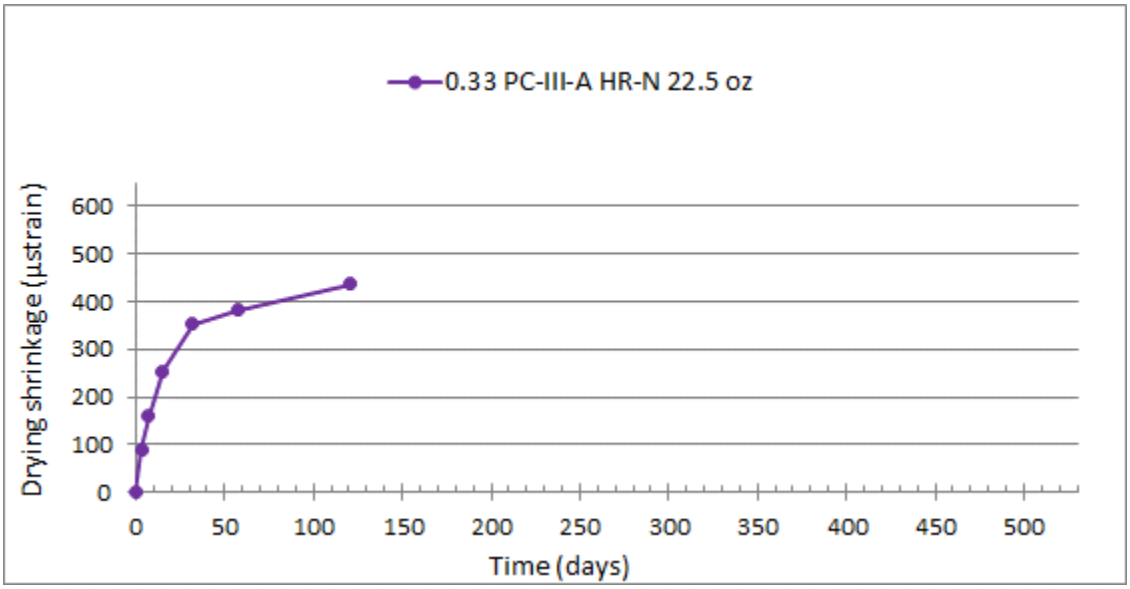

Fig.207 Drying Shrinkage 0.33 PC-III-A HR-N 22.5 oz

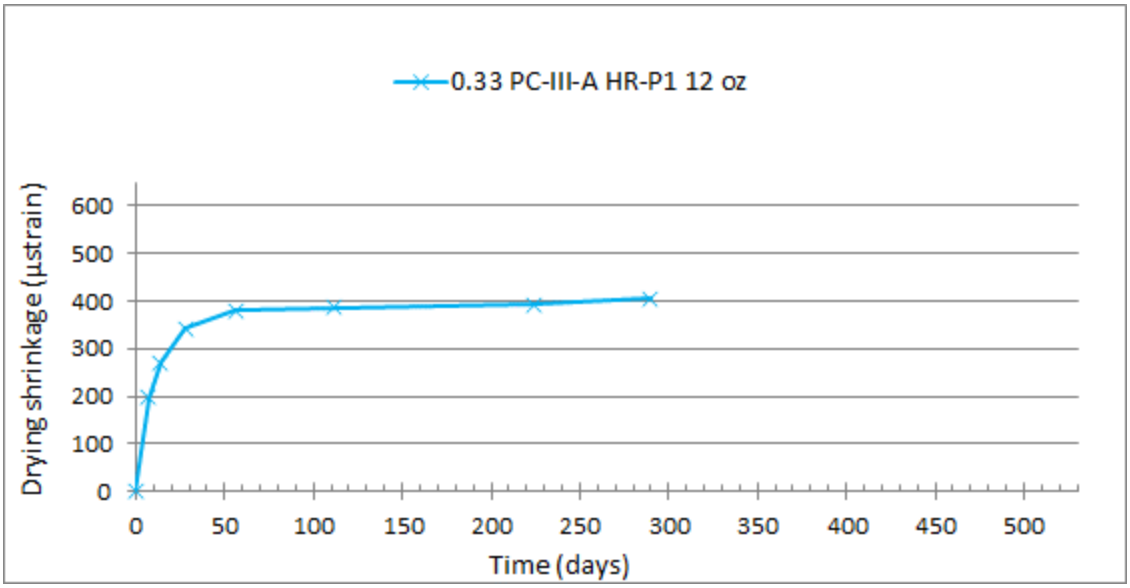

Fig.208 Drying Shrinkage 0.33 PC-III-A HR-P1 12 oz

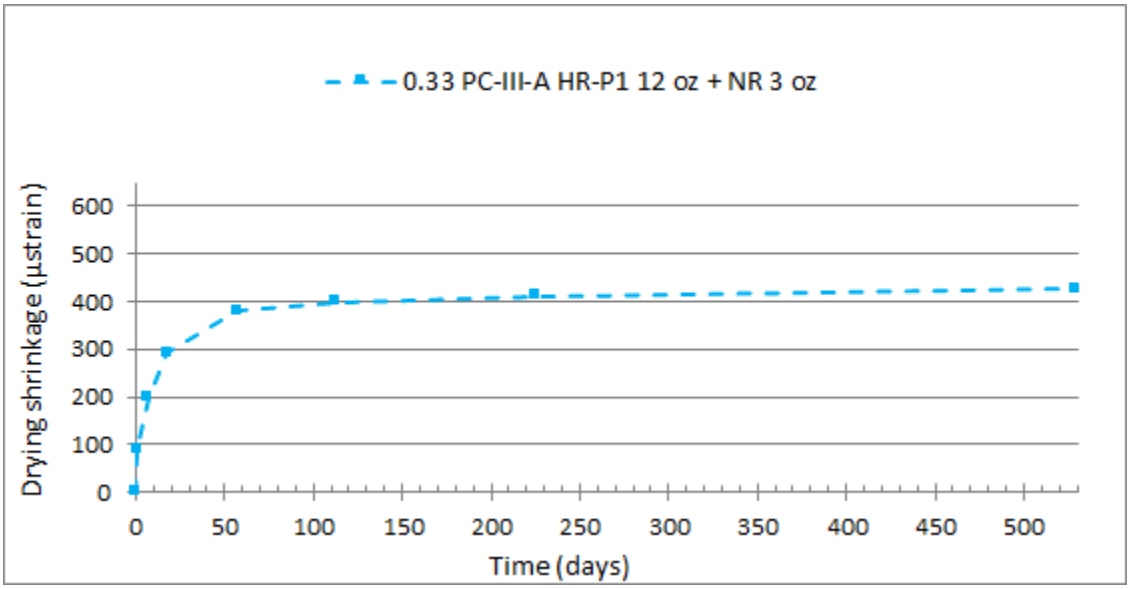

Fig.209 Drying Shrinkage 0.33 PC-III-A HR-P1 12 oz + NR 3 oz

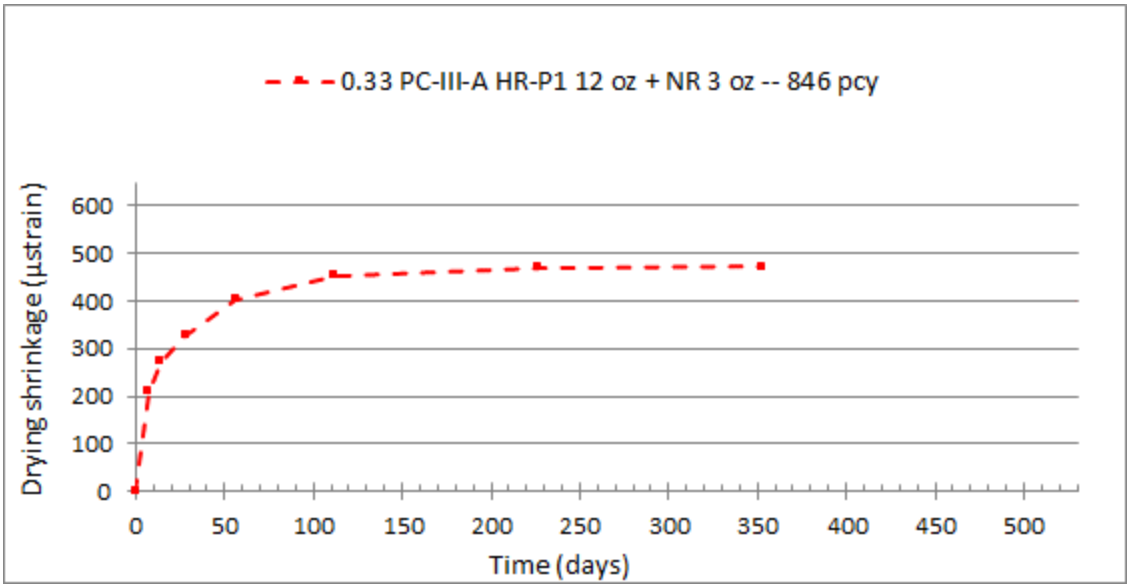

Fig.210 Drying Shrinkage 0.33 PC-III-A HR-P1 12 oz + NR 3 oz -- 846 pcy

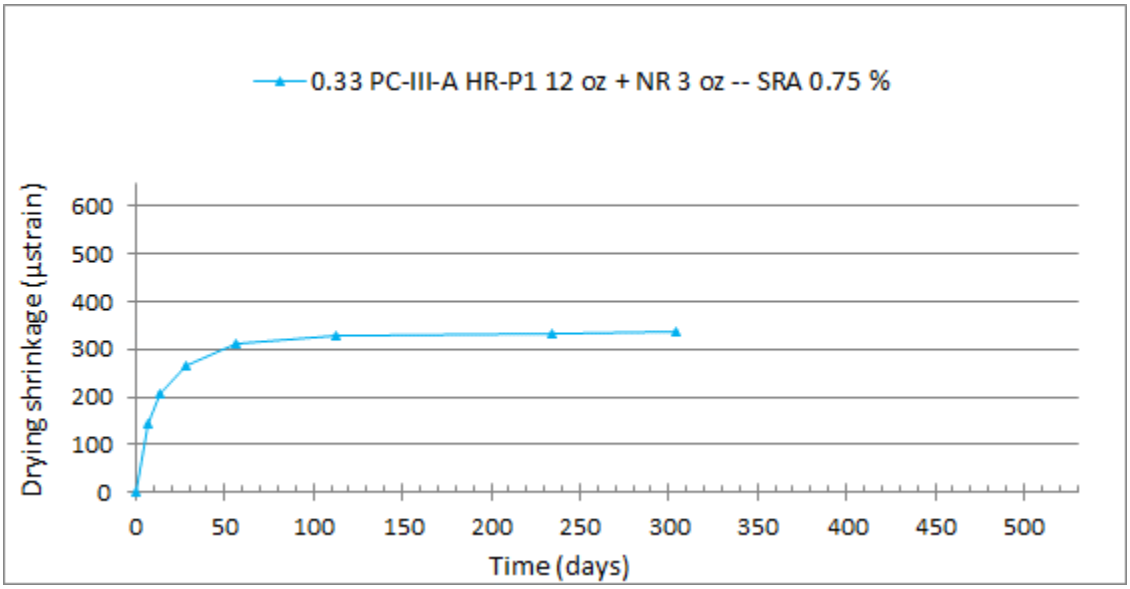

Fig.211 Drying Shrinkage 0.33 PC-III-A HR-P1 12 oz + NR 3 oz -- SRA 0.75 %

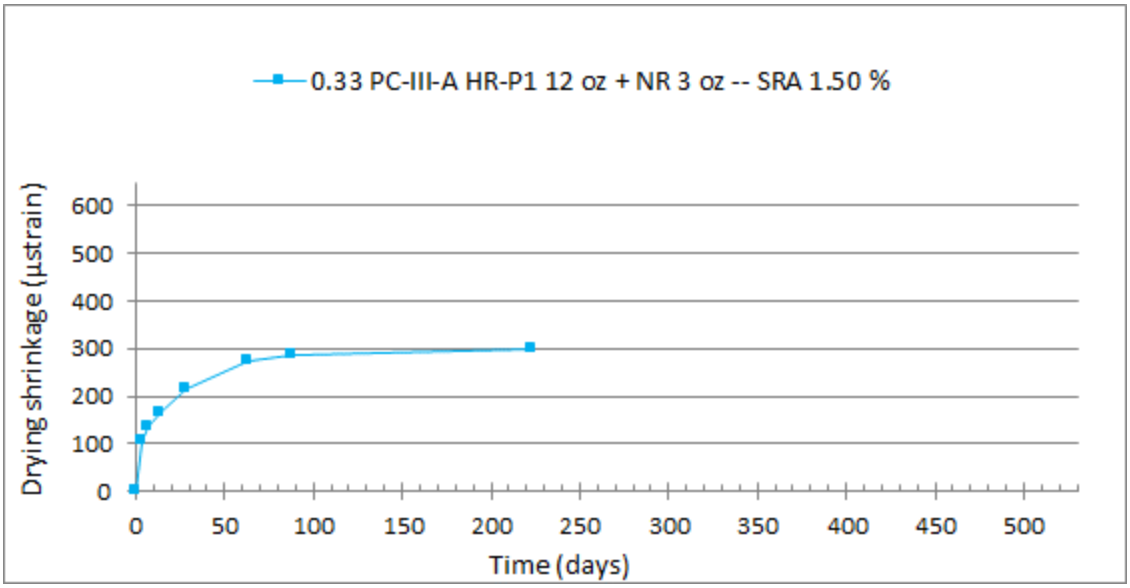

Fig.212 Drying Shrinkage 0.33 PC-III-A HR-P1 12 oz + NR 3 oz -- SRA 1.50 %

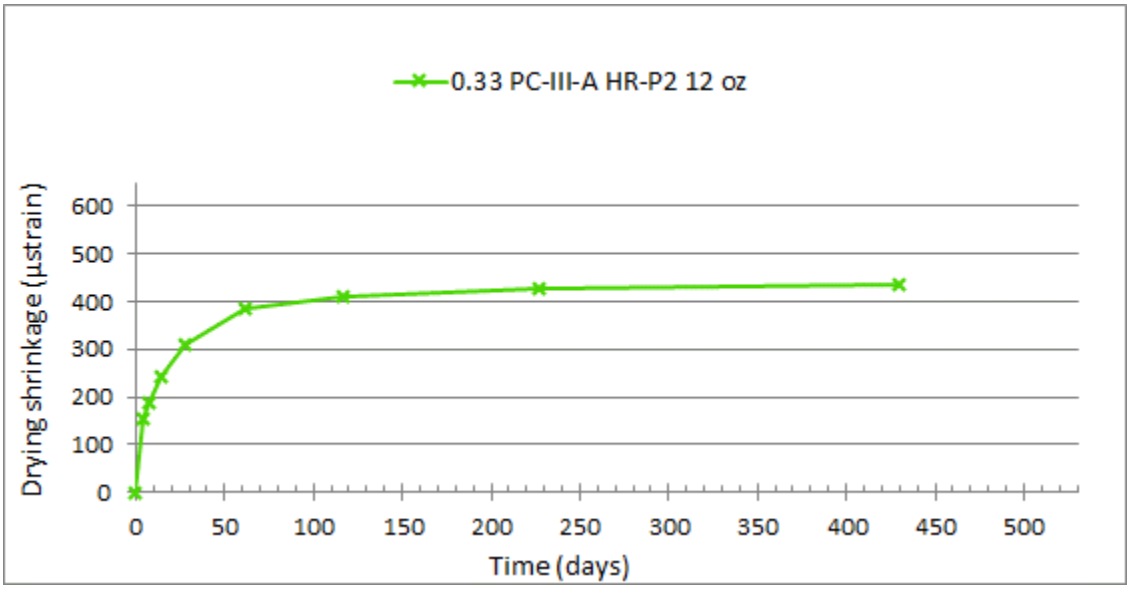

Fig.213 Drying Shrinkage 0.33 PC-III-A HR-P2 12 oz

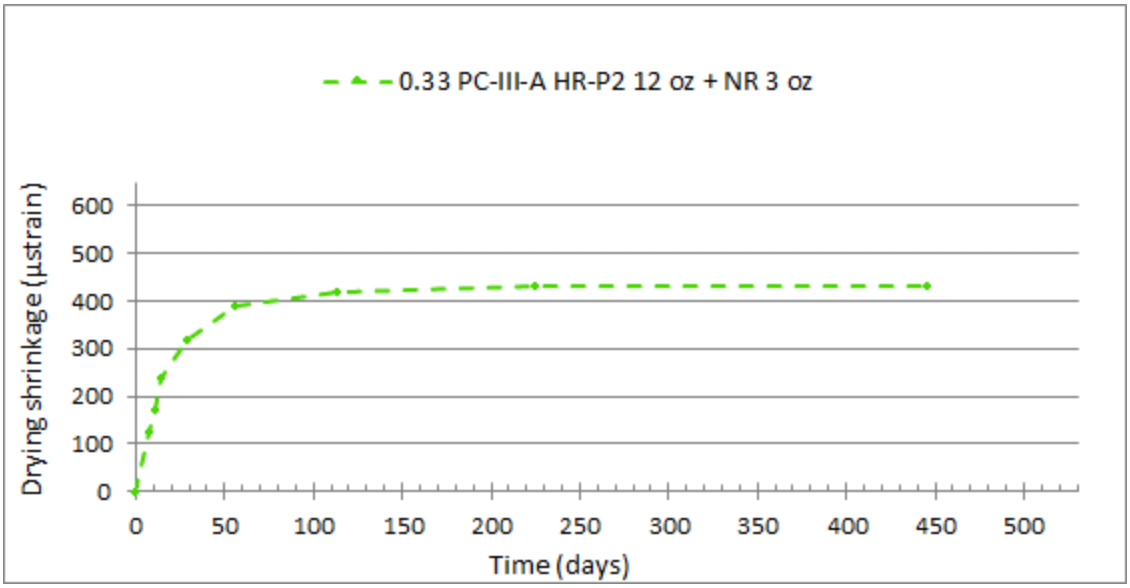

Fig.214 Drying Shrinkage 0.33 PC-III-A HR-P2 12 oz + NR 3 oz

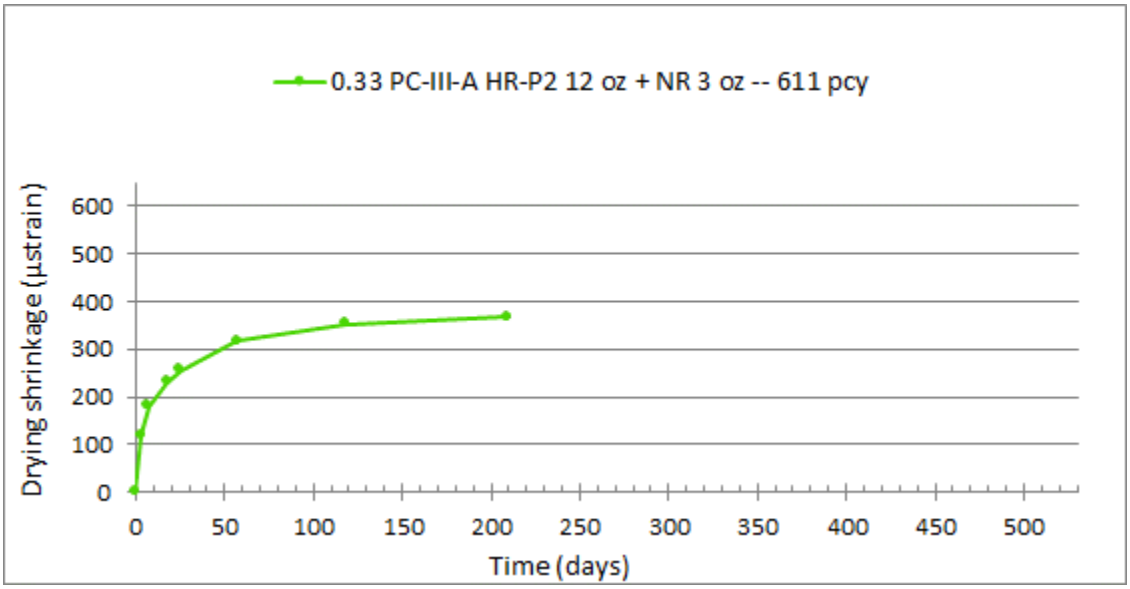

Fig.215 Drying Shrinkage 0.33 PC-III-A HR-P2 12 oz + NR 3 oz -- 611 pcy

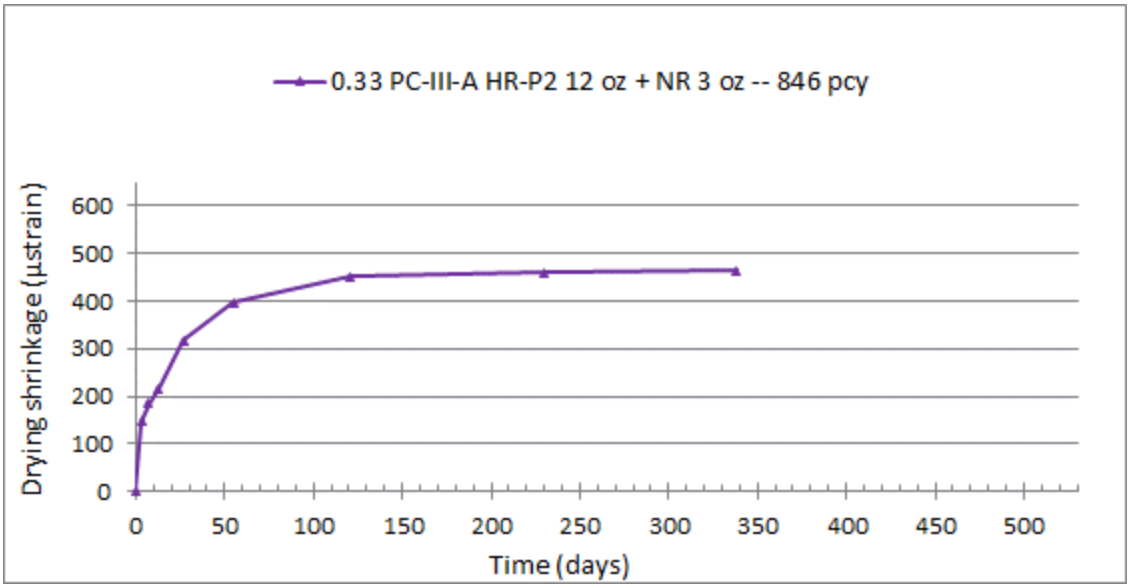

Fig.216 Drying Shrinkage 0.33 PC-III-A HR-P2 12 oz + NR 3 oz -- 846 pcy

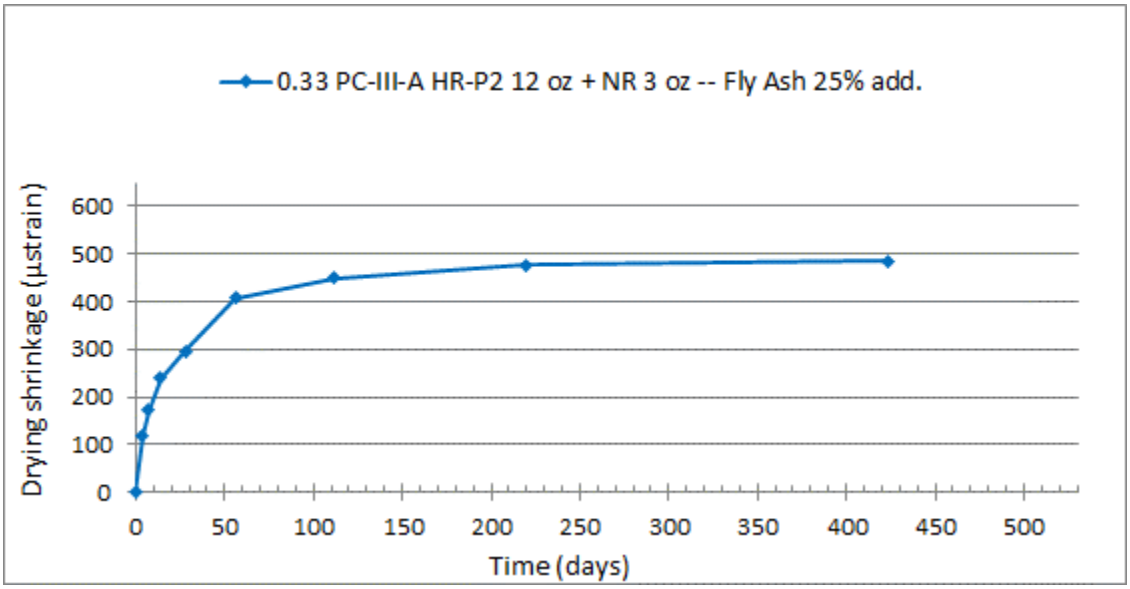

Fig.217 Drying Shrinkage 0.33 PC-III-A HR-P2 12 oz + NR 3 oz -- Fly Ash 25% add.

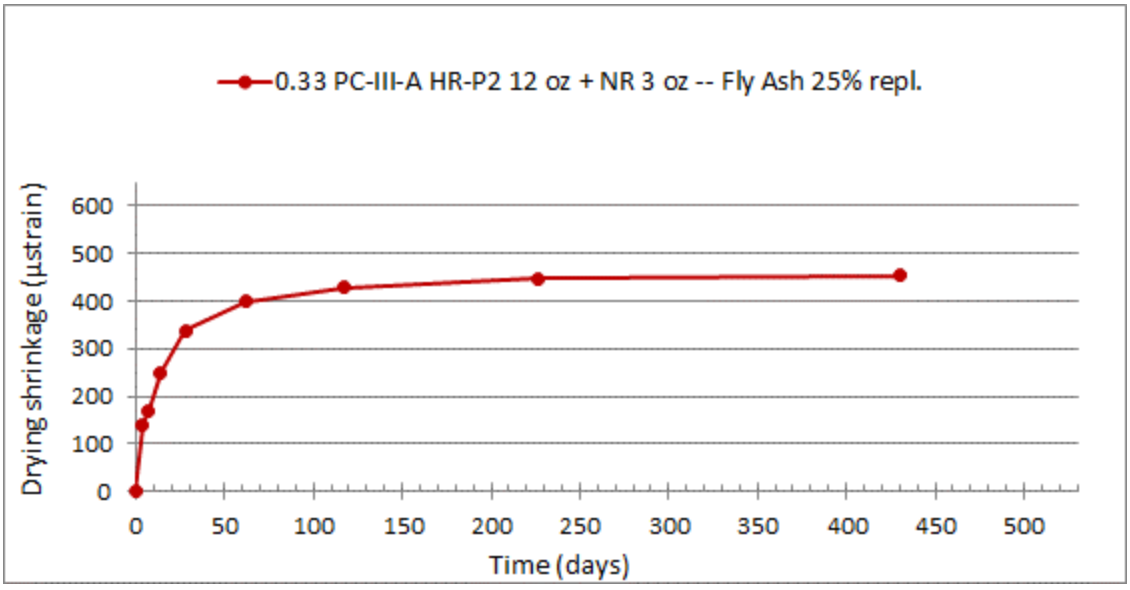

Fig. 218 Drying Shrinkage 0.33 PC-III-A HR-P2 12 oz + NR 3 oz -- Fly Ash 25% repl.

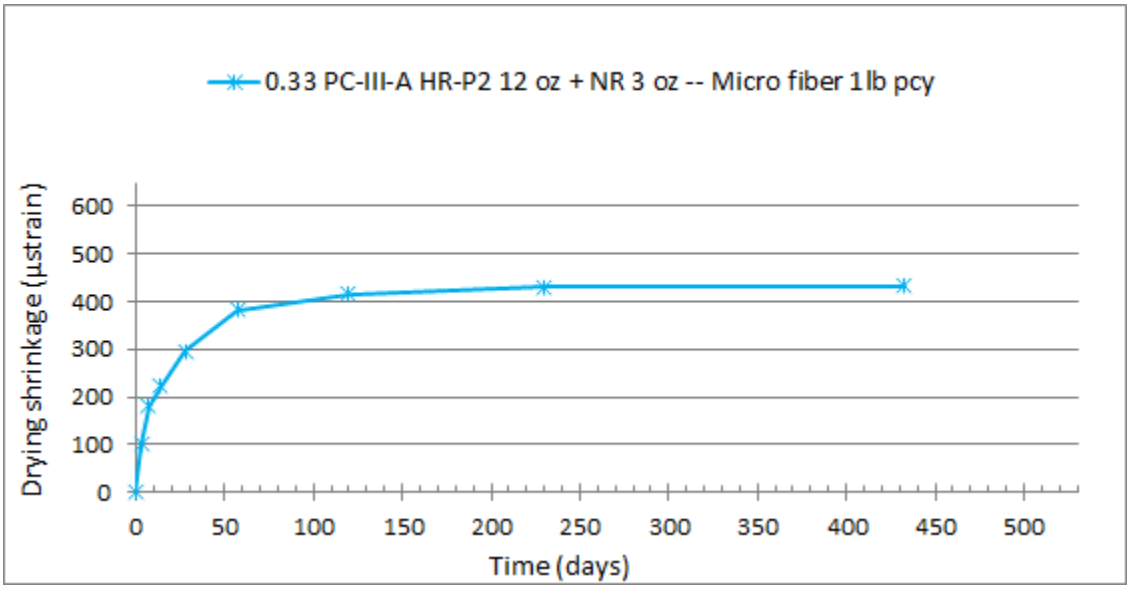

Fig. 219 Drying Shrinkage 0.33 PC-III-A HR-P2 12 oz + NR 3 oz -- Micro fiber 1lb pcy

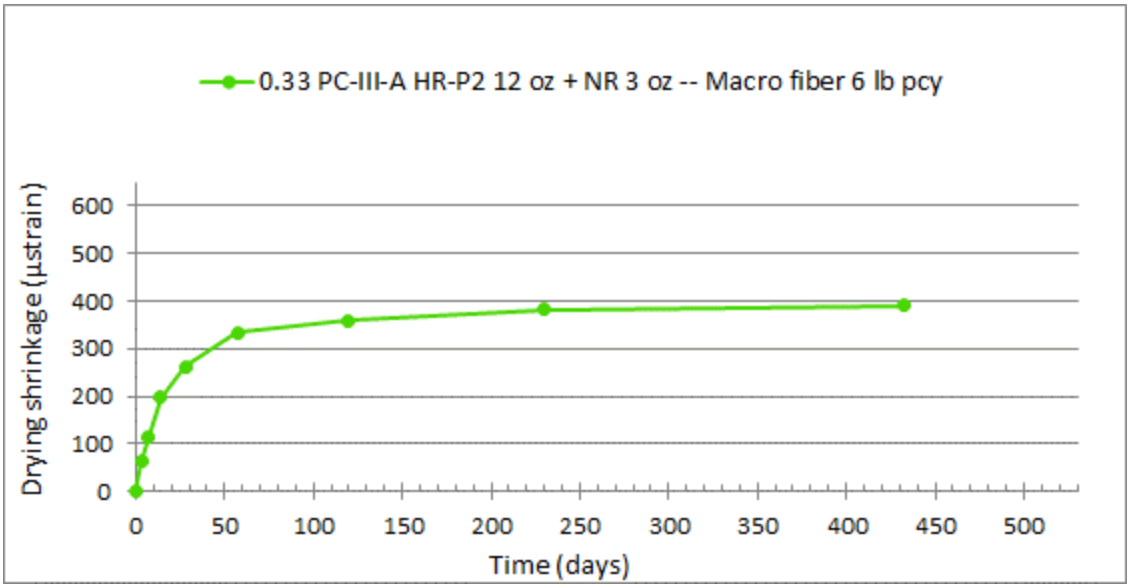

Fig.220 Drying Shrinkage 0.33 PC-III-A HR-P2 12 oz + NR 3 oz -- Macro fiber 6 lb pcy

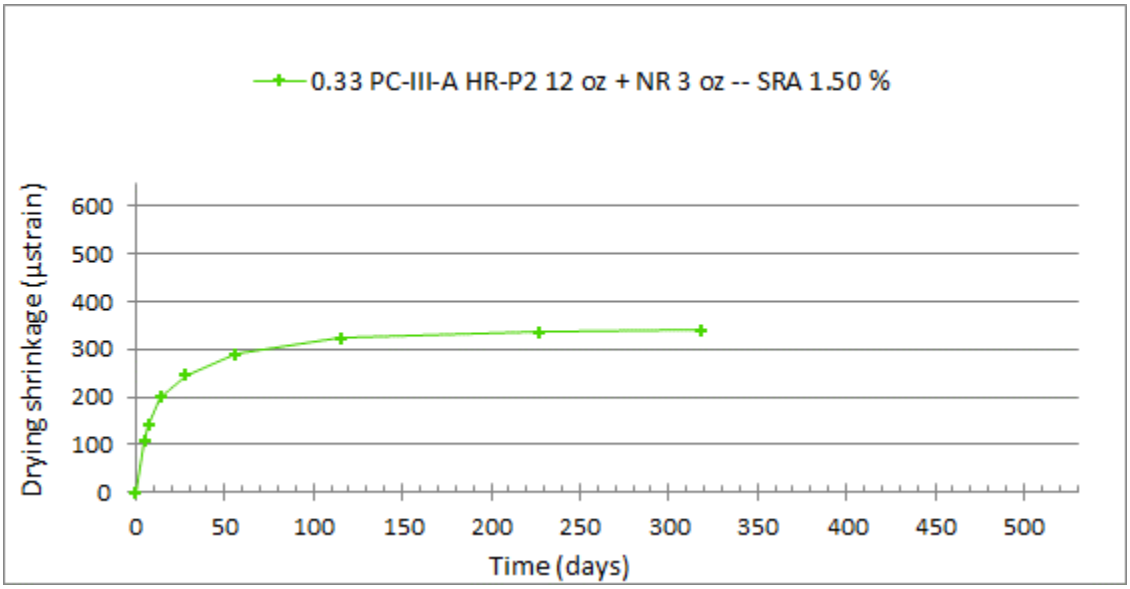

Fig.221 Drying Shrinkage 0.33 PC-III-A HR-P2 12 oz + NR 3 oz -- SRA 1.50 %

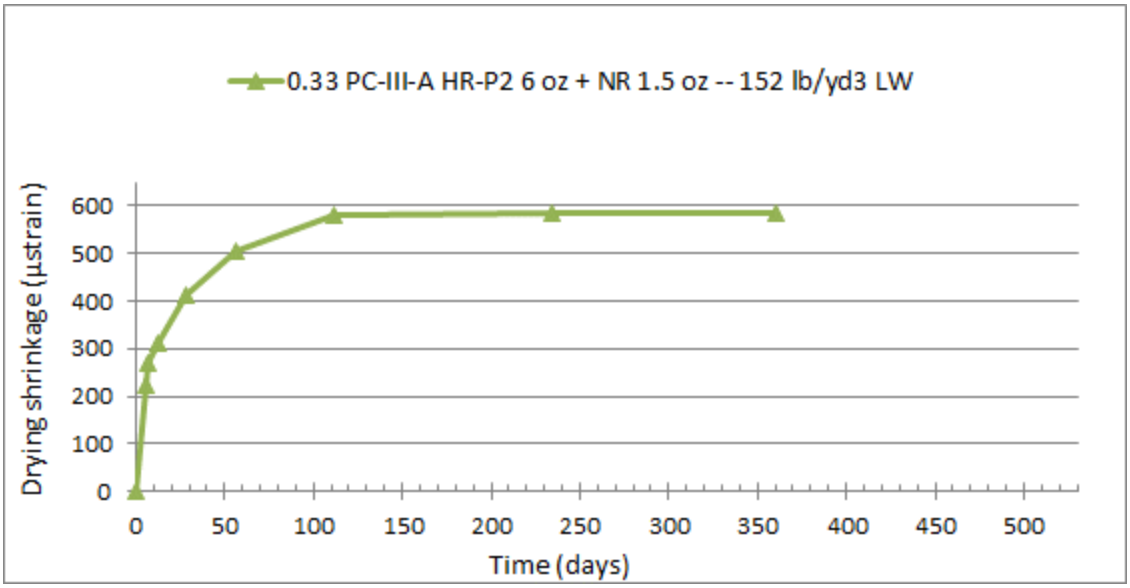

Fig.222 Drying Shrinkage 0.33 PC-III-A HR-P2 6 oz + NR 1.5 oz -- 152 lb/yd3 LW

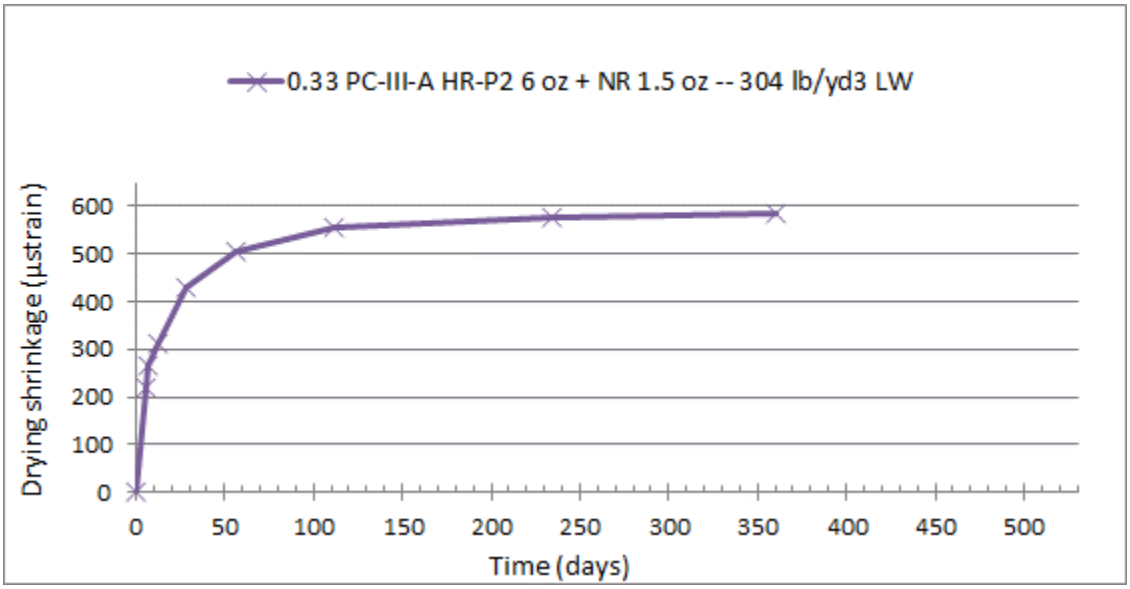

Fig.223 Drying Shrinkage 0.33 PC-III-A HR-P2 6 oz + NR 1.5 oz -- 304 lb/yd3 LW

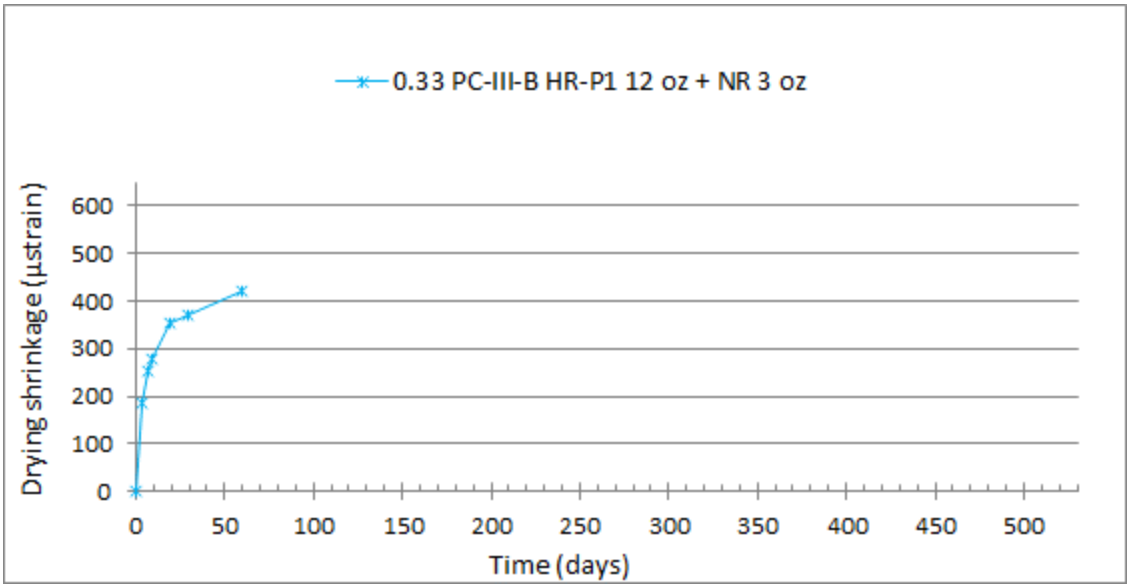

Fig.224 Drying Shrinkage 0.33 PC-III-B HR-P1 12 oz + NR 3 oz

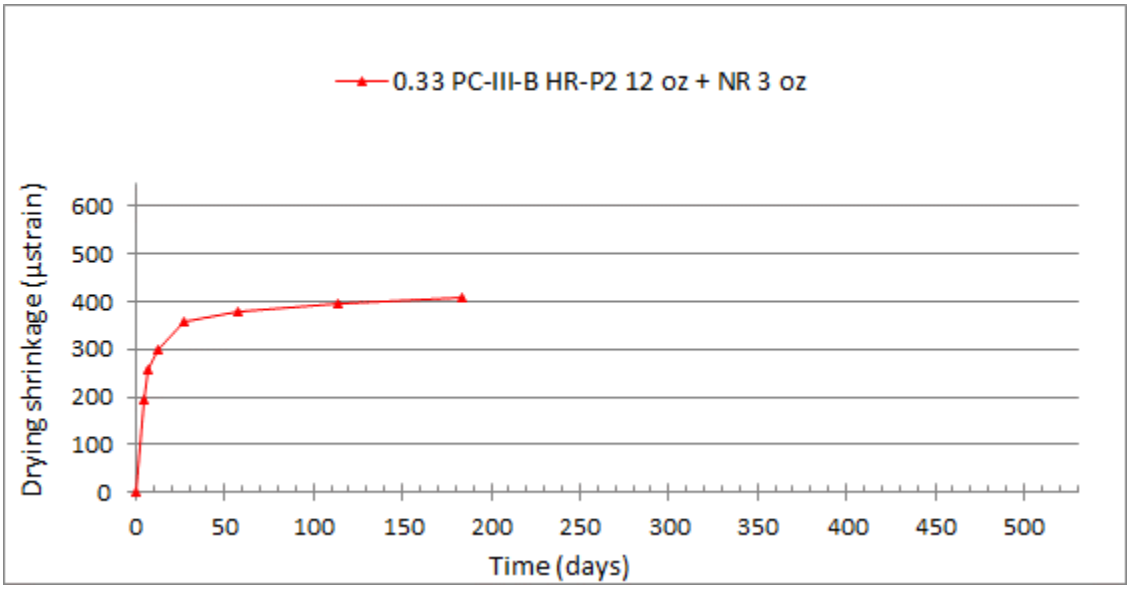

Fig.225 Drying Shrinkage 0.33 PC-III-B HR-P2 12 oz + NR 3 oz

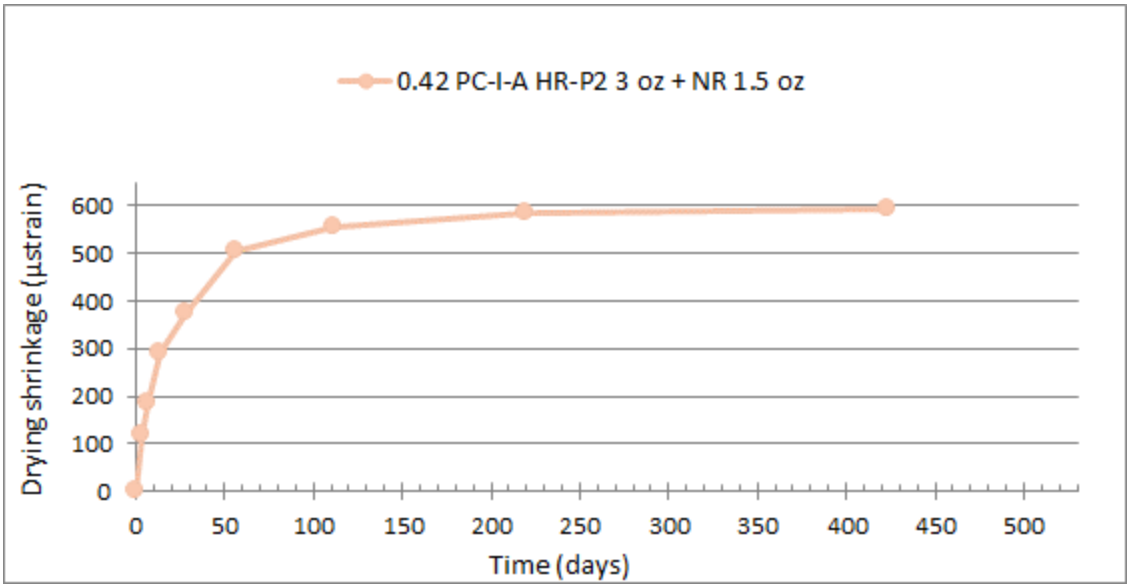

Fig.226 Drying Shrinkage 0.42 PC-I-A HR-P2 3 oz + NR 1.5 oz

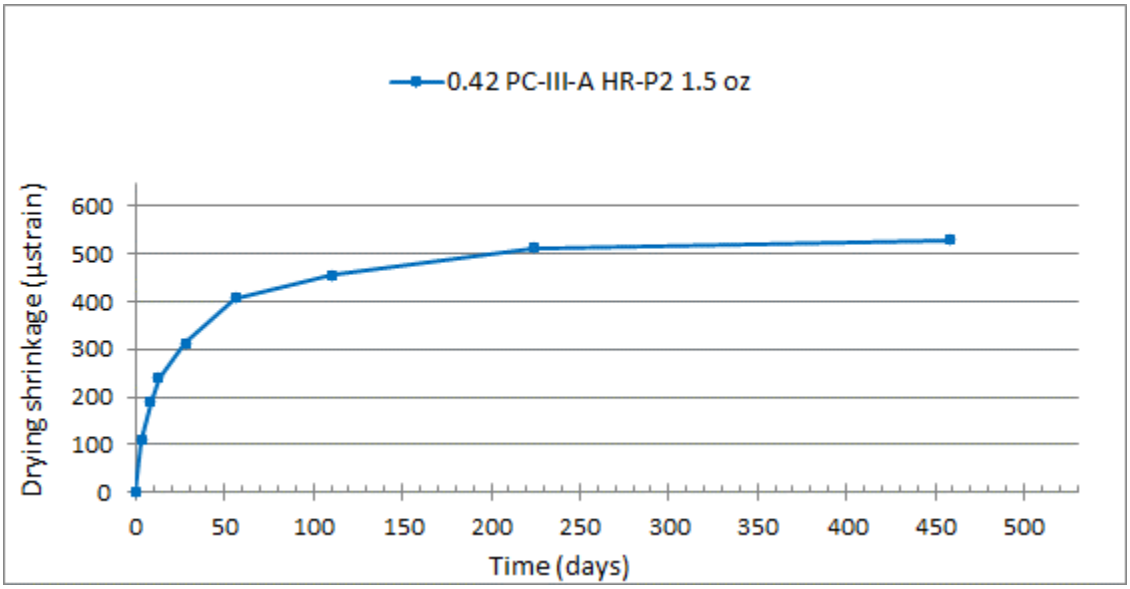

Fig.227 Drying Shrinkage 0.42 PC-III-A HR-P2 1.5 oz

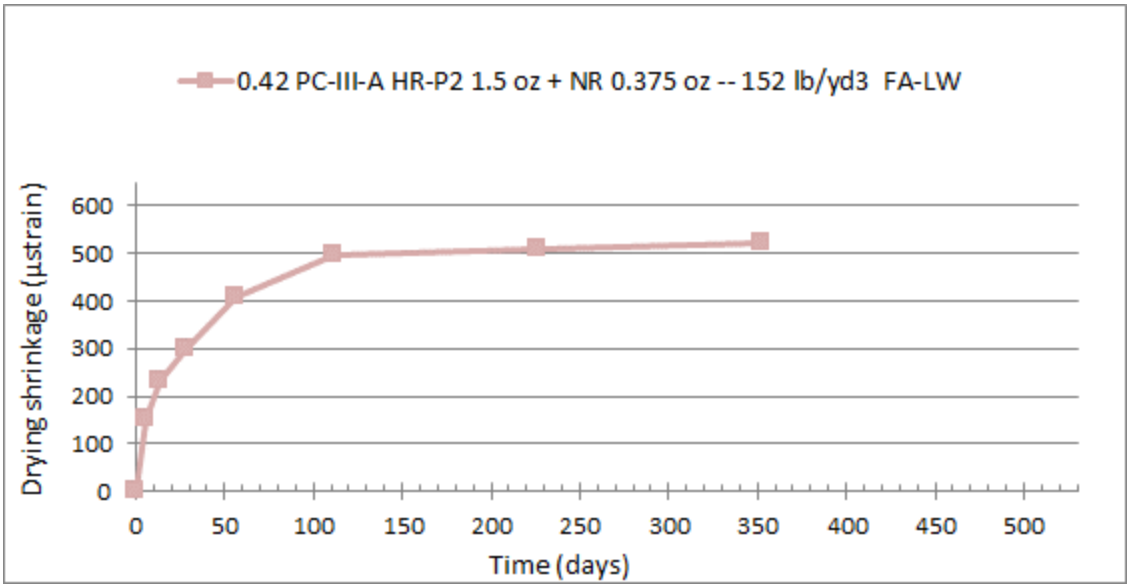

Fig.228 Drying Shrinkage 0.42 PC-III-A HR-P2 1.5 oz + NR 0.375 oz -- 152 lb/yd3 FA-LW

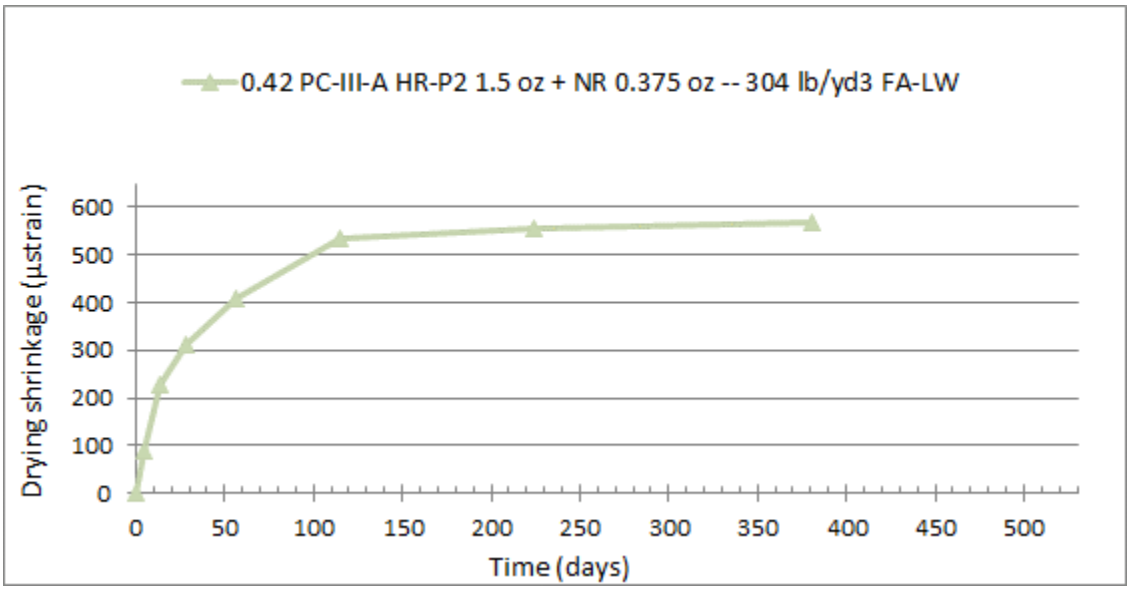

Fig.229 Drying Shrinkage 0.42 PC-III-A HR-P2 1.5 oz + NR 0.375 oz -- 304 lb/yd3 FA-LW

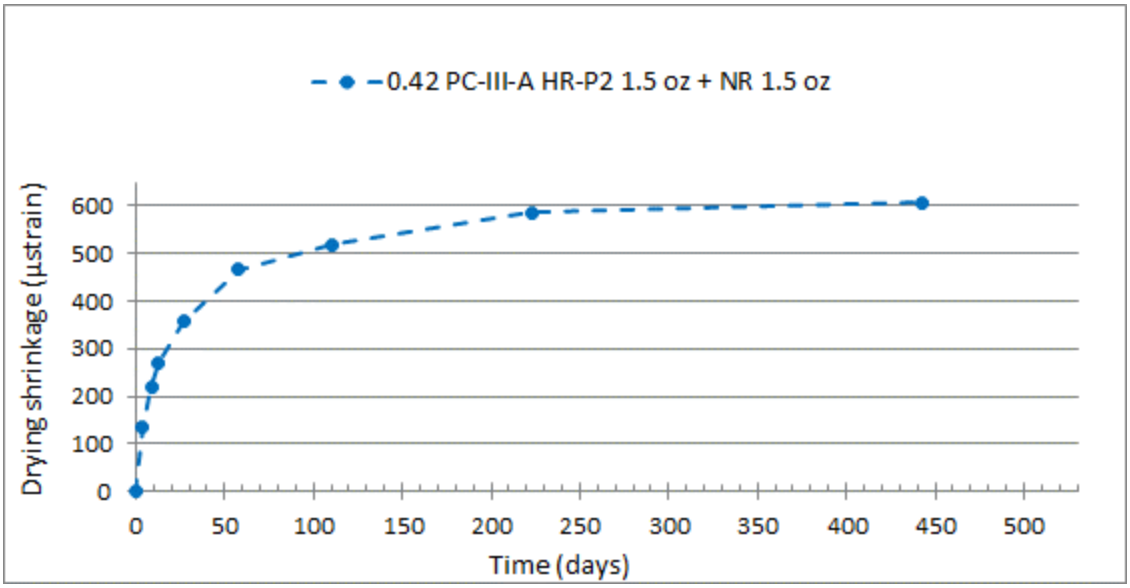

Fig.230 Drying Shrinkage 0.42 PC-III-A HR-P2 1.5 oz + NR 1.5 oz

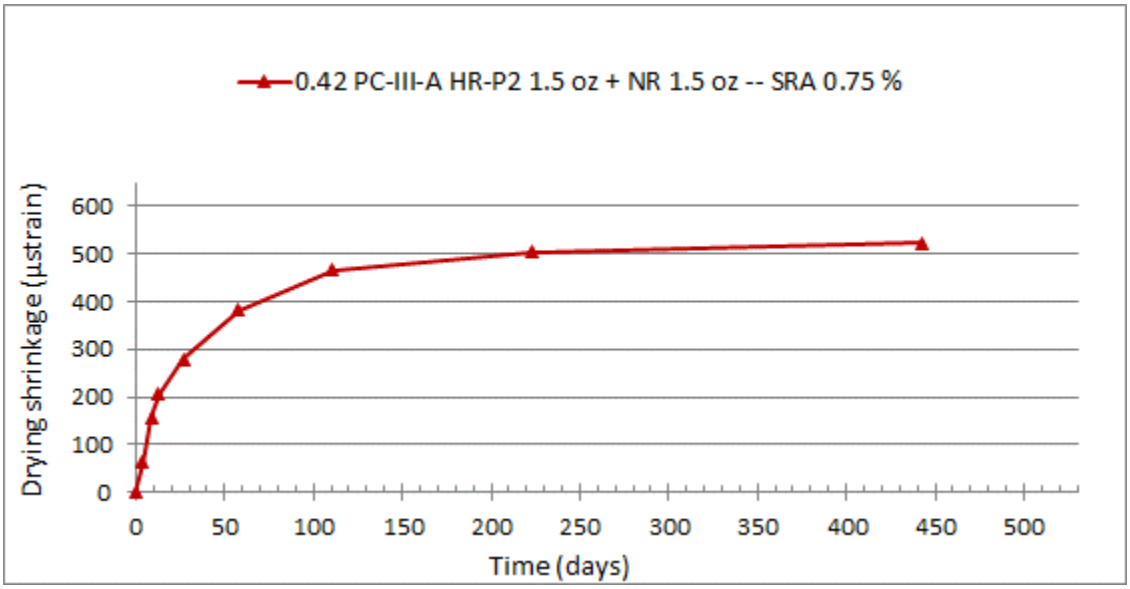

Fig.231 Drying Shrinkage 0.42 PC-III-A HR-P2 1.5 oz + NR 1.5 oz -- SRA 0.75 %

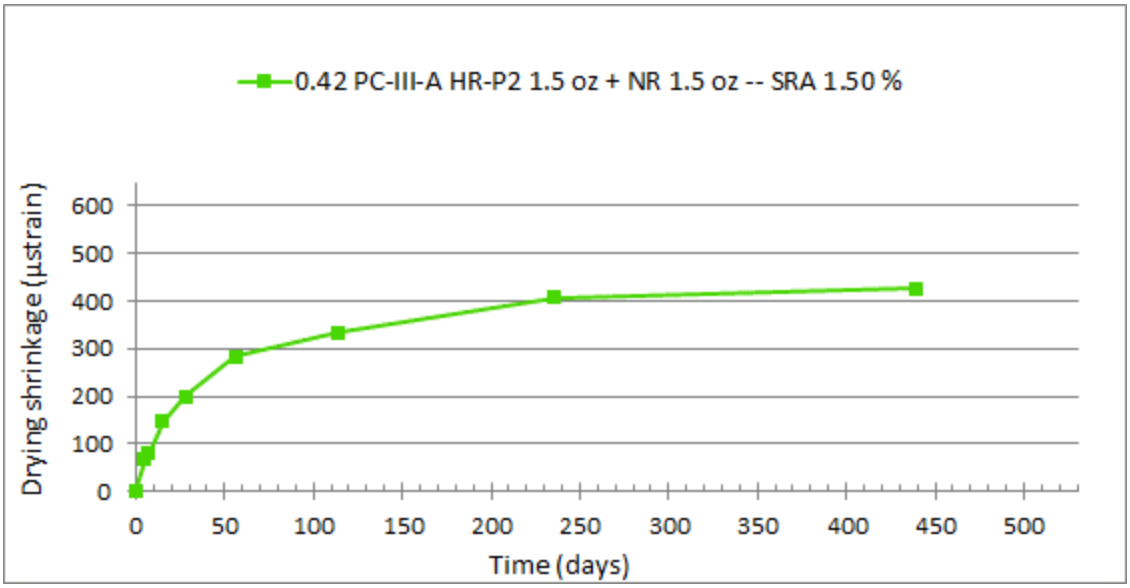

Fig.232 Drying Shrinkage 0.42 PC-III-A HR-P2 1.5 oz + NR 1.5 oz -- SRA 1.50 %

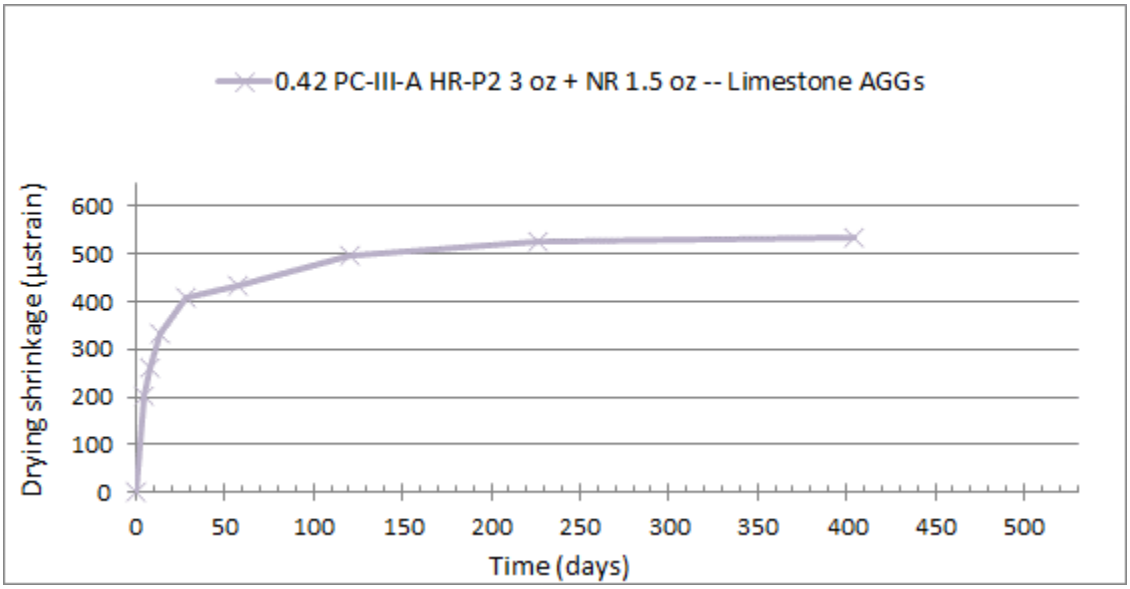

Fig.233 Drying Shrinkage 0.42 PC-III-A HR-P2 3 oz + NR 1.5 oz -- Limestone AGGs

Appendix V: TxDOT Exposure Site

Block Number	Cast Date	Cement/ Type	Admixture	w/cm	Cement (lbs/cu.yd)	**Visual rating 1st visit (5 is worst)**	**Visual rating 2nd visit (5 is worst)**	Comments
7	8/5/2010	PC-III-A	HRWR-Polycarboxylate + NR	0.33	564	**0**	**0**	
29	8/18/2010	PC-III-A	HRWR-Polycarboxylate + NR	0.33	658	**0**	**0.1**	
242	3/2/2011	PC-I-C	HRWR-Polycarboxylate + NR	0.45	700	**0**	**0.5**	
566	12/15/2011	PC-I-C	Mid-Range	0.37	708	**0**	**0.2**	Buff
567	12/15/2011	PC-I-C	Mid-Range	0.37	708	**0**	**0.25**	Buff
791	7/11/2012	PC-III-A	HRWR-Polycarboxylate + NR	0.33	564	**0**	**0.55**	SRA+ Type K cement
797	7/11/2012	PC-III-A	HRWR-Polycarboxylate + NR	0.33	564	**0**	**0**	

826	5/11/2012	K/PC-I/II-A	HRWR-Polycarboxylate	0.46	100/560	**0**	**0.1**	Type K cement
827	5/11/2012	K/PC-I/II-A	HRWR-Polycarboxylate	0.46	100/560	**0**	**0**	Type K cement
367	7/28/2011	PC-III-A	HRWR-HRWR-Polycarboxylate + NR	0.33	658	**0.2**	**0.5**	
796	3/21/2012	PC-I-C	None	0.45	680	**0.2**	**0.5**	
106	8/17/2010	PC-III-A	HRWR-Polycarboxylate + NR	0.25	564	**0.5**	**0.5**	
244 (big)	3/2/2011	PC-III-A	HRWR-Polycarboxylate + NR	0.33	658	**0.5**	**0.5**	Buff
287	3/30/2011	PC-III-A	HRWR-Polycarboxylate + NR	0.33	658	**0.5**	**1**	Buff
476	9/26/2012	PC-III-A	HRWR - Naphthalene	0.33	658	**0.5**	**1**	Cracked on top
617	3/14/2012	PC-III-A	HRWR-Polycarboxylate + NR	0.33	658	**0.5**	**1.75**	SRA+ Type K cement
750	10/24/2012	PC-III-A	HRWR-Polycarboxylate	0.33	658	**0.5**	**0.8**	Cracked on top
793	7/11/2012	PC-III-A	HRWR-Polycarboxylate + NR	0.33	564	**0.5**	**0.65**	SRA+ Type K cement

861	7/23/2012	K/PC-I-C	HRWR-Polycarboxylate	0.46	117.5/658	**0.5**	**1**	Type K cement - ASR cracking
876	10/25/2012	PC-III-A	HRWR-Polycarboxylate	0.33	658	**0.5**	**0.75**	Cracked on top
888	10/24/2012	PC-III-A	HRWR-Polycarboxylate	0.33	658	**0.5**	**0.6**	Cracked on top
792	7/20/2012	PC-III-A	HRWR-Polycarboxylate + NR	0.33	564	**0.65**	**0.65**	SRA+ Type K cement
794	7/11/2012	PC-III-A	HRWR-Polycarboxylate + NR	0.33	564	**0.5**	**0.5**	SRA+ Type K cement
522	9/26/2011	PC-I P-B	HRWR-Polycarboxylate + NR	0.33	658	**0.75**	**1.1**	
528	10/7/2011	PC-I P-B	HRWR-Polycarboxylate + NR	0.33	658	**0.75**	**0.75**	
616	3/14/2012	PC-III-A	HRWR-Polycarboxylate + NR	0.33	658	**1**	**1.25**	SRA+ Type K cement
619	3/14/2012	PC-III-A	HRWR-Polycarboxylate + NR	0.33	658	**1**	**2.25**	SRA+ Type K cement
646	10/5/2012	PC-III-A	HRWR - Naphthalene	0.33	658	**1**	**2**	
648	10/5/2012	PC-III-A	HRWR-Polycarboxylate	0.33	658	**1**	**1.5**	

366	7/28/2011	PC-III-A	HRWR-Polycarboxylate + NR	0.25	658	**1.2**	**-**	
531	10/7/2011	PC-III P-B	HRWR-Polycarboxylate + NR	0.33	658	**1.5**	**-**	
618	3/14/2012	PC-III-A	HRWR-Polycarboxylate + NR	0.33	658	**1.5**	**1.75**	SRA+ Type K cement
798	3/21/2012	PC-III-A	HRWR-Polycarboxylate + NR	0.33	658	**1.5**	**2**	
267	2/23/2011	PC-III-A	HRWR-Polycarboxylate + NR	0.33	658	**3**	**3**	
268	2/22/2011	PC-III-B	HRWR-Polycarboxylate + NR	0.33	658	**3**	**3**	
436	8/18/2011	PC-III-A	HRWR-Polycarboxylate + NR	0.25	658	**3**	**3**	Cracked on top
381	6/28/2011	PC-III-A	HRWR-Polycarboxylate + NR	0.25	658	**3.25**	**3.25**	Cracked on top
244	3/2/2011	PC-III-A	HRWR-Polycarboxylate + NR	0.33	658	**4**	**4**	
396	8/11/2011	PC-III-A	HRWR-Polycarboxylate + NR	0.25	658	**4**	**4**	Cracked on top - Buff

285	3/30/2011	PC-III-B	HRWR-Polycarboxylate + NR	0.33	700	-	**1**	Fly Ash 25 % Replacement
219	6/13/2011	PC-III-B	HRWR-Polycarboxylate + NR	0.33	806	-	**1.5**	Fly Ash 25 % Replacement
217	6/13/2011	PC-III-B	HRWR-Polycarboxylate + NR	0.33	575	-	**2**	Fly Ash 25 % Replacement
220	6/15/2011	PC-III-B	HRWR-Polycarboxylate + NR	0.33	586	-	**2**	Fly Ash 25 % Replacement
218	6/13/2011	PC-III-B	HRWR-Polycarboxylate + NR	0.33	691	-	**2.5**	Fly Ash 25 % Replacement
221	6/15/2011	PC-III-B	HRWR-Polycarboxylate + NR	0.33	703	-	**2.5**	Fly Ash 25 % Replacement
222	6/15/2011	PC-III-B	HRWR-Polycarboxylate + NR	0.33	820	-	**2.5**	Fly Ash 25 % Replacement
277	3/28/2011	PC-III-B	HRWR-Polycarboxylate + NR	0.33	700	-	**3.25**	
250	2/15/2011	PC-III-B	HRWR-Polycarboxylate + NR	0.33	658	-	**3.5**	
260	2/22/2011	PC-III-B	HRWR-Polycarboxylate + NR	0.33	658	-	**3.5**	

306	6/23/2011	PC-III-B	HRWR-Polycarboxylate + NR	0.33	658	-	**3.5**	
229	4/7/2011	PC-III-B	HRWR-Polycarboxylate + NR	0.33	719	-	**4.5**	

Table 19 Blocks at TxDOT exposure site

References

ACI Committee 231, Report on Early-Age Cracking: Causes, Measurement, and Mitigation, American Concrete Institute, (2010).

G.D. Alungbe, M. Tia, D. G. Bloomquist, Effects of Aggregate, Water/Cement Ratio, and Curing on the Coefficient of Linear Thermal Expansion of Concrete, Transportation Research Record: Journal of the Transportation Research Board No. 1335, 44–51, (1992).

ASTM C33, Standard Specification for Concrete Aggregates, American Society of Testing and Materials, (2013).

ASTM C39, Standard Test Method for Compressive Strength of Cylindrical Concrete Specimens, American Society of Testing and Materials, (2014).

ASTM C150, Standard Specification for Portland Cement, American Society of Testing and Materials, (2012).

ASTM C157, Standard Test Method for Length Change of Hardened Hydraulic-Cement Mortar and Concrete, American Society of Testing and Materials, (2008).

ASTM C305, Standard Practice for Mechanical Mixing of Hydraulic Cement Pastes and Mortars of Plastic Consistency, American Society of Testing and Materials, (2014).

ASTM C403, Test Method for Time of Setting of Concrete Mixtures by Penetration Resistance, ASTM International, (2008).

ASTM C469, Standard Test Method for Static Modulus of Elasticity and Poisson's Ratio of Concrete in Compression, American Society of Testing and Materials, (2010).

ASTM C494, Standard Specification for Chemical Admixtures for Concrete, American Society of Testing and Materials, (2013).

ASTM C496, Standard Test Method for Splitting Tensile Strength of Cylindrical Concrete Specimens, American Society of Testing and Materials, (2011).

ASTM C618, Standard Specification for Coal Fly Ash and Raw or Calcined Natural Pozzolan for Use in Concrete, American Society of Testing and Materials, (2012).

ASTM C1579, Standard Test Method for Evaluating Plastic Shrinkage Cracking of Restrained Fiber Reinforced Concrete (Using a Steel Form Insert), American Society of Testing and Materials, (2013).

ASTM C1581, Standard Test Method for Determining Age at Cracking and Induced Tensile Stress Characteristics of Mortar and Concrete under Restrained Shrinkage, (2009).

ASTM C1608, Standard Test Method for Chemical Shrinkage of Hydraulic Cement Paste, American Society of Testing and Materials, (2012).

ASTM C1679, Standard Practice for Measuring Hydration Kinetics of Hydraulic Cementitious Mixtures Using Isothermal Calorimetry, American Society of Testing and Materials, (2014).

N. Banthia, R. Gupta, Influence of polypropylene fiber geometry on plastic shrinkage cracking in concrete, Cement and Concrete Research 36, 1263–1267, (2006).

L. Barcelo, M. Moranville, B. Clavaud, Autogenous shrinkage of concrete: a balance between autogenous swelling and self-desiccation, Cement and Concrete Research 35 177–183, (2005).

V. Baroghel-Bouny, A. Kheirbek, Effect of mixture-parameters on autogenous deformations of cement pastes. Microstructural interpretations, Shrinkage of Concrete, International RILEM Workshop on Shrinkage of Concrete, 115-141, (2000).

V. Baroghel-Bouny, Hydration and Moisture Distribution, RILEM TC 181-EAS: Final Report 39-45 (2002).

V. Baroghel-Bouny, P. Mounanga, A. Khelidj, A. Loukili, N. Rafai, Autogenous deformations of cement pastes Part II. W/C effects, micro–macro correlations, and threshold values, Cement and Concrete Research 36, 123–136, (2006).

Z. P. Bazant, Delayed Thermal Dilatations of Cement Paste and Concrete due to Mass Transport, Nuclear Engineering and Design 14, 308-318, (1970).

A. F. Bentivegna, Multi-Scale Characterization, Implementation, and Monitoring of Calcium Aluminate Cement Based-Systems, PhD Dissertation, University of Texas at Austin, (2012).

A. Bentur, Chapter 1 - Introduction: Overview of Early Age Cracking, in Early Age Cracking In Cementitious Systems, RILEM TC 181-EAS: Final Report, (2002).

A. Bentur, K. Kovler, Evaluation of early age cracking characteristics in cementitious systems, Materials and Structures 36, 183-190, (2003).

D.P. Bentz, O.M. Jensen, Mitigation strategies for autogenous shrinkage cracking, Cement and Concrete Composites 26, 677–685, (2004).

D.P. Bentz, A review of early-age properties of cement-based materials, Cement and Concrete Research 38, 196–204, (2008).

S. Bishnoi, Automated Chemical Shrinkage Test and Shrinkage Suite Software. Lausanne, (2009).

J. Bisschop, Drying shrinkage cracking at early ages, RILEM TC 181-EAS: Final Report, 47-55, (2002).

M. Bouasker, P. Mounanga, P. Turcry, A. Loukili, and A. Khelidj, Chemical Shrinkage of Cement Pastes and Mortars at Very Early Age: Effect of Limestone Filler and Granular Inclusions, Cement and Concrete Composites 30, 13-22, (2008).

J.J. Brooks, X. Jiang, Cracking resistance of plasticized fly ash concrete, Proceedings Pro005: International Conference on the Role of Admixtures in High Performance Concrete, 493–506, (1999).

J. W. Bullard, H. M. Jennings, R. A. Livingston, A. Nonat, G. W. Scherer, J. S. Schweitzer, K. L. Scrivener, J. J. Thomas, Mechanisms of cement hydration, Cement and Concrete Research 41, 1208–1223, (2011).

B. E. Byard, A. K. Schindler, Modeling early-age stress development of restrained Concrete, Materials and Structures 48, 435–450, (2015).

V.T.N Dao, P.F. Dux, P.H. Morris and L. O' Moore, Plastic shrinkage cracking of concrete, Australian Journal of Structural Engineering, Vol. 10, No. 3, 207-214, (2010).

C.F. Ferraris, F.H. Wittmann, Shrinkage Mechanisms of Hardened Cement Paste, Cement and Concrete Research 17, 453-464, (1987).

K. J. Folliard, N. S. Berke, Properties of High-Performance Concrete Containing Shrinkage-Reducing Admixture, Cement and Concrete Research 27, 1357-1364 (1997).

T. Fu, Autogenous Deformation and Chemical Shrinkage of High Performance Cementitious Systems, Master's Thesis, Oregon State University, Corvallis, OR, (2011).

Z. C. Grasley, D. A. Lange, Thermal dilation and internal relative humidity of hardened cement paste, Materials and Structures 40, 311–317, (2007).

W. Hansen, Drying Shrinkage Mechanisms in Portland Cement Paste, Journal of the American Ceramic Society 70 (5), 323-328, (1987).

E. Holt, Contribution of mixture design to chemical and autogenous shrinkage of concrete at early ages, Cement and Concrete Research 35, 464– 472, (2005).

Jahangirnejad, Evaluation of Portland Cement Concrete Coefficient of Thermal Expansion Test Protocol and the impact of CTE on performance of Jointed Concrete Pavements, PhD Dissertation, Michigan State University, (2009).

D. Jansen, J. Neubauer, F. Goetz-Neunhoeffer, R. Haerzschel , W.D. Hergeth, Change in reaction kinetics of a Portland cement caused by a superplasticizer — Calculation of heat flow curves from XRD data, Cement and Concrete Research 42, 327–332, (2012).

O.M. Jensen, P.F. Hansen, A Dilatometer for Measuring Autogenous Deformation in Hardening Portland Cement Paste, Materials and Structures 28, 406-409, (1995).

O.M. Jensen, P.F. Hansen, Autogenous deformation and RH-change in perspective, Cement and Concrete Research 31, 1859–1865, (2001).

R. C. Joshi, R. P. Lohita, Fly Ash in Concrete: Production, Properties and Uses, Advances in concrete Technology, Volume 2, (1997).

H. Justnes, A.Van Gemert, A. Verboven, E. J. Sellevold, Total and External Chemical Shrinkage of Low W/C-ratio Cement Pastes, Advances in Cement Research, Vol. 8, No. 31, 121-126, (1996).

H. Justnes, E.J. Sellevold, B. Reyniers, D. Van Loo, A. Van Gemert, F. Verboven, D. Van Gemert, Chemical shrinkage of cement pastes with plasticizing admixtures, Nordic Concrete Research 24, 39–54, (2000).

H. Kada, M. Lachemi, N. Petrov, O. Bonnequ, P. C. Aïtcin, Determination of the Coefficient of Thermal Expansion of High Performance Concrete from Initial Setting, Materials and Structures 35, No. 245, 35-41 (2002).

A. Leemann, P. Nygaard, P. Lura, Impact of admixtures on the plastic shrinkage cracking of self-compacting concrete, Cement and Concrete Composites 46, 1-7, (2014).

P. Lura, O. M. Jensen, K. van Breugel, Autogenous shrinkage in high-performance cement paste: An evaluation of basic mechanisms, Cement and Concrete Research 33, 223–232, (2003).

P. Lura, O. M. Jensen, Measuring techniques for autogenous strain of cement paste, Materials and Structures 40, 431–440, (2007).

P. Lura, B. Pease, G. B. Mazzotta, F. Rajabipour, J. Weiss, Influence of Shrinkage-Reducing Admixtures on Development of Plastic Shrinkage Cracks, ACI Materials Journal, 187-194, March-April (2007).

P. Lura, O. M. Jensen, J. Weiss, Cracking in cement paste induced by autogenous shrinkage, Materials and Structures 42, 1089–1099, (2009).

M. Mangold, Methods for Experimental Determination of Thermal Stresses and Crack Sensitivity in the Laboratory, RILEM Report 15, Prevention of Thermal Cracking in Concrete at Early Ages, Edited by R. Springenschmid, E & Fn Spon, (1998).

I. Maruyama, Origin of Drying Shrinkage of Hardened Cement Paste: Hydration Pressure, Journal of Advanced Concrete Technology Vol. 8, No. 2, 187-200, (2010).

P.K Mehta, P.J.M Monteiro, Concrete: Structure, Properties and Materials, Third Edition, McGraw-Hill, (2006).

S. Mindess, J. F. Young, D. Darwin, Concrete, Second Edition, Prentice Hall, (2003).

J. Mora-Ruacho, R. Gettu, A. Aguado, Influence of shrinkage-reducing admixtures on the reduction of plastic shrinkage cracking in concrete, Cement and Concrete Research 39, 141–146, (2009).

J. Poole, Modeling Temperature Sensitivity and Heat Evolution of Concrete. PhD Dissertation, University of Texas at Austin, (2007).

C. Qi, J. Weiss and J. Olek, Characterization of plastic shrinkage cracking in fiber reinforced concrete using image analysis and a modified Weibull function, Materials and Structures 36, 386–395, (2003).

A. Radlinska, F. Rajabipour, B. Bucher, R. Henkensiefken, G. Sant, J. Weiss, Shrinkage Mitigation Strategies in Cementitious Systems. A Closer Look at Differences in Sealed and Unsealed Behavior, Transportation Research Record: Journal of the Transportation Research Board, No. 2070, 59–67, (2008).

F. Rajabipour, G. Sant, J. Weiss, Interactions between shrinkage reducing admixtures (SRA) and cement paste's pore solution, Cement and Concrete Research 38, 606–615, (2008).

A.A. Ramezanianpour, Cement Replacement Materials: Properties, Durability, Sustainability. Heidelberg: Springer, (2013).

K. Riding, Early age concrete thermal stress measurement and modeling. PhD Dissertation, University of Texas at Austin, (2007).

K. Riding, J. L. Poole, A. K. Schindler, M. C. G. Juenger, K. J. Folliard, Quantification of Effects of Fly Ash Type on Concrete Early-Age Cracking, ACI Materials Journal, March-April, (2008).

G. Sant, P. Lura, J. Weiss, Measurements of Volume Change in Cementitious Materials at Early Ages: Review of Testing Protocols and Interpretation of Results, Transportation Research Record: Journal of the Transportation Research Board, 21-29, (2006).

G. Sant, Examining volume change, stress development and cracking in cement-based materials, Master's Thesis, Purdue University, West Lafayette, IN, (2007).

G. Sant, B. Lothenbach, P. Juilland, G. Le Saout, J. Weiss, K. Scrivener, The origin of early age expansions induced in cementitious materials containing shrinkage reducing admixtures. Cement and Concrete Research 41, 218–229, (2011).

H. T. See, E. K. Attiogbe, M. A. Miltenberger, Potential for Restrained Shrinkage Cracking of Concrete and Mortar, Cement, Concrete and Aggregates 26, 123-130, (2004).

E.J. Sellevold, Ø. Bjøntegaard, Coefficient of thermal expansion of cement paste and concrete: Mechanisms of moisture interaction, Materials and Structures 39, 809–815, (2006).

S. Slatnick, K. A. Riding, K. J. Folliard, M. C. G. Juenger, Anton K. Schindler, Evaluation of Autogenous Deformation of Concrete at Early Ages, ACI Materials Journal, 21-28, January-February (2011).

M. D. A. Thomas, Optimizing the Use of Fly Ash in Concrete, IS548, Portland Cement Association, Skokie, IL, (2007).

N.H. Tran, K.D. Hall, M. James, Coefficient of Thermal Expansion of Concrete Materials: Characterization to Support Implementation of the Mechanistic-Empirical Pavement Design Guide, Transportation Research Record: Journal of the Transportation Research Board No. 2087, 51-56, (2008).

J. Weiss, Prediction of Early-Age Shrinkage Cracking in Concrete Elements. PhD thesis, Northwestern University, Evanston, IL, (1999).

J. Whigham, Evaluation of Restraint Stresses and Cracking in Early-Age Concrete with the Rigid Cracking Frame, Master's Thesis, Auburn University, (2005).

F. H. Wittmann, Heresies on shrinkage and creep mechanisms, in: Tanabe et al., Proceedings of Creep, Shrinkage and Durability Mechanics of Concrete and Concrete Structures, London: Taylor and Francis Group, 3-10, (2009).

M. Won, Improvements of Testing Procedures for Concrete Coefficient of Thermal Expansion, Transportation Research Record: Journal of the Transportation Research Board No. 1919, (2005).

M. Wyrzykowski, P. Lura, Controlling the coefficient of thermal expansion of cementitious materials – A new application for superabsorbent polymers, Cement & Concrete Composites 35, 49–58, (2013).

L. Xie, Influence of Mineral Admixtures on Early-Age Autogenous Shrinkage of High-Performance Concrete, Applied Mechanics and Materials, Vols. 457-458, pp 318-322, (2014).

Y.R. Zhang, X.M. Kong, Z.B. Lu, Z.C. Lu, S.S Hou, Effects of the charge characteristics of polycarboxylate superplasticizers on the adsorption and the retardation in cement pastes, Cement and Concrete Research 67, 184–196, (2015).